SAPIENZA
UNIVERSITÀ DI ROMA

Planck-scale-deformed relativistic symmetries and applications in astrophysics

Scuola di dottorato Vito Volterra

Dottorato di Ricerca in Fisica – XXXI Ciclo

Candidate

Giacomo D'Amico
ID number 1410623

Thesis Advisors

Prof. Giovanni Amelino-Camelia

Internal Thesis Advisors

Prof. Valeria Ferrari

October 2018

Thesis defended on 12 February 2019
in front of a Board of Examiners composed by:

Prof. Bruno Giacomazzo
Prof. Jerzy Kowalsky-Glickman
Prof. Marumi Marcello Kado (chairman)

Planck-scale-deformed relativistic symmetries and applications in astrophysics
Ph.D. thesis. Sapienza – University of Rome

This thesis has been typeset by LaTeX and the Sapthesis class.

Author's email: giacomo.damico@uniroma1.it

Contents

Introduction

The research work reported in this thesis is motivated by the possibility that we might yet be able to observe the first experimental evidence of quantum-gravity effects in astrophysical observations. This experimental evidence, if truly discovered, would shed light on the solution of the long-standing problem of Quantum Gravity. All observations performed so far can be described in terms of two theories, one is General Relativity (GR) which gives an accurate descriptions of gravitational phenomena, while the other is Quantum Mechanics (QM) which governs the Standard Model of particle physics. These theories, developed during the twentieth century, are the most fundamental physical theories known today. They have both had many experimental confirmations and now seem very robust in their predictions: QM in describing the microscopic phenomena involving fundamental particles, where gravity can be ignored, and GR in describing the motions of macroscopic bodies, whose quantum properties can be safely neglected. GR has been confirmed by experiments on scales between 10^{-6} m [93] and about 10^{20} m (at this scale one has to postulate the existence of dark matter in order to make general relativity agree with the experimental results), whereas the typical applications of QM and the Standard Model concern physical phenomena at scales between 10^{-8} m [112] and 10^{-20} m, the latter being the order of magnitude of the wavelength of the particles colliding at LHC.

There is a sort of "human discomfort" with the fact that we have on one side our present description of electromagnetic, weak and strong forces, "unified" within the Standard Model of particle physics, which is a quantum field theory, and on the other side gravity described by General Relativity, which is governed by the very different rules of classical mechanics. This, at first sight, might seem a purely philosophical problem: unity in science clearly cannot provide, on its own, the basis for introducing a truly scientific problem. But there is a well-defined scientific problem which can be naturally called "quantum-gravity problem", a problem which, as necessary in science, concerns the objective of obtaining quantitative predictions for the results of certain measurement procedures. If one applies GR and QM to the analysis of processes where neither gravity nor quantum properties can be safety neglected some logical and mathematical inconsistencies are encountered even before getting to the point of obtaining a numerical prediction. For example, as long as one ignores gravity, the Standard Model gives definite predictions on the results of a scattering process between two particles at energy scales of the order of the Planck energy

$$E_P = \sqrt{\frac{\hbar c^5}{G}} \sim 10^{28}\ eV.$$

Such high energy processes are not presently within our technological reach, but contemplating them sheds light on the conceptual structure of our theories. It is known that the gravitational interaction for collisions between two particles of energy approximately given by (or greater than) the Planck energy cannot be neglected, but we do not have any scientific information on how to introduce these gravitational properties in the theoretical framework of the standard model of particles physics. Estimating the gravitational contribution to the scattering amplitudes (from some effective-field-theory formulation of gravitational interactions) one obtains unmanageable divergences. The quantum-gravity problem is a scientific problem of a peculiar sort. The theories we have do not fail in reproducing any of the data we do have, but they do fail as a scientific theory in predicting the outcome of certain classes of measurement setups whose existence or availability is predicted by these theories presently in use. The search for "quantum gravity" is also justified by our limitation in describing the early stage of the universe, up to the Planck time $t_P \sim 10^{-44}\ s$. At this very early times, the size of the universe is so small that quantum gravitational fluctuations are expected to be important.

In physics every scientific problem should be handled combining mathematical-physics studies with experimental results. But for the last decades this has not been the case for search in quantum gravity. For various "historical" reasons, mostly connected with the lack of guidance from experiments [90], research on quantum gravity has wondered off the traditional strategy of progress in physics: the most popular quantum-gravity approaches, such as string theory and loop quantum gravity, could be described as "top-to-bottom approaches", since they start off with some key assumption about the structure of spacetime at the Planck scale and then they try to work their way back to the realm of doable experiments. It is notoriously difficult for these theories to translate their quantum-gravity framework into actual physical predictions which we can test. The main obstacle is given by the smallness of the scale at which the magnitudes of the effects of quantum mechanics and of gravitational effects become comparable, the Planck length

$$L_P = \sqrt{\frac{\hbar G}{c^3}} \sim 10^{-35}\,\mathrm{m}.$$

It was only rather recently, as a result of a research programme that started toward the end of the 1990s, that it was realized [24] that our chances to obtain at least indirect experimental access into the quantum-gravity realm might rely on those scenarios where the possible non-classical (quantum) properties of spacetime affects particle kinematics, usually allowing an effective low energy description characterized by nonlinear deformations of the relativistic symmetries. One of the most interesting aspects of the analysis of the quantum-gravity problem concerns the inadequacy of a standard classical description of space-time geometry. In GR we can measure the position of a particle of mass m with precision r only if [1] $r \gtrsim L_P^2 m$ (its Schwarzschild radius), otherwise a black hole forms and the localization procedure simply fails. Instead in relativistic QM it is possible to localize a particle of mass m in a region of space of size r only if $r \gtrsim 1/m$ (its Compton wavelength), otherwise

[1] From now natural units $\hbar = c = 1$ in which $G = L_P^2$ will be used and irrelevant numerical factors ignored.

the energy injected into the system required to localize the particle is sufficient to create another copy of the particle obstructing the measurement process. This argument, like many others (see Ref. [74]), for an intrinsic limit given by the Planck length in the localization of an event lead to a general expectation of the quantum gravity community that the abstraction of a classical spacetime must be abandoned in favor of a quantum description of spacetime. This has led many in the quantum-gravity community to argue that at the Planck scale Lorentz symmetry could be violated, with the associated emergence of a preferred reference frame (this theories are often labeled as Lorentz-symmetry-breaking theories). Another possibility is provided by the class of theories labeled as "DSR" (doubly-special, or, for some authors, deformed-special relativity) [22, 97, 102] in which the price to pay for introducing the Planck scale in the laws of relativistic kinematics is not the emergence of a preferred reference frame, but the fact that the transformation laws between inertial observers are deformed at the Planck scale. What is most noteworthy about this approaches to the quantum-gravity problem is that they are found to play a significant role in exploiting some of the few opportunities for Planck-scale phenomenology. For example, one can accommodate within a DSR framework a modification of the dispersion relation of the kind

$$E^2 - \vec{p}^2 + f(E, E_P) - m^2 = 0,$$

where the specific form of the function $f(E, E_P)$ can differ significantly from model to model. Assuming that the deformation admits a series expansion at small energies E, and parametrizing the deformation in terms of the Planck scale E_P, for a massless particle one would expect to be able to approximate the deformed dispersion relation at low energies according to

$$\vec{p}^2 \simeq E^2 \left(1 + \eta \left(\frac{E}{E_P}\right)^n\right),$$

where the power n and the parameter η would be fixed in a given dynamical framework. Because of the smallness of $1/E_P$ it was traditionally believed that this effect could not be seriously tested experimentally, but, for at least values of n as large as 1 (which is the most optimistic case), it will be shown in this thesis work that our current technological achievements, mainly in the detection of high-energy astrophysical photons and neutrinos, allow us to probe these Planck-scale deformations.

The deformed dispersion relation shown above may lead to a energy dependence in the speed of ultra-relativistic (or massless) particle, an effect which goes under the name of *in-vacuo dispersion*. In particular, the cosmological distances of gamma-ray bursts (GRBs) combine with their short duration provide ideal features for tests of possible in vacuo dispersion of electromagnetic and neutrino radiation from GRBs. Although the effect amounts to a correction of $E/E_P \sim 10^{-19}$ for photons of, say, GeV energies, for sources that are typically at cosmological distances, such as GRB, the long propagation times convert such tiny velocity deformations into an accumulated time-of-arrival effect which is macroscopic.

This thesis research work, whose results were published/announced in Refs. [26, 27, 31, 63, 30], has been mainly devoted to address the possibility that we might

be observing some GRB neutrinos affected by in vacuo dispersion; moreover, for GRB photons the abundance of observations cumulatively obtained by the Fermi telescope reached a level sufficient to allow to perform a statistical analyses over the whole collection of observed GRBs. The outline of the thesis will be the following: the first part is directed to a mathematical overview of relativistic symmetries and their representations, starting from Galilean relativity to Planck-scale-deformed special relativity, while the other parts of the thesis, after introducing the physics of GRBs and high-energy neutrinos, will concern the phenomenological results for both neutrinos and photons from GRBs, as well as the quantification of their statistical significance.

In chapter 1 it will be shown how the introduction of an invariant velocity scale (the velocity of light c) in the theory allows the transition from Galilean relativity to special relativity. This would be useful to recognize the essential features characterizing the striking concepts of Planck-scale deformed symmetries: the possibility of introducing the second observer-independent scale (the Planck scale) primitively in the spacetime structure. In doing so, we will also characterize the two essential phenomenological features explored in this thesis work: the already-mentioned in-vacuo dispersion and the "dual gravity lensing".

In chapter 2 it will be briefly exposed the physics of GRB: after an historical introduction of their discovery, the fireball theoretical model, that have been proposed to explain these particular objects, along with their predicted neutrino production, will be summarized.

In chapter 3 we will describe the original results obtained for the high-energy IceCube neutrinos. After briefly describing the currently largest neutrino observatory, the IceCube neutrino telescope at the South Pole, the high-energy neutrino physics, like the deep-inelastic scattering and the energy-dependent cross section of neutrino-nucleon interactions, is described. The main goal of this chapter will be to obtain, for the first time, an estimate of the posterior probability distribution for the most relevant properties, such as the neutrino energy and flavor, of the neutrino-nucleon interactions producing high-energy neutrino events in the IceCube detector.

In chapter 4 we propose a strategy of data analysis for exploring in-vacuo dispersion in neutrinos of 100 TeV from GRBs, which has the advantage of being applicable to several alternative possibilities. In all scenarios here of interest one should find a correlation between the energy of an observed neutrino and the difference between the time of observation of that neutrino and the trigger time of a GRB. We select accordingly some GRB-neutrino candidates among IceCube events, and our data analysis finds a rather strong such correlation. We also characterize the statistical significance of our findings.

In chapter 5, following the results obtained in the previous chapter, we explore the possibility that also dual lensing might play a role in the analysis of IceCube neutrinos. In doing so, we also investigate issues which are of broader interest, such

as the possibility of estimating the contribution by background neutrinos and some noteworthy differences between candidate "early neutrinos" and candidate "late neutrinos".

In chapter 6, from previous studies about what might be in-vacuo dispersion features for GRB neutrinos of 100 TeV and GRB photons with energy in the range of 10 GeV, we show that these two features are roughly compatible with a description such that the same effects apply over four orders of magnitude in energy. We also show that it should not happen so frequently that such pronounced features arise accidentally, as a result of (still unknown) aspects of the mechanisms producing photons at GRBs or as a result of background neutrinos accidentally fitting the profile of a GRB neutrino affected by in-vacuo dispersion.

Since previous results for GRBs were focused on the most energetic GRB particles, and in particular only included photons with energy at emission greater than 40 GeV, in chapter 7 we extend the window of the statistical analysis down to 5 GeV and find results that are consistent with what had been previously noticed at higher energies.

Chapter 1

Planck-scale-deformed relativistic symmetries

Whenever we need to build a physical theory in order to describe the *laws of nature*, the most important question that arises is how different observers will describe the same phenomena and how to confront their observations. This is possible only if the theory is a *relativistic* theory, which means that the mathematical formalism chosen to write these laws contains symmetries that maintains the theory *covariant* under a specified set of transformations between different observers. Mathematically, this means that, under a certain representation of the group of coordinate transformations, the form of physical laws must remains unchanged, i.e. invariant. Covariance does not necessary means that all observers will describe all the phenomena in the same way, but only that all the manifestation seen by all the observers are part of a single phenomenon. The most clear way to describe this concept is considering a charged particle at rest relative to an observer. This observer will detect a statical electric field, but a different observers, for which the particle is not at rest, will detect instead both electric and magnetic field. They are of course observing the same phenomenon and none of them is a special observer. On the contrary, there is a symmetry that preserves the invariance of the physical law that unifies these two seemingly distinct phenomena. The unchanging quality, or invariance, of physical laws for different observers represents a symmetry of space and time. In this particular example the symmetry is called Lorentz symmetry, which maintains the Maxwell equation covariant. The Lorentz symmetry of spacetime forms the core of special relativity, postulated by Einstein in 1905 in his historical paper [67]. Before Einsteins 1905 paper, one of the main difficulties which appeared in Classical (or Newtonian) Mechanics was its inconsistency with the electromagnetic phenomena, notably the fact that Maxwell equations involve a fundamental velocity scale, the speed of light $c \sim 3 \cdot 10^8 m/s$. The symmetry of Classical Mechanics is the Galilei symmetry, i.e. a set of transformations which leave invariant Newtonian mechanics. In Galilei relativity there is no observer-independent scale, thus the introduction of a fundamental velocity scale implies a preferred class of inertial observers (the "ether"). The negative result of the Michelson-Morley experiment, whose aim was measuring the translation velocity of the Earth in the ether, leads to the formulation of Einsteins Special Relativity in which the first observer-independent relativistic

scale was introduced. The presence of an observer-independent scale c in Maxwells equations was then understood not as a manifestation of the existence of a preferred class of inertial observers but as a manifestation of the necessity to deform the Galilei transformations.

The transition from Galilean Relativity to Special Relativity points out a general scheme for building new physical theories: having delineated all the symmetries that are inherent to the studied physical theory, one can discovers that there are some quantities which should be universal constant for all observers at some scale and not compatible with the original symmetries. Then one has to deform the symmetries in such a way to impose that all observers will agree on the values of these quantities. This is the case for Deformed (or Doubly) Special Relativity (DSR) [22], where an additional relativistically-invariant scale is introduced, usually thought to be, in the Quantum Gravity literature, the length/inverse-momentum Planck scale $\ell = M_P^{-1} \sim 10^{-35}$ m. Thus, DSR theories requires that the laws of physics involve both a fundamental velocity scale c and a fundamental inverse-momentum scale ℓ, and that each inertial observer can establish the same measurement procedure to determine the value of ℓ (besides the invariant measurement procedure to establish the value of c). In particular, since in DSR theories the speed of light could depend on its momentum, the value of c is assumed to be measured by each inertial observer as the value of the velocity of massless particles in the infrared limit, which is the limit in which the photons momentum is so small that one can neglect all the deformations at the Planck scale ℓ.

In this chapter we want first highlight, from a technial/mathematical point of view, the similarity in the logical structure between the transition from Galilean Relativity to Special Relativity and that from Special Relativity to DSR. On this purpose in Sec. 1.1, after introducing the Galilean symmetry, we present Special Relativity as a deformation of the Galilean framework, remarking the fact that the introduction of the absolute speed of light has the effect of turning the simple Galilean law of addition of velocities into a non commutative and nonassociative one, as well as the introduction of a new on-shell relation. Then in Sec. 1.1, following the same steps, we characterize DSR theories, along with their deformed on-shell relation. Finally in Sec. 1.2.1 and Sec. 1.2.2, for the purpose of the phenomenological research of this thesis work, it is introduced respectively the concept of "in-vacuo dispersion" and of "dual gravity lensing". The former is a feature that has the implication that the time needed for a ultra-relativistic particle to travel from a given source to a given detector receives an energy-dependent correction. The latter instead is a feature that allows in given DSR models deviations from the ordinary propagation in a direction orthogonal to the path connecting two distant observers, who could describe particles on parallel propagation as propagating along different directions.

1.1 From Galilean to special relativistic symmetries

The only postulate holding in Galilean relativity is the well-known Galilean relativity principle: the laws of physics take the same form in every inertial frame. This is manifest in all laws, and in particular in the on-shell relation $E = \vec{p}^2/2m$ and in the law of composition of velocities $\vec{v} \oplus \vec{u} = \vec{v} + \vec{u}$, which we use in particular

when connecting the description of a velocity $\vec{v}$ for a given observer Alice to the one of an observer Bob, when the relative Alice-Bob velocity is $\vec{u}$. The transition from Galilean Relativity to Special Relativity enforces the relativity of simultaneity and the associated law of absoluteness of the speed of light. The Galilean law of energy-momentum composition $p_\mu \oplus p'_{mu} = p_\mu + p'_{mu}$ is not challenged in any way, which is indeed maintained by the absoluteness of the speed of light . But the role of the speed of light as a relativistic invariant impose a change of on-shell relation $E^2 = c\vec{p}^2 + c^4 m^2$, and a change in the law of composition of velocities [1]

$$\vec{u} \oplus \vec{v} = \frac{1}{1 + \frac{\vec{u}\cdot\vec{v}}{c^2}} \left(\vec{u} + \frac{1}{\gamma}\vec{v} + \frac{1}{c^2}\frac{\gamma}{1+\gamma}(\vec{u}\cdot\vec{v})\vec{u} \right), \tag{1.1}$$

where as usual $\gamma = 1\sqrt{1 - \vec{u}\vec{u}/c^2}$.

The presence of an invariant velocity scale c is evidently inconsistent with the Galilean composition of velocities $\vec{v} \oplus \vec{u} = \vec{v} + \vec{u}$, whose special-relativistic version expressed in Eq. 1.1, which is non-commutative and non-associative, is well understood [78] as playing a central role in the logical consistency of Special Relativity.

In the following two sections it will be useful to describe the algebra of symmetries of the relativistic theory, both in Galilean (Sec. 1.1.1) and special relativity (Sec. 1.1.2). In this set up we will outline how the introduction of an invariant velocity scale (the velocity of light c) in the theory allows the transition from Galilean relativity to special relativity, and we will characterize such transition at the level of a generalization (c-deformation) of the algebra of symmetries. This framework will give us the opportunity to recognize, in Sec 1.2, the essential features characterizing the striking concepts we will develop in the transition (through ℓ-deformation) from special relativity to DSR theories.

1.1.1 Galilean-relativistic symmetries

As it is well known, the fundamental equations of Newtonian mechanics are invariant under the transformations of the 3+1D Galilei group: a ten-parameter group of linear transformations whose algebra of generators [2] of transformations can be represented in terms of the following set of Poisson brackets [3]

$$\begin{gathered} \{p_j, p_k\} = 0, \qquad \{p_0, p_k\} = 0, \\ \{R_j, R_k\} = \epsilon_{jkl} R_l, \quad \{R_j, p_0\} = 0, \quad \{R_j, p_k\} = \epsilon_{jkl} p_l, \\ \{N_j, N_k\} = 0, \quad \{R_j, N_k\} = \epsilon_{jkl} N_l, \quad \{N_j, p_0\} = p_j, \quad \{N_j, p_k\} = \delta_{jk} m, \end{gathered} \tag{1.2}$$

$$\mathcal{C} = m p_0 - \frac{\vec{p}^2}{2}, \tag{1.3}$$

[1] The reader might find more familiar the special case in which the velocities $\vec{u}$ and $\vec{v}$ are collinear: $\vec{u} \oplus \vec{v} = (\vec{u} + \vec{v})/(1 + (\vec{u}\cdot\vec{v})/c^2)$.

[2] A natural way to link the algebra of generators to its group is the exponential map [48].

[3] Recall that a Poisson bracket is defined as a bilinear map on the smooth functions $C^{\inf}$ (M) over a manifold M. The Poisson bracket gives the space of functions on the manifold the structure of a Lie algebra, so that Eqs. 1.2 reflect the properties of the Galilei algebra (the Lie algebra of the Galilei group). See for example Ref. [51] and references therein.

where p_0, $\vec{p}$, $\vec{R}$ and $\vec{N}$ are respectively the time translation, space translation, rotation and Galilean boost generators, m is the mass of the particle, while $\mathcal{C}$ is the (quadratic) Casimir of the algebra, having null Poisson bracket with all the generators. Having p_0 and $\vec{p}$ the physical interpretation of energy and momentum of the particle ($p_0 = E$), we can identify the quadratic Casimir (1.3) with the "on-shell relation" for the particle, giving the notorious Newtonian dispersion relation

$$E = \frac{\vec{p}^2}{2m} \tag{1.4}$$

Although this setup might seem redundant for the description of Galilean relativistic symmetries, it will prove useful for a comparison between Galilei relativity, special relativity and DSR.

At this point the elements of the symmetry algebra can be used to generate the symplectic transformations which map the coordinates between each inertial observer. We can define the symplectic structure of the system by introducing the spacetime coordinates x_0 and x_j (j = 1, 2, 3), canonically conjugate respectively to the energy p_0 and momenta p_j. The phase space x_0, x_j, p_0, p_j, can be described by the Poisson brackets

$$\begin{aligned} \{p_0, x_0\} &= 1, \quad \{p_0, x_i\} = 0, \\ \{p_i, x_0\} &= 0, \quad \{p_i, x_j\} = -\delta_{ij}, \end{aligned} \tag{1.5}$$

while the rotation and boost generators can be represented as

$$R_i = \epsilon_{ijk} x_j p_k, \quad N_i = x_i m - x_0 p_i. \tag{1.6}$$

One can then verify that the whole set of Poisson brackets in Eq. 1.2 and Eq. 1.5 satisfy the Jacoby identities [4], so that the symplectic structure is well defined, and is covariant.

Since the symplectic structure is canonical, the particles velocity can be obtained directly from Eq. 1.4 by the relation

$$v_i(\vec{p}) = \frac{dE(\vec{p})}{dp_j} = \frac{p_j}{m} \tag{1.7}$$

The velocity (1.7) can be derived also from the Hamiltonian analysis [5], where the equations of motions are [6]

$$\begin{aligned} \dot{x}_0 &= \frac{dx_0}{d\tau} = \{\mathcal{H}, x_0\} = m, \\ \dot{x}_j &= \frac{dx_j}{d\tau} = \{\mathcal{H}, x_j\} = p_j, \end{aligned} \tag{1.8}$$

[4] Given f, g, $h \in C^{\inf}(M)$, the Jacobi identity is $\{f, \{g, h\}\} + \{g, \{h, f\}\} + \{h, \{f, g\}\} = 0$.

[5] We can take as Hamiltonian of evolution the constraint $\mathcal{H} = \mathcal{C} - mw$, where w is the internal energy of the particle [43].

[6] We here introduce an "auxiliar" (not physically observable) parameter τ.

which can be integrated to give

$$\begin{aligned} x_0(\tau) - x_0(0) &= m\tau, \\ x_j(\tau) - x_j(0) &= p_j\tau. \end{aligned} \tag{1.9}$$

Finally eliminating τ we find the worldlines [7]

$$x_j(x_0) = \bar{x}_j + \frac{p_j}{m}(x_0 - \bar{x}_0). \tag{1.10}$$

We want to study now some properties of the symmetry transformations generated by the algebra defined in Eq. 1.2. In order to do so we introduce a scheme of analysis which will prove to be fruitful throughout this chapter. We specialize for simplicity to the 1+1D case, so that the phase space is characterized by the variables p_0, p_1, x_0, x_1.

Consider a first observer Alice, characterized by a set of phase space variables $k^A = (p_0^A, p_1^A, x_0^A, x_1^A)$. For the sake of brevity, being the translation sector trivial and similar for both Galilean and special relativistic symmetry, we focus only on the boost sector, which means that we consider Bob purely boosted respect to Alice, i.e. Bobs origin coincide with Alices, but he has velocity V_B relative to Alice. Observing that for each observer (labeling the coordinates of a generic observer by the suffix A for Alice and B for Bob) a given worldline can be specified by the parameters m, p_1, x_0, x_1, the worldlines in terms of which Alice and Bob will describe the motion of particles will have the same form expressed in Eq. 1.10, i.e.

$$x_1^A(x_0^A) = \bar{x}_1^A + \frac{p_1^A}{m}(x_0^A - \bar{x}_0^A), \tag{1.11}$$

$$x_1^B(x_0^B) = \bar{x}_1^B + \frac{p_1^B}{m}(x_0^B - \bar{x}_0^B). \tag{1.12}$$

One way to confront Alices and Bobs description is to express Bobs parameters in terms of Alices. We define the infinitesimal 1+1D boost trasformation to be given by [8]

$$\mathcal{B}_{V_B} \triangleright k^A = (\mathbb{1} - V_B\{N_1, \cdot\})k^A, \tag{1.13}$$

where $\triangleright$ is the action from left of the group element represented here by the boost trasformation $\mathcal{B}_{V_B}$.

Now using Eq. 1.6 and Eq. 1.5, one finds

$$\begin{aligned} \bar{x}_0^B &= \bar{x}_0^A - V_B\{x_1 m - x_0 p1, x_0\} = \bar{x}_0^A, \\ \bar{x}_1^B &= \bar{x}_1^A - V_B\{x_1 m - x_0 p1, x_0\} = \bar{x}_1^A - V_B\bar{x}_0^A, \\ p_1^B &= p_1^A - V_B\{x_1 m - x_0 p1, p_1\} = p_1^A - V_B m. \end{aligned} \tag{1.14}$$

[7] For simplicity we define $x(\tau = 0) \equiv \bar{x}$

[8] See Ref. [80] and reference therein for how to construct finite transformations by exponentiating the action of an infinitesimal transformation.

From the last expression of Eqs. 1.14 it is worth noticing, using the definition of velocity obtained in Eq. 1.7, that one can recover the law of composition of velocities and momentum in Galilean relativity:

$$\begin{aligned} v_1^B &= v_1^A - V_B, \\ p_1^B &= p_1^A - V_B m \end{aligned} \tag{1.15}$$

Then, substituting into Eq. 1.12, one gets

$$x_1^B(x_0^B) = \bar{x}_1^A - V_B x_0^A + \left(\frac{p_1^A}{m} - V_B\right)\left(x_0^B - \bar{x}_0^b\right), \tag{1.16}$$

from which one can recognize the well-known Galilean transformation between two boosted reference frames.

1.1.2 Special-relativistic symmetries

Following the same line of reasoning of the previous section, we now introduce the special relativistic symmetry, which arises when imposing the second postulate of special relativity, which can be restated as follows: the speed of light c in vacuum is the same for every inertial observer, and it is an upper bound for the speed of the other particles. The generators of the symmetry transformations for the special-relativistic case can be represented by the Poincaré Lie algebra given in terms of the Poisson brackets

$$\begin{gathered} \{p_j, p_k\} = 0, \qquad \{p_0, p_k\} = 0, \\ \{R_j, R_k\} = \epsilon_{jkl} R_l, \quad \{R_j, p_0\} = 0, \quad \{R_j, p_k\} = \epsilon_{jkl} p_l, \\ \{N_j, N_k\} = -\epsilon_{jkl} R_l, \quad \{R_j, N_k\} = \epsilon_{jkl} N_l, \quad \{N_j, p_0\} = p_j, \quad \{N_j, p_k\} = \delta_{jk} p_0, \end{gathered} \tag{1.17}$$

$$\mathcal{C} = p_0^2 - \vec{p}^2, \tag{1.18}$$

where as usual $\mathcal{C}$ is the (quadratic) Casimir of the algebra, having null Poisson bracket with all the generators, and N now is the Lorentz boost generator. One gets the special relativistic physical picture identifying the Casimir in Eq. 1.18 with the particles on-shell relation given by

$$\mathcal{C} = p_0^2 - \vec{p}^2 = m^2 c^2 \tag{1.19}$$

with c the invariant speed scale (the speed of light), while $\vec{p}$ is the particle momentum, and the physical interpretation of p_0 is given by the relation $p_0 = E/c$, with E the energy of the particle.

At this point we can describe the phase space by introducing the following Poisson brackets

$$\begin{aligned} \{p_0, x_0\} &= 1, \quad \{p_0, x_i\} = 0, \\ \{p_i, x_0\} &= 0, \quad \{p_i, x_j\} = -\delta_{ij}, \end{aligned} \tag{1.20}$$

where as usual x_μ ($\mu = 0, 1, 2, 3$) are the spacetime coordinates, canonically conjugate to the momenta p_μ. The rotation and boost generators are

$$R_i = \epsilon_{ijk} x_j p_k, \quad N_i = x_i p_0 - x_0 p_i, \qquad i, j, k = 1, 2, 3. \tag{1.21}$$

Now proceeding as in the previous section, since the symplectic structure is canonical, one can obtain the particle velocity from the on-shell relation in Eq. 1.19 (identifying $E = cp_0$) by the relation

$$v_i(\vec{p}) = \frac{dE(\vec{p})}{p_i} = \frac{cp_i}{\sqrt{\vec{p}^2 + m^2c^2}} = \frac{cp_i}{p_0}, \tag{1.22}$$

from which it is evident the interpretation of c as the speed of massless particles.

At this point we can derive the equation of motions using for the Hamiltonian the constraint $\mathcal{H} = \mathcal{C} - m^2c^2$:

$$\begin{aligned} \dot{x}_0 &= \frac{dx_0}{d\tau} = \{\mathcal{H}, x_0\} = p_0, \\ \dot{x}_j &= \frac{dx_j}{d\tau} = \{\mathcal{H}, x_j\} = p_j, \end{aligned} \tag{1.23}$$

which can be integrated to give

$$\begin{aligned} x_0(\tau) - x_0(0) &= p_o\tau, \\ x_j(\tau) - x_j(0) &= p_j\tau, \end{aligned} \tag{1.24}$$

and eliminating τ we find the worldlines [9]

$$x_j(x_0) = \bar{x}_j + \frac{p_j}{p_0}(x_0 - \bar{x}_0). \tag{1.25}$$

We are now ready to analyze some aspects of the symmetry transformations, restricting again for simplicity to the 1+1D case.. Using Eqs. 1.20 and 1.21, the Poisson brackets between the boost generator N_1 and the spacetime coordinates are given by

$$\{N_1, x_0\} = x_1, \qquad N_1, x_1 = x_0, \tag{1.26}$$

so that infinitesimal boost transformations are given by

$$\mathcal{B}_\xi \triangleright x_0 = x_0 - \xi x_1, \qquad \mathcal{B}_\xi \triangleright x_1 = x_1 - \xi x_0, \tag{1.27}$$

where ξ is the boost parameter called the "rapidity". Now, considering also the Poisson bracket between N_1 and p_1 defined in Eq. 1.17 one finds the transformation rules between Alices and (purely boosted) Bobs coordinates

$$\begin{aligned} x_0^B &= \cosh(\xi)x_0^A - \sinh(\xi)x_1^A, \qquad & x_1^B &= \cosh(\xi)x_1^A - \sinh(\xi)x_0^A, \\ p_0^B &= \cosh(\xi)p_0^A - \sinh(\xi)p_1^A, \qquad & p_1^B &= \cosh(\xi)p_1^A - \sinh(\xi)p_0^A, \end{aligned} \tag{1.28}$$

where as usual we have denoted the coordinates of a generic observer by the suffix A for Alice and B for Bob. Since Bob is purely boosted relative to Alice, we assume

[9] As in the previous section we define $x(\tau = 0) \equiv \bar{x}$

for simplicity that Bob is traveling inside a rocket, of mass M with speed V, whose frames origin coincide. In 1+1D case, the motion of the rocket is described by Alice in terms of the worldline given in Eq. 1.25, i.e. [10]

$$x_i^A(x_0^A) = \bar{x}_i^A + \frac{V}{c}\left(x_0^A - \bar{x}_0^A\right). \tag{1.29}$$

From the transformation laws of Eq. 1.28, being $v^A = cp_1^A/p_0^A$ the particle's velocity observed by Alice, Bob will observed the same velocity as

$$\begin{aligned} v^B = \frac{cp_1^B}{p_0^B} &= c\frac{\cosh(\xi)p_1^A - \sinh(\xi)p_0^A}{\cosh(\xi)p_0^A - \sinh(\xi)p_1^A} = \\ &= c\frac{\cosh(\xi)v^A/c - \sinh(\xi)}{\cosh(\xi) - \sinh(\xi)v^A/c}. \end{aligned} \tag{1.30}$$

From this last expression one can recognize the speed of light c as the same for the observer Alice and Bob (putting $v^A = c$ one also gets $v^B = c$) and as an upper bound for the speed of the other particles, which is indeed the second postulate of special relativity.

Being the rocket at rest relative to Bob, at this point we need just to set v^B equal to zero and find the relation

$$\sinh(\xi)p_0^A = \cosh(\xi)p_1^A, \tag{1.31}$$

i.e.

$$\tanh(\xi) = \frac{p_1^A}{p_0^A} = \frac{V}{c}. \tag{1.32}$$

This last equation express the relation between the rapidity and the speed of the moving frame. Then defining $\gamma = \cosh(\xi)$ and $\beta = V/c$, from Eq. 1.28 we recover the well-known Lorentz transformations for a collinear boost:

$$\begin{aligned} x_0^B &= \gamma x_0^A - \gamma\beta x_1^A, \qquad & x_1^B &= \gamma x_1^A - \gamma\beta x_0^A, \\ p_0^B &= \gamma p_0^A - \gamma\beta p_1^A, \qquad & p_1^B &= \gamma p_1^A - \gamma\beta p_0^A. \end{aligned} \tag{1.33}$$

At this point it is worth noticing that from Eq. 1.30 one can recover the non-commutative and non-associative law of composition of velocities in special relativity (see Eq. 1.1) for the case in which Bob is purely boosted and collinear respect to Alice:

$$v^B = \frac{v^A - V}{1 - \frac{Vv^A}{c^2}}. \tag{1.34}$$

Being useful when generalizing to DSR theories, we now want to show how the the Poincaré algebra $\mathcal{P}$ defined in Eq. 1.17 can be understood as a "c^{-1}-deformation" of Galilei relativity, emphasizing the characterization of special relativity as the introduction of an invariant velocity scale (the velocity of light c) in a relativistic theory. We first notice that, from a more formal point of view, the algebra of Eqs.

[10] Recalling that $x_0 = ct$, so that the rocket momentum p_R^A as observed by Alice is simply given by the relation $\frac{V}{c} = \frac{p_R^A}{\sqrt{(p_R^A)^2 + M^2c^2}}$

1.2 is not properly the Lie algebra $\mathcal{G}$ associated to the Galilei group, but it is the Lie algebra $\mathcal{G}\times < m >$ of the extended Galilei group, where m (the mass), is the central charge which commutes with all the generators of the Galilei group [43, 89]. Then, in order to obtain the Galilei algebra from the Poincaré algebra, we first have to perform a trivial central extension of the Poincaré algebra $\mathcal{P}$ (the Poincaré group does not admit non-trivial central extensions [43]), obtaining a new algebra $\mathcal{P}\times < \mu >$. Making the substitution $p_0 \to p_0 + \mu$ in the Poincarè algebra, we get that the only Poisson bracket that changes is the one between N_i and p_j, which now becomes

$$\{N_i, p_j\} = \delta_{ij}(p_0 + \mu), \tag{1.35}$$

The quadratic Casimir is now given by

$$\mathcal{C} = p_0^2 + 2p_0\mu + \mu^2 - \vec{p}^2 \tag{1.36}$$

from which one can subtract the unnecessary constant term μ^2.

At this point we apply what is called formally a Inönü-Wigner contraction [89], by rescaling the generators and the charge as

$$p_0 \to \epsilon p_0, \quad N_i \to \frac{N_i}{\epsilon}, \quad \mu \to \frac{m}{\epsilon}. \tag{1.37}$$

Once recalled that the physical interpretation adopted for the p_0 generator is $p_0 = E/c$ for special relativity, while $p_0 = E$ for Galilean relativity, with E the particles (kinetic) energy, this rescaling is easily understood as $\epsilon = 1/c$.

Finally we obtain the algebra

$$\begin{gathered}
\{p_j, p_k\} = 0, \qquad \{p_0, p_k\} = 0, \\
\{R_j, R_k\} = \epsilon_{jkl}R_l, \quad \{R_j, p_0\} = 0, \quad \{R_j, p_k\} = \epsilon_{jkl}p_l, \\
\{N_j, N_k\} = -\epsilon^2\epsilon_{jkl}R_l, \quad \{R_j, N_k\} = \epsilon_{jkl}N_l, \quad \{N_j, p_0\} = p_j, \quad \{N_j, p_k\} = \delta_{jk}(\epsilon^2 p_0 + m),
\end{gathered} \tag{1.38}$$

$$\mathcal{C} = \epsilon^2 p_0^2 + 2p_0 m - \vec{p}^2, \tag{1.39}$$

from which, taking the limit $\epsilon \to 0$, i.e. $c \to \infty$, we obtain the Galilei algebra.

1.2 Doubly-special relativity

We have shown in the previous sections how special relativity can be thought as the introduction in a relativistic theory (based on the principle of relativity) of an invariant velocity scale c (the speed of light), which has led us to the conclusion that special relativity is a c^{-1}-deformation of Galilean relativity. Moreover Einstein special relativity requires that the value of the fundamental velocity scale c can be measured by each inertial observer as the speed of light (speed of massless particles). Over last decade there have been certain approaches to the quantum-gravity problem, most notably the ones based on spacetime noncommutativity [38, 103] and loop quantum gravity [105, 110, 98], suggesting that there might be violations of some special-relativistic laws. The intuition that drives these proposals is that in the

quantum-gravity realm spacetime cannot be described as a smooth classical geometry, but rather it should have rich (and dynamical) short-distance structure, governed by a high-energy/short-distance scale ℓ, affecting in different ways particles of different wavelength. The interpretation of those results by the quantum-gravity community interested in these theories was that of a manifestation of a full breakdown of Lorentz symmetry, with the emergence of a preferred class of observers (an "ether"). But it was argued in Ref. [22] that the Relativity Principle, i.e. the principle of relativity of inertial observers, may well be compatible with the departures from Special Relativity governed by a high-energy/short-distance scale at the cost of allowing some consistent modifications of the Poincaré transformations, and particularly of the Lorentz-boost transformations. This suggestion gives birth to the DSR proposal in which the laws of physics involve both a fundamental velocity scale c and a fundamental inverse-momentum scale ℓ.

This proposal was then put forward (see Ref. [24] for instance) as a conceptual path for pursuing a broader class of scenarios of interest for fundamental physics, and in particular for the quantum-gravity phenomenology research. Most of the work in this line of research were concerning the possibility of introducing the second observer-independent scale ℓ primitively in the spacetime structure or at the level of the (deformed) de Broglie relation between wavelength and momentum, which in turn translates into a modified special-relativistic on-shell relation of the kind

$$E^2 - \vec{p}^2c^2 + f(p_\mu;\ell) - m^2c^4 = 0. \tag{1.40}$$

Where the function $f(p_\mu;\ell)$ depends on the kind of DSR scenario in which one is interested in. Evidently this on-shell relation is not Lorentz invariant. If we insist on this law and on the validity of classical (undeformed) special relativistic transformations between inertial observers (which we discussed in Sec. 1.1.2) we clearly end up with a preferred-frame picture, and the Principle of Relativity of inertial frames must be abandoned. The other option is that, preserving the relativity of inertial frames, in DSR theories the laws of transformation between inertial observers must be modified respect to the special relativistic ones, at the cost of modifying the action of boosts on momenta. This is achieved, in analogy with the c^{-1}-deformation that brings from the Galilei relativity description to Einstein relativity (as shown in the previous chapter), through a ℓ-deformation of special relativity transformation laws.

We now want to briefly review, following the same line of reasoning of the previous sections, the most studied formulation of DSR theories, which is the k-Poincaré/ k-Minkowski [11] model of DSR in the "bicrossproduct" (time-to-the-right) basis [103, 101], to which we will refer as illustrative example. We start by characterizing the algebra of symmetry generators in terms of Poisson brackets

$$\begin{aligned} \{p_\mu, p_\nu\} = 0, \quad \{R_j, R_k\} = \epsilon_{jkl}R_l, \quad \{N_j, N_k\} = -\epsilon_{jkl}R_l, \\ \{R_j, N_k\} = \epsilon_{jkl}N_l, \quad \{R_j, p_0\} = 0, \quad \{R_j, p_k\} = \epsilon_{jkl}p_l, \\ \{N_j, p_0\} = p_j, \quad \{N_j, p_k\} = \delta_{jk}\left(\frac{1-e^{-2\ell p_0}}{2\ell} + \frac{\ell}{2}\vec{p}^2\right) - \ell p_j p_k, \end{aligned} \tag{1.41}$$

[11] In the early literature [103, 101], the usage of the parameter $k = \ell^{-1}$, of the order of the huge Planck scale, was prefered.

$$\mathcal{C} = \left(\frac{2}{\ell}\right)^2 \sinh^2\left(\frac{\ell}{2}p_0\right) - e^{\ell p_0}\vec{p}^2. \tag{1.42}$$

Where $\mathcal{C}$ is the quadratic Casimir of the algebra (one can verify having null Poisson bracket with all the generators), which in the limit $\ell \to 0$ takes the form

$$\mathcal{C} = p_0^2 - \vec{p}^2 - \ell p_0 \vec{p}^2 + O(\ell^2). \tag{1.43}$$

The phase space is defined with the relations

$$\begin{gathered} \{p_0, x_0\} = 1, \quad \{p_0, x_j\} = 0, \\ \{p_j, x_0\} = -\ell p_j, \quad \{x_j, x_k\} = -\delta_{jk}, \\ \{x_j, x_0\} = \ell x_j \end{gathered} \tag{1.44}$$

In terms of the phase space variables p_μ, x_μ, the rotation and boost generators have representations

$$R_i = \epsilon_{ijk} x_j p_k, \quad N_i = -x_0 p_j + x_j \left(\frac{1 - e^{-2\ell p_0}}{2\ell} + \frac{\ell}{2}\vec{p}^2\right). \tag{1.45}$$

Using the representations given in this last expression, one can verify that given the Poisson brackets defined by Eqs. 1.41 and 1.44, the Jacobi identities for the whole set of phase space functions p_μ, x_μ, N_j ,R_j , are satisfied. It is also worth noticing that if $\{x_j, x_0\}$ were zero, the Jacoby identities would not be satisfied by the relations given in Eqs. 1.44. This ensures that the symplectic transformations generated by the elements of the algebra 1.41 preserve the Poisson structure itself, in such a way that every inertial observer connected by such transformations describes the same symplectic structure in his coordinates.

The relations in Eqs. 1.41 and 1.44 define the k-Poincaré algebra, i.e. the ℓ-deformation of the Poincaré algebra discussed in the previous section. In order to complete the characterization of DRS symmetries, we introduce now, as made in Sec. 1.1.1 and 1.1.2 for the Galilean and special relativistic case, the action of the symmetry transformations on the phase space coordinates.

For simplicity we will develop this analysis in 1+1D dimension and, due to the smallness of the deformation scale ℓ we want to contemplate for our physical interpretation (close to the inverse of the Planck scale) of the theory we will limit our analysis to the first order in the deformation parameter ℓ, neglecting higher orders contributes. This means that the ℓ-deformed Poisson structure is now given by the relations [12]

$$\begin{gathered} \{x_1, x_0\} = \ell x_1, \quad \{p_1, x_0\} = \ell p_1, \quad \{x_j, x_0\} = -\ell x_j, \\ \{N, p_1\} = p_0 + \ell p_0^2 + \frac{\ell}{2} p_1^2, \end{gathered} \tag{1.46}$$

$$\mathcal{C} = p_0^2 - p_1^2 + \ell p_0 p_1^2, \tag{1.47}$$

[12] We take the opposite sign of ℓ respect to the formulas given in Eqs. 1.41 and 1.44 , in order to describe, consistently throughout this thesis, subluminal (superluminal) deviations from speed-of-light for positive (negative) ℓ.

while all the other relations of Eqs. 1.41 and 1.44 are unchanged. The boost generators N (in the x_1 direction) is now given by

$$N = -x_0 p_1 + x_1 p_0 + \ell x_1 \left(p_0^2 - \frac{p_1^2}{2} \right). \tag{1.48}$$

From the Hamiltonian constraint $\mathcal{H} = \mathcal{C} - m^2$, we get the equation of motion

$$\begin{aligned} \dot{x}_1 &= \{\mathcal{H}, x_1\} = 2p_1 - 2\ell p_0 p_1, \\ \dot{x}_0 &= \{\mathcal{H}, x_0\} = 2p_0 - \frac{1}{2}\ell p_1^2, \end{aligned} \tag{1.49}$$

which can be integrated to get the worldline

$$x_1 = \bar{x}_1 + \left(\frac{p_1}{p_0} - \ell \left(p_1 - \frac{p_1^3}{2p_0^2} \right) \right) (x_0 - \bar{x}_0). \tag{1.50}$$

Notice that after enforcing the on-shell relation $\mathcal{H} = 0$, one gets the on-shell dispersion relation

$$p_0 = \sqrt{p_1^2 + m^2} - \frac{\ell}{2} p_1^2. \tag{1.51}$$

This relation can be used to get from Eq. 1.50, the following expression for the worldline

$$x_1 = \bar{x}_1 + \left(\frac{p_1}{\sqrt{p_1^2 + m^2}} - \ell \frac{m^2 p_1}{p_1^2 + m^2} \right) (x_0 - \bar{x}_0), \tag{1.52}$$

which, for a massless particle, becomes

$$x_1 = \bar{x}_1 + \frac{p_1}{|p_1|}(x_0 - \bar{x}_0). \tag{1.53}$$

One can then verify that the worldline of Eq. 1.52 are covariant under the transformations generated by p_μ and N by Poisson brackets. We now consider a first observer, Alice, local to an emitter, and a second observer, Bob, at rest respect to Alice and local to a detector. Since the worldlines are covariant they take the same form for all "inertial" observers, i.e. Alice and Bob respectively describe the motion of the particles in their coordinates in terms of the worldlines

$$\begin{aligned} x_1^A &= \bar{x}_1^A + v(p_1^A)(x_0^A - \bar{x}_0^A), \\ x_1^B &= \bar{x}_1^B + v(p_1^B)(x_0^B - \bar{x}_0^B), \end{aligned} \tag{1.54}$$

where we have defined

$$v(p_1) = \left(\frac{p_1}{\sqrt{p_1^2 + m^2}} - \ell \frac{m^2 p_1}{p_1^2 + m^2} \right). \tag{1.55}$$

Consider now the worldines of two photons (massless particles) emitted simultaneously in Alice origin ($\bar{x}_0^A = \bar{x}_1^A = 0$) propagating towards the positive x_1^A axis direction:

$$\begin{aligned} x_1^{A,1} &= x_0^A, \\ x_1^{A,2} &= x_0^A. \end{aligned} \tag{1.56}$$

In Alices description, the two worldline would reach the detector simultaneously, at $x_0^A = L$. But Alice is distant from the detector, so she is not a reliable observer to measure their arrival time . We consider then the second observer Bob, local to the detector. Bob worldlines are obtained from Alice worldlines using the translation transformation $\mathcal{T}$, whose action on the set of phase space variables $k = (p_\mu, x_\mu)$ is given by

$$k^B = \mathcal{T} \triangleright k^A = k^A - a_0\{p_0, k^A\} + a_1\{p_1, k^A\}, \tag{1.57}$$

where a_0 and a_1 are respectively the time and spatial component of the translation parameter a, i.e. the vector separating the two observers. Using the algebra of Eqs. 1.46 we get that Bobs coordinates are related to Alices by

$$\begin{aligned} x_0^B = x_0^A - a_0 + \ell a_1 p_1^A, \quad \bar{x}_0^B = \bar{x}_0^A - a_0 + \ell a_1 p_1^A, \\ x_1^B = x_1^A - a_1, \quad \bar{x}_1^B = \bar{x}_1^A - a_1, \\ p_1^B = p_1^A. \end{aligned} \tag{1.58}$$

Assuming that Bob detects the soft particle in his spacetime origin, so that the translation parameters are $a_1 = a_0 = L$, and using the relations in Eqs. 1.58, we get that the two particles are described by Bob in terms of the worldlines

$$\begin{aligned} x_1^{B,1} &= x_0^B, \\ x_1^{B,2} &= x_0^B - \ell L p_1^{B,2}, \end{aligned} \tag{1.59}$$

where we have used the fact that one photon is a low energy (soft) one, such that all the effects of deformation to its motion can be neglected $\ell p_1^{A,1} = \ell p_1^{B,1} = 0$, while the other photon is a high energy (hard) one, for which the effects of the ℓ-deformation are tangible $\ell p_1^{A,2} = \ell p_1^{B,2} \neq 0$. Setting to zero the last two equations, we find that while Bob detects the soft particle in his spacetime origin, he detects the hard particle with a delay

$$\Delta t^B = \ell L p_1^{B,2}. \tag{1.60}$$

Bob, local to the detector, describes distinct worldlines for the soft and hard photons and "witnesses" different arrival times. Conversely Bob, distant to the event of emission, describes the two particles to be emitted at different times, while Alice, local to the emission event, witnesses it to be simultaneous. We thus understand that in this k-Minkowski inspired DSR theory, what appears as a distantly local event to an observer may not be local for an observer witness to the event. To be more precise, we established that what actually happens to locality is that it remains objective to observers local to the coincidence of events, but observers who are distant in their coordinatization of spacetime see those same pairs of events as not coincident: locality becomes relative. The transition from Galilean relativity to special relativity, and in particular the introduction of an observer-invariant velocity scale c, enforces one to abandon the idealization of absolute simultaneity. In the same way having one more thing invariant requires rendering one more thing relative. The effects of relative locality in DSR scenarios have been pushed forward in the framework of Refs. [34, 35], based on the recently proposed "principle of relative locality": the possibility of linking the non-trivial geometry for momentum space to some effects of relative locality.

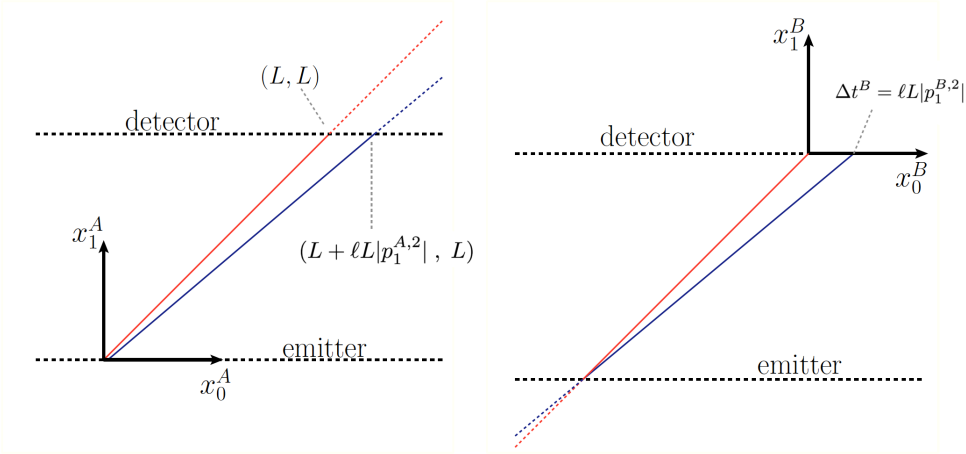

Figure 1.1. On the left (right) panel is shown Alices (Bobs) description of the emission and detection of the twho photons.

1.2.1 In-vacuo dispersion

We have seen in the previous sections how DSR theories allow us to consider deformed dispersion relations of the kind

$$E^2 - \vec{p}^2 c^2 + f(p_\mu; \ell) - m^2 c^4 = 0, \tag{1.61}$$

and how these deformed deformed dispersion relations can be maintained relativistically covariant at the cost of modifying the action of boosts on momenta. This has also led us to allow an energy-dependent speed for massless particles. We focused on the case in which, at leading order in ℓ (we assume $\ell^{-1} \sim M_P \sim 10^{19}$ GeV) , the velocity of massless particles takes the form (setting $c = 1$)

$$v = 1 + \eta \frac{E}{M_P}, \tag{1.62}$$

where η is a parameter whose value and sign depend on the DSR scenario one is intended to study.

It is also emerging that the most powerful perspective on this feature is that the relevant models have their momentum space curved (see e.g. Refs. [40, 34, 37, 28, 56] and references therein), and an effect dual to redshift produces the energy dependence of travel times. Famously ordinary redshift due to spacetime curvature is such that particles emitted at different times with the same energy by the same source reach the detector with different en- ergy, while the curvature of momentum space induces the feature that ultrarelativistic particles emitted at the same time with different energy by the same source reach the detector at different times. This is why the feature of in-vacio dispersion is also referred to as "dual redshfit".

The possibility of energy dependence of speed of light is considerably relevant for Planck scale phenomenology, as it has been shown to lead to testable predictions [42, 39]. As shown in the rest of this thesis work, these effects are within the reach of present experiments due mainly to an effective amplification, as for instance in the observations of gamma-ray bursts. Take for instance two photons, a hard one

with energy of $\sim$ GeV, which is in the range of energies for photons produced by the most energetic gamma ray bursts, and a relative soft one with energy of $\sim$ KeV, both emitted simultaneously [13] by a gamma-ray burst whose cosmological distance from our telescopes is of $\sim 10^{18}$ s. Assuming the deformation scale ℓ to be close to the Planck scale the delay accumulated by the hard photon relative to the soft photon, due to the in-vacuo disperion, would be of the order of 10^{-1} s, within the reach of the sensibility of presently available astronomical telescopes. An even higher sensitivity to a possible energy dependence of the speed of photons could be achieved by exploiting the fact that, according to current models (see Ref [130] and Chap. 2), gamma-ray bursters should also emit a substantial amount of high-energy neutrinos. Presently available neutrino observatories, like the IceCube neutrino observatory, can observe neutrinos with energies greater than 100 TeV, and one could, as shown in Chap. 4, compare the times of arrival of these neutrinos emitted by gamma-ray bursts to the corresponding times of arrival of low-energy photons.

This computation can be considered to be only an approximate estimate of the magnitude of the effect, because it is clear that with the huge, cosmological distances traveled by the GRB photons, one cannot neglect the effects of spacetime curvature in the estimate of the photons time of arrival: light propagation from remote objects is affected by the expansion of the Universe and depends upon the cosmological model. Two particles, that are emitted simultaneously from a source and have different propagation speeds, will arrive on Earth at different times. If the source is at a cosmological distance, then as a result of the universes expansion, the proper (physical) distances traveled by the particles will also differ. A length that is by definition always fixed between the source and the observer (provided they move together with the universes expansion) is the "comoving distance". In order to determine the cosmological delay between the two particles we have to inspect their comoving trajectories. Neglecting higher order Planck scale corrections and using the velocity given in Eq. 1.62, we write the comoving path as [92]

$$x(z,E) = \frac{1}{H_0}\int_0^z \left(1+\eta\frac{E}{M_P}(1+\zeta)\right)\frac{d\zeta}{\sqrt{\Omega_\Lambda+(1+\zeta)^3\Omega_m}}, \tag{1.63}$$

where E is the redshifted particle energy measured at present and H_0, Ω_Λ and Ω_m are the cosmological parameters evaluated today, to which we assign throughout this thesis the standard values [17]. We examine a low-energy photon, that was emitted at redshift z and reaches us at redshift 0 , and a highly energetic one, that was also emitted at redshift z and arrives with a delay at redshift $-\Delta$ z. The comoving distance, traveled by both particles, emitted from the same source and reaching Earth, is the same. Equating the two paths and taking again only the leading order corrections yields:

$$\int_{-\Delta z}^0 \frac{d\zeta}{\sqrt{\Omega_\Lambda+(1+\zeta)^3\Omega_m}} = \int_0^z \left(1+\eta\frac{E}{M_P}(1+\zeta)\right)\frac{d\zeta}{\sqrt{\Omega_\Lambda+(1+\zeta)^3\Omega_m}}. \tag{1.64}$$

[13] The fact that both particle has to be emitted simultaneously is a key element in this kind of phenomenological line of research, as it will be clear throughout this thesis work. In principle any observed delay between particle at the Earth can be attributed to some effect at the source. This is also why GRB are a perfect tool to explore in-vacuo dispersion, being their duration relative small.

Since for all delays that may be considered Δz is a very small number, we neglect second order corrections in Δz and we finally arrive at the expression for the time delay of a cosmological high-energy massless particle:

$$\Delta t = \eta \frac{E}{M_P} D(z), \tag{1.65}$$

where we have defined [14]

$$D(z) = \frac{1}{H_0} \int_0^z d\zeta \frac{1+\zeta}{\sqrt{\Omega_\Lambda + (1+\zeta)^3 \Omega_m}}. \tag{1.66}$$

Let us now conclude this section about in-vacuo dispersion mentioning the possibility of effects of quantum gravity on particle propagation mainly concerned stochastic or so-called fuzzy effects. These were inspired by speculations that quantum spacetime, like the k-Minkowski description of spacetime introduced in the previous section, can provide a characterization of spacetime fuzziness at the Planck length: spacetime is "foamy" in the sense that spacetime structure would not affect the average arrival time of a group of particles, but would instead contribute to the spreading of results of repeated measurements. In particular, one can consider the picture introduced in Refs. [21, 41], which implies the following description of the relationship between the energy and speed of a particle

$$v = 1 + \eta \frac{E}{M_P} \pm \delta \frac{E}{M_P}, \tag{1.67}$$

where η parametrizes the type of "systematic" effect we have already considered, while the notation "$\pm\delta$" parametrizes the fuzziness of the relationship between the energy and speed. In light of these considerations, Eq. 1.65 can be rewritten as

$$\Delta t = \eta \frac{E}{M_P} D(z) \pm \delta \frac{E}{M_P} D(z). \tag{1.68}$$

1.2.2 Dual-gravity lensing

For the line of research that will be exposed in Chap. 5, it is now useful to briefly describe an interesting feature that emerges when investigating the emission and observation of different signals in distinct reference frames boosted one respect the other in the DSR framework. First, we need to point out that the delay of Eq. 1.60 is a feature purely longitudinal, meaning that it lies along the direction connecting the two observers. In this section we will instead study the emergence of effects of transverse relative locality. The distinction between longitudinal relative locality and transverse relative locality is that with longitudinal relative locality coincidences of events established by nearby observers are described by distant observers as events that are non-coincident along the direction connecting the observer to the events, whereas with transverse relative locality the distant observer describes the events as non-coincident along a direction orthogonal to the direction connecting observer to

[14] The interplay between quantum-spacetime effects and curvature of spacetime is still a lively subject of investigation, and, while (1.66) is by far the most studied scenario, some alternatives to (1.66) are also under consideration [123].

events. First mentions of a feature of transverse relative locality can be found in Refs. [70, 40], where it was introduced the effect of "dual-gravity lensing" [15], intended as a manifestation of relative locality such that particles on parallel propagation according to some observers could be described by other observers as propagating along different directions.

The strategy we are going to follow is very tight to the one shown in the previous section for the study of longitudinal time delays. We start from the parametric 2+1D DSR algebra used in Ref. [29]

$$\begin{aligned}
&\{p_0, p_i\} = 0, \quad \{p_i, p_j\} = 0, \quad \{N_i, p_0\} = (1 - \ell\alpha p_0)p_i, \quad \{R, p_i\} = \epsilon_{ij}p_j, \\
&\{R, N_i\} = \epsilon_{ij}N_j, \quad \{R, p_0\} = 0, \quad \{N_i, N_j\} = (1 + 3(\alpha - \beta - \gamma - \frac{1}{2})\ell p_0)\epsilon_{ij}R, \\
&\{N_i, p_j\} = \delta_{ij}p_0 + \ell\left(\delta_{ij}(\beta\vec{p}^2 + (1 - \alpha + \gamma)p_0^2) - (\beta + \gamma - \frac{1}{2})p_j p_j\right),
\end{aligned} \tag{1.69}$$

$$\mathcal{C} = p_0^2 - \vec{p}^2 + \ell\left(2\gamma p_0^3 + (1 - 2\gamma)p_0\vec{p}^2\right), \tag{1.70}$$

with $i, j = 1, 2$ and α, β and γ three real parameters. The phase space is defined with the relations

$$\begin{aligned}
\{x_0, x_i\} = \{x_j, x_k\} = &\{p_0, p_i\} = \{p_j, p_k\} = 0, \\
\{p_0, x_0\} = 1, \quad &\{p_i, x_j\} = -\delta_{ij},
\end{aligned} \tag{1.71}$$

Thus in terms of the phase space variables p_μ, x_μ, the rotation and boost generators reads

$$\begin{aligned}
&R = \epsilon_{ij}x_j p_j, \\
&N_i = x_i p_0 + x_0 p_i + \ell\left(\alpha x_0 p_0 p_i + x_i(\beta\vec{p}^2 + (1 + \gamma - \alpha)p_0^2) - (\gamma + \beta\frac{1}{2})x_k p^k p_i\right).
\end{aligned} \tag{1.72}$$

It is easy to verify [40] that all Jacobi identities are satisfied by these choices of Poisson brackets. Then in order to obtain the worldline, following the same procedure used throughout this chapter, we use the on-shell relation as Hamiltonian of evolution in an auxiliary worldline parameter τ, i.e.

$$\begin{aligned}
\dot{x}_i = \{\mathcal{C}, x_i\} &= 2p_i\left(1 - \ell(1 - 2\gamma)p_0\right), \\
\dot{x}_0 = \{\mathcal{C}, x_0\} &= 2p_0 - +\ell\left(6\gamma p_0^2 + (1 - e\gamma)\vec{p}^2\right),
\end{aligned} \tag{1.73}$$

from which in particular one obtains that for massless particles the worldlines are governed by

$$x_i = \bar{x}_i + (1 - \ell|\vec{p}|)\frac{p_i}{|\vec{p}|}(x_0 - \bar{x}_0). \tag{1.74}$$

[15] One can qualify this sort of effects as "dual-gravity lensing" in light of the thesis put forward in Refs. [34, 35] which characterizes relative locality as a manifestation of the, possibly curved, geometry of momentum space. The standard gravitational lensing is caused by spacetime curvature, and this relative-locality-induced "lensing" can be attributed to the "dual gravity" of momentum space.

Now let us first establish how a single massless particle emitted in Alices origin and propagating along its x_1^A axis is described by an observer Bob, translated with respect to Alice along the x_1^A direction, and by an observer Camilla, purely boosted with respect to Bob along the direction x_2^B. The boost regarding Camilla is central in this analysis: she is boosted in a direction transverse to that connecting Alice and Bob. Evidently, in light of the equations for worldlines of massless particles derived above, according to Alice such a particle has worldline

$$x_1^A = (1 - \ell p)x_0^A, \quad x_2^A = 0, \tag{1.75}$$

where we denote with p the specific value of spatial momentum of this particle.

In order to obtain Bobs description of this same worldline we must use the translation generators:

$$\begin{aligned} &\mathcal{T} \triangleright x_0^A = x_0^A + a\{p_1, x_0^A\} - a\{p_0, x_0^A\} = x_0^A - a, \\ &\mathcal{T} \triangleright x_1^A = x_1^A + a\{p_1, x_1^A\} - a\{p_0, x_1^A\} = x_1^A - a, \\ &\mathcal{T} \triangleright x_2^A = x_2^A, \quad \mathcal{T} \triangleright p_i^A = p_i^A, \quad \mathcal{T} \triangleright p_0^A = p_0^A, \end{aligned} \tag{1.76}$$

where we have used as transaltion paramaters $a_0 = a_1 = a$ and $a_2 = 0$. We therefore find Alices worldline of Eq. 1.75 is described by Bob as follows

$$x_1^B = -a + (1 + \ell p)(x_0^B + a), \quad x_2^B = 0. \tag{1.77}$$

We are now ready for the final step of our planned analysis of the massless particle of generic momentum p emitted in Alices origin along Alices x1 axis, i.e. we can now perform the DSR-deformed boost along the x_2 direction to obtain the description of that particle according to observer Camilla. Using the representation given in Eq. 1.72 we obtain the following action of the boosts on coordinates:

$$\begin{aligned} \{N_i, x_0\} &= x_i + \ell \left(2(1 + \gamma - \alpha)x_i p_0 + \alpha x_0 p_i\right), \\ \{N_i, x_j\} &= x_0\delta_{ij} - \alpha\ell x_0 p_0 \delta_{ij} + \ell\left(\gamma + \beta - \frac{1}{2}\right)\left(\delta_{ij}x_k p^k + p_i x_j\right) - 2\beta\ell x_i p_j. \end{aligned} \tag{1.78}$$

Specializing these formulas to the case of a boost purely in the x_2 direction, and acting with it on the worldline of Eq. 1.77 we arrive at the sought Camilla description:

$$\begin{aligned} x_1^C &= -a + (1 - \ell p)(x_0^C + a), \\ x_2^C &= \xi_2 a - \ell\xi_2 a\left(\alpha - \beta - \gamma + \frac{1}{2}\right)p - \xi_2\left(1 - \left(\alpha - \beta - \gamma + \frac{1}{2}\right)\ell p\right)(x_0^C + a), \end{aligned} \tag{1.79}$$

where ξ_2 is the boost parameter for the transformation from Bob to Camilla, which is a pure boost along the x_2 direction. By eliminating x_0^C one obtains the projection of the worldline in the x_1^C, x_2^C plane

$$x_2^C = -\xi_2\left(1 - \left(\alpha - \beta - \gamma + \frac{1}{2}\right)\ell p\right)x_1^C - \ell p a \xi_2, \tag{1.80}$$

which has some remarkable properties. The detection at Camilla presents, besides the the usual delay $\Delta t^C = \ell a p$, a rigid shift from the origin in the x_2 direction [16]

$$\Delta x_2^C = \xi_2 \ell a p, \tag{1.81}$$

and an angular deviation, that we identified as a "dual gravity lensing" [17]

$$\Delta\theta = \left(\alpha - \beta - \gamma + \frac{1}{2}\right) \ell p. \tag{1.82}$$

[16] When distances of order $\xi_2 \ell a p$ are within the reach of available experimental sensitivities it will be appreciated that the worldline does not cross Camillas spatial origin, a feature we shall find convenient to label as "shift".

[17] When $\ell \xi_2 p$ is within the reach of available angular resolutions and $\left(\alpha - \beta - \gamma + \frac{1}{2}\right) \neq 0$ the angle in the x_1, x_2 plane by which Camilla sees the arrival of the particle is momentum dependent, which is the mentioned "dual-gravity lensing".

Chapter 2

Gamma-ray bursts

In this chapter we will introduce Gamma-Ray Bursts (GRBs), short and intense bursts of $\sim$ 100 keV-1 GeV photons. They are one of the brightest and most interesting phenomena in the Universe, which are going to play a crucial role throughout the rest of this thesis. After an historical introduction of their discovery, the theoretical model that have been proposed to explain these particular objects will be summarised. Being GRBs promising sources of Ultra-High Energy Cosmic Rays (UHECRs) and high-energy neutrinos, the predicted neutrino production from GRBs will be also briefly described. Finally, a brief description of the gamma-ray detectors, used to observe GRBs, is exposed.

2.1 Historical introduction

The Vela satellites, a US military satellite system looking for clandestine nuclear tests, deployed by the United States Department of Defense, discovered GRBs in 1967 [94]. Initially they observed several bursts of gamma-rays which did not look like nuclear events. Then convincing evidence that those bursts were not coming from Earth were provided by identical observations recorded by satellites on opposite sides of the Earth. The Vela data, initially classified, was finally made public only in 1973.

For almost 20 years the science community thought that due to their incredible fluence emitted over very short time periods (time-integrated energy $\approx 10^{51} - 10^{53}$ ergs) [118] , GRBs had a galactic origin. To explain the origin of the GBRs a lot of possible progenitors were proposed, but little progress was made, mainly because of their unpredictability and of their short duration, between 0.1 seconds and 1000 seconds.

The nature of GRBs began to be revealed only in 1991, when the CGRO (Compton Gamma Ray Observatory) satellite was launched with the BATSE (Burst And Transient Satellite Experiment) detector [69] on board. Thanks to this experiment the first map of GRBs [106] was released (see Fig. 2.1), revealing to the community the isotropic distribution of the 2704 GRBs observed over several years of operation. This discovery was a strong hint that GRBs were of extragalactic origin.

The extra-galactic origin was confirmed in 1997 with the first observation of X-ray afterglow by the Beppo-SAX satellite [61] a hard x-ray telescope which was

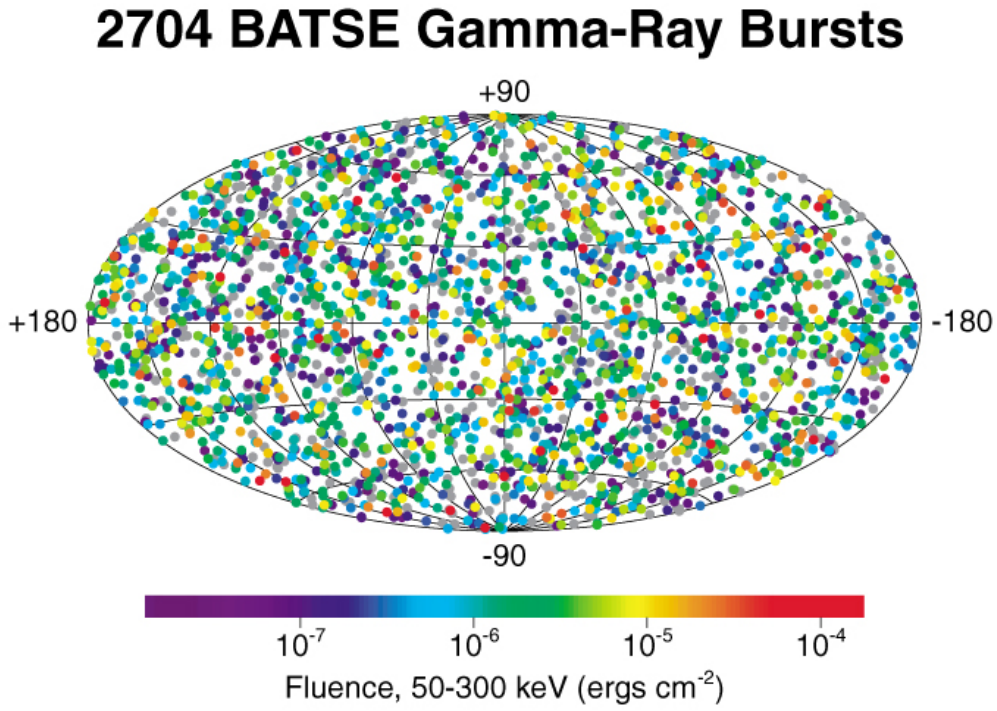

Figure 2.1. The above figure illustrates the locations of 2704 gamma-ray bursts detected by the BATSE instrument during nine years of observations. The projection is in galactic coordinates; the plane of the Milky Way Galaxy is along the horizontal line at the middle of the figure. The burst locations are color-coded based on fluence, which is the energy flux of the burst integrated over the total duration of the event. Bright bursts appear in red, and dim bursts appear in purple, grey indicates bursts for which the fluence cannot be calculated due to incomplete data. Figure taken from [113].

the first instrument able to localize quickly GRBs to arcminutes, which allowed follow up in the optical and radio band. This new technology led to the first redshift measurement for the GRB970508 [109], giving proof of a cosmological origin of GRBs. More recently the INTEGRAL (2002), Swift (2004) and Fermi (2008) missions have significantly increased our knowledge of GRBs. Despite all these new observations, the mystery of the GRB progenitors and of their inner engines remains mainly unresolved.

For instance, short-duration gamma-ray bursts are widely believed to be powered by the mergers of compact binaries, such as binary neutron stars or possibly neutron star-black hole binaries. The very recent observation of the gravitational wave GW170817 by the Advanced LIGO and Advanced Virgo detectors on August 17, 2017 in association with the gamma-ray burst GRB170817A, detected by Fermi-GBM, provides the first direct evidence of a link between neutron star mergers and short gamma-ray bursts [14].

2.2 The phenomenological model

Despite the enormous variety displayed by the gamma-ray bursts, there are some basic features that hold for every GRB. The GRB prompt emission can last from millisecond to several minutes and are followed by an afterglow - lower energy, long lasting emission in the X-ray, optical and radio. In almost all cases, if the afterglow position is detected narrowly, the identification of host galaxies enabled the determination of the corresponding redshifts that range from 0.009727 (GRB170817A [14]) to 9.4 (GRB090429B [62]).

The clearest classification of GRBs is based on their duration. GRBs can be divided to two distinct groups [96]: long burst with $T_{90} > 2$ sec [1] and short bursts with $T_{90} < 2$ sec. Initially this classification of GRBs in two groups comes from the bimodal distribution of burst duration and spectral hardness, as one can see from Fig. 2.2. Since the launch of the Swift satellite in 2004 [75], which, thanks to its quick localization capability, allows the identification of the X-ray and optical afterglow for short GRBs, it has been possible to show that short GRBs tipically have associated galaxies at relatively low redshifts with a median redshift of $z \sim 0.5$ [47]. Instead long GRBs are localized at higher redshifts ~ 2.

Another important distinction between these two population is the progenitor. Based on both photometric and spectroscopic observations, long GRBs were shown to be associated with Type Ic supernovae, moreover the environments and supernova associations indicated that long GRBs arise from the death of massive stars. On the other hand, mounting evidence are accruing in favor to the hypothesis that short GRBs come from the merger of neutron stars, either with another neutron star, or a black hole. An hypothesis which has been confirmed by the observation of GW170817, produced by a neutron-star merger, in association with the short GRB170817A. Also the host galaxies of short GRBs are diverse from their long-duration counterparts. They are more massive and less actively star-forming on average than long GRB hosts. The most accepted models for GRBs progenitors are

[1] T_{90} is defined as the time interval of gamma-ray photons collected (from 5 % to 95 % of the total GRB counts) by a given instrument.

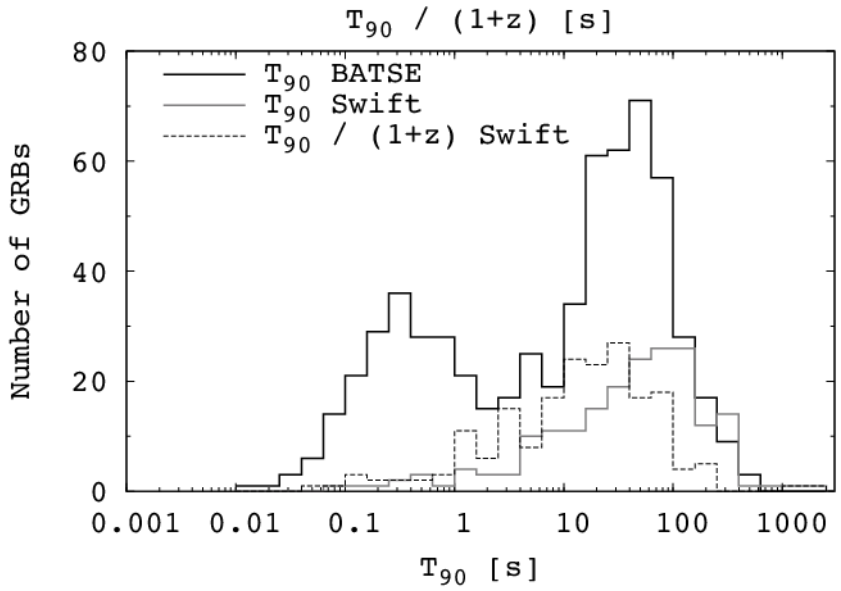

Figure 2.2. Duration T_{90} of the 4B BATSE Catalog of Gamma-Ray Bursts shows two classes of GRBs (solid black line): those with $T_{90} < 2$ s are called short GRBs, and those with $T_{90} > 2$ s are long GRBs. For comparison, results from more recent Swift satellite observations are shown: the grey line is the distribution of Swift bursts with known redshift over T_{90} (in the observers frame); the dashed line is the distribution of Swift bursts with known redshift over $T_{90}/(1 + z)$, i.e. approximate time of duration in the GRBs rest frame. Figure taken from [81].

now the collapsar model for long GRBs and the compact binary merger for short GRBs.

2.2.1 The fireball model

The fireball internal-external shocks model is the dominant picture that describes what happens in a GRB [117]. It is generally accepted that, whatever the progenitor or central engine, the evolution of the explosion after tremendous energy injection can be characterized independently of the details of the progenitor. According to the fireball model, after the progenitor has converted the gravitational energy (of order of a solar rest mass) into kinetic energy, GRBs are produced by the dissipation in internal collisions of the kinetic energy of an ultra-relativistic flow. When this flow is slowed down by shocks with the surrounding matter the afterglow is produced. The prediction of the afterglow itself, or the prediction of jet breaks in the afterglow light curve and of an optical flash that accompanies the GRBs themselves, are just some of the numerous successful predictions that this model has made.

The initial jets contain a plasma of leptons, photons and baryons and are optically thick. The optical depth τ can be expressed in terms of

$$\tau \approx \frac{f\sigma 4\pi d^2 F}{\bar{E}c^4 \delta t\, m}, \tag{2.1}$$

where f is a numerical factor denoting the average probability that one kind of particle of mass m and average energy $\bar{E}$ will collide with a cross section σ, F is the observed flux and $4\pi d^2 F/\bar{E}c^3\delta t$ yields the particle density in a volume $c\delta t$ (being δt the time-scale fluctuations). A naive calculation from Eq. 2.1 for pair e^+e^- production processes gives, for typical and reasonable set of parameters [2] and cosmological distances, an extremely large value of $\tau_{e^\pm} \sim 10^{15}$, i.e. the source is optically thick and the resulting radiation should be thermal. This is, of course, inconsistent with the non-thermal spectrum observed in GRBs. This problem is known as the compactness problem and can be resolved if the emitting matter is moving relativistically towards the observer. When considering the Lorentz factor Γ one has to make two major corrections to Eq. 2.1. First, the observed photons are blue shifted so that their energy at the source must be lowered by a factor Γ. The second correction one has to include regards the size of the source, which now is given by $c\delta t\Gamma^2$. Together these effects result in an overall factor of $\Gamma^{-4-2\alpha}$, where α is the photons index of the observed γ-rays (namely the number of observed photons per unit energy is proportional to $E^{-\alpha}$.). For a typical value $\alpha \sim 2$ one finds that in order to obtain an optically thin source $\Gamma \gtrsim 100$ [87]. Such extreme-relativistic motion is larger than the relativistic motion observed in any other celestial source.

The basic picture proceeds as follows: since this flow of plasma is initially optically thick, it undergoes adiabatic expansion and cools, becoming optically thin at distances $> 10^{11}$ m ~ 1 a.u. from the central engine (which has a size of about 10-100 km) and only at this point can γ-rays escape. Only a fraction of the energy of the outflow is carried by the emitted γ-rays. The rest is produced at larger distances

[2] One has to use the Thomson cross-section $\sigma_T \sim 6.25 \cdot 10^{-25}\, cm^2$, $m_e c^2 = 0.511$ MeV and the typical observed photon energy $\bar{E}_\gamma \sim 1$ MeV

of $10^{14} - 10^{16}$ m ~ 0.001 lyr - 1 lyr, when the outflow collides with the surrounding medium resulting in the so-called afterglow which we observe in lower frequencies.

Another crucial ingredient in the fireball model for GRBs is the radial inhomogeneity of the shell which was produced by the source. Evidence of the radial inhomogeneities in the shell is given by the observed temporal variability. One has to imagine the expanding plasma structured as several shells with slightly different Lorentz factors, generating multiple shock fronts when a faster shell catches up with a slower one. The assumption that the short structures arising in GRB spectra is caused by internal shocks has been confirmed by numerical simulations [121]. When the fireball collides with the surrounding medium, a reverse shock appears, going backwards through the expanding fireball. Depending on the model, the reverse shock could contribute to all wavelengths from X-ray to radio, resulting also in a bright and rapidly fading optical emission called optical flash [82].

In order to conclude this brief description of the fireball model one has to explain why beamed jets are necessary to explain GRBs. The inferred isotropic energy for a GRB can be of $\sim 10^{54}$ ergs, which is more than $M_{\odot}c^2$ transformed to γ-ray emission, and therefore is difficult to explain from core collapses or from compact object mergers, giving rise to a serious problem for any stellar mass model of GRBs. The solution to this problem is given by the not isotropic, but instead collimated emission. If the emission is collimated in two opposite jets with an angle $\theta \ll 1$, this would lower the required energy budget by a factor of θ^2. If a burst is expanding with a Lorentz factor of Γ, then, due to aberration of light, the emission is strongly beamed within an angle $\sim 1/\Gamma$. As long as $\theta > 1/\Gamma$ the light cone of outflow will not include the observer, which can not distinguish between spherical or collimated outflow. However once the flow slows down, moving through the interstellar material, the beam angle increases and the observer begins to see the edge of the jet cone and receives less light than in the case of a spherical outflow. Evidence for this expected steepening, referred to as an achromatic break or a jet break, is seen in the light curve simultaneously at all wavelengths emitted by the outflow. From the time of the break, typical values of the beam opening angle are 2° - 4° and rarely exceed 10°. These values relax the energy requirement to the more reasonable value of 10^{51} ergs, similar to the total output in a standard supernova. Finally, using this data for the beaming angles and an average rate of one observed GRB per day, it has been possible to estimate, , since we can observe only those GRBs that accidentally point in our direction, that there are about $\sim$ 100 - 1000 GRBs/day occurring in the observable Universe.

2.3 Neutrino production

As mentioned above, different kind of particles, such as neutrinos, gravitational waves and cosmic rays, with various energies are expected to be produced in GRBs. For instance, nucleons in the fireball will have $\gtrsim 100$ GeV kinetic energies in the observer frame, which can lead to inelastic collisions resulting in pions, muons, neutrinos and electrons as well as their anti-particles. The internal-shocks model of the fireball described in Sec. 2.2.1 is capable of accelerating by Fermi's mechanism protons and other heavier nuclei present in the outflow up to energies of 10^{20} eV, the energies

required in the observed ultra-high energy cosmic rays spectrum [129]. Magnetic field irregularities keep scattering the particles back so that they keep crossing the same shock. The competition between the average energy gain per shock crossing cycle and the escape probability per cycle leads to a power-law spectrum

$$N(E)dE \propto E^{-p}dE. \tag{2.2}$$

For shocks in an ideal monotonic gas, the value of p can be shown to be 2, as typically expected for Fermi acceleration and which would produce the observed spectrum of ultrahigh energy cosmic rays [129].

Assuming protons are accelerated along with the electrons in the fireball to an E^{-2} spectrum, the neutrino production in GRBs mainly occurs through pγ interactions. Protons will interact with the γ-rays to produce pions via the Δ^+ resonance:

$$p + \gamma \rightarrow \Delta^+ \rightarrow \begin{cases} p + \pi^0 \\ n + \pi^+ \end{cases} \tag{2.3}$$

In the observer frame the energy threshold for this process is given by

$$E_p \cdot E_\gamma \geq \left(\frac{\Gamma}{1+z}\right)^2 \frac{m_\Delta^2 - m_p^2}{4}, \tag{2.4}$$

where as usual Γ denotes the bulk Lorentz factor of the expanding fireball and z is the redshift of the GRB.

The pions produced will ultimately decay in γ-rays and neutrinos:

$$\pi^+ \rightarrow \mu^+ + \nu_\mu \rightarrow e^+ + \nu_e + \bar{\nu}_\mu + \nu_\mu \tag{2.5}$$

$$\pi^0 \rightarrow \gamma + \gamma \tag{2.6}$$

This process produces a neutrino flavor ratio at the source of $(\nu_e : \nu_\mu : \nu_\tau) = (1 : 2 : 0)$, which, due to oscillations between flavors over cosmological distances, will result in an expected flavor ration of $(1 : 1 : 1)$ at the Earth.

2.3.1 Neutrino flux and spectrum

Though there is a general agreement on the global mechanism described above in order to produce neutrinos from GRBs, many different methods to calculate the neutrino flux from GRBs have been proposed. One of the most preferable scenario, proposed by Waxman and Bahcall [130], calculated the resulting neutrino flux observed at the Earth, assuming that GRBs are the sources of ultrahigh energy cosmic rays. There are manly two reasons for which this assumption might be true: the GRBs (as well as the Active Galactic Nuclei) are among the most energetic events in the Universe, making these objects the perfect candidates for the highest energy cosmic rays, and secondly, the spectrum of ultrahigh energy cosmic rays (above 10^{19} eV) is consistent [129] with that expected from Fermi acceleration of protons in GRBs.

Their derivation of the expected neutrino spectrum takes the form of a broken power-law

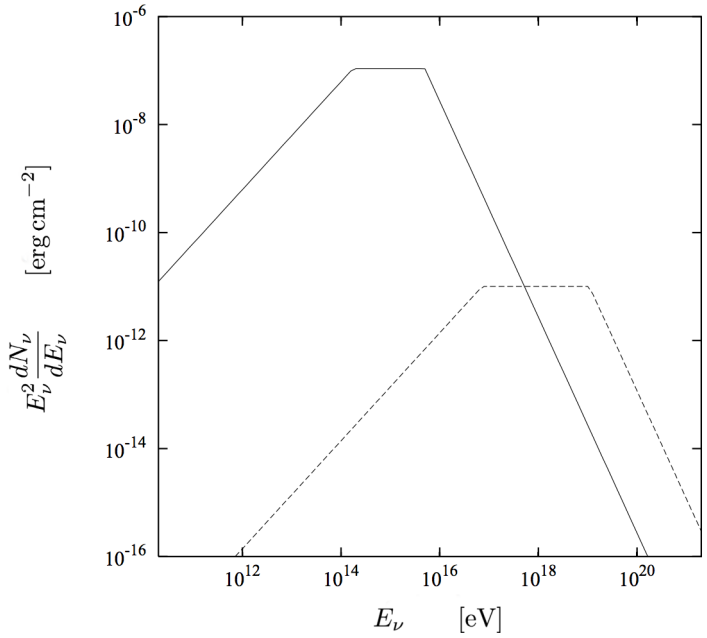

Figure 2.3. The muon neutrino spectrum, $E_\nu^2 \frac{dN_\nu}{dE_\nu}$, for fiducial parameters in the models described in [85]. The solid line is for a typical GRB with $\Gamma = 300$ and time variability of 10 ms, while the dashed line is for a X-ray flash candidate with $\Gamma = 1440$ and time variability of 50 ms.. Figure taken from [85].

$$E_\nu^2 \frac{dN_\nu}{dE_\nu} = \Phi_0 \cdot \begin{cases} (E_\nu/\epsilon_\nu^b)^\beta, & E_\nu \leq \epsilon_\nu^b \\ (E_\nu/\epsilon_\nu^b)^\alpha, & \epsilon_\nu^b < E_\nu \leq \epsilon_\nu^s \\ (E_\nu/\epsilon_\nu^b)^\alpha (E_\nu/\epsilon_\nu^s)^{-2}, & \epsilon_\nu^s < E_\nu \end{cases} \tag{2.7}$$

where ϵ_ν^b and ϵ_ν^s are respectively the break energy (of order 1 PeV in the observer frame), resulting when fitting the gamma-ray spectra in the BATSE data, and the energy threshold at which radiative losses become important. The specific form of the neutrino flux described in Eq. 2.7 depends on a number of somewhat tenuous assumptions, which requires a better understanding of the fireball phenomenology than we have now. For instance, making a series of fiducial assumptions for the model parameters [85], one can derive the expected neutrino spectrum shown in Fig. 2.3.

This model predicts that neutrinos will be emitted at the same time as the gamma-rays, and is therefore often called the prompt model . The prediction of a neutrino emission from GRBs is generic within the most widely accepted models: for instance, one should also expect from different models low-energy precursor neutrinos [108], high-energy neutrinos in the afterglow [132], and so on. But all of these models predict fluxes which result in much lower observable signal than the prompt model. The observation of high-energy neutrinos from GRBs would be crucial in order to update our current knowledge of the fireball model for GRB. Due to the small interaction cross-section of neutrinos, the detection of high-energy neutrinos is only possible in a detector sufficiently large in volume, such as the

IceCube Neutrinos Observatory in Antarctica, whose operation and observational properties will be described in the following chapter.

2.4 Gamma-ray detectors

We conclude this chapter about gamma-ray bursts giving a brief description of the gamma-ray detectors that oberved those GRBs used in this thesis work. All the temporal, spatial, and spectral information for all observed GRB used in this dissertation are provided by the GRBweb database [83], a tabulated and publicly available website. One can also find in App. B all their relevant properties. As it will be clear in Chaps. 4 and 5, the temporal information of a GRB is used to correlate neutrino candidate events with the prompt gamma-ray emission of a GRB, while the localization information of GRBs is used to correlate neutrino candidate events spatially with a GRB. The remainder of this section briefly describes the properties of the major gamma-ray detectors.

Swift Swift is a satellite launched into orbit around Earth in 2004 and designed primarily to study GRBs [75]. It consists of three instruments: a wide-field Burst Alert Telescope(BAT), the X-ray Telescope(XRT), and the Ultraviolet/Optical Telescope (UVOT). Swift continuously scans the sky with the BAT with a 1.4 sr field of view to detect GRBs over the 15-150 keV hard x-ray and gamma-ray energy range. The Swift-XRT and UVOT detectors can then observe GRB afterglows, resulting in GRB localizations of arcsec (XRT) to sub-arcsec (UVOT) precision as well as redshift determination.

Fermi The Fermi Gamma-Ray Space Telescope is a wide field of view high-energy γ-ray telescope, that was launched into orbit around Earth in 2008. It consists of of two instruments: the Gamma-ray Burst Monitor (GBM) [107] and Large Area Telescope (LAT) [44] detectors. The LAT is a pair converter detector with an energy sensitivity range of 20 MeV to 300 GeV, while the GBM, with its 12 activated sodium iodide (NaI) and 2 bismuth germanate (BGO) scintillation detectors have an energy response of 8 keV - 40 MeV. The angular resolution is of the order of 1° - 15°. Taken together, Fermi-GBM observes the entire sky not occulted by the Earth ($\geq$ 8 sr). Together the Swift and Fermi detectors contribute the majority of the observed GRB used in this analysis. The following two experiments are useful when adding information to GRBs in the final sample.

INTEGRAL The International Gamma-Ray Astrophysics Laboratory (INTEGRAL) experiment was launched into a highly eccentric orbit, with an apogee of 0.5 lightseconds, around Earth in 2002 [134]. It contains three different coded aperture mask gamma-ray instruments. The Imager on board INTEGRAL (IBIS) is capable of $12'$ angular precision and is capable to observe the gamma-ray sky with an energy sensitivity of 15 keV to 10 MeV.

AGILE The AGILE satellite, launched in 2007 into low-Earth orbit, consists of a Gamma-Ray Imaging Detector (GRID), a CsI minicalorimeter, a plastic scintillator

anticoincidence shield, and the SuperAGILE x-ray monitor [126]. The detector can image an area of 0.8 sr in the range 10-40 keV, allowing simultaneous measurement of GRBs in both gamma-rays and hard x-rays.

Chapter 3

High-energy IceCube neutrinos

In this chapter we present a flavor and energy inference analysis for each down-going high-energy astrophysical neutrino event observed by the IceCube observatory during six years of data taking. Our goal is to obtain, for the first time, an estimate of the posterior probability distribution for the most relevant properties, such as the neutrino energy and flavor, of the neutrino-nucleon interactions producing shower and track events in the IceCube detector. For each event the main observables in the IceCube detector are the deposited energy and the event topology (showers or tracks) produced by the Cherenkov light by the transit through a medium of charged particles created in neutrino interactions. In order to suggest that some properties of these IceCube neutrinos might be manifestations of in-vacuo dispersion, we shall show in this chapter, using Bayesian inference and Markov chain Monte Carlo methods, how to reconstruct from these observables the properties of the neutrino which generated such event.

The structure of this chapter is as follows. We start in Sec. 3.1 by introducing the IceCube neutrino observatory and then in Sec. 3.2 we describe our assumptions on energy and flavor flux for the astrophysical neutrinos. Sec. 3.3 provides a description of the deep-inelastic scattering, the energy-dependent cross section of neutrino-nucleon interactions and the neutrino energy loss. Branching fractions of tau-decay channel, along with the energy distribution of the decay products, are presented in Sec. 3.4. A summary of all parameters used in this analysis and a brief description of the Bayesian method can be found in Sec. 3.6. Finally in Sec. 3.7 we highlight our results and discuss their implications.

3.1 The IceCube neutrino observatory

The largest neutrino telescope to date is the IceCube Neutrino Observatory at the geographic South Pole, whose first sensors were deployed at the South Pole during the austral summer of 2004-2005 and have been producing data since February 2005 [16]. IceCube instruments one cubic kilometer of ice with 86 cables, called ”strings”, each of which contains 60 Digital Optical Modules (DOMs), deployed between 1450 m and 2450 m deep in the ice. Most of the strings are horizontally separated by 120 m (see Fig. 3.1). The DOM is a glass pressure vessel containing a 10-inch photomultiplier tube (PMTs), digitizing electronics, and LED flashers for calibration.

After six years of data taking [13], from early 2010 to early 2016 for a total of 2078 days, 74 cointened "high-energy starting event" (HESE) with deposited energies above 30 TeV have provided the evidence for the existence of an extraterrestrial neutrino flux. Only three events with deposited energy above 1 PeV have been observed, with the 2 PeV event being the most energetic one. The discovery of this flux has motivated a vigorous program of studies to unravel their origin [12] and their properties [116, 9, 5].

IceCube detects neutrinos by observing Cherenkov light produced by charged particles created in neutrino interactions as they transit the ice within the detector. DOMs record light from particle interactions in the ice. The time and amplitude of signals recorded by the PMTs are used to reconstruct the direction and energy of the particles. At this range of energies, the way neutrinos interact is deep-inelastic scattering with nuclei in the detector material. There are two possible interactions: charged-current (CC) or neutral-current (NC) interactions. In both a cascades of hadrons is created at the neutrino interaction vertex and for CC interaction this shower is accompanied by an outgoing charged lepton which may itself trigger another overlaid cascades. IceCube events have two basic topologies: tracks and showers. Considering the energy involved for this analysis we assume tracks are made only by ν_μ CC interactions and by ν_τ CC interactions in which the tau lepton decays in $\nu_\tau\mu\nu_\mu$. Showers instead are those events without visible muon tracks and are formed by particle showers near the neutrino vertex. While the particle content of showers created by final-state hadrons, electrons, and taus is different, the IceCube detector is currently insensitive to the difference. This means that a shower is produced in ν_e CC interaction, ν_τ CC interactions (where the produced τ does not decay in the muonic channel), and in all-flavor NC interactions.

In previou works IceCube data have been analyzed and discussed in detail (see Ref. [12, 54, 116] and references therein) using a maximum-likelihood approach over the whole collection of events. Although useful informations about the energy behavior and the flavor composition has already been explored, it has never been performed an inference analysis of the properties of each single astrophysical neutrino. This work differs from previous analyses also for the statistical approach used: having to deal, one by one, with just one single event the frequentist approach is unsuitable and may be misleading. For this reason we prefer the Bayesian approach which we discuss in Sec. 3.6.

3.2 Assumptions on neutrino fluxes

Working with neutrinos implies the knowledge of its energy and flavor, which are not direct observables. We can only infer this quantities by the deposited energy in the detector and by the event topology. This is possible only if we assume *a priori* the expected fluxes of astrophysical incoming-neutrino energy and flavor.

A limited class of the contained HESE events observed by IceCube is considered in this analysis in order to use few assumptions as possible: to neglect neutrino absorption in the Earth we select those events arriving at the detector from above, the so-called down-going neutrinos, i.e., with the cosine of the zenith angle greater than zero. The single zenith angle coordinate is sufficient to calculate the neutrino

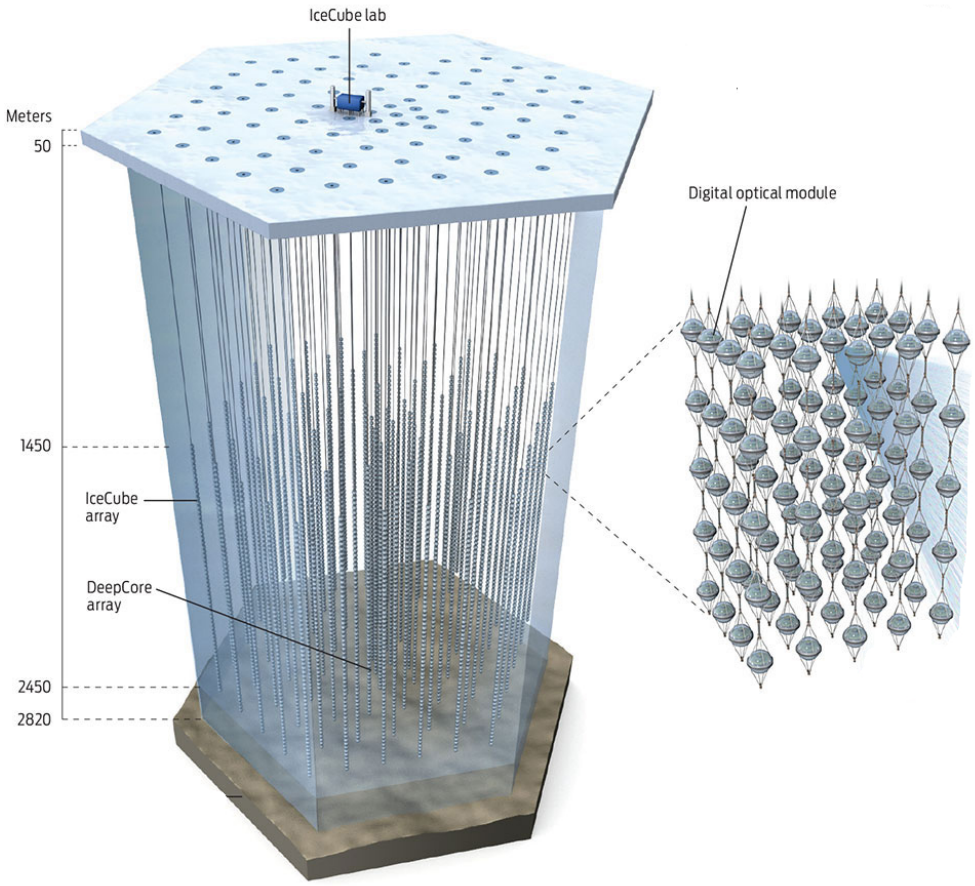

Figure 3.1. Layout of the IceCube detector. Here the 80 strings of the detector are shown, as well as the digital optical modules.

attenuation inside the Earth: above the horizon, attenuation is negligible at all energies [11, 50]. A key assumption throughout this analysis is the astrophysical origin of neutrino events. This means that all inferred properties are only valid if we neglect contribution from sources of background for astrophysical neutrinos in IceCube, the so-called atmospheric muon and neutrino fluxes. According to the cut considered by the IceCube collaboration we consider only neutrino events with deposited energy in the range 60 TeV - 3 PeV, which is a cut often used when performing statistical analyses of the astrophysical flux. The minimum deposited energy of 60 TeV is intended to remove the majority of the backgrounds from muons and atmospheric neutrinos [1], while the limit of 3 PeV deposited energy would discard the Glashow resonance at $E_\nu \simeq 6.3$ PeV [79], which should give rise to yet-unobserved events in the few PeV region.

These assumptions restrict our inference analysis from 74 HESE neutrinos to only 35: 28 showers and 7 tracks.

We assume an equal spectrum and flux for neutrinos and anti-neutrinos at the Earth. When fitting the current available data, the assumption that neutrino and anti-neutrino flavor fractions are the same at the Earth seems reasonable [111] [2].

The flavor ratio at the Earth $(f_e : f_\mu : f_\tau)_\oplus$ is one of the most studied properties of astrophysical neutrinos. This is due mainly to the fact that the flavor ratio of astrophysical neutrinos is both a probe of the source of high energy cosmic rays and a test of fundamental particle physics. A deviation from the expected flavor ratio at the Earth would be a signal of new physics in the neutrino sector. Consistently with the $(1 : 1 : 1)_\oplus$ flavor ratio at Earth commonly expected [104] and with the results reported by the IceCube collaboration in Ref. [7], a uniformly-distributed prior probability for the neutrino flavor will be used in this analysis. Thus

$$f(\ell) = \begin{cases} 1/3, & \ell = e \\ 1/3, & \ell = \mu \\ 1/3, & \ell = \tau, \end{cases} \tag{3.1}$$

where ℓ is the leptonic flavor and $f(\ell)$ its probability distribution.

As discussed in detail in the previous chapter, astrophysical neutrinos from cosmic accelerators are generically expected to have a hard energy spectrum. Waxman and Bahcall [131] predicted a cosmic neutrino flux proportional to E_ν^{-2}, as originally predicted by Fermi. But the spectral index may depends on the source properties and the acceleration mechanism, as pointed out in some recent works (see Ref. [46] for instance). It is also possible that the neutrino fluxes may be described by more than one component [54, 55]. In this analysis we assume a single astrophysical component parametrized in terms of an unbroken power-law per neutrino flavor described by two parameters, the normalization $\Phi_{\rm astro}$ at 100 TeV neutrino energy

[1] At $> 5\ \sigma$ significance, the event sample above 60 TeV is dominated by extragalactic sources [65].

[2] All parameters and their properties, if not otherwise specified, are obtained for the sum of neutrino plus anti-neutrino contributions. For the sake of brevity, here and in the rest of this article, we imply also anti-neutrinos when we speak of neutrinos and we will refer to both neutrinos and anti-neutrinos as ν.

and the spectral index γ:

$$\Phi(E_\nu)_{\nu+\bar{\nu}} = \Phi_{\text{astro}} \cdot \left(\frac{E_\nu}{100\ \text{TeV}}\right)^{-\gamma}. \tag{3.2}$$

Since in this analysis we are mainly interested in inferring the energy E_ν for each single astrophysical neutrino, the only parameter that matters for us is the spectral index γ, for which a value of 2 is assumed [3].

From all these considerations we use

$$\frac{E_\nu^{-2}}{(60\,\text{TeV})^{-1} - (3\,\text{PeV})^{-1}} \tag{3.3}$$

with $E_\nu \in$ [60 TeV, 3 PeV], as our prior probability distribution for the neutrino energy E_ν.

3.3 Neutrino-Nucleon deep-inelastic scattering

Our current knowledge of the proton's parton distributions allows us to calculate the neutrino-nucleon cross sections with confidence up to neutrino energies of about 10 PeV [72]. At neutrino energies E_ν above some 10 GeV, as relevant for this analysis, neutrino-nucleon reactions are dominated by deep-inelastic scattering. The processes that go into our evaluation are the CC channel, where the ν scatters off a quark in the nucleon N via exchange of a virtual W-boson,

$$\nu_\ell N \to X + \ell$$

and the NC channel, via exchange of a virtual Z-boson,

$$\nu_\ell N \to X + \nu_\ell,$$

where $\ell = \{e, \mu, \tau\}$, and X represents hadrons. In Fig. 3.2 both interactions are schematically represented. The neutrino-nucleon CC and NC cross-sections have

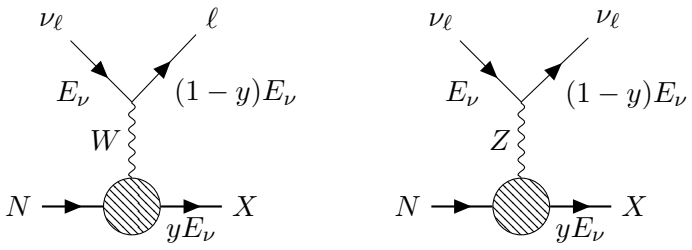

Figure 3.2. Diagrams for charged (left) and neutral (right) current neutrino-nucleon interaction. Time runs from left to right and the flavor index ℓ represents e, μ, or τ.

been measured by several experiments. A complete review can be found in Ref. [73, 60], from which we report in Table 3.1 and 3.2 the values of cross-sections respectively for CC and NC interaction for given energy values in the range 60 TeV-3 PeV. For the purpose of this analysis, we need to know the probability that

Table 3.1. Charged-current cross sections for neutrino, anti-neutrino and their sum for neutrino-nucleon interactions.

E_ν [TeV]	σ^{ν}_{CC} $[10^{-33}\,cm^2]$	$\sigma^{\bar{\nu}}_{CC}$ $[10^{-33}\,cm^2]$	σ_{CC} $[10^{-33}\,cm^2]$
60	0.1514	0.1199	0.2713
100	0.2022	0.1683	0.3705
250	0.3255	0.2909	0.6164
600	0.4985	0.4667	0.9652
10^3	0.6342	0.6051	1.2393
$2.5 \cdot 10^3$	0.9601	0.9365	1.8966

Table 3.2. Neutral-current cross sections for neutrino, anti-neutrino and their sum for neutrino-nucleon interactions.

E_ν [TeV]	σ^{ν}_{NC} $[10^{-33}\,cm^2]$	$\sigma^{\bar{\nu}}_{NC}$ $[10^{-33}\,cm^2]$	σ_{NC} $[10^{-33}\,cm^2]$
60	0.05615	0.04570	0.10185
100	0.07667	0.06515	0.14182
250	0.1280	0.1158	0.2438
600	0.2017	0.1901	0.3918
10^3	0.2600	0.2493	0.5093
$2.5 \cdot 10^3$	0.4018	0.3929	0.7947

a neutrino interacts with a nucleon via CC or NC channel. In order to estimate this probability we use the values given in Table 3.1 and 3.2 from which we get the fraction of NC events

$$\frac{\sigma_{NC}}{\sigma_{CC} + \sigma_{NC}}. \tag{3.4}$$

These values are then fitted, as shown in Fig. 3.3, in order to obtain the following parametrization in terms of $\epsilon = \mathrm{Log}_{10}(E_\nu/\mathrm{TeV})$

$$A_1 + A_2 \cdot \log(\epsilon - A_3), \tag{3.5}$$

with $A_1 = 0.2595$, $A_2 = 0.0313$ and $A_3 = 0.2484$. From Fig. 3.3 one can see that the probability that a neutrino interacts with a nucleon via NC is $\sim 30\%$ and in the range of energies we are interested in depends slightly on the neutrino energy E_ν. Eq. 3.5 will be then used as the prior probability for NC interactions.

An important parameter that plays a crucial role in this analysis is the inelasticity parameter y: as schematically shown in Fig. 3.2, in both CC and NC interactions a

[3] When fitting all the 6-years HESE data, with an isotropic, unbroken power law flux, a spectral index of $2.92^{+0.33}_{-0.29}$ is obtained [13]. Since we assume in our analysis an astrophysical origin for all neutrinos, selecting only down-going events above 60 TeV, a value of 2 for the spectral index seems to us more consistent with our analysis.

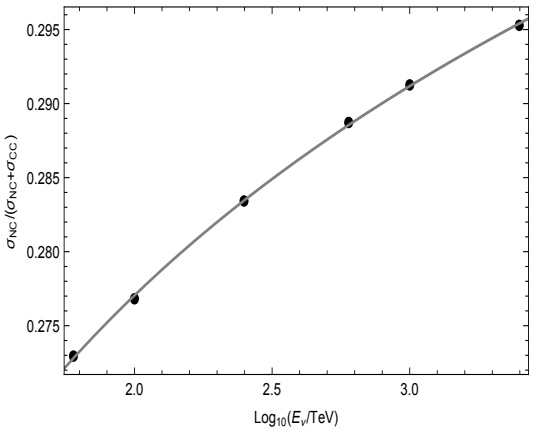

Figure 3.3. Fraction of NC events. Points are taken from Table 3.1 and 3.2 using Eq. 3.4, while the curve is obtained from Eq. 3.5.

fraction $(1-y)$ of the neutrino energy E_ν goes to the final-state lepton; the remaining fraction y goes to the final-state hadrons.

The differential cross section for CC interactions in terms of y and of the Bjorken scaling variables x (the fraction of the nucleon momentum carried by the struck quark) is given by (in natural units $\hbar = c = 1$)

$$\frac{d\sigma_{CC}}{dydx} = \frac{2G_F^2 M_N E_\nu}{\pi}\left(\frac{M_W^2}{Q^2+M_W^2}\right)^2\left(q+(1-y)^2\bar{q}\right). \tag{3.6}$$

Likewise, the NC differential cross section is given by

$$\frac{d\sigma_{NC}}{dydx} = \frac{2G_F^2 M_N E_\nu}{\pi}\left(\frac{M_Z^2}{Q^2+M_Z^2}\right)^2\left(q^0+(1-y)^2\bar{q}^0\right). \tag{3.7}$$

In these equations q, $\bar{q}$, q^0 and $\bar{q}^0$ are quark and antiquark distribution functions [59, 73], M_N, M_W and M_Z are respectively the nucleon, W and Z mass, G_F is the Fermi coupling constant and $Q^2 \approx 2xyE_\nu M_N$ is the negative four-momentum transfer squared.

In order to simulate in our code the y-distribution given by Eq. 3.6 and 3.7, we used the algorithm described in Ref. [59].

3.4 τ-decay channels

When a ν_τ and a nucleon interacts via CC interaction a τ of energy $E_\tau = (1-y)E_\nu$ is produced. The τ is the heaviest of the leptons with a mass m_τ of 1.78 GeV and therefore it has a very short lifetime of about $3 \cdot 10^{-13}\,s$. It can decay in the lepton channel or in the hadronic channel, as shown schematically in Fig. 3.5. The leptonic decays have a total branching fraction of $\sim 35\%$ and the hadronic decays have a total branching fraction of $\sim 65\%$, which is consistent with the expected branching fraction when the color charges of the quarks are included. The branching fraction

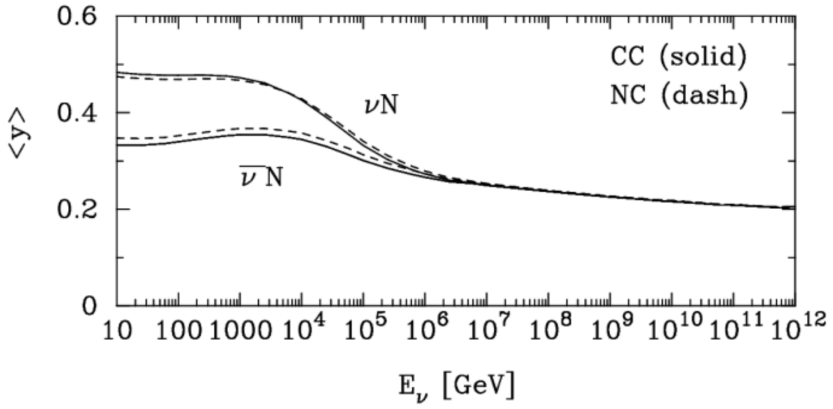

Figure 3.4. Average y as a function of neutrino energy E_ν, for CC (solid lines) and NC (dashed) reactions. Figure taken from Ref. [72].

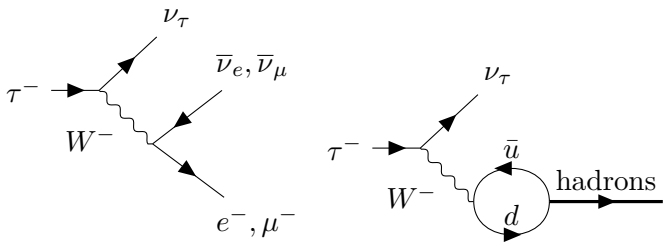

Figure 3.5. Diagrams for leptonic (left) and hadronic (right) decay of the τ lepton. Time runs from left to right.

into each decay channel is approximately [66]

$$\begin{aligned} &0.18 \quad \text{for } \tau \to \nu_\tau e \nu_e, \\ &0.18 \quad \text{for } \tau \to \nu_\tau \mu \nu_\mu, \\ &0.12 \quad \text{for } \tau \to \nu_\tau \pi, \\ &0.26 \quad \text{for } \tau \to \nu_\tau \rho, \\ &0.13 \quad \text{for } \tau \to \nu_\tau a_1, \\ &0.13 \quad \text{for } \tau \to \nu_\tau X \quad (X \neq \pi, \rho, a_1). \end{aligned} \tag{3.8}$$

Due to its very short lifetime the track produced inside the detector by the τ has generally a length of $50\,m \cdot (E_\tau/\text{PeV})$ [10]. At energies below PeV, the double cascade signature is difficult to distinguish from a single cascade, due to the sparse spacing of digital optical modules. Thus a track produced by a τ below a few PeV is unresolvable by IceCube. At higher energy ($\gtrsim 1$ PeV) a signature of ν_τ CC interactions would be two cascades joined by a short track, referred as a "double bang", which has not yet been observed. Considering the energies of our interest, in this analysis we assume that ν_τ CC interactions followed by $\tau \to \nu_\tau \mu \nu_\mu$ are undistinguishable from a track event produced in ν_μ CC interactions, while all the other τ-decay channels produce a shower event.

The ν_τ spectra for τ-leptonic decay has the following form in term of $z = E_{\nu_\tau}/E_\tau$

[99]

$$\frac{d\sigma}{dz} \propto \left(\frac{5}{3} - 3z^2 + \frac{4z^3}{3}\right) - P_\tau \left(\frac{1}{3} - 3z^2 + \frac{8z^3}{3}\right), \tag{3.9}$$

while the ν_ℓ ($\ell = \{e, \mu\}$) spectra in term of $z' = E_{\nu_\ell}/E_\tau$ reads

$$\frac{d\sigma}{dz'} \propto \left(2 - 6z'^2 + 4z'^3\right) - P_\tau \left(-2 + 12z' - 18z'^2 + 8z'^3\right), \tag{3.10}$$

where P_τ is the polarization of the τ.

In the case of hadronic decays $\tau \to \nu_\tau X$ the distribution depends on the kind of hadrons produced. An approximation of the distribution for each hadronic channel i, in terms of $z = E_{\nu_\tau}/E_\tau$ and $r_i = m_i^2/m_\tau^2$, can be found in Ref. [66]:

$$\frac{d\sigma}{dz} \propto \begin{cases} \frac{1}{1-r_\pi}\theta(1-r_\pi-z) + P_\tau \frac{2z-1+r_\pi}{(1-r_\pi)^2}\theta(1-r_\pi-z), & \tau \to \nu_\tau \pi, \\ \frac{1}{1-r_\rho}\theta(1-r_\rho-z) + P_\tau \left(\frac{2z-1+r_\rho}{1-r_\rho}\right)\left(\frac{1-2r_\rho}{1+2r_\rho}\right)\theta(1-r_\rho-z), & \tau \to \nu_\tau \rho, \\ \frac{1}{1-r_{a_1}}\theta(1-r_{a_1}-z) + P_\tau \left(\frac{2z-1+r_{a_1}}{1-r_{a_1}}\right)\left(\frac{1-2r_{a_1}}{1+2r_{a_1}}\right)\theta(1-r_{a_1}-z), & \tau \to \nu_\tau a1, \\ \frac{1}{0.3}\theta(0.3-z), & \tau \to \nu_\tau X \\ & (X \neq \pi, \rho, a1). \end{cases} \tag{3.11}$$

For energies of our interest we have $m_\tau/E_\tau \ll 1$, thus it is safe to assume [86, 49] the τ being almost fully polarized, i.e., $P_\tau = 1$.

The distributions in Eq. 3.9, 3.10 and 3.11 , along with their respective branching fraction in Eq. 3.8, will be then used as prior distributions in those CC interactions involving a ν_τ and its subsequent decay.

3.5 Deposited energy

All charged particles produced in the neutrino-nucleon interaction propagate through ice emitting Cherenkov radiation. This Cherenkov radiation is ultimately measured by the IceCube detectors producing a deposited energy $E_{dep.}$, which is proportional to the total energy E_ν of the neutrino. Each channel has different efficiencies when it comes to producing a measured energy deposition in the IceCube detector. First of all one has to distinguish electromagnetic cascades from hadronic cascades, which are both recognize in the detector as showers. For electromagnetic cascades one can safely assume the deposited energy being equal to the energy of the electron produced in the neutrino-nucleon interaction. On the other hand, the deposited energy in hadronic cascade is less reliable due to the presence of more neutral particles like neutrons, to large losses due to the binding energies in hadronic processes and to a higher Cherenkov threshold for hadrons [120].

Following Ref. [116], being E_X the energy of the cascade-initiating particle, we define the deposited energy in hadronic cascade as

$$E_h(E_X) = \left(1 - f \cdot \left(\frac{E_X}{E_0}\right)^{-m}\right) \cdot E_X, \tag{3.12}$$

where $f = 0.533$, $E_0 = 0.399\,GeV$ and $m = 0.130$, resulting from a fit to simulations of hadronic cascades [120].

For track events, being the lifetime of a muon much larger than the time it takes to cross the detector, a fraction of the initial muon energy E_μ is lost. As explicited stated by the authors of Ref. [116], although at these energies muon energy losses can be stochastic and large fluctuations around the mean are expected, it is reasonable to treat them as continuous and approximate the average deposited energy along a track E_t by

$$E_t(E_\mu) = F_\mu \cdot (E_\mu + a/b), \tag{3.13}$$

where [4] $a = 0.206\,GeV/m$, $b = 3.21 \cdot 10^{-4}\,m^{-1}$ and $F_\mu = 0.119$.

If the track is produced in a tau decay of energy E_τ, one has to take into account also that a significant fraction of tau leptons would escape the detector volume before decaying, so that F_μ has to be multiplied by a factor given by

$$\frac{1 + p_1 \cdot (E_\tau/10\,PeV)}{1 + q_1 \cdot (E_\tau/10\,PeV) + q_2 \cdot (E_\tau/10\,PeV)^2}, \tag{3.14}$$

where $p_1 = 0.984$, $q_1 = 1.01$ and $q_2 = 1.03$ [116].

Finally, for all the neutrino-nucleon interactions we have considered, the total deposited energy $E_{dep.}$ is given by

$$E_{dep.} = \begin{cases} E_h(E_X), & NC, \\ E_h(E_X) + E_\ell, & \nu_e\,CC, \\ E_h(E_X) + E_t(E_\ell), & \nu_\mu\,CC, \\ E_h(E_X) + E_\ell \cdot (1 - z - z'), & \nu_\tau\,CC \quad \tau \to \nu_\tau e \nu_e, \\ E_h(E_X) + E_t\left(E_\ell \cdot (1 - z - z')\right), & \nu_\tau\,CC \quad \tau \to \nu_\tau \mu \nu_\mu, \\ E_h(E_X) + E_h\left(E_\ell \cdot (1 - z)\right), & \nu_\tau\,CC \quad \tau \to \nu_\tau X, \end{cases} \tag{3.15}$$

where $E_X = yE_\nu$, $E_\ell = (1-y)E_\nu$ with $\ell = \{e, \mu, \tau\}$, while y has been discussed in Sec. 3.3. The parameters z and z' have been discussed in Sec. 3.4, which are respectively E_{ν_τ}/E_τ and $E_{\nu_{e,\mu}}/E_\tau$.

One has also to make distinction between the true deposited energy $E_{dep.}$ and the observed-deposited energy $E^{obs.}_{dep.}$. For this analysis we simply assume that $E^{obs.}_{dep.}$ follows a normal distribution with mean value given by $E_{dep.}$ and standard deviation $\sigma_{E_{dep.}}$:

$$\mathcal{N}(E^{obs.}_{dep.} \,|\, E_{dep.}, \sigma_{E_{dep.}}) = \frac{1}{\sigma_{E_{dep.}}\sqrt{2\pi}} e^{-\left(E^{obs.}_{dep.} - E_{dep.}\right)^2 \Big/ 2\sigma^2_{E_{dep.}}}. \tag{3.16}$$

For each neutrino event the value of $\sigma_{E_{dep.}}$ is taken from the uncertainty in the deposited energy provided by IceCube [13, 8].

3.6 Analysis

In Table 3.3 we summarize all parameters and the sequence of events that, given a neutrino with energy E_ν, cause an observed-deposited energy $E^{obs.}_{dep.}$ in the detector. In a certain sense, we need to go backwards through the whole chain of events in order to infer the neutrino energy E_ν from the observed-deposited energy $E^{obs.}_{dep.}$ and its topology [5]. In this section we briefly describe how this goal can be achieved using

[4] the parameters a and b vary slowly in the energy range of interest [116].

[5] For convenience in the rest of this paper we occasionally abbreviate "topology" with "top.".

Table 3.3. Table of all parameters used in this analysis along with their associated prior probability distribution. The right two columns show the sections and the references where these parameters are discussed in detail. The values of a and b in the z-parameter row can be obtained from Eq. 3.11 with $P_\tau = 1$.

Parameters		Prior probability distribution	Sec.	Ref.
		Flux parameters		
r	(anti-neutrino/neutrino ratio)	$\delta(r-1)$	3.2	[111]
ℓ	(neutrino flavor)	$1/3, \quad \ell = e$ $1/3, \quad \ell = \mu$ $1/3, \quad \ell = \tau$	3.2	[7]
γ	(spectral index)	$\delta(\gamma-2)$	3.2	[13, 131]
E_ν	(neutrino energy)	$E_\nu^{-2} / \left((60\,\mathrm{TeV})^{-1} - (3\,\mathrm{PeV})^{-1}\right)$	3.2	[13, 131]
		Deep-inelastic scattering parameters		
k	(neutrino-nucleon interaction)	$A_1 + A_2 \cdot \ln(\epsilon - A_3), \quad k = \mathrm{NC}$ $1 - A_1 - A_2 \cdot \ln(\epsilon - A_3), \quad k = \mathrm{CC}$	3.3	[72, 60]
y	(inelasticity parameter)	$d\sigma_k(E_\nu)/dy$ (see Eq. 3.6 and 3.7)	3.3	[72, 59]
		τ-decay parameters		
j	(τ-decay channel)	$0.18, \quad j = \tau \to \nu_\tau e \nu_e$ $0.18, \quad j = \tau \to \nu_\tau \mu \nu_\mu$ $0.12, \quad j = \tau \to \nu_\tau \pi$ $0.26, \quad j = \tau \to \nu_\tau \rho$ $0.13, \quad j = \tau \to \nu_\tau a_1$ $0.13, \quad j = \tau \to \nu_\tau X \quad (X \neq \pi, \rho, a_1)$	3.4	[66]
z	(energy fraction E_{ν_τ}/E_τ)	$4/3\left(1-z^3\right), \quad$ if $j = \tau \to \nu_\tau e \nu_e$ or $\nu_\tau \mu \nu_\mu$ $(a_\pi + b_\pi \cdot z)\,\theta(1 - r_\pi - z), \quad$ if $j = \tau \to \nu_\tau \pi$ $(a_\rho + b_\rho \cdot z)\,\theta(1 - r_\rho - z), \quad$ if $j = \tau \to \nu_\tau \rho$ $(a_{a_1} + b_{a_1} \cdot z)\,\theta(1 - r_{a_1} - z), \quad$ if $j = \tau \to \nu_\tau a_1$ $1/0.3\,\theta(0.3 - z), \quad$ if $j = \tau \to \nu_\tau X \quad (X \neq \pi, \rho, a_1)$	3.4	[66, 99, 86]
z'	(energy fraction E_ℓ/E_τ)	$4 - 12z' + 12z'^2 - 4z'^3, \quad$ if $j = \tau \to \nu_\tau e \nu_e$ or $\nu_\tau \mu \nu_\mu$	3.4	[66, 99]
		Deposited Energy		
$E_{dep.}^{obs.}$	(observed deposited energy)	$\mathcal{N}(E_{dep.}^{obs.} \,|\, E_{dep.}, \sigma_{E_{dep.}})$ with $E_{dep.}$ defined in Eq. 3.15	3.5	[116, 5]

Bayesian inference.

As usually done in literature, let D denote the observed data, in our case the deposited energy $E_{dep.}$ and the event topology (track or shower), and θ denote the model parameters, which are summarized in the first column of Table 3.3. Formal inference then requires setting up a joint probability distribution $f(D, \theta)$ (here and in the rest of this paper we will refer simply as f to all distributions). This joint distribution comprises two parts: a prior distribution $f(\theta)$ (see the second column of Table 3.3) and a likelihood $f(D|\theta)$. Defining $f(\theta)$ and $f(D|\theta)$ gives the full probability distribution

$$f(D, \theta) = f(D|\theta) \cdot f(\theta). \tag{3.17}$$

Having observed D, one can then obtain the distribution of θ conditional on D by applying the Bayes theorem

$$f(\theta|D) = \frac{f(D|\theta) \cdot f(\theta)}{\int f(D|\theta) \cdot f(\theta)\, d\theta}. \tag{3.18}$$

This is called the posterior distribution of θ and is the object of our Bayesian-inference analysis. From the posterior distribution of θ one can then obtain the expected value of a given parameter by integrating over the remaining parameters or study the dependence between parameters x and y by applying the product rule $f(x|y, D) = f(x, y|D)/f(y|D)$.

From Eq. 3.18, one recovers the maximum likelihood approach as a special case that holds under particular conditions, such as many data points and vague priors, which clearly are not satisfied in this analysis.

In theory, Bayesian methods are straightforward: the posterior distribution contains everything you need to carry out inference. In practice, the posterior distribution can be difficult to estimate precisely. A useful tool to derive the posterior distribution of Eq. 3.18 is the Markov Chain Monte Carlo (MCMC) technique. In a MCMC instead of having each point being generated one independently from another (like in a Monte Carlo), the sequence of generated points takes a kind of random walk in parameter space. Moreover, the probability of jumping from one point to an other depends only on the last point and not on the entire previous history (this is the peculiar property of a Markov chain). In particular, for this work we performed the MCMC using the Gibbs sampling algorithm [76], in order to explore the entire parameter space of the posterior distribution. This allows us to derive the unknown and potentially complex distribution $f(\theta|D)$ and estimate all neutrino properties we are interested in. The results of this inference analysis are presented and discussed in Sec. 3.7.

3.7 Results of the inference analysis for the high-energy neutrinos

In Table 3.4 we show for each of the 28 down-going shower events above 60 TeV, denoted by its ID number and observed-deposited energy $E_{dep.}^{obs.}$, the mean values (mean) and the standard deviations (s.d.) of the posterior distribution of neutrino energy E_ν. The mean and s.d. values are given assuming different flavors ℓ (e, μ or τ) and type of interaction k (CC or NC), where for the meaning of parameters ℓ and k we remind the reader to see Table 3.3. In the last columns, one can also find for each neutrino the probability $f(\ell|E_{dep.}^{obs.}, \text{top.})$ of being of electronic, muonic and tauonic flavor and the probability $f(k|E_{dep.}^{obs.}, \text{top.})$ of having scattered with nucleon via CC or NC interaction. We show the same results for the 7 down-going track events above 60 TeV in Table 3.5. But in this case the probabilities for neutrinos of being electronic or having scattered with nucleon via CC or NC interaction are absent: as we learned in the previous sections, tracks can only be produced in CC interactions by muonic or tauonic neutrinos.

For shower events the neutrino energy E_ν is, as expected, approximately equal to the observed-deposited energy $E_{dep.}^{obs.}$ only in ν_e CC interactions, where the uncertainty (given by the s.d.) for E_ν is also approximately equal to the uncertainty $\sigma_{E_{dep.}}$ in the observed-deposited energy. For ν_τ CC interactions and all-flavors NC interactions instead the situation is different: due mainly to neutrinos energy loss in neutrino-nucleon deep-inelastic scattering and to the τ-decay products escaping the detector, the neutrino energy results being higher than the observed-deposited energy with

a more dispersed distribution. This behaviour is manifest in Fig. 3.6, where the posterior distribution

$$f(E_\nu|\ell, k, E^{obs.}_{dep.}, \text{top.}) \tag{3.19}$$

is shown for two shower events. In the bottom part of these plots is also shown the neutrino-energetic distribution $f(E_\nu|E^{obs.}_{dep.}, \text{top.})$ making no assumption on ℓ and k, i.e., marginalizing over these parameters

$$f(E_\nu|E^{obs.}_{dep.}, \text{top.}) = \sum_{\ell,k} f(E_\nu|\ell, k, E^{obs.}_{dep.}, \text{top.}) \cdot f(\ell|E^{obs.}_{dep.}, \text{top.}) \cdot f(k|E^{obs.}_{dep.}, \text{top.}). \tag{3.20}$$

As one can see from Fig. 3.6, for showers, having to guess about the neutrino energy, the observed-deposited energy in the detector is the best choice, being this value approximately equal to the mode of the distribution $f(E_\nu|E^{obs.}_{dep.}, \text{top.})$. Instead the mean value feels the effect of the pronounced tail at higher energy produced by NC and ν_τ CC interactions. Thus the mean value of E_ν results being higher than the observed-deposited energy: in Fig. 3.8 we show, for different kinds of interaction, the neutrino-energy mean value as a function of the observed-deposited energy and the *relative standard deviation* (RSD), which is a measure of dispersion of a probability distribution (defined as the ratio of the standard deviation to the mean value), as a function of the observed-deposited energy.

We show the same plots for track events: in Fig. 3.7 one can find the posterior distributions for two track events, while in Fig. 3.9 we show the neutrino-energy mean value and RSD as a function of the observed-deposited energy. The main difference between the energetic distribution for showers $f(E_\nu|E^{obs.}_{dep.}, \text{shower})$ and tracks $f(E_\nu|E^{obs.}_{dep.}, \text{track})$ is that for the latter the distribution mode is higher than the observed-deposited energy with a tail more pronounced at higher energy. This is mainly due to the fact that tracks are produced by muons, whose energy loss in the detector is only a fraction of the muon energy.

An important feature that emerges from this analysis, in particular from the right plots of Fig. 3.8 and 3.9, is that, as we approach higher observed-deposited energy, the neutrino-energy distributions become less dispersed, a fact which is illustrated by the decreasing values taken by the RSD at higher energy. This behaviour can be understood taking into account the very steeply falling of the neutrino spectrum: at higher energy the right tail of the neutrino-energy distribution becomes less pronounced, because higher energies become less frequent, and this results in a less relative dispersion in the density distribution. The very steeply falling of neutrino spectrum (with a spectral index of 2) plays also a crucial role when estimating the posterior flavor probabilities $f(\ell|E^{obs.}_{dep.}, \text{shower})$. For instance, considering that a ν_μ produces a shower only in NC interactions, one should expect *a priori* that the probability for a shower event of being generated by a muonic neutrino is $\sim 10\%$, being $\sim 30\,\%$ the probability for a neutrino of scattering via NC interaction (see Fig. 3.3) and 1/3 the probability of being muonic. Instead our Bayesian inference gives us a value of $\sim 4\,\%$. As mentioned above, this value, which is smaller than the expected one, can be explained only considering the neutrino spectrum and the existence of other mechanisms with better efficiency in producing a deposited energy (such as the ν_e CC interaction): higher energies are less frequent, thus the more particles can escape the detector after a neutrino-nucleon interaction, the less chance there is of

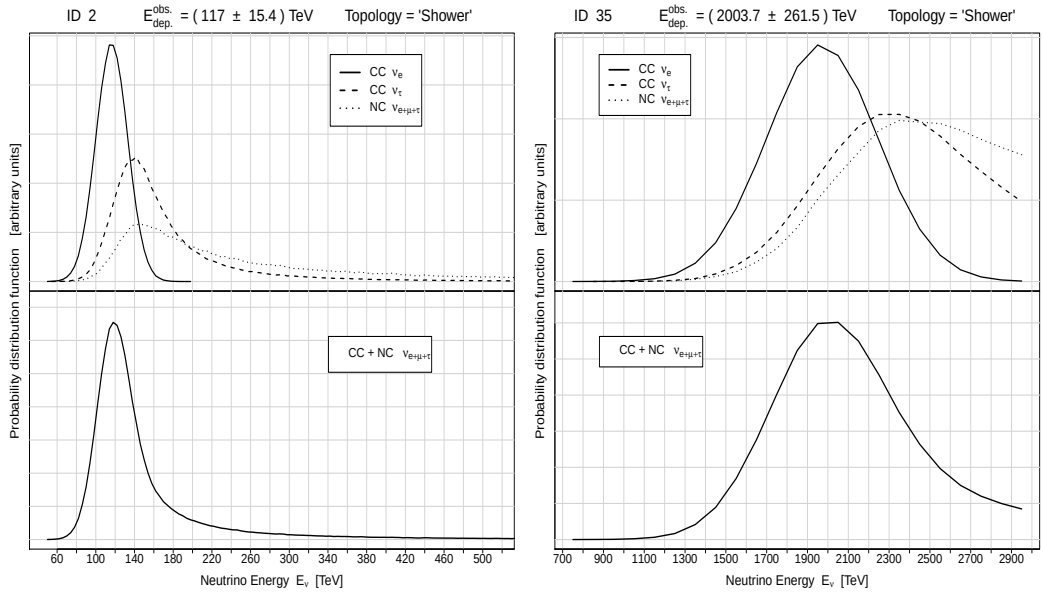

Figure 3.6. Posterior probability distributions $f(E_\nu|\ell, k, E^{obs.}_{dep.}, \text{shower})$ of the neutrino energy for two shower events. In the top panel the distributions assuming ν_e CC interaction (solid line), ν_τ CC interaction (dashed line) and NC interaction (dotted line) are shown. In the bottom panel the distribution $f(E_\nu|E^{obs.}_{dep.}, \text{shower})$, obtained marginalizing over ℓ and k, is shown.

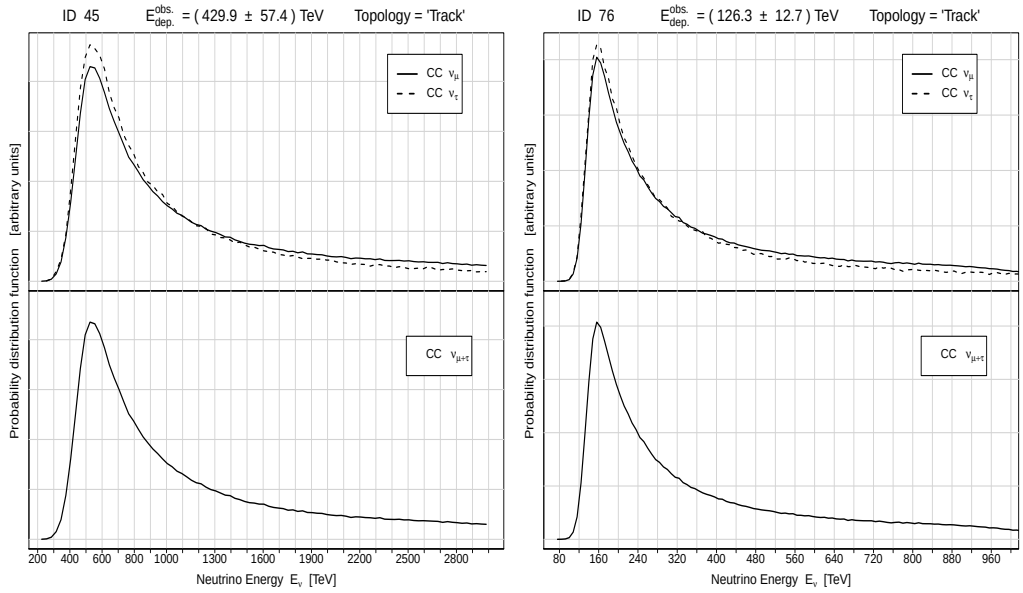

Figure 3.7. Posterior probability distributions $f(E_\nu|\ell, k, E^{obs.}_{dep.}, \text{track})$ of the neutrino energy for two track events. In the top panel the distributions assuming ν_μ CC interaction (solid line) and ν_τ CC interaction (dashed line) are shown. In the bottom panel the distribution $f(E_\nu|E^{obs.}_{dep.}, \text{track})$, obtained marginalizing over ℓ and k, is shown.

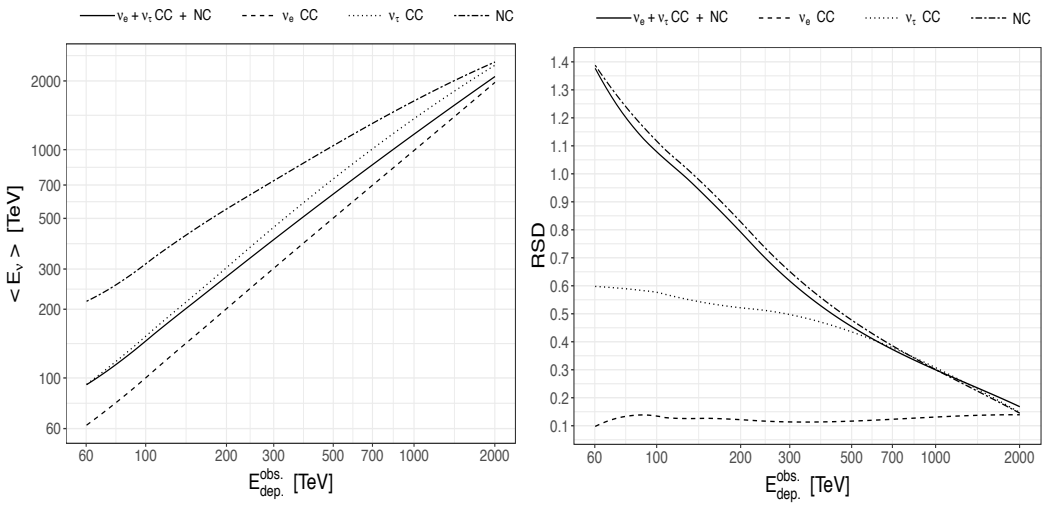

Figure 3.8. The mean value of the neutrino energy E_ν (left) and its RSD value (right) are shown as a function of the observed-deposited energy in shower events making no assumption (solid line), assuming ν_e CC interaction (dashed line), ν_τ CC interaction (dotted line) and NC interaction (dot-dashed line).

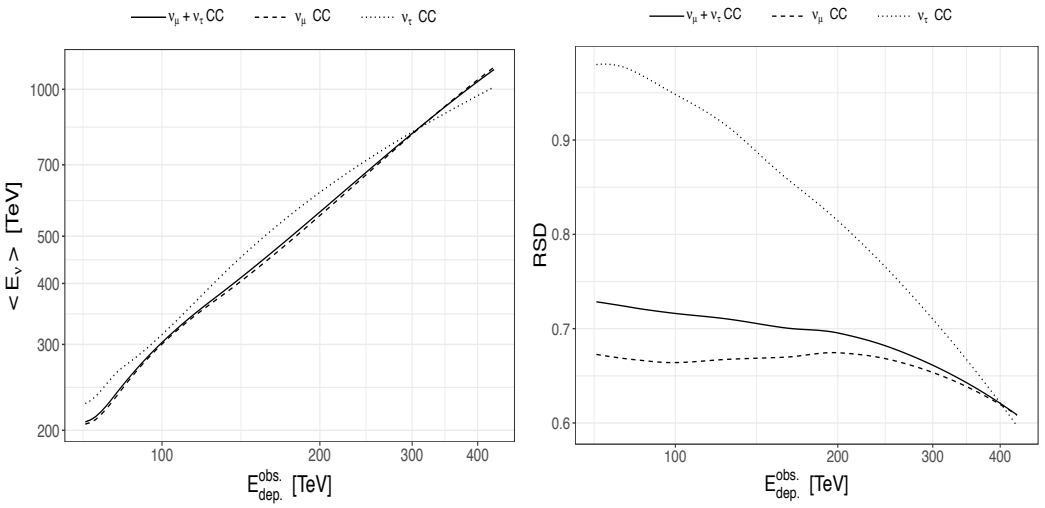

Figure 3.9. The mean value of the neutrino energy E_ν (left) and its RSD value (right) are shown as a function of the observed-deposited energy in track events making no assumption (solid line), assuming ν_μ CC interaction (dashed line) and ν_τ CC interaction (dotted line).

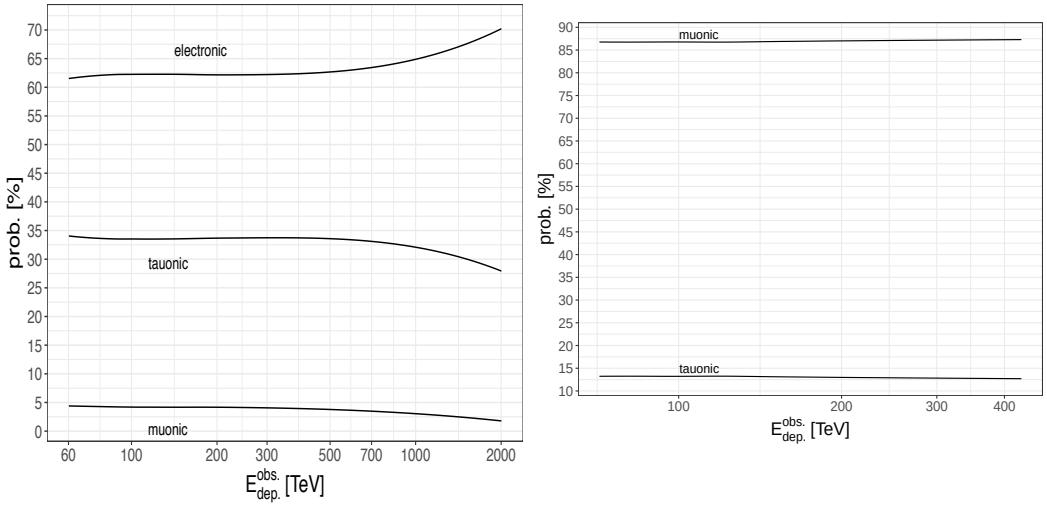

Figure 3.10. The probability of being of electronic, muonic or tauonic flavor is shown as a function of the observed-deposited energy for a shower event (left) or a track event (right).

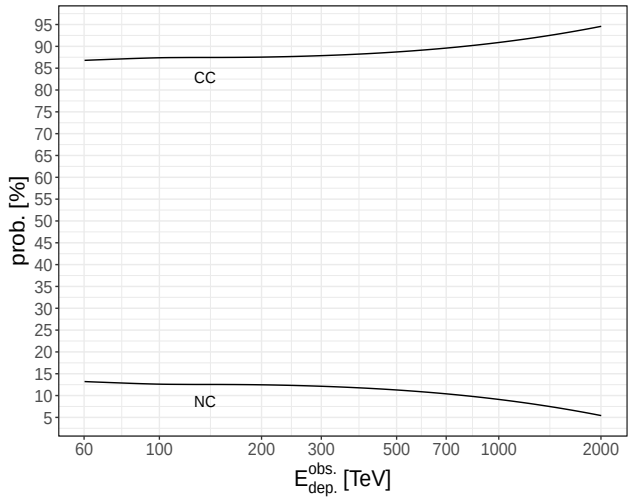

Figure 3.11. The probability for a shower event of having scattered via CC or NC interaction is shown as a function of the observed-deposited energy.

this interaction having occurred in the detector. From this considerations it is not surprising that a neutrino producing a shower event has the best chance of being electronic: from Table 3.4 we have about $\sim 61\,\%$ of chance that its flavor is electronic, $\sim 5\,\%$ muonic and $\sim 34\,\%$ tauonic. For track events the situation is simpler: we need to consider only ν_μ and ν_τ (followed by $\tau \to \nu_\tau \mu \nu_\mu$) CC interactions. Both interactions have similar efficiency in producing a deposited energy (as illustrated by the top panels of Fig. 3.7), thus for track events when estimating the chance of being muonic or tauonic the most important thing to consider is the branching fraction for the muonic τ-decay channel (see Eq. 3.8). Our Bayesian inference for track events (see Table 3.5) ends up giving to neutrinos a $\sim 87\,\%$ chance of being muonic and $\sim 13\,\%$ tauonic.

Performing an inference analysis of neutrino fluxes over the whole data sample goes beyond the scope of this work, as we are interested only in inferring properties of each single neutrino event. But it is worth noticing that, combining our flavor probabilities with the observed track-to-shower ratio, we obtain that the expected flavor ratio $(1:1:1)_\oplus$ is currently disfavored. The current track-to-shower ratio for down-going events above 60 TeV is 7/35, thus the flavor flux is approximately given by

$$\sim \frac{1}{35}\,(28\cdot 61\,\%\;:\;28\cdot 5\,\%+7\cdot 87\,\%\;:\;28\cdot 34\,\%+7\cdot 13\,\%)_\oplus \propto (1:0.44:0.61)_\oplus. \tag{3.21}$$

This finding is in agreement with previous results obtained independently in other analyses [7, 115, 114]. Thus the current observed track-to-shower ratio implies that the electronic flavor is almost two times more frequent than the muonic or tauonic flavor. Although it is not statistically significant at present and a complete discussion of its implications goes beyond the scope of this paper, this result may be explained either by a misidentification of tracks as showers [6] or, even more compellingly, by some new physics that goes beyond the standard model. Therefore, a further investigation in this direction will be crucial when more data will be collected.

In this work we performed, for the first time, a detailed Bayesian inference analysis for each of the 35 down-going high-energy neutrino events above 60 TeV detected by IceCube in 6 years of data taking. We have shown how from the observed-deposited energy and the topology event one can obtain an estimate of the neutrino energy and flavor. We have also explained how this analysis depends on the assumptions made for neutrino fluxes and for the physics involved in all processes producing shower and track events in the detector. From these assumptions we selected those prior probability distributions which seem, at present, the most reasonable ones. Further investigations in high-energy neutrino physics may change the current situation, improving our knowledge of the prior probability distribution for the parameters involved in this inference analysis.

Neutrino astronomy has just started with IceCube providing the first evidence of astrophysical high-energy neutrinos. Inference analyses, as the one here exposed, for the properties of each high-energy neutrino have become impelling in searches for new physics and in order to shed some light on many of the questions raised by

[6] according to IceCube the fraction of track misidentification is about $\sim 30\,\%$ [7], while the reverse, i.e., a shower being misclassified as a track, is very rare [6].

the observation of these events.

Table 3.4. Here we show the relevant properties of the 28 down-going shower events with observed-deposited energy above 60 TeV. The first three columns are respectively the ID number, the observed-deposited energy and its uncertainty for each shower event. From the fourth to the seventh columns we have the mean value (mean) and the standard deviation (s.d.) of the posterior distributions of E_ν assuming different neutrino flavor and kind of interaction. In the last columns the probabilities for each shower event of being generated by a electronic, muonic and tauonic neutrino and of having scattered with nucleon via CC or NC interaction are shown.

ID	$E^{obs.}_{dep.}$ [TeV]	$\sigma_{E_{dep.}}$ [TeV]	E_ν [TeV]								prob. [%]				
			CC + NC		CC		CC		NC						
			$\nu_e + \nu_\mu + \nu_\tau$		ν_e		ν_τ		$\nu_e + \nu_\mu + \nu_\tau$		ν_e	ν_μ	ν_τ	CC	NC
			mean	s.d.	mean	s.d.	mean	s.d.	mean	s.d.					
2	117	15.4	168	176	117	17	177	102	363	390	61.0	4.6	34.4	86.2	13.8
4	165.4	19.8	233	203	166	21	249	124	479	439	61.1	4.4	34.5	86.7	13.3
10	97.2	12.4	142	161	97	13	147	82	319	367	61.3	4.6	34.1	86.3	13.7
11	88.4	12.5	127	140	88	13	135	86	274	318	60.9	4.4	34.6	86.6	13.4
12	104.1	13.2	151	158	104	14	158	86	328	351	60.9	4.6	34.5	86.2	13.8
14	1040.7	144.4	1205	388	1022	152	1412	417	1690	534	63.2	3.2	33.5	90.3	9.7
19	71.5	7.2	109	136	73	8	110	60	249	316	60.8	4.6	34.5	86.1	13.9
20	1140.8	142.8	1313	381	1129	150	1537	411	1795	512	63.7	3.0	33.3	91.0	9.0
22	219.5	24.4	303	227	221	26	335	174	586	460	61.0	4.3	34.7	86.9	13.1
27	60.2	5.6	94	131	62	6	94	57	219	306	60.2	4.7	35.1	85.8	14.2
30	128.7	13.8	184	176	130	15	196	101	387	389	61.2	4.5	34.3	86.4	13.6
35	2003.7	261.5	2090	347	1973	274	2339	347	2417	346	70.9	1.8	27.4	94.7	5.3
39	101.3	13.3	148	166	101	14	154	92	328	374	60.9	4.6	34.5	86.3	13.7
40	157.3	16.7	226	208	159	18	241	135	477	442	61.3	4.5	34.2	86.5	13.5
42	76.3	11.6	112	139	76	12	114	65	252	324	60.7	4.6	34.7	86.1	13.9
46	158	16.6	221	190	159	18	241	128	446	411	61.5	4.4	34.1	86.8	13.2
48	104.7	13.5	152	160	105	14	160	91	329	359	61.0	4.5	34.5	86.5	13.5
52	158.1	18.4	223	200	159	20	240	129	462	434	61.2	4.4	34.4	86.8	13.2
56	104.2	10	151	156	106	11	161	90	322	354	61.2	4.5	34.3	86.6	13.4
57	132.1	18.1	186	179	131	19	199	108	389	399	61.1	4.4	34.4	86.7	13.3
59	124.6	11.7	184	188	127	13	194	115	396	405	60.9	4.7	34.5	86.0	14.0
60	93	12.9	134	147	92	14	141	86	290	336	61.1	4.5	34.4	86.6	13.4
64	70.8	8.1	106	133	72	9	109	65	241	308	60.8	4.6	34.6	86.2	13.8
70	98.8	12	143	150	99	13	150	84	307	337	61.1	4.5	34.4	86.4	13.6
74	71.3	9.1	104	125	72	9	109	68	228	289	60.8	4.5	34.6	86.4	13.6
79	158.2	20.3	225	208	158	22	240	134	470	441	61.1	4.6	34.4	86.3	13.7
80	85.6	11.1	126	146	86	12	130	73	280	333	60.9	4.6	34.5	86.2	13.8
81	151.8	21.6	211	191	150	23	227	120	434	414	61.1	4.5	34.4	86.6	13.4

Table 3.5. Same as for Table 3.4, but for the 7 down-going track events with observed-deposited energy above 60 TeV.

ID	$E_{dep.}^{obs.}$ [TeV]	$\sigma_{E_{dep.}}$ [TeV]	E_ν [TeV]						prob. [%]	
			CC $\nu_\mu + \nu_\tau$		CC ν_μ		CC ν_τ		ν_μ	ν_τ
			mean	s.d.	mean	s.d.	mean	s.d.		
3	78.7	10.8	225	167	222	149	249	254	86.7	13.3
5	71.4	9	208	151	206	136	227	226	86.9	13.1
23	82.2	8.6	242	174	238	157	267	258	86.7	13.3
44	84.6	7.9	248	177	245	161	269	256	86.8	13.2
45	429.9	57.4	1098	659	1110	667	1011	597	87.3	12.7
71	73.5	10.5	211	155	208	139	231	232	86.6	13.4
76	126.3	12.7	374	264	369	244	403	366	86.8	13.2

Chapter 4

IceCube and GRB neutrinos propagating in quantum spacetime

As discussed in Chap. 2 the prediction of a neutrino emission associated with gamma ray bursts (GRBs) is generic within the most widely accepted astrophysical models. After a few years of operation IceCube still reports [4] no conclusive detection of GRB neutrinos, contradicting some influential predictions [130, 131, 119, 84, 18] of the GRB-neutrino observation rate by IceCube. Of course, it may well be the case that the efficiency of neutrino production at GRBs is much lower than had been previously estimated [45, 88, 137]. However, from the viewpoint of quantum-gravity/quantum-spacetime research it is interesting to speculate that the IceCube results for GRB neutrinos might be misleading because of the assumption that GRB neutrinos should be detected in very close temporal coincidence with the associated γ-rays: a sizeable mismatch between GRB-neutrino detection time and trigger time for the GRB is expected in several much-studied models of neutrino propagation in a quantum spacetime (see Refs. [24, 91, 42, 32, 71, 19, 38, 110, 36, 124] and references therein).

This possibility was preliminarily explored in Ref. [36] using only IceCube data from April 2008 to May 2010, and focusing on 3 weak but intriguing candidate GRB neutrinos (see Refs. [64, 133]): a 1.3 TeV neutrino 1.95^o off GRB090417B with detection time 2249 seconds before the trigger of GRB090417B, a 3.3 TeV neutrino 6.11^o off GRB 090219 and detection time 3594 seconds before the GRB 090219 trigger, and a 109 TeV neutrino 0.2^o off GRB091230A and detection time some 14 hours before the GRB091230A trigger. The analysis reported in Ref. [36] would have been more intriguing if the 109 TeV event could be viewed as a promising cosmological-neutrino candidate, but for that event there was a IceTop-tank trigger coincidence. A single IceTop-tank trigger is not enough to firmly conclude that the event was part of a cosmic-ray air shower, but of course that casts a shadow on the interpretation of the 109-TeV event as a GRB neutrino.

Unaware of the observations reported in Ref. [36], recently Stecker *et al.* reported in Ref. [124] an observation which also might encourage speculations about neutrino propagation in quantum spacetime. Ref. [124] noticed that IceCube data are

presently consistent with a ~ 2 PeV cutoff for the cosmological-neutrino spectrum, and that this could be due to novel processes (like "neutrino splitting" [124, 24]) that become kinematically allowed in the same class of quantum-spacetime models considered in Ref. [36].

The study we are here reporting in this chapter was motivated by these previous observations of Refs.[36] and [124]. Like Ref. [36] our focus is on the hypothesis of GRB neutrinos with quantum-spacetime properties, also exploiting the fact that, while Ref. [36] was limited to IceCube data up to May 2010, the amount of data now available from IceCube [3] is significantly larger. Conceptually the main issue we wanted to face is indeed related to the amount of IceCube data: as studies like these start to contemplate larger and larger groups of "GRB-neutrino candidates" some suitable techniques of statistical analysis must be adopted, and (unlike Refs.[36] and [124]) we wanted to devise a strategy of analysis applicable not only to one "preferred model", but to a rather wide class of scenarios for the properties of the laws of propagation of neutrinos in a quantum spacetime.

As discussed in Sec. 1.2.1 and more quantitatively below, the effects on propagation due to spacetime quantization can be systematic or of "fuzzy" type. Combinations of systematic effects and fuzziness are also possible, and this is the hypothesis most challenging from the viewpoint of data analysis. We came to notice that in all these scenarios one should anyway find a correlation between the energy of the observed GRB neutrino and the difference between the time of observation of that neutrino and the trigger time of the relevant GRB. Intriguingly our data analysis finds a rather strong such correlation, and we therefore argue that our findings should motivate a vigorous program of investigation following the strategy here advocated.

The structure of this chapter is as follows. In Sec. 4.1 we charactareize in detail our strategy of analysis for exploring in-vacuo dispersion in the astrophysical IceCube neutrinos. The results of this analysis are then reported in Sec. 4.2, in which we also quantify the statistical significance of our findings by introducing the concept of "false alarm probability". Finally, in Sec. 4.3 we discuss the interpretation of our results in searching for evidence of quantum-spacetime effects on neutrino propagation.

4.1 Quantum-spacetime-propagation models and strategy of analysis

As discussed in detail in Chap. 1, the class of scenarios we intend to contemplate finds motivation in some much-studied models of spacetime quantization (see, *e.g.*, [91, 42, 24, 32, 71, 19, 38, 110] and references therein) and, for the type of data analyses we are interested in, has the implication that the time needed for a ultrarelativistic particle [1] to travel from a given source to a given detector receives a quantum-spacetime correction, here denoted with Δt. We focus on the class of scenarios whose predictions for energy (E) dependence of Δt can all be described in terms of

[1] Of course the only regime of particle propagation that is relevant for this thesis work is the ultrarelativistic regime, since photons have no mass and for the neutrinos we are contemplating (energy of tens or hundreds of TeVs) the mass is completely negligible.

the formula (working in units with the speed-of-light scale "c" set to 1)

$$\Delta t = \eta_X \frac{E}{M_P} D(z) \pm \delta_X \frac{E}{M_P} D(z)\,. \tag{4.1}$$

Here the redshift- (z-)dependent $D(z)$ carries the information on the distance between source and detector, and it factors in the interplay between quantum-spacetime effects and the curvature of spacetime. As usually done in the relevant literature [91, 42, 24] and as discussed in detail in Sec. 1.2.1, we take for $D(z)$ the following form: [2]

$$D(z) = \int_0^z d\zeta \frac{(1+\zeta)}{H_0\sqrt{\Omega_\Lambda + (1+\zeta)^3\Omega_m}}\,, \tag{4.2}$$

where Ω_Λ, H_0 and Ω_0 denote, as usual, respectively the cosmological constant, the Hubble parameter and the matter fraction, for which we take the values given in Ref. [17]. With M_P we denote the Planck scale ($\simeq 1.2 \cdot 10^{28} eV$) while the values of the parameters η_X and δ_X in Eq. 4.1 characterize the specific scenario one intends to study. In particular, in Eq. 4.1 we used the notation "$\pm\delta_X$" to reflect the fact that δ_X parametrizes the size of quantum-uncertainty (fuzziness) effects. Instead the parameter η_X characterizes systematic effects: for example in our conventions for positive η_X and $\delta_X = 0$ a high-energy neutrino is detected systematically after a low-energy neutrino (if the two neutrinos are emitted simultaneously).

The dimensionless parameters η_X and δ_X can take different values for different particles [24, 110, 105, 125], and it is of particular interest for our study that in particular for neutrinos some arguments have led to the expectation of an helicity dependence of the effects (see, *e.g.*, Refs.[24, 105] and references therein). Therefore even when focusing only on neutrinos one should contemplate four parameters, η_+, δ_+, η_-, δ_- (with the indices + and − referring of course to the helicity). The parameters η_X, δ_X are to be determined experimentally. When non-vanishing, they are expected to take values somewhere in a neighborhood of 1, but values as large as 10^3 are plausible if the solution to the quantum-gravity problem is somehow connected with the unification of non-gravitational forces [24, 122, 52] while values smaller than 1 find support in some renormalization-group arguments (see, *e.g.*, Ref.[53]).

Presently for photons the limits on η_γ and δ_γ are at the level of $|\eta_\gamma| \lesssim 1$ and $\delta_\gamma \lesssim 1$ [15, 127], but for neutrinos we are still several orders of magnitude below 1 [124, 24]. This is mainly due to the fact that the observation of cosmological neutrinos is rather recent, still without any firm identification of a source of cosmological neutrinos [3], and therefore the limits are obtained from terrestrial experiments [4] (where the distances travelled are of course much smaller than the ones relevant in astrophysics).

[2] The interplay between quantum-spacetime effects and curvature of spacetime is still a lively subject of investigation, and, while Eq. 4.2 is by far the most studied scenario, some alternatives to Eq. 4.2 are also under consideration [123].

[3] Very recently, the IceCube Collaboration has reported the observation of a high-energy neutrino from the direction of the blazar TXS 0506+056 [58]. Some authors [68] have used this event to put the limit on η_ν for neutrinos at the level of $|\eta_\nu| \lesssim 400$.

[4] Supernova 1987a was rather close by astrophysics standards and the signal detected in neutrinos was of relatively low energy.

For reasons that shall soon be clear we find convenient to introduce a "distance-rescaled time delay" Δt^* defined as

$$\Delta t^* \equiv \Delta t \frac{D(1)}{D(z)} \tag{4.3}$$

so that Eq.4.1 can be rewritten as

$$\Delta t^* = \eta_X \frac{E}{M_P} D(1) \pm \delta_X \frac{E}{M_P} D(1)\,. \tag{4.4}$$

This reformulation of Eq. 4.1 allows to describe the relevant quantum-spacetime effects, which in general depend both on redshift and energy, as effects that depend exclusively on energy, through the simple expedient of focusing on the relationship between Δt and energy when the redshift has a certain chosen value, which in particular we chose to be $z = 1$. If one measures a certain Δt for a candidate GRB neutrino and the redshift z of the relevant GRB is well known, then one gets a firm determination of Δt^* by simply rescaling the measured Δt by the factor $D(1)/D(z)$. And even when the redshift of the relevant GRB is not known accurately one will be able to convert a measured Δt into a determined Δt^* with accuracy governed by how much one is able to still assume about the redshift of the relevant GRB. In particular, even just the information on whether a GRB is long or short can be converted into at least a very rough estimate of redshift.

Of course a crucial role is played in analyses such as ours by the criteria for selecting GRB-neutrino candidates. We need a temporal window (how large can the Δt be in order for us to consider a IceCube event as a potential GRB-neutrino candidate) and we need criteria of directional selection (how well the directions estimated for the IceCube event and for the GRB should agree in order for us to consider that IceCube event as a potential GRB-neutrino candidate). While our analysis shall not include the above-mentioned 109-TeV neutrino (from Ref.[36]), we do use it to inspire a choice of the temporal window: assuming a 109-TeV GRB neutrino could be detected within 14 hours of the relevant GRB trigger time, an analysis involving neutrinos with energies up to 500 TeV should allow for a temporal window of about 3 days, and an analysis involving neutrinos with energies up to, say, 1000 TeV should allow for a temporal window of about 6 days. Considering the rate of GRB observations of about 1 per day, we opt for focusing on neutrinos with energies between 60 TeV [5] and 500 TeV, allowing for a temporal window of 3 days. Widening the range of energies up to, say, 1000 TeV would impose us indeed a temporal window of about 6 days, rendering even more severe one of the key challenges for this sort of analysis, which is the one of multiple GRB candidates for a single IceCube event. As directional criteria for the selection of GRB-neutrino candidates we consider the signal direction PDF depending on the space angle difference between GRB and neutrino: $P(\nu, GRB) = (2\pi\sigma^2)^{-1} \exp(-\frac{|\vec{x}_\nu - \vec{x}_{GRB}|^2}{2\sigma^2})$, a two dimensional circular Gaussian whose standard deviation is

$$\sigma = \sqrt{\sigma_{GRB}^2 + \sigma_\nu^2}\,, \tag{4.5}$$

[5] The 60-TeV lower limit of our range of energies is consistent with the analogous choice made by other studies whose scopes, like ours, require keeping the contribution of background neutrinos relatively low, as discussed in Chap. 3 and in Refs. [1, 6].

asking the pair composed by the neutrino and the GRB to be at angular distance compatible within a 2σ region.

A key observation for our analysis is that whenever η_+, η_-, δ_+, δ_- do not vanish one should expect on the basis of Eq. 4.4 a correlation between the $|\Delta t^*|$ and the energy of the candidate GRB neutrinos. The interested reader will immediately see that this is obvious when $\delta_+ = \delta_- = 0$. It takes only a little bit more thinking to notice that such a correlation should be present also when $\delta_+ \neq 0$ and/or $\delta_- \neq 0$ with $\eta_+ = \eta_- = 0$, as a result of how the fuzzy effects have range that grows with the energy of the GRB neutrinos. We provide support for this conclusion in Fig. 4.1.

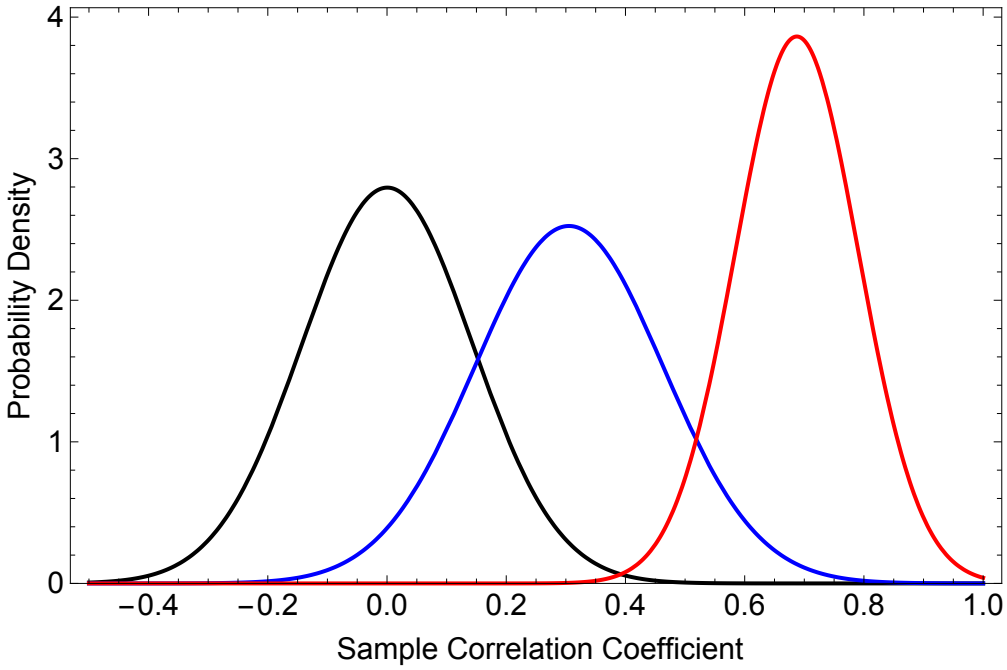

Figure 4.1. Here we illustrate the different expectations one should have for the correlation on which we focus, assuming all neutrinos are just background neutrinos (black), assuming 10% of neutrinos are background while 90% are GRB neutrinos with $\eta_+ = \eta_- = 0$, $\delta_+ = \delta_- = 5$ (blue), or assuming 10% of neutrinos are background while 90% are GRB neutrinos with $|\eta_+| = |\eta_-| = 15$, $\delta_+ = \delta_- = 5$ (red). The probability densities were computed assuming that the spectrum of the neutrinos decreases quadratically with energy (E^{-2}) between 60 and 500 TeV, that the neutrinos would be observed only if within a 3-day window of the relevant GRB, and, for simplicity, that all relevant GRBs are exactly at redshift of 1. This probability densities were obtained for the hypothetical case of 50 candidate GRB neutrinos. The figure shows that 50 candidate GRB neutrinos would be enough for the most likely correlation outcome in the scenario with $\eta_+ = \eta_- = 0$, $\delta_+ = \delta_- = 5$ to be a rather unlikely outcome for the "pure-background hypothesis". Actually, much less than 50 candidate GRB neutrinos would be enough for the most likely correlation outcome in the scenario with $|\eta_+| = |\eta_-| = 15$, $\delta_+ = \delta_- = 5$ to be a very unlikely outcome for the pure-background hypothesis.

4.2 Results for in-vacuo dispersion in GRB-neutrinos

Our data set[6] is for four years of operation of IceCube [1, 8, 3], from June 2010 to May 2014. Since the determination of the energy of the neutrino plays such a crucial role in our analysis we include only IceCube "shower events". This is becouse, as shown in detail in Chap. 3, for "track events" the reconstruction of the neutrino energy is far more problematic and less reliable, while for "shower events" the best- guess value for the neutrino energy is the deposited energy [2]. We have 21 such events within our 60-500 TeV energy window, and we find that 9 of them fit the requirements introduced in the previous section for candidate GRB neutrinos. The properties of these 9 candidates that are most relevant for our analysis are summarized in Table 4.1 and Fig. 4.2.

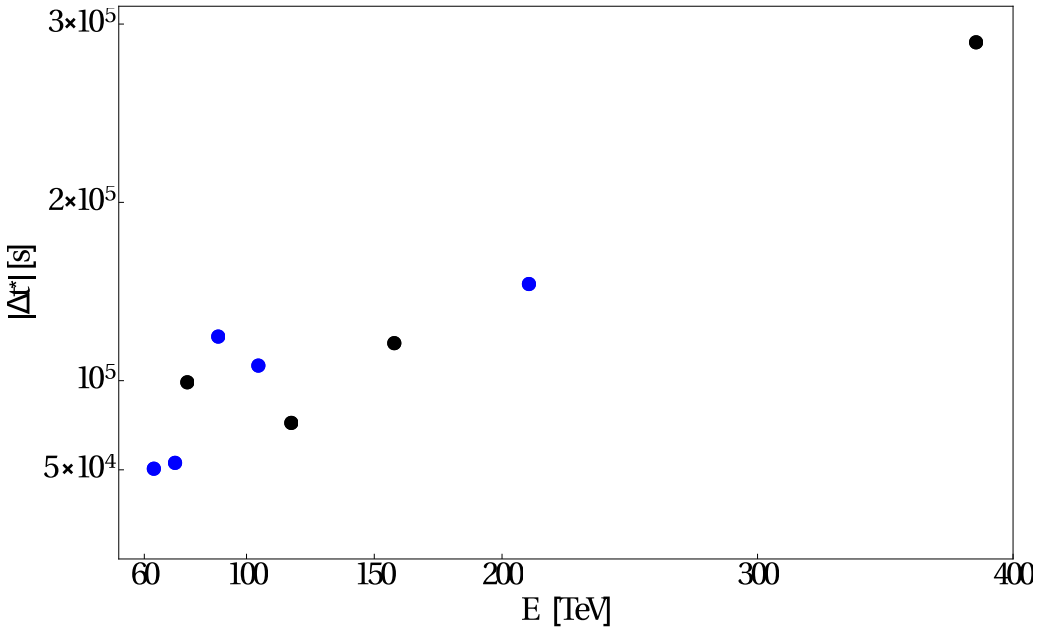

Figure 4.2. Points here in figure correspond to the 9 GRB-neutrino candidates highlighted with an asterisk in the last column of Table 1. Blue points correspond to "late neutrinos" ($\Delta t^* > 0$), while black points correspond to "early neutrinos" ($\Delta t^* < 0$).

In commenting Table 4.1 we start by noticing that for some IceCube events our selection criteria produce multiple GRB-neutrino candidates (and the situation would have been much worse if we had considered a wider energy range and a correspondingly wider temporal window). Since we have two cases with 3 possible GRB partners and one case with a pair of possible GRB partners, we must contemplate 18 alternative descriptions of our 9 GRB-neutrino candidates. As neutrino telescopes gradually accrue more and more such events the number of combinations to be considered in analyses such as ours will grow very large. We propose that in general this issue of multiple candidates should be handled, consistently with the nature of the hypothesis being tested, by focusing on the case that provides the highest

[6]Both IceCube-neutrino data and GRB data used for this study were gathered from https://icecube.wisc.edu/science/tools. A list of the relevant properties for IceCube neutrinos and GRBs can also be found respectivetely in Appxs. A and B.

	E[TeV]	GRB	z	Δt^* [s]	
IC9	63.2	110503A	1.613	50227	*
IC19	71.5	111229A	1.3805	53512	*
IC42	76.3	131117A	4.042	5620	
		131118A	1.497 *	-98694	*
		131119A	?	-146475	
IC11	88.4	110531A	1.497 *	124338	*
IC12	104.1	110625B	1.497 *	108061	*
IC2	117.0	100604A	?	10372	
		100605A	1.497 *	-75921	*
		100606A	?	-135456	
IC40	157.3	130730A	1.497 *	-120641	*
IC26	210.0	120219A	1.497 *	153815	*
		120224B	?	-117619	
IC33	384.7	121023A	0.6 *	-289371	*

Table 4.1. Among the 21 "shower neutrinos" with energy between 60 and 500 TeV observed by IceCube between June 2010 and May 2014 only 9 fit our directional and temporal criteria for GRB-neutrino candidates, and yet for 3 of them there is more than one GRB to be considered when pairing up neutrinos and GRBs. The last column highlights with an asterisk the 9 GRB-neutrino candidates ultimately selected by our additional criterion of maximal correlation. Also shown in table are the values of redshift attributed to the relevant GRBs: the redshift is known only for GRB111229A and GRB110503A (plus GRB131117A, which however ends up not being among the GRBs selected by the maximal-correlation criterion). GRB111229A and GRB110503A are long GRBs and we assume that the average of their redshifts (1.497) could be a reasonably good estimate of the redshifts of the other long GRBs relevant for our 9 GRB-neutrino candidates. These are the 6 estimated values of redshift $z = 1.497^*$, the asterisk reminding that it is a "best guess" value. For analogous reasons we place an asterisk close to the value of 0.6 which is our best guess for the redshift of the only short GRB in our sample. The first column lists the "names" given by IceCube to the neutrinos that end up being relevant for our analysis. Also notice that 5 of our GRB-neutrino candidates are "late neutrinos" ($\Delta t^* > 0$), while the other 4 are "early neutrinos" ($\Delta t^* < 0$): this might be of interest to some readers but plays no role in our study since our correlations involve the absolute value of Δt^*.

correlation. This might appear to introduce a bias toward higher values of the correlation, but, as we shall soon argue, the significance of such an analysis is not given by the correlation itself but rather requires the evaluation of a "false alarm probability", and for the false alarm probability this criterion for handling multiple candidates introduces no bias (see below).

Another issue reflected by Table 4.1 comes from the fact that for only 3 of the GRBs involved in this analysis the redshift is known. We must handle only one short GRB of unknown redshift, and we assume for it a redshift of 0.6, which is a rather reasonable rough estimate for a short GRB (but we shall contemplate also values of 0.5 and of 0.7). For some of our long GRBs we do have a redshift determination and we believe that consistently with the hypothesis here being tested one should use those known values of redshift for obtaining at least a rough estimate of the redshift of long GRBs for which the redshift is unknown. This is illustrated by the 9 GRB-neutrino candidates marked by an asterisk in table 1: those 9 candidates include 8 long GRBs, 2 of which have known redshift, and we assign to the other 6 long GRBs the average $\bar{z}$ of those two values of redshift ($\bar{z} = 1.497$). These results do not depend strongly on the what is assumed about unknown redshifts, be it assuming that these redshifts follow the distribution of GRBs observed in photons or simply assuming different values of $\bar{z}$. We shall document a bit of this insight here below, by providing our results both assuming this criterion of the $\bar{z}$ and assuming simply a redshift of 2 for all long GRBs of unknown redshift. We feel that estimating a $\bar{z}$ from the "data points" is the only reasonable way to proceed, since we do not expect that the redshift distribution of GRBs observed also in neutrinos should look much like the redshift distribution of GRBs observed only in photons. However we imagine that some readers might have been more comfortable if we assumed for our long GRBs of unknown redshift the average value of redshift of GRBs observed in photons, which is indeed of about 2.

Having specified these further prescriptions, we can proceed to compute the correlation between $|\Delta t^*|$ and energy for our 9 GRB-neutrino candidates. Because of the fact that for some of our neutrinos there is more than one possible GRB partner we end up having 18 such values of correlation, and remarkably they are all very high: the highest of these 18 values is of 0.951 (the corresponding 9 neutrino-GRB pairs are highlighted by an asterisk in Table 4.1 and are shown in Figure 4.2), and even the lowest of these 18 values of correlation is still of 0.802. In Table 4.2 we show how the evaluation of the maximum correlation for our 9 GRB-neutrino candidates would change upon replacing our $\bar{z}$ with a redshift of 2, for long GRBs, and upon replacing the value of 0.6 we assumed for the redshift of the short GRB in our collection with 0.5 or 0.7.

The class of quantum-spacetime scenarios we are considering predicts a non-vanishing (and possibly large) correlation, and we did find on data very high values of correlation. This in itself however does not quantify what is evidently the most interesting quantity here of interest, which must be some sort of "false alarm probability": how likely it would be to have accidentally data with such good agreement with the expectations of the quantum-spacetime models here contemplated? We need to estimate how often a sample composed exclusively of background neutrinos[7]

[7]Consistently with the objectives of our analysis we consider as "background neutrinos" all neutrinos that are unrelated to a GRB, neutrinos of atmospheric or other astrophysical origin which

	$z_{long} = \bar{z}$	$z_{long} = 2$
$z_{short} = 0.5$	0.958	0.953
$z_{short} = 0.6$	0.951	0.960
$z_{short} = 0.7$	0.941	0.964

Table 4.2. Adopting our "$\bar{z}$ criterion" for long GRBs whose redshift is not known and z=0.6 for short GRBs one gets as maximal correlation for our data the impressive value of 0.951. Here we show how this estimate changes if one assigns to short GRBs the alternative values of redshift of 0.5 and 0.7 and/or one replaces our $\bar{z}$ with a redshift of 2.

would produce accidentally 9 or more GRB-neutrino candidates with correlation comparable to (or greater than) those we found in data. We do this by performing 10^5 randomizations of the times of detection of the 21 IceCube neutrinos relevant for our analysis, keeping their energies fixed, and for each of these time randomizations we redo the analysis just as if they were real data. Our observable is a time-energy correlation and by randomizing the times we get a robust estimate of how easy (or how hard) it is for a sample composed exclusively of background neutrinos to produce accidentally a certain correlation result. In the analysis of these fictitious data obtained by randomizing the detection times of the neutrinos we handle cases with neutrinos for which there is more than one possible GRB partner by maximizing the correlation, in the sense already discussed above for the true data. We ask how often this time-randomization procedure produces 9 or more GRB-neutrino candidates with correlation ≥ 0.951, and remarkably we find that this happens only in 0.03% of cases.

In Table 4.3 we report a preliminary investigation of how this result of a 0.03% false alarm probability depends on the assumptions we made for redshifts. Table 4.3 is in the same spirit of what was reported in our Table 4.2 for the estimates of the correlation. Each entry in Table 4.2 recalculates the false alarm probability just like we did above to obtain the result of 0.03%, but now considering some alternative possibilities for the assignment of redshifts to GRBs whose redshift is actually unknown. Once again for long GRBs we consider two possibilities, the $\bar{z}$ discussed above and redshift of 2, while for short GRBs we consider values of redshift of 0.5, 0.6 and 0.7. Table 4.3 shows that our false alarm probability does not change much within this range of exploration of the redshift assignments.

Our next objective is to see how things change if one is "unreasonably conservative" in assessing the implications of our prescription for handling cases where there is more than one possible GRB partner for a neutrino. We are proposing that one should address this multi-candidate issue in the way that maximizes the correlation, and this evidently introduces some bias toward higher values of the correlation. However, as already stressed above, when we randomize (fictitious) detection times we handle the multi-candidate issue in exactly the same way, by maximizing the correlation, so that overall there is no bias for the false alarm probability. It is nonetheless interesting

end up being selected as GRB-neutrino candidates just because accidentally their time of detection and angular direction happen to fit our selection criteria.

	$z_{long} = \bar{z}$	$z_{long} = 2$
$z_{short} = 0.5$	0.03 %	0.04 %
$z_{short} = 0.6$	0.03 %	0.02 %
$z_{short} = 0.7$	0.04 %	0.01 %

Table 4.3. Adopting our "$\bar{z}$ criterion" for long GRBs whose redshift is not known and z=0.6 for short GRBs one gets a false alarm probability of 0.03%. Here we show how this estimate changes if one assigns to short GRBs the alternative values of redshift of 0.5 and 0.7 and/or one replaces our $\bar{z}$ with a redshift of 2.

to notice that one still obtains a rather low false alarm probability even when comparing the minimum correlation for our true data to the maximum correlation for the fictitious data obtained by randomizing neutrino detection times. So we now ask how often the fictitious data obtained by randomizing neutrino detection times produce 9 or more GRB-neutrino candidates with correlation ≥ 0.803 (0.803 being, as noticed above, the lowest possible value of correlation for our true data), but for the fictitious data we still handle cases with neutrinos having more than one possible GRB partner by maximizing the correlation. Even this procedure, which is evidently biased toward lower values of the false alarm probability, only gives a false alarm probability of $\simeq 1\%$. Table 4.4 explores the dependence on assumptions for redshift of the value of 0.803 for the lowest correlation obtainable from the true data, while Table 4.5 explores analogously the dependence on assumptions for redshift of our result for the "unreasonably conservative estimate of the false alarm probability".

	$z_{long} = \bar{z}$	$z_{long} = 2$
$z_{short} = 0.5$	0.844	0.869
$z_{short} = 0.6$	0.803	0.849
$z_{short} = 0.7$	0.751	0.822

Table 4.4. Adopting our "$\bar{z}$ criterion" for long GRBs whose redshift is not known and z=0.6 for short GRBs one gets as minimal correlation for our data a still high value of 0.803. Here we show how this estimate changes if one assigns to short GRBs the alternative values of redshift of 0.5 and 0.7 and/or one replaces our $\bar{z}$ with a redshift of 2.

	$z_{long} = \bar{z}$	$z_{long} = 2$
$z_{short} = 0.5$	0.7 %	0.6 %
$z_{short} = 0.6$	1.0 %	0.6 %
$z_{short} = 0.7$	1.5 %	0.8 %

Table 4.5. Adopting our "$\bar{z}$ criterion" for long GRBs whose redshift is not known and z=0.6 for short GRBs we obtain an "unreasonably conservative estimate of the false alarm probability" which is still only 1.0%. Here we show how this estimate changes if one assigns to short GRBs the alternative values of redshift of 0.5 and 0.7 and/or one replaces our $\bar{z}$ with a redshift of 2.

4.3 Challenges for the interpretation of the data

In searching for evidence of quantum-spacetime effects on neutrino propagation our approach has the advantage of allowing to study at once a variety of scenarios, the scenarios obtainable by all sorts of combinations of values for η_+, η_-, δ_+, δ_-. This is due to the fact that positive correlation between $|\Delta t^*|$ and E is expected whenever one or more of the parameters η_+, η_-, δ_+, δ_- are non-zero. Our approach performs very well in comparing the hypothesis "all the GRB-neutrino candidates actually are background neutrinos" to the hypothesis "some of the GRB-neutrino candidates truly are GRB neutrinos governed by Eq. 4.1 with one or more of the parameters η_+, η_-, δ_+, δ_- having non-zero value". It does so in ways that are rather robust with respect to the assumptions made about the redshift of the relevant GRBs and with respect to the presence of some background neutrinos among the GRB-neutrino candidates.

If it happens that the experimental situation develops positively for our scenario then one will of course be interested in estimating model parameters, *i.e.* comparing how well different choices of values of the parameters of the model match the available data. Our false-alarm probabilities are still not small enough to worry about that, but we find appropriate to offer here some related observations, hoping that this will ignite a debate in the community on how the relevant challenges could be handled.

4.3.1 Challenges for handling background neutrinos

The role of background neutrinos in the correlation studies here proposed is not very troublesome. In absence of background neutrinos our correlation would take statistically-significant values already with a few candidate GRB neutrinos, while in presence of a sizable contribution by background neutrinos one should expect our correlation to take statistically-significant values only with larger numbers of GRB-neutrino candidates. The approach is robust against contamination by background neutrinos in the sense that this contamination only increases the amount of data needed, without affecting the strategy of analysis.

As mentioned, this is true only when comparing the hypothesis "all the GRB-neutrino candidates actually are background neutrinos" to the hypothesis "some of the GRB-neutrino candidates truly are GRB neutrinos governed by Eq. 4.1 with one or more of the parameters η_+, η_-, δ_+, δ_- having non-zero value". However, if we ever get to the point of having a statistically-significant value of the correlation we will want to estimate model parameters, and that task would be rather challenging in presence of a large amount of background neutrinos.

One could compare different models predicting our correlation by establishing how likely it would be to produce, with a given model, the actual value of correlation seen in data. This of course requires some estimate of the contamination by background neutrinos, since evidently a given model of the correlation expected for GRB neutrinos will ultimately give rise to different predictions for the observed correlation, depending on how many background neutrinos contaminate the sample. This is a severe challenge since, as already stressed above, for the type of analysis we are proposing, one should consider as background neutrinos not only atmospheric neutrinos (whose frequency at the energies here of interest is anyway not well known), but also

cosmological neutrinos which do not originate from GRBs (or originate from GRBs which have not been observed).

4.3.2 LIV interpretation and neutrino splitting

If we ever get to the point of having a statistically-significant correlation, its interpretation in terms of models (and values of model parameters) will not only require appropriate handling of background neutrinos but also some carefulness with relativistic issues. We illustrate this point first for the scenario in which the effects here contemplated are manifestations of a loss of relativistic invariance, i.e. the already discussed "LIV scenario" [8] (see Chap. 1).

Such a LIV interpretation would introduce some challenges particularly in presence of early neutrinos, neutrinos being detected before the associated GRB. In LIV scenarios with neutrinos traveling faster than photons, governed by Eq. 4.1, one ends up having a picture in which the neutrinos cannot propagate freely from a given source to a given distant detector, at least not in general. Above a certain threshold energy, the neutrino could loose energy along the way[9] by emitting electron-positron pairs, or by splitting into 3 neutrinos [124, 57]. Of course, in the case of neutrino splitting we would be observing one of the 3 neutrino "daughters" produced along the way by the mother neutrino emitted at the source. Depending on how frequent such splits are, we might be seeing a granddaughter or a grand-granddaughter (and so on...) of the mother neutrino emitted at the source. As discussed in Ref.[124] this "neutrino splitting" should play a more significant role than electron-positron-pair production by the neutrinos.

Imagine then for simplicity a case when all neutrinos are early neutrinos, such as the case described by our model for $\eta_+ = \eta_- < 0$ and $\delta_+ = \delta_- = 0$. In absence of neutrino splitting this would imply that all GRB neutrinos are observed with a negative Δt^* and with values of $|\Delta t^*|$ that grow linearly with the observed energy. But, in presence of neutrino splitting, a neutrino observed with energy E would have traveled most of the time with energy significantly greater than E, so that, particularly for neutrinos of lower energies, one would expect the relationship between $|\Delta t^*|$ and energy to be affected by departures from the linear behavior, possibly large departures. In principle the departures could be high enough to reduce significantly our correlation, giving rise to "false-negative results" for our correlation-based test of hypothesis (the correlation would be found to be small not because $|\eta_+|$ and $|\eta_-|$ are small but rather because there are large neutrino-splitting effects). However, the impact of neutrino-splitting on our analysis is bigger at lower energies, so one could avoid the false-negative results by focusing on neutrinos of higher energies. For example, as more of our GRB-neutrino candidates are accumulated by IceCube, we might reach a situation in which the value of the correlation between 60 and 500 TeV is not at all statistically significant, while the value of the correlation between 200 and 500 TeV is very significant statistically; that would be a situation favoring an interpretation in terms of neutrino splitting.

In scenarios in which all neutrinos are late neutrinos (traveling slower than

[8] We recall that LIV stands for Lorentz Invariance Violation

[9] We are grateful to an anonymous referee who encouraged us to comment on the role of neutrino splitting and electron-positron-pair production.

low-energy photons), splitting and electron-positron pair production are not possible. An interesting situation arises if some neutrinos are early and some neutrinos are late, a case we can contemplate by assuming within our model that $\eta_+ > 0$ and $\eta_- < 0$ (still with $\delta_+ = \delta_- = 0$, for simplicity). If the observed neutrino is characterized by η_+, but that neutrino originates from a process of neutrino splitting of a mother neutrino characterized by η_-, we would have not only that the energy of the observed neutrino is lower than the energy of the mother neutrino, but also that the total travel time would be composed of a portion of the trip with a neutrino traveling faster than light, followed by a second part of the trip made by a neutrino traveling slower than light. Partial cancelation of the overall effect would be possible in such cases. And one should keep in mind that there might be more than one process of neutrino splitting along the way. Also in this case the implications of neutrino splitting would be naturally stronger a lower energies, and one could achieve a certain degree of immunity to the implications of neutrino splitting by focusing on the GRB-neutrino candidates of highest energies.

In summarizing the points made in this subsection, we first observe that the interpretation in terms of a LIV scenario with exclusively late neutrinos should be relatively unproblematic. Our data analysis however found 4 early GRB-neutrino candidates, so it tentatively invites one to contemplate LIV scenarios with at least some early neutrinos, and in that case neutrino splitting (and electron-positron-pair production by neutrinos) should be taken into account. Neutrino splitting would first of all manifest itself as a neutrino spectrum unusually tilted toward lower energies, and with our correlation becoming stronger at higher energies. If these features are ever found, one should then proceed to test models that explicitly make room for neutrino splitting, producing predictions for the correlation (and its associated energy dependence) by suitable simulations that take into account the relevant decay processes and their probabilities of occurrence (mean free path).

4.3.3 DSR interpretation and the Cherenkov effect

A much studied alternative to the LIV scenario is the interpretation of the effects here contemplated within a "DSR-relativistic scenario" [10]. This is a possibility that was first proposed in Refs. [22, 20] (also see the follow-up studies in Refs. [97, 102]) and discussed in detail in Chap. 1: it describes the departures from standard relativistic laws not as the result of the presence of a preferred frame, but rather as the manifestation of new laws of transformation among observers, within a framework which is still fully relativistic (no preferred frame). Such theories have two non-trivial relativistic invariants, not only the "speed-of-light scale" (which in DSR exclusively has the role of speed of massless particles in the infrared limit), but also a energy scale characteristic of the new effects.

It is well-established (see, *e.g.*, Ref. [23] and references therein) that in these novel relativistic theories processes like neutrino splitting and electron-positron-pair production by neutrinos are kinematically forbidden. Therefore the challenges discussed in the previous subsection for the LIV-scenario interpretation would not have to be faced when exploring a DSR-relativistic interpretation.

[10] We recall that DSR stands for Doubly Special Relativity

We should mention however that the development of quantum field theories with DSR-relativistic symmetries is still rather preliminary. This might be relevant for example in light of the fact that IceCube is a Cherenkov detector. At the present level of understanding of DSR-relativistic quantum field theories one is unable to establish rigorously that the Cherenkov effect is unaffected (or negligibly affected) by the new features. Since the DSR-relativistic scenario has been found to introduce in many ways rather smooth departures from an ordinarily relativistic theory (smoother than in a LIV scenario), it is natural to expect that nothing much would change for phenomena like the Cherenkov effect involving neutrinos of energy not higher than 500 TeV (very small in comparison to the scale characteristic of the new effects). However, if at some point the type of properties contemplated for neutrinos in this thesis work finds stronger support in data, one should assign a very high priority to the challenge of describing a Cherenkov detector within the DSR-relativistic framework.

4.3.4 A simple-minded analysis

As clarified in the other parts of this section, the interpretation of a possible statistically-significant correlation of the type here proposed would be challenging and should take into account several factors. The current situation, while intriguing, does not impose yet any such interpretation. Still, in closing this section we do find appropriate to offer at least a rudimentary attempt of interpretation of the data, as they are now, mainly as an excuse for seeing in action some of the issues discussed in this section.

We start by noticing that the data reported in Fig. 4.2 evidently provide some support for a linear correlation between $|\Delta t^*|$ and energy. Looking in greater detail at the data reported in Fig. 4.2 one cannot fail to also notice that they support a linear dependence of $|\Delta t^*|$ on energy more strongly at higher energies and less strongly (with more spread) at lower energies. This can be quantified by noticing that the correlation of the 5 data points of Fig.2 of highest energy is 0.983, even higher than the correlation of 0.951 we found for all 9 points.

Since the results of our whole analysis are only preliminarily encouraging, evidently at present one should not attach much significance to this more refined feature of the strengthening of the correlation at higher energies. It is however a useful exercise to contemplate it. In particular, it is interesting that more than one of the issues mentioned in this section could be responsible for such a feature. We already stressed that neutrino splitting is expected to produce something of this sort, with the correlation becoming stronger at higher energies. Also the presence of background neutrinos could produce such a feature, since surely background neutrinos are more abundant at lower energies. Moreover, the same feature could also be produced accidentally even in absence of neutrino splitting and in absence of background neutrinos, as a result of the fact that for most of our candidate GRB neutrinos the redshift of the relevant GRB is to a large extent unknown (effectively introducing a possibly large uncertainty in the values attributed to $|\Delta t^*|$). We want to give support to this later claim within a simplified analysis: we assume $\eta_+ + \eta_- = 0$, which is reasonably consistent with the fact that in Fig. 4.2 one sees about an equal number of candidate "early neutrinos" and candidate "late

neutrinos", and we further restrict our attention to the case $\delta_+ = \delta_-$, so that we must only be concerned with the parameters η_+ and δ_+ (with then $\eta_- = -\eta_+$, $\delta_- = \delta_+$). We want to see if, adopting these restrictions, one could reasonably describe the features shown in Fig. 4.2 exclusively in terms of Eq. 4.1 and taking into account the uncertainties on GRB redshifts, without allowing for neutrino splitting and without making room for any contribution by background neutrinos.

As a first step we make the further optimistic assumption that the estimates of GRB redshifts given in table 1 are exact, and that points in Fig. 4.2 fail to be on a straight line exclusively because of the effects of the parameter δ_+ (and δ_-, with $\delta_- = \delta_+$). We observe that then one has a rather good fit with $|\eta_+| = 22 \pm 2$ and $\delta_+ = 6 \pm 2$.

Next we perform a Bayesian analysis to derive posterior distributions of unknown parameters. We handle as unknown parameters not only the parameters of our model, $|\eta_+|$ and δ_+, but also the standard deviation δz of the normal distribution that we tentatively assume to describe the redshift distribution of long GRBs observed also in neutrinos. As mean value of this normal distribution we take 1.497, following the argument discussed in the previous section. For the redshift distribution of short GRBs observed also in neutrinos (which is relevant for only one of our GRB-neutrino candidates) we simply assume a normal distribution with mean value 0.6 and standard deviation of 0.2. In order to evaluate the marginalized posterior probability density functions of the parameters $|\eta_+|$, δ_+ and δz we use the Markov chain Monte Carlo technique, with uniform priors with ranges $0 \leq |\eta_+| \leq 50$, $0 \leq \delta_+ \leq 10$ and $0 \leq \delta z \leq 1$. Uncertainties for the energies of the neutrinos (see Ref. [3]) were also taken into account. This Bayesian analysis determines δz to be $\delta z = 0.45 \pm 0.17$, and for the parameters of our model gives $|\eta_+| = 23 \pm 2$, $\delta_+ = 4.7 \pm 1.5$, which is consistent with what we had concluded in the previous paragraph ($|\eta_+| = 22 \pm 2$, $\delta_+ = 6 \pm 2$) on the basis of more simple-minded considerations.

The fact that this analysis assigns a relatively small value to δ_+ and a relatively small value to δz implies that the presently available data could be described within the model here adopted even without advocating a role for background neutrinos and/or for neutrino splitting. This of course may well change as more data are accumulated by IceCube, particularly if the feature of sharper correlation at higher energies becomes more pronounced.

Chapter 5

Probing quantum-gravity-induced dual lensing with IceCube neutrinos

As discussed in Sec.1.2.2 it was recently realized [70, 29, 100, 25] that typically curvature of momentum space also produces, in addition to dual redshift (or in-vacuo dispersion), the effect of "dual lensing", which affects the direction of detection: just like ordinary spacetime-curvature lensing, with dual lensing the direction by which a particle is detected might not point to where actually the source is located.

While dual redshift has been much studied and is at this point rather well understood, for dual lensing there have been so far only a few exploratory studies and several grey areas remain for its understanding. The few toy models which have been shown to exhibit it [70, 29, 100, 25] are probably not representative of the variety of possibilities one should consider for dual lensing in the quantum-gravity realm. Correspondingly there is nothing much on model building for dual lensing in phenomenology. Aware of these challenges, in this chapter, we nonetheless explore the possibility that dual lensing might play a role in observations by the IceCube neutrino telescope.

In the previous chapter we observed that allowing for dual redshift one gets a rather plausible picture in which some of the neutrinos observed by IceCube actually are GRB neutrinos. We here explore the possibility that also dual lensing might play a role in the analysis of IceCube neutrinos. In doing so we investigate issues which are also relevant for more refined analyses of dual redshift, such as the possibility of estimating the contribution by background neutrinos and some noteworthy differences between candidate "early neutrinos" and candidate "late neutrinos". We shall here adopt an exploratory attitude. The key point for us is just to explore the issue that GRB neutrinos might not be identified as such both because of time-of-arrival effects (dual redshift) and directional effects (dual lensing).

This chapter is organized as follows: in Sec. 5.1 we try to estimate the number of background neutrinos among our GRB-neutrinos candidates found in the previous chapter. Then in Sec. 5.2 we probe the effect of dual lensing assuming that the directional uncertainty of the neutrinos has received an additional energy-independent contribution. Finally in Sec. 5.3, adopting the strategy of analysis of the previous

chapter, we differentiate between early neutrinos (neutrinos observed before the relevant GRB) and late neutrinos (neutrinos observed after the relevant GRB).

5.1 Background neutrinos and dual lensing

In the previous chapter the directional analysis was limited to the requirement that the pair composed by the neutrino and the GRB should be at angular distance compatible within a 2σ region. It is however interesting that (as one can easily check from the useful tools provided by the IceCube collaboration[1] and from the Appxs. A and B) for only 2 of our 9 GRB-neutrino candidates the pair composed by the neutrino is at angular distance compatible within one σ. The 2 relevant GRB-neutrino candidates are IC9/GRB110503A and IC40/GRB130730A. It is interesting to contemplate this fact taking as working assumption, just for the sake of this exercise, that the model we are considering is correct, and therefore there are GRB neutrinos of the type here considered. If our 9 GRB-neutrino candidates were all "signal" neutrinos, and if the directional uncertainties were correctly estimated, we should expect 6 or 7 candidates at one sigma (since there are 9 candidates at 2 sigma). Finding 2 instead of 6 or 7 could be significant.

In part this can be blamed on our selection criteria: for cases in which for one neutrino there was more than one GRB possibly associated to it we handled the multiplicity by selecting the maximum-correlation option, as explained above. We could have used the maximum correlation criterion only at a lower level of selection, giving priority instead to GRB-neutrino candidates such that the pair composed by the neutrino and the GRB is at angular distance compatible within one σ. However, if this alternative criterion had been adopted only 1 of our 9 candidates would be affected: we would select IC42/GRB131119A instead of IC42/GRB131118A, with the end result that 3 out of the 9 candidates would have direction compatible at one sigma.

Having 3 at one sigma out of 9 at two sigmas is still not very satisfactory. However, there are at least two possible explanations:

(i) We surely have some background neutrinos among our candidates and if, say, 4 of the 9 are background then one would be in the situation of having 3 out of 5 signal neutrinos with direction acceptable at one sigma, which is satisfactory.

(ii) Dual lensing could be responsible: the low number of GRB-neutrino candidates "at one sigma" would be expected if there is a sizable mismatch between the apparent direction of observation of the neutrino and the actual direction pointing to its source.

In this section we mainly explore the first hypothesis, (i), while the next section is focused on the second hypothesis.

5.1.1 Estimating background

In light of the observations reported at the beginning of this section it is of paramount importance to have at least a rough estimate of how many of our 9 GRB-neutrino candidates should be expected to be background. For this purpose it is useful

[1] See at http://grbweb.icecube.wisc.edu/

to notice that out of the 21 neutrinos in our sample only 9 turned out to fit our requirements for GRB-neutrino candidates. We have therefore 12 neutrinos which are background in both of the scenarios we are comparing: if all 21 neutrinos are background of course also those 12 are background, and even if some of the neutrinos are GRB neutrinos of the type we are contemplating we find that those 12 still must be interpreted as background.

We can therefore ask how likely it would have been for one or more of those 12 neutrinos to accidentally appear to be GRB neutrinos of the type we are looking for. This can be estimated by randomizing the times of those 12 neutrinos. Of course, if, say, it is likely that 4 of those neutrinos could appear as GRB neutrinos, we will assume that a proportionate number of our 9 GRB-neutrino candidates are background. It is evidently an estimate to be performed by self-consistence: one starts with 12 neutrinos which are surely background, but then one is led to increase the estimated number of background neutrinos, since the analysis itself suggests that also some of our 9 GRB-neutrino candidates actually are background.

Among the results obtained applying this logic of analysis, randomizing the times of the 12 sure-background neutrinos, we stress in particular that there is a probability of 66% that 3, 4 or 5 of our 9 GRB-neutrino candidates are background (19% that 3 of them are background, 26% that 4 of them are background, and 21% that 5 of them are background). This by itself renders already less surprising the fact that we have only 3 GRB-neutrino candidates at one sigma, with 6 more at two sigmas: it may well be that the 3 at one sigma are all signal, while, say, 4 of the remaining 6 are background.

5.1.2 Overachieving background neutrinos

The fact that it is very likely that 3, 4 or 5 of our 9 GRB-neutrino candidates actually are background renders the "directional story" of our analysis less surprising, but in turn brings up some questions concerning the very high correlation we found in the previous chapter. We have a monstrous correlation of 0.951 for our 9 GRB-neutrino candidates even though very likely 4 or 5 of them are background! In the corresponding sense our 9 candidates overachieved.

It is interesting to estimate at least roughly by how much our 9-plet overachieved. Let us do that by taking as reference the case that 4 among our 9 GRB-neutrino candidates are background. We can then exploratively assume that the 5-plet of "true" GRB neutrinos is the maximum-correlation 5-plet among the 5-plets obtainable from our 9 candidates. These are IC9/GRB110503A, IC19/GRB111229A, IC40/GRB130730A, IC26/GRB120219A, IC33/GRB121023A. Accordingly we would have that the remaining four, IC11/GRB110531A, IC42/GRB131118A, IC12/GRB110625B, IC2/GRB100605A, are background. But these remaining four still contribute rather strongly to the correlation: the correlation of 0.9996 of the maximum-correlation 5-plet is only decreased to 0.951 when we include all 9 candidates. Within the assumptions we are making this means that the 4 background neutrino "overachieved", *i.e.* they did not behave like standard background neutrinos, but rather, accidentally, looked like signal neutrinos. We can quantify this overachievement by randomizing the times of detection of IC11/GRB110531A, IC42/GRB131118A, IC12/GRB110625B, IC2/GRB100605A (keeping the times of detection of the other

5 neutrinos fixed) and seeing what is the expected value of correlation. This value is 0.903. Interestingly if we take as reference the value of correlation of 0.903 the corresponding false alarm probability, computed just as prescribed in the previous chpater, is of 0.21% (still very small but significantly higher than the false alarm probability of 0.03% one estimates ignoring this issue of the overachieving background neutrinos).

When taking as working assumption a certain number of background neutrinos it makes sense to compute a false alarm probability defined in a slightly different way from the one introduced in the previous chapter. We introduce this notion focusing again, for illustrative purposes, on the case in which one takes as working assumption that 4 among our 9 GRB-neutrino candidates are background, then computing for the true data the maximum value of correlation obtainable by considering 5 out of our 9 candidates (the highest value of correlation found among the 126 possible 5-plets of candidates obtainable from our total of 9 candidates). We can define a false alarm probability based on how frequently simulated data, obtained by randomizing the times of detection of the 21 neutrinos in our sample, include a 5-plet of candidates with correlation greater or equal to the one found for the best 5-plet in the real data (so, if, say, a given time randomization produces 11 candidates one assigns to the randomization a value of correlation given by the highest correlation found by considering all possible choices of 5 out of the 11 candidates). We find that this false alarm probability is of 0.16%.

5.2 Probing the possible presence of dual lensing

In the previous section we showed that the "directional story" of our analysis is not so surprising in light of a plausible estimate of the role played by background neutrinos. Since probably 4 or 5 of our 9 candidates are background neutrinos that only accidentally we selected as candidates, it is not surprising that only 2 (3 with another criterion discussed above) candidates are "at one sigma" among the total of 9 candidates that we have "at two sigmas". This renders less compelling the hypothesis that dual lensing might have payed a role, but of course, one may nonetheless explore the possible role of dual lensing. We shall do this knowing that, as the interested reader will easily realize, analyses such as ours would be affected tangibly by dual lensing only if rather large directional mismatches are produced, at least as large as a few degrees. We find it hard to believe that a quantum-gravity effect could be this large, but of course we still rely on data rather than prejudice to investigate the issue.

As shown in Sec.1.2.2 the magnitude of dual lensing will likely depend on the energy of the particle [70, 29, 100, 25]; however, for this exploratory study we shall be satisfied with a rudimentary and limited description of dual lensing: we shall simply assume that the directional uncertainty of the neutrinos, for which we used above the notation σ_ν, receives an additional energy-independent contribution $\sigma_{d.l.}$,

$$\sigma_\nu \to \sigma'_\nu = \sigma_\nu + \sigma_{d.l.}$$

We are therefore adopting a rudimentary description of dual lensing which is energy

independent and is of "fuzzy type" (non-systematic), so that Eq. 4.5 is replaced by

$$\sigma' = \sqrt{\sigma_{GRB}^2 + (\sigma_\nu + \sigma_{d.l.})^2}\,, \tag{5.1}$$

We only consider a few values of $\sigma_{d.l.}$, specifically 5, 10, 15 and 20 degrees. With more data it would make sense to probe $\sigma_{d.l.}$ more finely, but in the present situation this is evidently sufficient. What we are looking for is establishing whether or not the additional GRB-neutrino candidates picked up by allowing for $\sigma_{d.l.}$ manifest any connection with the 9 GRB-neutrino candidates we had in Chap. 4. We select candidates just as discussed in Sec. 4.2, but now replacing the σ of Eq. 4.5 with the σ' of Eq. 5.1, for the few mentioned values of $\sigma_{d.l.}$. We find that for $\sigma_{d.l.} = 5$ degrees one picks up 2 additional GRB-neutrino candidates in addition to the 9 candidates we already had for $\sigma_{d.l.} = 0$. These two "dual-lensing candidates" selected with with $\sigma_{d.l.} = 5$ degrees are IC39/GRB130707A and IC46/GRB140129C. The correlation of our original 9 candidates was 0.951 and with addition of IC39/GRB130707A and IC46/GRB140129C the correlation goes down to 0.830. The fact that the correlation goes down does not in itself provide an indication against dual lensing, since 0.830 is still a very high value. The relevant issue for assessing the "performance of dual lensing" concerns whether these 2 additional candidates "look like background" or rather appear to be in reasonably good agreement with the 9 candidates we already had. For luck of a better name we shall label this as the "variation probability". While it is intuitively clear what one intends to characterize with such a variation probability, there are, as we shall see, at least a couple of possibility for its definition that one should consider. Let us start by estimating a variation probability by randomizing the times of the 12 IceCube neutrinos not involved in our original 9 candidates, and seeing how frequently one picks up extra candidates, by allowing for $\sigma_{d.l.}$ of 5 degrees, such that the overall correlation is of 0.831 or higher. We find that this "variation probability" is 35%, providing an indication which is (however mildly) favorable for the dual-lensing hypothesis with $\sigma_{d.l.} = 5$ degrees: if the 12 relevant neutrinos are all background then in 65% of cases one would expect to find a correlation lower than 0.831. An alternative definition of the variation probability could fix the number of "dual-lensing candidates" found in simulations: one would randomize the times of the 12 IceCube neutrinos not involved in our original 9 candidates, and focus on cases when such randomizations produce a number of dual-lensing candidates equal to the number of dual-lensing candidates found on true data. We shall label this second notion of variation probability as the "fixed-number variation probability", and we find that for $\sigma_{d.l.}$ of 5 degrees, this fixed-number variation probability is of 69%, which is evidently less encouraging for dual lensing. The main reason for contemplating the possibility of fixing the number of dual-lensing candidates in simulations to be equal to the number of dual-lensing candidates found in true data is that we are focusing on variations of the correlation and the typical size of such variations depends of course on how many additional candidates contribute. Starting with 9 candidates, if we only add, say, one more candidate the variation typically will be small, significantly smaller than what one typically should find for cases with, say, 5 additional candidates.

Next we consider the case $\sigma_{d.l.} = 10$ degrees, finding that in that case one picks up 3 additional GRB-neutrino candidates in addition to the 9 candidates we already

had for $\sigma_{d.l.} = 0$, one more, which is IC22/GRB120114B, in addition to the 2 already found for $\sigma_{d.l.} = 5$ degrees. For the total of 12 GRB-neutrino candidates selected for $\sigma_{d.l.} = 10$ degrees one has correlation of 0.770. Moreover we find a variation probability of 45% by randomizing the times of the 12 IceCube neutrinos not involved in our original 9 candidates, and seeing how frequently one picks up extra candidates, by allowing for $\sigma_{d.l.}$ of 10 degrees, such that the overall correlation is of 0.770 or higher. A variation probability of 45% is not at all encouraging: it just means that overall the extra candidates picked up for $\sigma_{d.l.} = 10$ degrees behaves just like typically one would expect pure background to behave. This is confirmed by computing the fixed-number false alarm probability, which turns out to be of 73%.

For $\sigma_{d.l.} = 15$ degrees and $\sigma_{d.l.} = 20$ degrees one gets a picture very similar to what we just reported for $\sigma_{d.l.} = 10$ degrees, not favorable to dual lensing. For $\sigma_{d.l.} = 15$ degrees one picks up one more candidate, which is IC30/GRB120709A, and the candidate IC39/GRB130705A, selected already at $\sigma_{d.l.} = 5$ degrees, is replaced [2] by IC39/GRB130707A; the correlation for the total of 13 candidates is 0.767, giving a variation probability of 44% (and a fixed-number variation probability of 72%). At $\sigma_{d.l.}$ of 20 degrees one picks up 4 more candidates, for a total of 17 (the 9 candidates we already had for $\sigma_{d.l.} = 0$, the 4 other candidates we had already picked up going up to $\sigma_{d.l.} = 15$ degrees, plus 4 more candidates). The correlation for this 17 candidates is 0.716, giving a variation probability of 62% (and a fixed-number variation probability of 67%).

5.3 Differentiating between early neutrinos and late neutrinos

We have so far, like in the previous chapter, considered values of correlation between energy and the absolute value of Δt^*, thereby having a situation such that both early neutrinos (neutrinos observed before the relevant GRB) and late neutrinos (neutrinos observed after the relevant GRB) contribute on the same footing to the same correlation study. On the theory side this is relevant for scenarios in which, in the sense of our Eq. 4.1 (and of comments to Eq. 4.1 which we offered in Sec. 4.1), one has that[3] $\eta_+ \simeq -\eta_-$. A posteriori this found some motivation in the content of our data set, since we found about an equal number of early neutrinos and late neutrinos. However, we here argued that quite a few of our GRB-neutrino candidates (as many as 4 or 5 out of 9) are likely background and if these were mostly of one type (say, all late neutrinos) our perspective on the data could change significantly. This motivates us to also consider separately early neutrinos and late neutrinos.

In the next subsection we do this adopting the strategy of analysis of the previous chapter, which in particular required that the pair composed by the neutrino and

[2] As explained above and in the previous chapter, we are consistently using a criterion such that, when a given neutrino has available more than one GRB partner, the GRB-neutrino candidate is taken to be the one that maximizes the correlation. For the neutrino IC39 up to $\sigma_{d.l.} = 10$ degrees one has only one possible GRB partner, which is GRB130707A, but at $\sigma_{d.l.} = 10$ degrees one has that also GRB130705A becomes directionally compatible with IC39, and actually the candidate IC39/GRB130705A leads to higher correlation than IC39/GRB130707A.

[3] Evidently δ_+ and δ_- automatically do not discriminate between early and late neutrinos since they govern uncertainty-type effects.

the GRB should be at angular distance compatible within a 2σ region ($\sigma_{d.l.} = 0$). Then we also perform the same analysis making room for dual lensing, requiring that the pair composed by the neutrino and the GRB should be at angular distance compatible within a $2\sigma'$ region, for values of $\sigma_{d.l.}$ of 5, 10, 15 and 20.

5.3.1 Early and late neutrinos without dual lensing

So let us start by going back to $\sigma_{d.l.} = 0$, as in the previous chapter, but now looking separately at early neutrinos and late neutrinos. For the 21 IceCube shower neutrinos of energy between 60 and 500 GeV we ask that a potential GRB partner for a late (early) neutrino should be observed up to 3 days earlier (later) than the neutrino, and that the pair composed by the neutrino and the GRB should be at angular distance compatible within a 2σ region ($\sigma_{d.l.} = 0$).

We find 5 "early GRB-neutrino candidates", which we list in Table 5.1. Of course this is a subset of the content of Table 4.1. Fig. 5.1 illustrates these findings.

	E[TeV]	GRB	z	Δt^* [s]	
IC42	76.3	131118A	1.497 *	-98694	*
		131119A	?	-146475	
IC2	117.0	100605A	1.497 *	-75921	*
		100606A	?	-135456	
IC40	157.3	130730A	1.497 *	-120641	*
IC26	210.0	120224B	1.497 *	-117619	*
IC33	384.7	121023A	0.6 *	-289371	*

Table 5.1. This table uses the same conventions as Table 1, but includes exclusively early neutrinos.

For these 5 early neutrinos the correlation between energy and[4] $-\Delta t^*$ takes the very high value of 0.945. The resulting false alarm probability (computed as in the previous chapter but now focusing only on early neutrinos) is correspondingly very low, a false alarm probability of only 0.56%.

We of course redo the same exercise for late neutrinos. We find 7 "late GRB-neutrino candidates", which we list in Table 5.2, while Fig. 5.2 illustrates these findings.

For these 7 late neutrinos the correlation between energy and Δt^* takes the value of 0.502, which is still rather high, but significantly smaller than the one found for early neutrinos. Of course, in light of the estimates concerning background neutrinos offered above, this does not necessarily imply that the case for early neutrino is stronger than than for late neutrinos (as many as 3 or 4 of these 7 late neutrinos could be coherently interpreted as background, even if one took as working assumption the presence of dual redshift). Setting aside the possible role

[4]For early neutrinos it is natural to consider the correlation between energy and $-\Delta t^*$, since by changing the overall sign of Δt^* for early neutrinos one gets results more readily comparable to the ones obtained for the correlation between energy and Δt^* for late neutrinos.

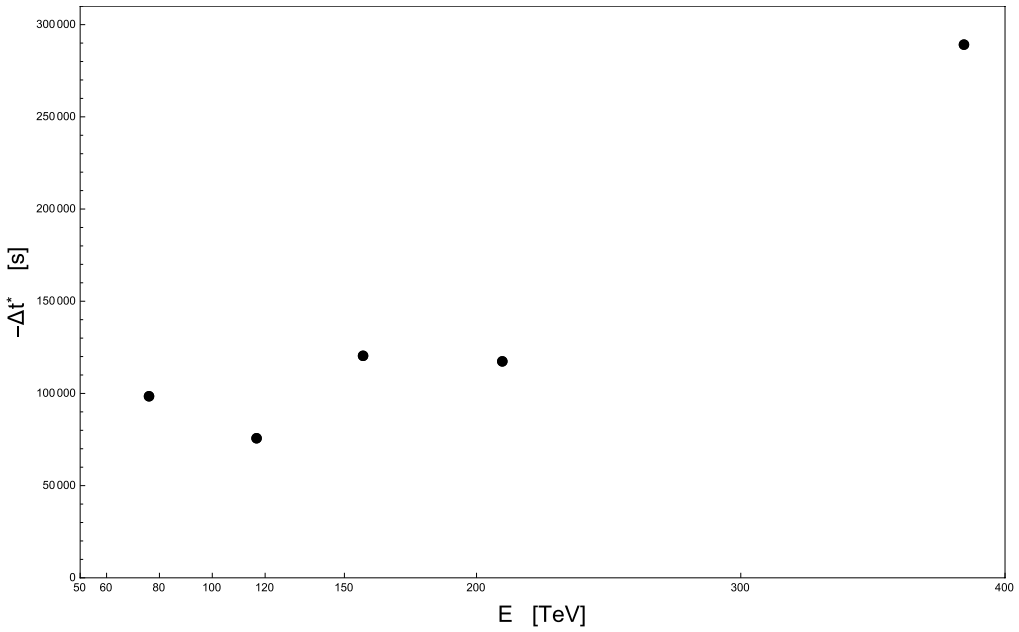

Figure 5.1. Points here in figure correspond to the 5 "early GRB-neutrino candidates" highlighted with an asterisk in the last column of Table 2.

of background neutrinos, one can observe that the resulting false alarm probability (computed as in the previous chapter but now focusing only on late neutrinos) is of 2.6%, indeed rather small but not as small as for the early-neutrino case.

We should also stress than when differentiating between early and late neutrinos one does not necessarily have to focus on one or the other, in the sense that some valuable information could be found also by searching for both early and late neutrinos while keeping track of their difference. This could be particularly valuable if η_+ and η_- have opposite sign and significantly different size (the effect for late neutrinos having different size from the effect for early neutrinos). In such a case one could compute separately the correlation found in late neutrinos, which one could denote by ρ_+, and the correlation found for early neutrinos, which one could denote by ρ_-, then probing the statistical significance of what one has found in terms of the product of these correlations. Let us be satisfied here illustrating this strategy of analysis for the candidates listed in table 1. First we address the issue of multiple candidate GRB partners for some of the neutrinos in table 1, by picking up the set of GRB-neutrino candidates that maximizes the product of ρ_+ and ρ_-. This leads to selecting as the 9 GRB-neutrino candidates 4 early neutrinos and 5 late neutrinos[5]. The resulting value of the product of correlations is $\rho_+ \cdot \rho_- = 0.812$ (with correlation of 0.981 for early neutrinos and of 0.828 for late neutrinos). We introduce a false alarm probability for this case by producing as usual simulated

[5]These 9 candidates selected with the criterion of maximizing the product $\rho_+ \cdot \rho_-$ differ from the 9 candidates with an asterisk in table 1 only in one respect: they include IC2/GRB100606A in place of IC2/GRB100605A.

	E[TeV]	GRB	z	Δt^* [s]	
IC9	63.2	110503A	1.613	50227	*
IC19	71.5	111229A	1.3805	53512	*
IC42	76.3	131117A	4.042	5620	*
IC11	88.4	110531A	2.345 *	124338	*
IC12	104.1	110625B	2.345 *	108061	*
IC2	117.0	100604A	2.345 *	10372	*
IC26	210.0	120219A	2.345 *	153815	*

Table 5.2. This table uses the same conventions as Table 1, but includes exclusively late neutrinos.

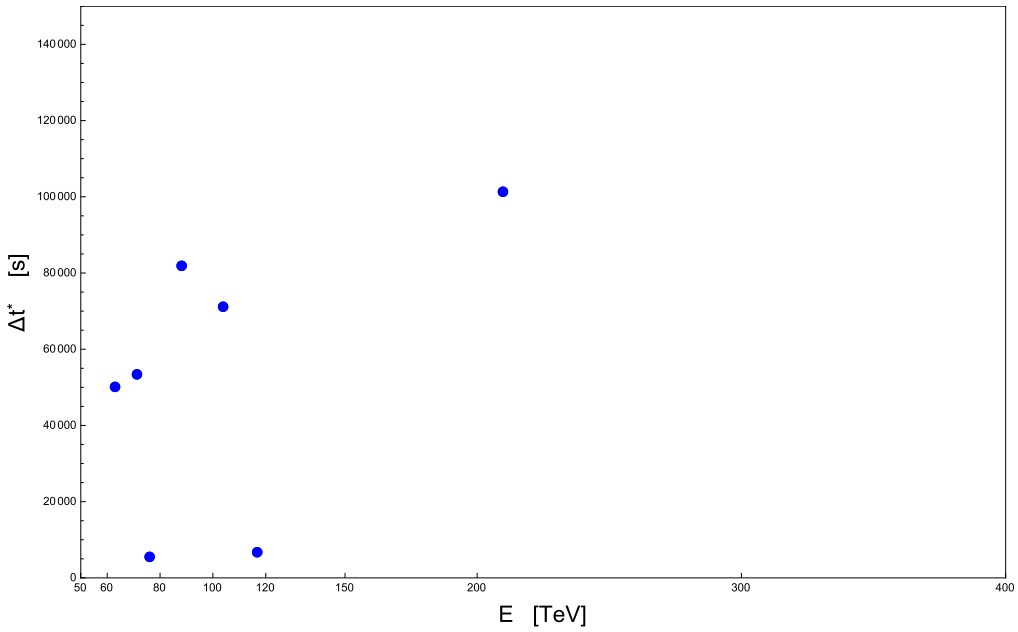

Figure 5.2. Points here in figure correspond to the 7 "late GRB-neutrino candidates" highlighted with an asterisk in the last column of Table 3.

data obtained by ramdomizing the times of observation of the 21 neutrinos in our sample (keeping as usual their energies and directions unchanged), and seeing how frequently such simulations have at least 4 early-neutrino candidates and at least 5 late-neutrino candidates, with the product of ρ_+ and ρ_- greater or equal to 0.812. We find that this false alarm probability is 0.11%.

5.3.2 Early neutrinos with dual lensing

Next we allow for dual lensing also for the analysis that focuses on early neutrinos. For $\sigma_{d.l.} = 5$ degrees and for $\sigma_{d.l.} = 10$ degrees one does not pick up any additional GRB-neutrino candidates. At $\sigma_{d.l.} = 15$ degrees one picks up a single additional early GRB-neutrino candidate, which is IC30/GRB120709A. This is a rather intriguing dual-lensing candidate: as shown in Fig. 5.3 it matches very naturally the 5 early-GRB-neutrino candidates we started with (for $\sigma_{d.l.} = 0$).

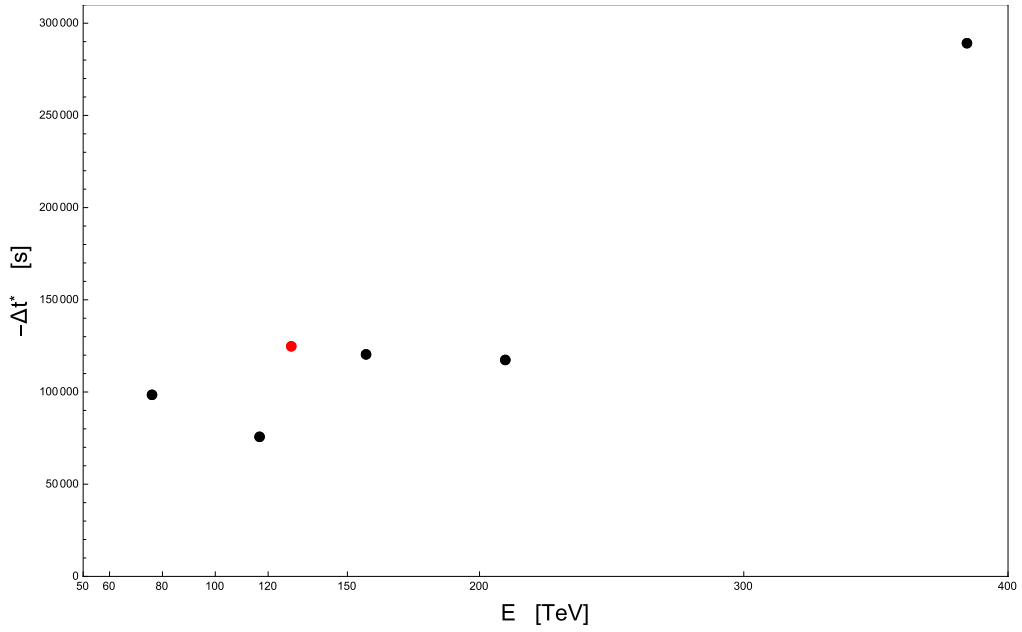

Figure 5.3. Here in figure we just highlight the noteworthy consistency between the "dual-lensing early neutrino candidate" (red) picked up at $\sigma_{d.l.}$ of 15 degrees and the 5 early-neutrino candidates (black) we already had without dual lensing ($\sigma_{d.l.} = 0$).

Indeed adding this 6th candidate IC30/GRB120709A to the 5 early-GRB-neutrino candidates we started with the correlation essentially remains unchanged: it changes from 0.945 to 0.937. Computing our variation probability for this case, we find that only in 1.0% of cases by randomizing the times of detection of the 12 neutrinos excluded at $\sigma_{d.l.} = 0$ one would get accidentally a value of correlation ≥ 0.937. Evidently this is of some (however tentative) encouragement for the hypothesis of dual-lensing for early neutrinos. Note however that this is a case where on true data we picked up only one dual-lensing candidate, and therefore the smallness of the variation of the correlation must be attribute not only to the good match between the dual-lensing candidate and the other candidates, shown in Fig. 5.3, but also to the fact that with only 1 dual-lensing candidate it is difficult to produce large variations of a correlation initially built out of 5 candidates. Simulations (obtained by time randomization for the 21 neutrinos in our sample) producing several dual-lensing candidates would lead to a larger variation of the correlation even if each of these

dual-lensing candidates was a reasonably good match to the original 5 candidates. Evidently this is a case where one should be particularly interested in checking the value of what we labeled as the "fixed-number variation probability", which we find to be of 39%. This value of 39% is still at least marginally encouraging for dual lensing of early neutrinos, since it means that in 61% of cases simulations producing one and only one dual-lensing candidate lead to values of correlation smaller than the value of 0.937 found in the analysis of the true data.

Increasing then $\sigma_{d.l.}$ to 20 degrees the numbers are even less intriguing. For $\sigma_{d.l.} = 20$ degrees one picks up two more candidates, which are IC51/GRB140414B and IC22/GRB120118A, and one has a correlation of 0.826 for the total of 8 early-GRB-neutrino candidates (the 5 candidates we already had for $\sigma_{d.l.} = 0$, the additional candidate picked up at $\sigma_{d.l.} = 15$ degrees, plus the 2 additional candidates picked up at $\sigma_{d.l.} = 20$ degrees). The corresponding variation probability is 18%, while the fixed-number variation probability is 59%.

5.3.3 Late neutrinos with dual lensing

Next we allow for dual lensing for the analysis that focuses on late neutrinos. Something intriguing is immediately found by allowing for $\sigma_{d.l.}$ of 5 degrees. One picks up two additional GRB-neutrino candidates, which are IC39/GRB130707A and IC46/GRB140129C. Adding these 2 dual-lensing candidates to the 7 late-neutrino candidates we started with (for $\sigma_{d.l.} = 0$) one has a total of 9 candidates for which the correlation between energy and Δt^* is of 0.544, actually higher than the correlation of 0.502 which we started with, for the 7 late-neutrino candidates already picked up at $\sigma_{d.l.} = 0$. This is of course the type of quantitative behavior that supporters of dual lensing would want to see. In this particular case its significance is not very high, mainly as a result of the fact that we started with a value of correlation, for $\sigma_{d.l.} = 0$, which was not very high (0.502), so it is not too difficult to pick up background neutrinos that accidentally look like dual-lensing candidates producing an increase of the correlation. Indeed computing our variation probability for this case, we find that in 19% of cases by randomizing the times of detection of the 12 neutrinos excluded at $\sigma_{d.l.} = 0$ one would get accidentally a value of correlation ≥ 0.544. As done in other analogous situations, we also consider more prudently the fixed-number variation probability, which in this case comes out to be of 25%. So focusing on late neutrinos and $\sigma_{d.l.}$ of 5 degrees both in terms of our variation probability and in terms of our fixed-number variation probability one finds that the true data are a bit more consistent with the dual-lensing hypothesis than one would typically expect assuming instead that all neutrinos in our sample are background.

At $\sigma_{d.l.} = 10$ degrees one picks up a single additional late GRB-neutrino candidate, which is IC22/GRB120114B, so the total number of candidates goes up to 10, and the corresponding 10-candidate correlation is of 0.404 (lower than the 9-candidate correlation found at $\sigma_{d.l.} = 5$ degrees and actually also lower than the 7-candidate correlation we started with at $\sigma_{d.l.} = 0$). Computing our variation probability for this case, we find that at $\sigma_{d.l.} = 10$ degrees in 39% of cases by randomizing the times of detection of the 12 neutrinos excluded at $\sigma_{d.l.} = 0$ one would get accidentally a value of correlation ≥ 0.404. The corresponding value of the fixed-number variation probability is of 46%. Evidently the (however moderate) encouragement for dual

lensing for late neutrinos found at $\sigma_{d.l.} = 5$ degrees vanishes already at $\sigma_{d.l.} = 10$ degrees.

At $\sigma_{d.l.} = 15$ degrees one does not pick up any additional late GRB-neutrino candidate, so one still has 10 candidates with correlation of 0.404. Recomputing the variation probability for this case (with $\sigma_{d.l.} = 15$ degrees in the time-randomization analysis) one finds for it the value of 37%. The corresponding value of the fixed-number variation probability is of 53%. So nothing much changes for the dual-lensing late-neutrino analysis in going from $\sigma_{d.l.} = 10$ degrees to $\sigma_{d.l.} = 15$ degrees.

Finally increasing $\sigma_{d.l.}$ to 20 degrees one picks up 4 more candidates, for a total of 14, the correlation goes down to 0.317, the variation probability is of 48%, and the fixed-number variation probability is also 48%.

5.4 Strategy for future analyses

This is the first ever truly quantitative phenomenological study centered on dual lensing, which in itself should be viewed as an added value of the analysis exposed in the previous chapter. Indeed previous studies of dual lensing had mostly focused on the conceptual issues that still need to be addressed for its full understanding [70, 29, 100, 25]. In this chapter we essentially showed that these open conceptual issues do not obstruct the way for initiating an associated phenomenological program. Actually we would argue that progress in this phenomenological effort needs most urgently not necessarily some theory work, but rather data of improved quality. For example, if the sample of high-energy neutrinos at our disposal had been larger we could have probed dual lensing more finely, making room in particular for the expected energy dependence of the "dual-lensing angle".

Because of these limitations concerning the quality of data, we expected this study to turn into a merely academic exercise, just introducing techniques of analysis that might be valuable once indeed the quality of data improves. What we ended up finding goes somewhat beyond the merely academic exercise, even though it is evidently just barely enough to provide motivation for future related studies. One might want to take notice in particular of the fact that our analysis of early neutrinos found for dual-lensing angle of 15 degrees a result which is encouraging, though rather weakly. Similar remarks would apply to our findings for late neutrinos at dual-lensing angle of 5 degrees. Moreover, it is intriguing that these results providing (however weak) encouragement for dual lensing were exclusively found for small dual-lensing angles. For dual-lensing angle of 20 degrees all our results provide no encouragement for dual lensing. Whether or not this difference between findings at smaller dual-lensing angles and findings at larger dual-lensing angles is accidental (it is a quantitatively small difference anyway), it serves us well in illustrating how in principle one could use an analysis such as ours not only to possibly establish the presence of dual lensing, but also to estimate its magnitude.

We also believe that some of the observations and results we here reported will indeed be valuable also for studies assuming that dual lensing is absent, as we anticipated in our opening remarks. Estimating background for such studies is particularly challenging, and the strategy for estimating background here proposed in Sec. 5.1.1 is a valuable step toward that goal. Moreover we here introduced 3

levels of analysis which we feel should become a standard for similar studies, the level of the correlation for all neutrinos between energy and $|\Delta t^*|$, the level of the correlation exclusively for late neutrinos between energy and Δt^*, and the level of the correlation exclusively for early neutrinos between energy and $-\Delta t^*$.

Chapter 6

In-vacuo-dispersion features for GRB photons

For more than a decade the analyses of GRB data from the in-vacuo-dispersion perspective were done considering only photons and focusing on what could be tentatively inferred from each single GRB. Recently, thanks mainly to the IceCube telescope, it became possible to contemplate, as done Chaps. 4 and 5, the possibility that we might be observing also some GRB neutrinos affected by in-vacuo dispersion; moreover, for GRB photons the abundance of observations cumulatively obtained by the Fermi telescope reached the level sufficient for attempting to perform statistical analyses over the whole collection of Fermi-observed GRBs. Intriguing statistical analyses of in-vacuo dispersion over the whole collection of Fermi-observed GRBs were perfomed in a series of studies by Bo-Qiang Ma and collaborators [138, 136, 135]. The neutrino studies reported in the previous chapters led to exposing a feature in the IceCube neutrino data which could plausibly be a manifestation of in-vacuo dispersion. The possibility that this feature could be the result of background neutrinos just accidentally arranging themselves as if they were GRB neutrinos affected by in vacuo dispersion was considered using statistical tools of analysis, finding that it would be "very untypical" for background neutrinos to produce accidentally such a pronounced in-vacuo dispersion feature. The GRB-photon studies reported in Refs. [138, 136, 135] also led to exposing a feature which could be a manifestation of in-vacuo dispersion. While this feature for GRB photons is certainly striking, as observed most convincingly in Ref. [135], there was so far no attempt to characterize quantitatively its statistical significance.

The main objective of this chapter is to characterize the statistical significance of the feature exposed in Refs. [138, 136, 135] for photons, and to show that this feature is surprisingly consistent with the feature exposed in the previous chapters for neutrinos of much higher energies (the relevant photons have energies of the order of 10 GeV, while the neutrinos have energies of the order of 100 TeV). We also offer some preliminary observations which might become relevant if any of the features here contemplated find greater support as more data are accrued, concerning the possible interpretation of such features as manifestations of (so far unknown) astrophysical mechanisms, rather than as manifestations of in-vacuo dispersion.

6.1 Modeling quantum-gravity-induced in-vacuo dispersion

Following Refs. [138, 136, 135], we find convenient to introduce a "distance-rescaled energy" E^* defined as [1]

$$E^* \equiv E\frac{D(z)}{D(1)} \tag{6.1}$$

so that Eq. 4.1 can be rewritten as

$$\Delta t = \eta_X D(1)\frac{E^*}{M_P} \pm \delta_X D(1)\frac{E^*}{M_P}\,. \tag{6.2}$$

This reformulation of Eq. 4.1 allows to describe the relevant quantum-spacetime effects, which in general depend both on redshift and energy, as effects that depend exclusively on energy, through the simple expedient of focusing on the relationship between Δt and energy when the redshift has a certain chosen value, which in particular we chose to be $z = 1$. If one measures a certain Δt and the redshift z of the relevant GRB is well known, then one gets a firm determination of E^* by simply rescaling the measured E by the factor $D(z)/D(1)$. And even when the redshift of the relevant GRB is not known accurately one will be able to convert a measured E into a determined E^* with accuracy governed by how much one is able to still assume about the redshift of the relevant GRB. In particular, even just the information on whether a GRB is long or short can be converted into at least a very rough estimate of redshift.

Eq. 6.2, which follows the strategy of analysis proposed in Refs. [138, 136, 135], is ideally structured to handle the possibility that there be a (roughly) systematic time offset at emission between the time of emission of the low-energy particles used as reference (we shall later take as reference the time of observation of the first peak of the low-energy-gamma-ray component of a GRB) and the higher-energy particle of interest. Such an astrophysical mechanism for time offset at the source, would imply, within the modelization we are assuming for the quantum-spacetime effects, that Δt is not exactly proportional to E^*, since the observed Δt would receive both a contribution from the quantum-spacetime effects given by the right-hand side of Eq. 6.2 and a contribution due to the time offset at the source. This latter contribution can be described as $(1 + z)t_{off}$, where t_{off} is the time offset at the source and the factor $(1 + z)$ takes into account time dilatation. Following Refs. [138, 136, 135] these observations can be fruitfully used to replace Eq. 6.2 with

$$\frac{\Delta t}{1+z} = t_{off} + \frac{\eta_X}{M_P}D(1)\frac{E^*}{(1+z)} \pm \frac{\delta_X}{M_P}D(1)\frac{E^*}{(1+z)}\,. \tag{6.3}$$

[1] While here and in Refs. [138, 136, 135] the analysis is set up in terms of correlations between Δt and a "distance-rescaled energy" E^*, in the previous chapters, which focused on neutrinos, the analysis was set up in terms of correlations between energy and a "distance-rescaled time delay" Δt^*. The two setups are evidently equivalent, but the one we adopt here is best suited for handling the possibility of a (roughly-)systematic time offset at the source (see later). For the values of Δt that are relevant for the neutrino part of the analysis this possibility of a time offset has a negligible role, and therefore the two setups are actually equally convenient, but for part of the analysis based on photons it is advantageous to set up the analysis in terms of correlations between Δt and a "distance-rescaled energy" E^*.

Notice that in allowing for the mentioned possibility of a time offset at the source we also found appropriate to set up our equation as a relationship between $\frac{\Delta t}{1+z}$ and $\frac{E^*}{(1+z)}$, so that the term involving t_{off} is just a constant contribution, redshift independent and energy independent. Later, in our graphs showing $\frac{\Delta t}{1+z}$ versus $\frac{E^*}{(1+z)}$, this will facilitate the visualization of t_{off}. We stress that here, just like in Refs. [138, 136, 135], we shall not allow for different values of t_{off} for different photons[2]. We just allow for one value of t_{off} valid for all photons of all GRBs in the analysis, and we shall show that the present data situation fits rather nicely this apparently simplistic assumption.

6.2 Summary of previous analysis of GRB-neutrino candidates in terms of E^*

As stressed above, the main objective of the study we are here reporting is to characterize the statistical significance of the in-vacuo-dispersion feature exposed in Refs.[138, 136, 135] for photons, and to show that this feature is surprisingly consistent with the feature exposed in the previous chapters for neutrinos. For this reason, we here arrange the quantitative characterization of the statistical significance of the in-vacuo-dispersion feature found for neutrinos in Chap. 4, in which the analysis was arranged in terms of correlations between energy and a "distance-rescaled time-of-arrival difference" Δt^* (see Eq. 4.1). These two arrangements of the analysis are evidently equivalent for the neutrino case [3], but it is a good preparation for the later discussion of the photon case to have the discussion of neutrinos arranged in terms of correlations between $\Delta t/(1+z)$ and $E^*/(1+z)$.

In Table 6.1 and Fig. 6.1 we report in terms of $\Delta t/(1+z)$ and $E^*/(1+z)$ the properties of the 9 GRB-neutrinos candidates (see Chap. 4) that are most relevant for our analysis.

In Fig. 6.1 it is striking that the correlation between $|\Delta t|/(1+z)$ and $E^*/(1+z)$ gets stronger at higher energies. Interestingly, as observed in Chap. 4, this too fits the expectations of some quantum-spacetime models: as stressed in particular in Ref.[124], in some of these quantum-spacetime models neutrinos can undergo processes of "neutrino splitting", and in turn this could plausibly (see Chap. 4) affect a in-vacuo-dispersion study such as ours just in the way of rendering the correlation weaker at lower energies. While this was worth mentioning, we shall here prudently not take it into account: we shall ignore neutrino splitting and handle all our 9 GRB-neutrino candidates on the same footing.

The correlation between $|\Delta t|/(1+z)$ and $E^*/(1+z)$ for the 9 GRB-neutrino candidates highlighted in Fig. 6.1 is of[4] 0.866. This is a strikingly high value of

[2]The interested reader can easily see that by allowing different values of t_{off} for different photons one could never test the in-vacuo-dispersion hypothesis, since any measured value of Δt could always be attributed to a corresponding value of t_{off} at the source.

[3]The two arrangements of the analysis are completely equivalent for our neutrinos, since for them the hypothesis of a time offset at the source is irrelevant, as we shall soon observe. For photons, were a time offset at the source could have tangible consequences, it is truly convenient (as first observed in Refs. [138, 136, 135]) to arrange the analysis in terms of correlations between $\Delta t/(1+z)$ and $E^*/(1+z)$.

[4]In Chap. 4, where the correlation study was arranged for energy versus a time-of-observation

	E[TeV]	E^*[TeV]	Δt [s]	z	GRB	
IC9	63.2	101.1	80335	1.613	110503A	*
IC19	71.5	98.5	73960	1.3805	111229A	*
IC42	76.3	273.3	20134	4.042	131117A	
		113.6	-146960	1.497 *	131118A	*
		?	-218109	?	131119A	
IC11	88.4	131.7	185146	1.497 *	110531A	*
IC12	104.1	155.0	160909	1.497 *	110625B	*
IC2	117.0	?	15445	?	100604A	
		174.2	-113051	1.497 *	100605A	*
		?	-201702	?	100606A	
IC40	157.3	234.3	-179641	1.497 *	130730A	*
IC26	210.0	312.8	229039	1.497 *	120219A	*
		?	-175141	?	120224B	
IC33	384.7	227.4	-171072	0.6 *	121023A	*

Table 6.1. Same for Table 4.1, but here we report the values of the Δt and E^* defined in the main text.

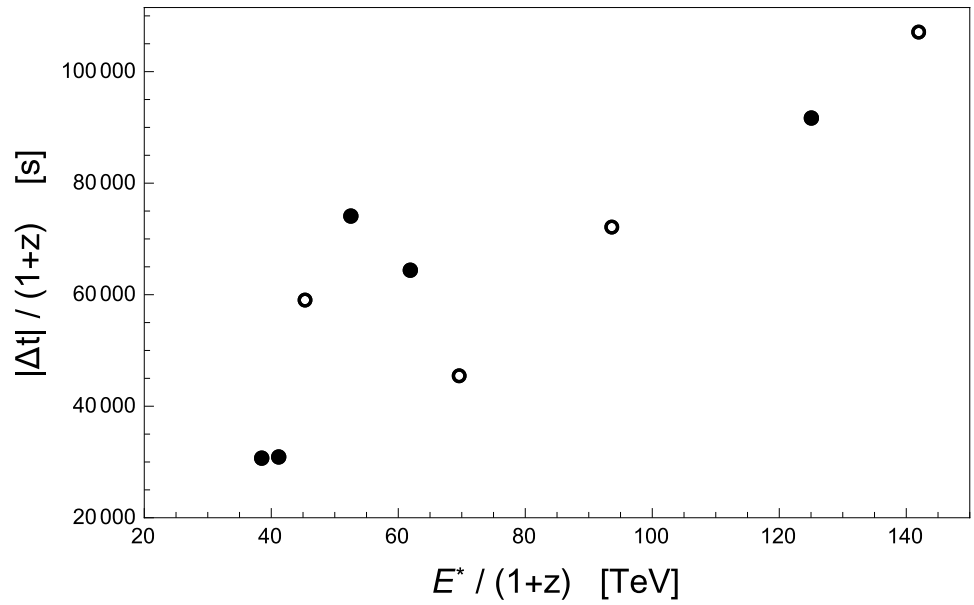

Figure 6.1. Points here in figure correspond to the 9 GRB-neutrino candidates highlighted with an asterisk in the last column of Table 6.1. Filled points correspond to "late neutrinos" ($\Delta t > 0$), while open points correspond to "early neutrinos" ($\Delta t < 0$).

difference rescaled by a function of redshift, we had found for the same 9 candidates a correlation of 0.951.This 0.951 goes down to 0.866 when arranging the analysis for correlation between $\Delta t/(1+z)$

correlation but in itself does not provide what is evidently the most interesting quantity here of interest, which must be some sort of "false alarm probability": how likely it would be to have accidentally data with such good agreement with the expectations of the quantum-spacetime models here contemplated? As done in Chap. 4. for these purposes one could estimate how often a sample composed exclusively of background neutrinos [5] would produce accidentally 9 or more GRB-neutrino candidates with correlation comparable to (or greater than) those we found in data. We did this by performing 10^5 randomizations of the times of detection of the 21 IceCube neutrinos relevant for our analysis, keeping their energies and directions fixed, and for each of these time randomizations we redo the analysis [6] just as if they were real data. Our observable is a time-energy correlation and by randomizing the times we get a robust estimate of how easy (or how hard) it is for a sample composed exclusively of background neutrinos to produce accidentally a certain correlation result. Also in the analysis of these fictitious data obtained by randomizing the detection times of the neutrinos we handle cases with neutrinos for which there is more than one possible GRB partner by maximizing the correlation, in the sense already discussed in Chap. 4 for the true data. We ask how often this time-randomization procedure produces 9 or more GRB-neutrino candidates with correlation ≥ 0.866, and remarkably we find that this happens only in 0.11% of cases.

Having correlation as high as 0.866 (and false alarm probability of 0.11%) is particularly striking considering that surely at least some of our 9 GRB-neutrino candidates are just background neutrinos accidentally fitting our criteria for the selection of GRB-neutrino candidates. This issue has been addressed in Chap. 5. Important for us here is that this line of reasoning leads to the conclusion that it is very likely that at least 3 of our 9 GRB-neutrino candidates are background. This renders somewhat striking the fact that, in spite of these contributions by background neutrinos, we found a value of correlation as high as 0.866. Taking as working assumption that 3 among our 9 GRB-neutrino candidates surely are background, we can then exploratively assume that the 6-plet of "true" GRB neutrinos is the maximum-correlation 6-plet among the 6-plets obtainable from our 9 candidates, and take as reference for the analysis the value of correlation found for this maximum-correlation 6-plet, which is 0.995. One can then define a false alarm probability based on how frequently simulated data, obtained by randomizing the

and $E^*/(1+z)$. These two types of correlation studies are based on two equations which are equivalent to each other, one obtained from the other by simply dividing both members of the equation by the same function of redshift. Therefore in the ideal case of an infinite amount of data the indications emerging from the two types of correlation studies would be exactly coincident, but only 9 data points intervene in our analysis, spread over a wide range of values of redshift, and this results in the (however small) difference between 0.951 and 0.866.

[5] Consistently with the objectives of our analysis we consider as "background neutrinos" all neutrinos that are unrelated to a GRB, neutrinos of atmospheric or other astrophysical origin which end up being selected as GRB-neutrino candidates just because accidentally their time of detection and direction of detection happen to fit our selection criteria.

[6] In particular for any given realization of the fictitious GRB-neutrino candidates we identify those of known redshift and use them to estimate the "typical fictitious GRB-neutrino redshift", then attributed to those candidates of unknown redshift (procedure done separately for long and for short GRBs). When in the given realization of the fictitious GRB-neutrino candidates there is no long (short) GRB of known redshift we attribute to all of them a redshift of 1.497 (0.6).

times of detection of all the 21 neutrinos in our sample, include a 6-plet of candidates with correlation greater or equal to the value of 0.995 found for the best 6-plet in the real data (so, if, say, a given time randomization produces 11 candidates one would assign to the randomization a value of correlation given by the highest correlation found by considering all possible choices of 6 out of the 11 candidates). We find that this false alarm probability is of 0.6%.

6.3 In-vacuo dispersion for high-energy Fermi-telescope photons

6.3.1 Selection criteria

Having reviewed briefly in terms of $\Delta t/(1+z)$ and $E^*/(1+z)$ the "case for in-vacuo dispersion for neutrinos", and the characterization of its statistical significance provided in the previous chapters, we are ready to proceed with our analysis of the "case for in-vacuo dispersion for photons", emerging from the investigations reported in Refs. [138, 136, 135]. For this photon case, while Ref. [135] convincingly characterized the relevant feature as striking, there was so far no characterization of the statistical significance, so one of our main objectives here is to provide such a characterization.

The analyses reported by Ma and collaborators in Refs. [138, 136, 135] focus on the highest-energy photons among those observed for GRBs by the Fermi telescope, and implements some time-window selection criteria. Evidently, in spite of the many differences between the two contexts, there are challenges in this sort of analysis of GRB photons, which are rather similar to the challenges faced in the analysis of candidate GRB neutrinos reported above.

We find appropriate to here contemplate not only the energy-window and time-window criteria adopted by Ma and collaborators but also to propose some alternative criteria of our own, which (while keeping close to the criteria introduced by Ma and collaborators) we feel might be a natural alternative to be considered as this research program further advances, especially as new data are accumulated.

Ma and collaborators focus on GRB photons observed within 90 seconds of the first peak in the GBM and with observed energy greater than 10 GeV. In our alternative criteria we choose to specify the time window by mainly exploiting the fact that, as already observed in Ref. [135], a surprisingly high percentage of the photons selected by the criteria of Ma and collaborators are consistent with roughly the same value of the time offset at the source t_{off}. We attempt to exploit this aspect in our time-window selection criteria by essentially characterizing the time window in terms of emission times, rather than observed times. We require that at the source the time of emission of our selected photons be consistent with an offset with respect to the time of emission of the first GBM peak of up to 20 seconds, but of course also allowing in addition for a sizeable range of effects possibly due to in-vacuo dispersion. When expressed in terms of the difference Δt between the time of observation of the relevant photon and the time of observation of the first GBM peak, our time selection criterion takes the form

$$|\Delta t| \leq 10^{-16} D(z) + (1+z)20s\,. \tag{6.4}$$

Here the $20s$ are our mentioned window on t_{off}, while the parameter we fix at 10^{-16} allows for in-vacuo-dispersion effects of amount roughly comparable to the corresponding range of effects probed by Ma and collaborators. The main difference here is that our time window has the same quantitative interpretation for all GRBs when described in terms of emission times at the source, but when expressed as a window on observed times it depends on the redshift of the GRB. The 90 seconds of redshift-independent observed-time window adopted by Ma and collaborators roughly coincide with our window on observed times at redshift of 1. For GRBs at redshift greater than 1 (where both time dilatation of the offset and the possible in-vacuo dispersion would produce bigger effects on the time of observation) our Eq. 6.4 allows for an observed-time window larger than 90 seconds, while for GRBs at redshift smaller than 1 it allows for an observed-time window smaller than 90 seconds.

For what concerns our window on photon energies, consistently with our focus on properties at the source (rather than observed properties), we require that our selected photons be emitted at the source with energy greater than[7] 40 GeV. So in terms of observed energy our window is $E \geq 40\text{GeV}/(1+z)$, an alternative to the 10-GeV redshift-independent observed-energy window of Ma and collaborators. We picked 40 GeV as our cut on the energy at the source because the selection process for this choice gives results rather close to those obtained with the cut at 10 GeV of observed energy adopted by Ma and collaborators.

At the present time (as confirmed by our analysis) there is no evidence that our criteria might be more advantageous than those of Ma and collaborators. We are only proposing them as an alternative which might play a role as this research program advances. Accordingly, while we keep at center stage our proposed criteria, in this chapter we shall also report some results that we obtained using the selection criteria of Ma and collaborators.

An important final remark on selection criteria concerns redshifts. For our neutrino analysis it was possible, as shown above, to allow for GRB-neutrino candidates for which the GRB redshift had not been measured. We expect, as argued more extensively in Chap. 4, that by using as reference some estimated average value of redshifts for long and short GRBs observed in neutrinos we should eventually, as more data is accrued, reach conclusive findings, in spite of handling GRBs which, for the most part, have no precise redshift assignment. Such conclusive findings would have been reached faster in presence of more measured values of redshift, but without such measured values the analysis still works in the long run. We believe, however, that for the analogous photon analyses the role of redshift measurements must be handled differently. A challenge for this sort of photon analyses is that the size of the conjectured effects, often of a few seconds, is comparable to the time scales of the astrophysical mechanisms at work in a GRB. Any eventual in-vacuo dispersion effect would have to be deduced finely within the sort of "background noise" produced by the (largely unknown) mechanisms that cause the specific time variability of a given GRB. As a result we propose

[7]For what concerns this energy-selection criteria, we should mention that as we were finalizing the study here reported, in private conversations with Bo-Qiang Ma, we learned that Ma and collaborators are independently contemplating the possibility of implementing the selection in terms of energy at emission, also leaning toward the possibility of setting the cut at 40 GeV.

that in-vacuo-dispersion photon analyses should confine themselves to GRBs of measured redshift. Also Ma and collaborators rather strictly adopt this attitude toward redshifts, though they have handled cases [8] where the GRB redshift had been guessed on the basis of some theoretical argument but had not been measured. We shall assume that it is safer for photon analyses to focus strictly on GRBs on measured redshift.

6.3.2 Properties of selected photons and statistical analysis

We show in Table 6.2 and Fig. 6.2 the 11 Fermi-telescope photons selected by the time window of our Eq. 6.4 and our requirement of an energy of at least 40 GeV at emission. The fact that our criteria are to a large extent compatible with the criteria of Ma and collaborators is also suggested by Figure 2: all our 11 photons were also selected by Ma and collaborators; the only difference is that 2 of the photons selected by Ma and collaborators are not picked up by our criteria. These 2 additional photons are also shown in Table 6.2 and Fig. 6.2.

	$E_{\rm em}$[GeV]	$E_{\rm obs}$[GeV]	E^*[GeV]	Δt [s]	z	GRB
1	40.1	14.2	25.4	4.40	1.82	090902B
2	43.5	15.4	27.6	35.84	1.82	090902B
3	51.1	18.1	32.4	16.40	1.82	090902B
4	56.9	29.9	26.9	0.86	0.90	090510
5	60.5	19.5	40.0	20.51	2.11	090926A
6	66.5	12.4	47.1	10.56	4.35	080916C
7	70.6	29.8	40.7	33.08	1.37	100414A
8	103.3	77.1	25.2	18.10	0.34	130427A
9	112.5	39.9	71.5	71.98	1.82	090902B
10	112.6	51.9	60.7	62.59	1.17	160509A
11	146.7	27.4	104.1	34.53	4.35	080916C
12*	33.6	11.9	21.3	1.90	1.82	090902B
13*	35.8	12.7	22.8	32.61	1.82	090902B

Table 6.2. Here reported are some properties of the 13 photons picked up by the selection criteria of Ma and collaborators. Our selection criteria pick up 11 of these 13 photons (we place an asterisk on the 12th and 13th entries in the table in order to highlight that they are not picked up by our selection criteria). The second and third columns report respectively the values of energy at emission and energy at observation. The fourth column reports the difference in times of observation between the relevant photon and the peak of the GBM signal. The last column identifies the relevant GRB, while the fifth column reports its redshift.

[8] The only case of this type included so far in studies by Ma and collaborators is GRB140619B [136, 135], a GRB for which no redshift measurement is available. We shall here not consider GRB140619b.

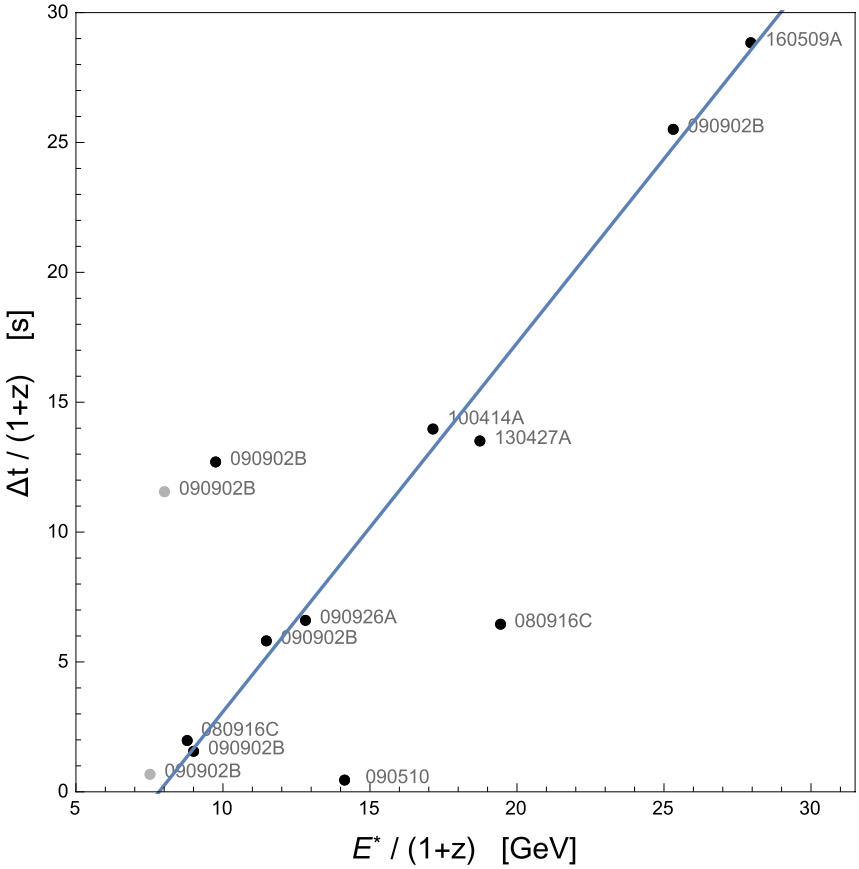

Figure 6.2. Black points here in figure correspond to the 11 photons picked up by our selection criteria, characterized in terms of their values of $\Delta t/(1+z)$ and $E^*/(1+z)$. Gray points are for the 12th and 13th entries in table 2 (photons picked up by the criteria of Ma and collabroators, but not by our criteria). The strikingly visible feature of 8 black points (plus 1 gray point) falling nicely on a straight line is also highlighted in figure by the presence of a best-fit line (which however we find appropriate to discuss in detail only later, in Sec. 6.4).

The content of Fig. 6.2, as already efficaciously stressed in Ref. [135], is rather striking. Following Ma and collaborators, we notice that all 13 photons (the 11 picked up by our criteria, plus the two additional ones picked up by the criteria of Ma and collaborators) are well consistent with the same value of η, upon allowing for only 3 values of t_{off}. We shall not however attempt to quantify the statistical significance of this more complex thesis based on 3 values of t_{off}: evidently the most striking feature is that 8 of our 11 photons (9 of the 13 photons of Ma and collaborators) are all compatible with the same value of η and t_{off}. This sets up a rather easy question that one can investigate statistically: if there is no in-vacuo dispersion, and therefore the correlation shown by the data is just accidental, how likely it would be for such 11 photons to include 8 that line up so nicely?

We address this question quantitatively by first computing the correlation of the 8 among our 11 photons that line up nicely in Fig. 6.2, finding that this correlation is 0.9959. We then estimate an associated "false alarm probability" (see Chap. 4) by

performing simulations in which (while keeping their energy fixed at the observed value) we randomize, within the time window specified by our time-selection criterion, the time delay of each of our 11 high-energy photons with respect to the GBM peak of the relevant GRB, and we assign to each of these randomizations a value of correlation given by the maximum value of correlation found by taking in all possible ways 8 out of the 11 photons. We find that these simulated values of correlation are ≥ 0.9959 only in 0.0013% of cases, about 1 chance in 100000.

We stress that this impressive quantification of the statistical significance of the feature exposed by Ma and collaborators does not depend on the fact that we adopted our own novel selection criteria. For this purpose we redo the analysis including also the 2 photons that should be included according to the criteria of Ma and collaborators. In this case we have 9 out of 13 photons that line up very nicely. The value of correlation found for those 9 photons is 0.9961. We then perform simulations in which we randomize the time of observation of all the 13 photons within the time window specified by the time-selection criterion of Ma and collaborators and to each of these randomizations we assign a value of correlation given by the maximum value of correlation found by taking in all possible ways 9 out of the 13 photons. We find that these simulated values of correlation are ≥ 0.9961 only in 0.0009% of cases, very close to the 0.0013% obtained with our selection criteria.

6.3.3 Predictive power

The values of correlation reported in the previous subsection, and especially the values of false alarm probability found in the previous subsection, are rather impressive. However, as discussed in the next section, the interpretation of these data presents us with some challenges. In light of this we find appropriate to stress that the picture emerging from this photon feature has intrinsic model-independent "predictive power". We illustrate this notion by considering the situation set up by the first two papers by Ma and collaborators, Refs. [138, 136], which were written before May 2016 (*i.e.* before the observation of GRB160509a). At that point Ma and collaborators had already discussed the photon feature using all the photons in our figure 2, of course with the exception of the photon from GRB160509a which had not yet been observed. That photon from GRB160509a allowed then Ma and Xu, in Ref. [135], to appropriately emphasize that the picture was finding additional support.

In a sense which we shall attempt to quantify, the picture Ma and collaborators had been developing exhibited some predictive power upon the observation of GRB160509a. Our quantification of this predictive power takes off by computing the value of correlation obtained with the other 8 photons on the "main line" of Fig. 6.2 (*i.e.* not including the photon from GRB160509a, but including the photon on the "main line" picked up by the selection criteria of Ma and collaborators but not picked up by our selection criteria), finding that this correlation is of 0.9935. With the observation of the photon from GRB160509a the resulting 9-photon correlation moved up to 0.9961. We shall characterize the predictive power by asking how likely it would be for a photon unrelated to those previous 8 photons on the "main line" to produce accidentally such an increase of correlation. We randomize the time of

observation of that photon from GRB160509a (within the time window specified by the time-selection criterion of Ma and collaborators) and we find that an increase of correlation from 0.9935 to 0.9961 (or higher) occurs only in 1.9% of cases.

We perform the same estimate also adopting our selection criteria, as a mere academic exercise (our selection criteria are being proposed here, after the observation of GRB160509a). With our selection criteria one has only 7 photons on the "main line", when considering data available before GRB160509a. Those 7 photons have correlation of 0.9932. Adding the photon from GRB160509a one then has a 8-photon correlation of 0.9960. We randomize the time of observation of that photon from GRB160509a (within the time window specified by our time-selection criterion) and we find that an increase of correlation from 0.9932 to 0.9960 (or higher) occurs only in 0.79 % of cases.

6.4 Observations relevant for the interpretation of the data

Our quantification of statistical significance gave rather impressive results both for the neutrino feature and for the photon feature. We still feel that the overall situation should be assessed prudently, since both analyses still rely on only a small group of photons and neutrinos. There is no reason to jump to any conclusions, also because both the Fermi telescope and the IceCube observatory will continue to report new data still for some time to come. It is nonetheless interesting to assess the present situation both from the viewpoint of possible interpretations and from the viewpoint of a possible consistency between different analyses.

6.4.1 Concerning photons outside the "main line"

A first step of interpretation must concerns the 3 photons that in Fig. 6.2 do not line up with the other 8 photons, the 8 photons which lie on the "main line" [138, 136, 135] of Ma and collaborators. The tentative interpretation one must give within the setup of these analyses is that those 3 photons were not emitted in coincidence with the fist peak of the GBM signal. The time window of our selection criterion (and similarly the one of the selection criterion adopted by Ma and collaborators) is structured in such a way to "catch" those high-energy photons that were emitted roughly at the same time when the first peak of the GBM was emitted, but if truly in-vacuo dispersion is at work evidently it would happen occasionally that just because of in-vacuo dispersion some photons not emitted in coincidence with the first peak of the GBM end up being observed within our time window. While it is evidently difficult to quantify how frequently this should occur, at least qualitatively what is shown in figure 2 is just what one should expect if in-vacuo dispersion truly occurs, including the presence of some photons outside the "main line".

As an aside, let us however notice that the significance of what is shown in Fig. 6.2 is not washed away if we include in the analysis of statistical significance also the photons outside the "main line". For this purpose we first notice that the value of correlation obtained by taking into account all 11 photons is 0.845, still rather high. In our simulations, in which we randomize the time of observation of the 11 photons

(within the time window specified by our time-selection criterion), we find that a value of correlation for all 11 photons ≥ 0.845 is obtained only in 0.035 % of cases.

Similar conclusions are reached adopting the criteria of Ma and collaborators. In that case one has 13 photons under consideration, and the value of correlation computed for those 13 photons is 0.805. Randomizing the times of observation of those 13 photons (within the time window specified by the time-selection criterion of Ma and collaborators) we find that a value of correlation for all 13 photons $\geq$ 0.805 is obtained only in 0.037% of cases.

6.4.2 Trigger time without offsset

In light of the observations made in the previous subsection one feels encouraged to set aside the 3 photons that fall off the "main line", and focus on the other 8 photons. A significant characterization of those 8 photons is obtained by assuming $\delta_\gamma = 0$, so that the whole feature is due to a nonzero value for η_γ. This assumption $\delta_\gamma = 0$ is very restrictive but still the "main line" of 8 photons in Fig. 6.2 is very well described by the model of Eq. 6.3, for $t_{off} = -11s \pm 1s$ and $\eta_\gamma = 34 \pm 1$. These are the parameters of the line shown in Fig. 6.2, where the goodness of the fit of the 8 photons on the "main line" is visible.

The story with the "main line", the single time offset shared by 8 photons, and $\delta_\gamma = 0$ fits indeed in remarkably nice way, in spite of being based on very restrictive assumptions. This is surely striking, but we are nonetheless inclined to proceed cautiously. There is evidently a pronounced feature, of the type here characterized, in these available GRB-photon data, but its description does not necessarily have to be the one that presently fits the data so nicely. First we should stress that in spite of our impressive findings for the false alarm probabilities, we still consider as most likely the hypothesis that the feature is accidental, rather than a truly physical (in-vacuo-dispersion-like) feature. Perhaps more surprisingly, even when taking as temporary working assumption that the feature is physical we give priority to the hypothesis that the feature might not really be describable in terms of the ingredients composed by the "main line", the same time offset for 8 photons and $\delta_\gamma = 0$. We are inclined to adopt this attitude because our intuitive assessment is that, even if the overall feature is physical, at least part of present picture, with these few data available, could be accidental. We feel that such level of prudence is methodologically correct in general, and in this case might find additional motivation in the fact that the offset time favored by the analysis summarized in Fig. 6.2 would require, as observed above, a majority of our photons to have been emitted at the source some 11 seconds before the time of emission of the GBM peak. (We might have had a slightly different intuition had we found a similar result but for 11 seconds after the GBM peak.)

We give tangibility to these considerations by taking temporarily as working assumption, as an illustrative example, a hypothesis such that the feature is truly physical but the way it manifested itself so far is in part accidental. For this purpose we "scramble" the nice picture of Fig. 6.2 by not taking under consideration the Δt, time difference with respect to time of observation of GBM peak, but rather a $\Delta t_{trigger}$, time difference with respect to trigger time of the GBM signal. We do this just to probe the dependence of our results on the perspective adopted in the

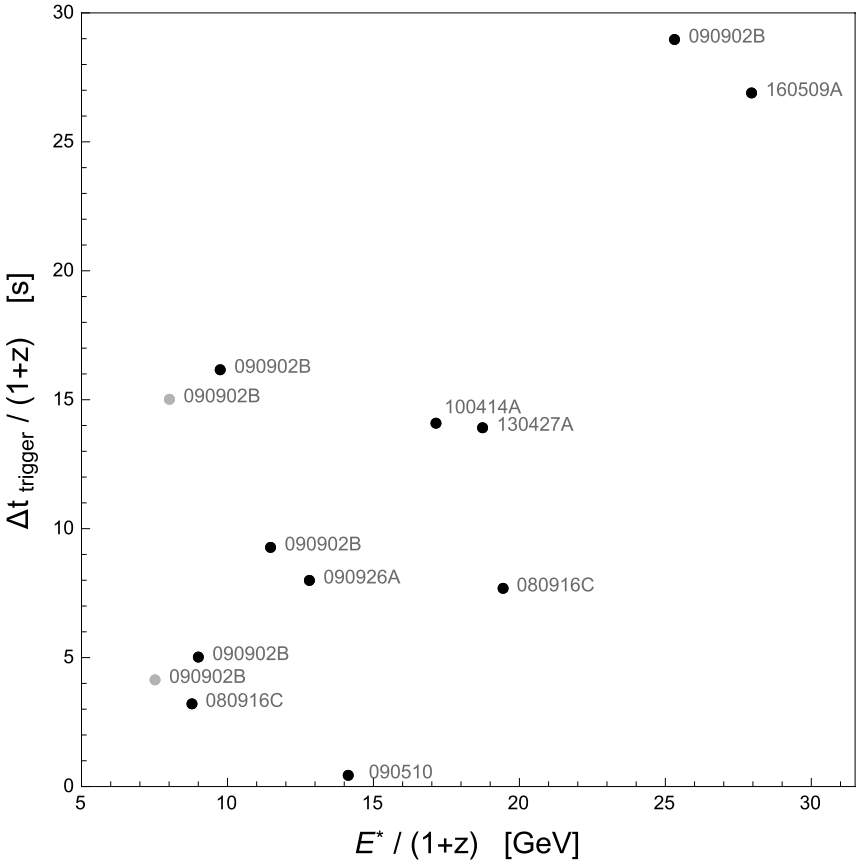

Figure 6.3. Same as figure 2, but replacing Δt with $\Delta t_{trigger}$.

analysis: we would not really expect that $\Delta t_{trigger}$ is better than Δt at exposing the sought correlation, but it is interesting for us to see whether the feature completely disappears by replacing Δt with $\Delta t_{trigger}$.

What we get upon relying on $\Delta t_{trigger}$ in place of Δt is the picture given by Fig. 6.3. In Fig. 6.3 there is no neat "main line", but this is after all what we would have expected before looking at the data: we would have expected the time offset at the source (with respect to the first GBM peak or to the GBM trigger) to be at least a bit different for different photons; moreover, with a nonvanishing δ_γ the time of observation of each photon would receive an additional random component.

Importantly for our purposes, one should notice that, while Fig. 6.3 is surely less striking than Fig. 6.2, the feature has not disappeared: it is less pronounced but the overall picture of Fig. 6.3 still shows a surprisingly high correlation. This is what we mean by contemplating the hypothesis that only part of what is shown in Fig. 6.2 might be physical, with the rest being just accidental result of how these first 11 photons usable for our purposes happened to match very neatly a particular set of hypothesis for the interpretation and the analysis. Quantitatively we have that for the data analyzed in the way reflected by figure 3 we have correlation of 0.775, over all 11 photons picked up by our selection criteria. Randomizing, within the time window specified by our time-selection criterion, the time delay of each of our 11 high-energy photons with respect to the GBM trigger of the relevant GRB, we find

correlation ≥ 0.775 in only 0.17% of cases, which is (not as small as the 0.0013% found above for the analysis with Δt, but) still a very small false alarm probability.

6.4.3 Consistency between the features for photons and the feature for neutrinos

In light of the observations made in the previous subsection we now set aside the 3 photons that fall off the "main line", and focus on the other 8 photons. A significant characterization of those 8 photons is obtained by assuming $\delta_\gamma = 0$, so that the whole feature is due to a nonzero value for η_γ. This assumption $\delta_\gamma = 0$ is restrictive but still the "main line" of 8 photons in figure 1 is very well described by the model of Eq. 6.3, for $t_{off} = -11s \pm 1s$ and $\eta_\gamma = 34 \pm 1$.

It is interesting to compare this estimate of η_γ with the estimate of η_ν that one can obtain from the neutrino data discussed in Sec. 4.3.4 . This comparison should be handled with some care, since some quantum-spacetime models predict (see, *e.g.*, Ref. [24] and references therein) independent in-vacuo dispersion parameters for different particles, and also a possible dependence of the effects on polarization for photons and on helicity for neutrinos. Still one would tentatively expect comparable magnitude of the effects for different particles (including the possible dependence on polarization/helicity). A first important observation is the Fig. 6.1 includes 5 neutrinos whose interpretation in terms of in-vacuo dispersion would require positive η_ν and 4 neutrinos whose interpretation in terms of in-vacuo dispersion would require negative η_ν (this is why in figure 1 we consider the absolute value of Δt). Another complication for our purposes originates in the fact that, as mentioned, there are reasons, as exposed in Chap. 5, to expect that 3 or 4 of those 9 GRB-neutrino candidates are actually background neutrinos that happened to fit accidentally our profile of a GRB-neutrino candidate. What we can do is to attempt an estimate of the absolute value $|\eta_\nu|$ and to perform this estimate by assuming that 3 of the 9 GRB-neutrino candidates are background: essentially we estimate $|\eta_\nu|$ for each possible group of 6 neutrinos among our 9 GRB-neutrino candidates, and we combine these estimates into a single overall estimate. This leads to the estimate $|\eta_\nu| = 19 \pm 4$.

So we have an estimate of $\eta_\gamma = 34 \pm 1$ and an estimate of $|\eta_\nu| = 19 \pm 4$, which are closely comparable, as theoretical prejudice would lead us to expect. Perhaps more importantly, the hypothesis that both features are accidental should also face the challenge introduced by this correspondence of values. If actually there is no in-vacuo dispersion both features should be just accidental. All 9 of our GRB-neutrino candidates would just be background neutrinos who happened to fit our criteria for selection of GRB-neutrino candidates and whose energies and times of observation just happened to produce the high correlation shown in Fig. 6.1. And similarly all 11 of the photons selected by our criteria would have accidentally produced the correlation visible in Fig. 6.2: they would be photons whose time of observation (with respect to the time of observation of the GBM peak) is not really correlated with energy, the correlation with energy emerging just accidentally. All these assumptions about neutrinos and photons are needed if there is no in-vacuo dispersion, with the additional observation that all these accidental facts end up producing comparable estimates of η_γ and $|\eta_\nu|$.

The level of "consistency" (in the sense discussed above) between the neutrino

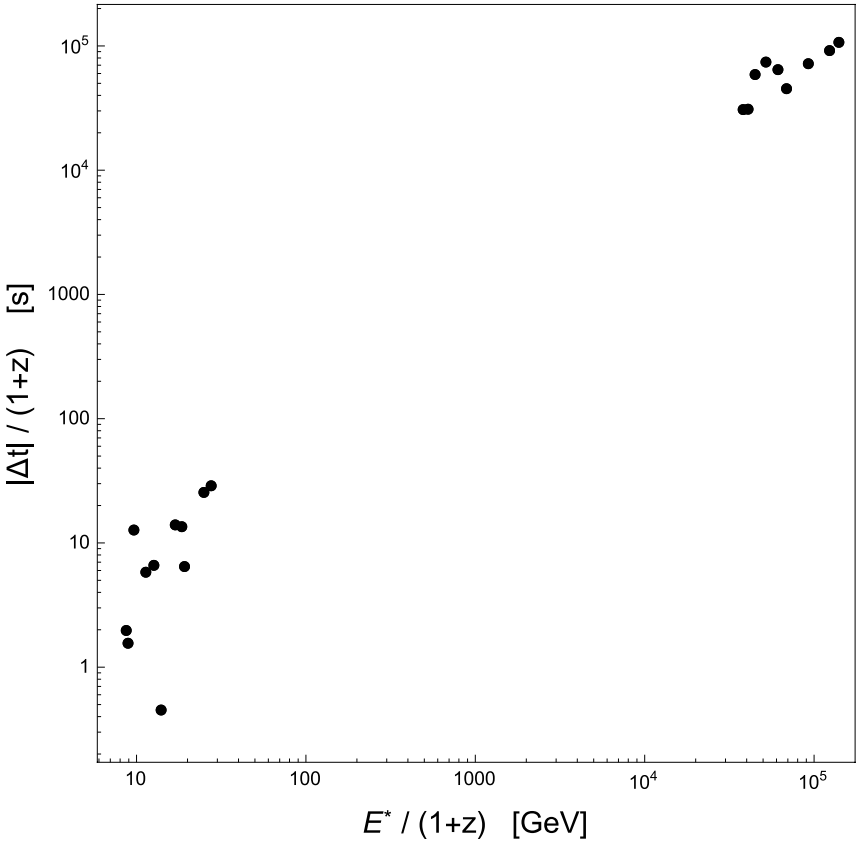

Figure 6.4. Here we show together the content of Figs. 6.1 and 6.2, so that one can appreciate the overall picture for what concerns the correlation between $|\Delta t|$ and E^*.

feature and the photon feature is visually illustrated in our Fig. 6.4, showing both our 11 photons and our 9 GRB-neutrino candidates in a plot of E^* versus the absolute value of Δt.

6.4.4 On a possible astrophysical interpretation of the photon feature

So far we only considered two alternative hypotheses: either the two features shown in Figs. 6.1 and 6.2 are due to in-vacuo dispersion or there is no in-vacuo dispersion and those two features are accidental. One should of course contemplate a third possibility: there might be no in-vacuo dispersion but still at least one of those two features is not accidental, but rather the result of some other physical mechanism. This leads us naturally to wonder whether the two features could be the result of some (so far unknown) astrophysical properties of the sources.

We believe the hypothesis that the neutrino feature be of astrophysical origin should be discarded: the relevant effects are of the order of a couple of days, and neutrinos observed two days before or after a GRB could not possibly be GRB neutrinos (unless in-vacuo dispersion takes place). If the neutrino feature is confirmed when more abundant data become available we would know that something not of astrophysical origin has been discovered.

In this respect the photon feature is very different. The size of the effects is between a few and ~ 100 seconds, which may well be the time scale of some mechanisms intrinsic of GRBs. The main reason to be skeptical about the astrophysical interpretation comes from the fact that the content of Fig. 6.2 reflects the properties of the $D(z)$: the data points (those on the "main line") line up only because we have factored the $D(z)$ in the analysis, and the $D(z)$ is a form of dependence on redshift which reflects propagation. So the astrophysical interpretation of the photon feature still requires assuming that at least part of the content of Fig. 6.2 is accidental: we cannot exclude some mechanism at the GRB producing some level of correlation between energy of the photon and difference in time of emission with respect to the GBM peak, but such a mechanism could produce the feature of Fig. 6.2 only if accidentally (on those few data points) it ended up taking values lending themselves to the sort of $D(z)$-dependent analysis which we performed.

So the astrophysical interpretation of the photon feature is possible but must face some issues. However, we should stress that also the interpretation of the photon feature in terms of the model of Eq. 6.3 has to face a challenge connected with GRB090510. One of 3 photons off the "main line" is a 30 GeV photon from the short GRB090510. As discussed above, when taking as working assumption that in-vacuo dispersion actually takes place, these photons off the "main line" should be interpreted as photons emitted not in (however rough) coincidence with the first peak of Fermi's GBM. Such an interpretation is certainly plausible in general, but the case of the 30 GeV photon from GRB090510 is a challenge. That 30GeV photon was observed [15] within the half-second time window where most GRB090510 photons with energy between 1 and 10 GeV were also observed (see Fig. 7.1 in the next chapter). In light of this, it is certainly very natural to assume that the 30 GeV photon could not have accrued an in-vacuo-dispersion effect of more than half a second, travelling from redshift of 0.9 (the redshift of GRB090510), which implies $|\eta_\gamma| < 1$. For $\eta_\gamma \sim 30$, as suggested by the points on the "main line", the in-vacuo-dispersion effect for that 30 GeV photon should be of more than 15 seconds. It should have arrived together with that half-second-wide peak of 1-10 GeV photons because of an accidental and strong cancellation between an effect of ~ 15 seconds due to emission-time differences at the source and a 15-second in-vacuo-dispersion effect accrued propagating.

We feel the the 30 GeV photon from GRB090510 poses a very severe challenge for the interpretation of the photon feature in terms of our model (6.3), even though all other photons in our data fit so nicely (6.3). In connection with this one should notice that the 30 GeV photon is the only photon in our sample coming from a short GRB (GRB090510). All other photons in our sample come from long GRBs. If the effect is present for long GRBs and absent for short GRBs, then the interpretation should be astrophysical. One can also notice however that GRB090510, with its redshift of 0.9, is one of the closest GRBs relevant for our photon analysis. All other GRBs in our photon analysis, with the exception of GRB130427a, are at redshift greater than 1. A scenario in which the effect is pronounced only at large redshifts could be of quantum-spacetime origin, but of course would require a quantum-spacetime picture in which the dependence on redshift of the effects is not exactly governed by the function $D(z)$.

Any attempt of quantum gravity interpretation of the feature discussed here

should also explain why the previous analysis [128] obtains negative results. We note that we used selection criteria very different from those of the previous study [128]: for each of the GRBs considered, that study [128] focused on a tight temporal window, much tighter than the one that would be achieved for those same GRBs our criterion (see Eq. 6.4). The end result is that the previous analysis [128] does not include 9 of our 11 photons (Fig. 6.2). Also potentially noteworthy is the fact that we only consider photons with energy at emission greater than 40 GeV, while the previous analysis [128] obtained statistical results involving all photons with observed energy greater than 30 MeV: only two of our photons with energy greater than 40 GeV are included in that analysis [128], and it can be assumed that those two photons do not carry much weight in that analysis, since the statistical study is dominated by the more abundant photons of energy between 30 MeV and 40 GeV [128].

Chapter 7

In-vacuo-dispersion-like spectral lags in gamma-ray bursts

In the previous chapter we exposed a rather strong statistical evidence of in-vacuo-dispersion-like spectral lags for gamma-ray bursts, i.e. a linear correlation between time of observation and energy of GRB particles. This is particularly evident by the content of Fig. 6.4: the linear correlation between Δt and E^* visible is just of the type expected for quantum-gravity-induced in-vacuo dispersion. It might of course be accidental, but it has been estimated in the previous chapters that for the relevant GRB-neutrino candidates such a high level of correlation would occur accidentally only in less than 1% of cases, while GRB photons could produce such high correlation (in absence of in-vacuo dispersion) only in less than 0.1% of cases. However, the results we obtained focused on testing in-vacuo dispersion for the most energetic GRB particles, and in particular only included photons with energy at emission greater than 40 GeV. The "statistical evidence" summarized in Fig. 6.4 is evidently intriguing enough to motivate us to explore whether or not the in-vacuo-dispersion-like spectral lags persist at lower energies. The main goal of the analysis we will expose in this chapter is to extend the window of the statistical analysis down to 5 GeV. In doing so we find results that are consistent with what had been previously noticed at higher energies for GRB photons (see Chap. 6).

7.1 New strategy of analysis

When lowering the cutoff for GRB photons down to 5 GeV, the main challenge one has to address is that we cannot simply apply to lower-energy photons the reasoning exposed in Chap. 6 which led to Fig. 6.4. This is because the Δt in Fig. 6.4 is the difference between the time of observation of the relevant particle and the time of observation of the first low-energy peak in the GRB, so it is a Δt which makes sense for in-vacuo-dispersion studies only for photons which one might think were emitted in (near) coincidence with the first peak of the GRB. This assumption is (challengeable [77] but) plausible [135] for the few highest-energy GRB photons relevant for Fig. 6.4, with energy at emission greater than 40 GeV, but of course it cannot apply to all photons in a GRB. Conceptually the main aspect of novelty of our analysis concerns a strategy for handling this challenge.

Our analysis focuses on the same GRBs whose photons took part in the analyses which led to the picture here summarized in Fig. 6.4, but now including all photons from those GRBs with energy at the source greater than 5 GeV, thereby lowering the cutoff by nearly an order of magnitude. These are the GRBs that provide us the full range of energies relevant for our analysis: GRB080916C, GRB090510, GRB090902B, GRB090926A, GRB100414A, GRB130427A, GRB160509A. Only 11 photons took part in the previous analyses whose findings were summarized in our Fig. 6.4, whereas the analysis we are here reporting involves a total of 148 photons. We report the relevant properties of these 148 photons in Fig. 7.1 and in Table 7.1. The relevant data were downloaded from the Fermi-LAT archive and they were calibrated and cleaned using the LAT ScienceTools-v10r0p5 package, which is available from the Fermi Science Support Center.

For the reasons discussed above, we do not consider the Δt (with reference to the first peak of the GRB), but rather we consider a Δt_{pair}, which gives for each pair of photons in our sample their difference of time of observation. Essentially each pair of photons (from the same GRB) in our sample is taken to give us an estimated value of η_γ, by simply computing

$$\eta_\gamma^{[pair]} \equiv \frac{M_P \Delta t_{pair}}{D(1) E^*_{pair}}\,, \tag{7.1}$$

where E^*_{pair} is the difference in values of E^* for the two photons in the pair. Of course the Δt_{pair} for many pairs of photons in our sample could not possibly have anything to do with in-vacuo dispersion: if the two photons were produced from different phases of the GRB (different peaks) their Δt_{pair} will be dominated by the intrinsic time-of-emission difference. Those values of $\eta_\gamma^{[pair]}$ will be spurious, they will be "noise" for our analysis. However we also of course expect that some pairs of photons in our sample were emitted nearly simultaneously, and for those pairs the Δt_{pair} could truly estimate η_γ. Since estimating η_γ from the photons in Fig. 6.4 one gets $\eta_\gamma = 30 \pm 6$, the preliminary evidence summarized in Fig. 6.4 would find additional support if this sort of analysis showed that values of $\eta_\gamma^{[pair]}$ of about 30 are surprisingly frequent, more frequent than expected without a relationship between arrival times and energy of the type produced by in-vacuo dispersion.

7.2 Results for all photon pairs

We first take into account all pairs of photons (of course from the same GRB) within our data set (see. Table 7.1) and we compute for each pair the value of $\eta_\gamma^{[pair]}$ given in Eq. 7.1. Being in the previous chapter our previous estimation of $\eta_\gamma = 30 \pm 6$, we select those values of $\eta_\gamma^{[pair]}$ in the range [-95,95] divided in 19 bins of equal size, so that we can then focus our statistical analysis on the bin between 25 and 35. Each pair of photon typically contributes to more than one of our bins, considering that the energies of the photons are not known very precisely. The contribution of a given pair to each bin is computed generating a gaussian distribution with mean value η_γ (calculated with Eq. (7.1)) and standard deviation σ_γ obtained by error

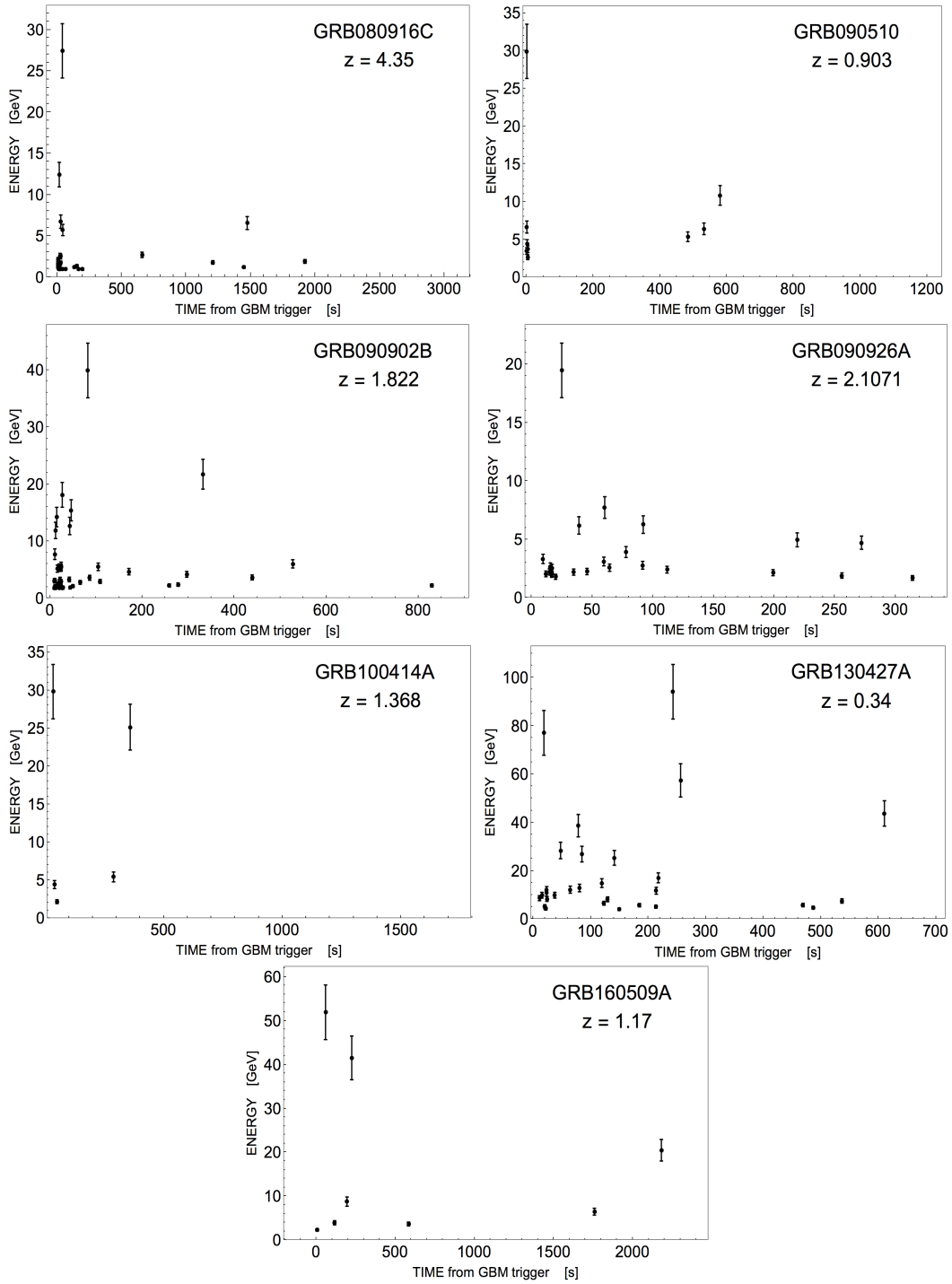

Figure 7.1. For each of the 7 GRBs used in this analysis, values of the time of arrival from the GBM trigger versus the observed energy for all 148 photons with energy at the source greater than 5 GeV. In each plot it is also reported on the top the name of the GRB and its redshift. The error bar for the energy results from assuming a 10 % uncertainty.

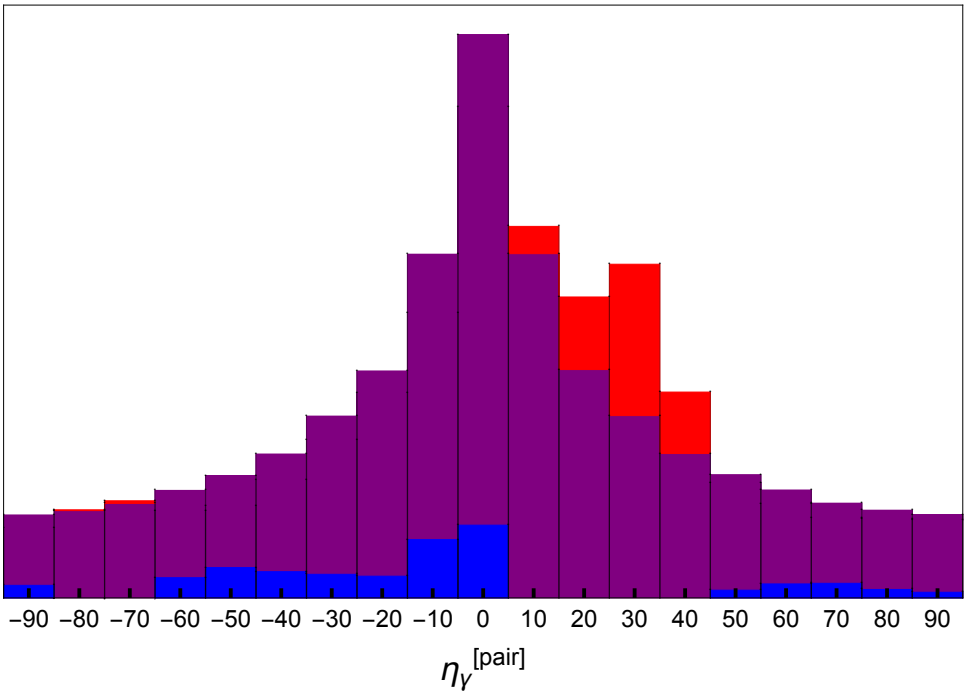

Figure 7.2. Normalized distribution of $\eta_\gamma^{[pair]}$ for all pairs of photons (from the same GRB) within our data set. For bins where the observed population is higher than expected we color the bar in purple up to the level expected, showing then the excess in red. For bins where the observed population is lower than expected the bar height gives the expected population, while the blue portion of the bar quantifies the amount by which the observed population is lower than expected.

propagation of the energy uncertainty, which we assume to be of 10%:

$$\sigma_\gamma = \frac{M_P |\Delta t_{pair}|}{D(1) E^{*2}_{pair}} \cdot 0.1 \cdot \sqrt{E^{*2}_1 + E^{*2}_2}, \tag{7.2}$$

where E^*_1 and E^*_2 are respectively the distance-rescaled energy for the first and second photon in a given pair. Then, we compute the area of this distribution, which we limit in the interval $[\eta_\gamma - \sigma_\eta, \eta_\gamma + \sigma_\eta]$, falling within each bin, in order to evaluate the value to assign to a given bin. Thus, each pair in general contributes to more than one bin and does that with a gaussian weight. The expected frequency of occurrence of values of $\eta_\gamma^{[pair]}$ corresponding to a given bin was estimated instead by producing 10^5 sets of simulated data, each obtained by reshuffling randomly the times of observation of the photons (of each GRB) in our sample, and by redoing the analysis just as if they were real data. Thus for each of the 19 bins in the range [-95,95], having obtained 10^5 values we then take their mean value as the expected frequency of occurrence. The results of this analysis is illustrated in Fig. 7.2.

Of particular significance for our objective is the higher than expected observed frequency of values of $\eta_\gamma^{[pair]}$ between 25 and 35, as shown perhaps most vividly by the content of Fig. 7.2. The main point to be noticed in Fig. 7.2 is that we find in our sample a frequency of occurrence of values of $\eta_\gamma^{[pair]}$ between 25 and 35 which is tangibly higher than one would have expected in absence of a correlation between

Δt_{pair} and E^*_{pair}. Following a standard strategy of analysis (see, *e.g.*, Refs.[33, 128]) we estimate how frequently $25 \leq \eta_\gamma^{[pair]} \leq 35$ should occur in absence of correlation between Δt_{pair} and E^*_{pair} by producing 10^5 sets of simulated data, each obtained by reshuffling randomly the times of observation of the photons in our sample. Interestingly we find, using our simulated data obtained by time reshuffling, that the excess in bin $25 \leq \eta_\gamma^{[pair]} \leq 35$ visible in Fig. 7.2 is expected to occur accidentally only in 1.2 % of cases.

7.3 High, medium and low energy photons

For reasons that shall soon be clear it was valuable for us to divide our data sample in different subgroups, characterized by different ranges of values for the energy at emission, which we denote by E_0. We label as "high" the photons in our sample with $E_0 > 40$ GeV , with "medium" those with 15 GeV $\leq E_0 \leq 40$ GeV , and with "low" those with 5 GeV $\leq E_0 \leq 15$ GeV . As it will be soon shown in this section, It is noteworthy that a higher than expected observed frequency of values of $\eta_\gamma^{[pair]}$ between 25 and 35 is present also if we constrain the two photons in a pair to be of different type, for what concerns our categories of "high", "medium" and "low". Most notably, values of $\eta_\gamma^{[pair]}$ between 25 and 35 occur at a rate higher than expected even if we exclude from the analysis the photons whose energy at emission is greater than 40 GeV (the photons that were taken into account in the analyses leading to the content of our Fig. 6.4).

Our "high" photons were already taken into account in the previous studies (see Chap. 6) which led to Fig. 6.2, so it is particularly valuable to keep them distinct from the other photons in our sample (the ones we label as "medium" and "low"). In Fig. 7.3 we report the results of an analysis that is just like the analysis that produced Fig. 7.2, but now excludes the contributions from the "high" photons (with energy at emission greater than 40 GeV). It is noteworthy that one still has a higher than expected observed frequency of values of $\eta_\gamma^{[pair]}$ between 25 and 35, and for this case we estimate, using our simulated data obtained by time reshuffling (as described in the previous section), that the excess of occupancy of the bin $25 \leq \eta_\gamma^{[pair]} \leq 35$ visible in Fig. 7.3 should occur accidentally only in 0.6 % of cases.

Also intriguing is the content of our Fig. 7.4, which offers an intuitive characterization of the consistency that emerged from our analysis between what had been found in previous studies of GRB photons with energy at emission greater than 40 GeV, and what we now find for GRB photons with energy between 5 and 40 GeV.

In Fig. 7.5 we show the results we obtain for pairs composed of a "high" ($E_0 > 40$ GeV) and a "low" (5 GeV $\leq E_0 \leq 15$ GeV) photon. As visible in Fig. 7.5, once again we find a higher than expected observed frequency of values of $\eta_\gamma^{[pair]}$ between 25 and 35, even though in this case the statistical significance is less striking: using our simulated data obtained by time reshuffling, we find that the excess of occupancy of the bin $25 \leq \eta_\gamma^{[pair]} \leq 35$ visible in Fig. 7.5 should occur accidentally in about 14 % of cases (though this result reflects in part also the fact that we do not have high statistics of high-low pairs).

In Fig. 7.6 we show the results we obtain for pairs composed of a "medium"

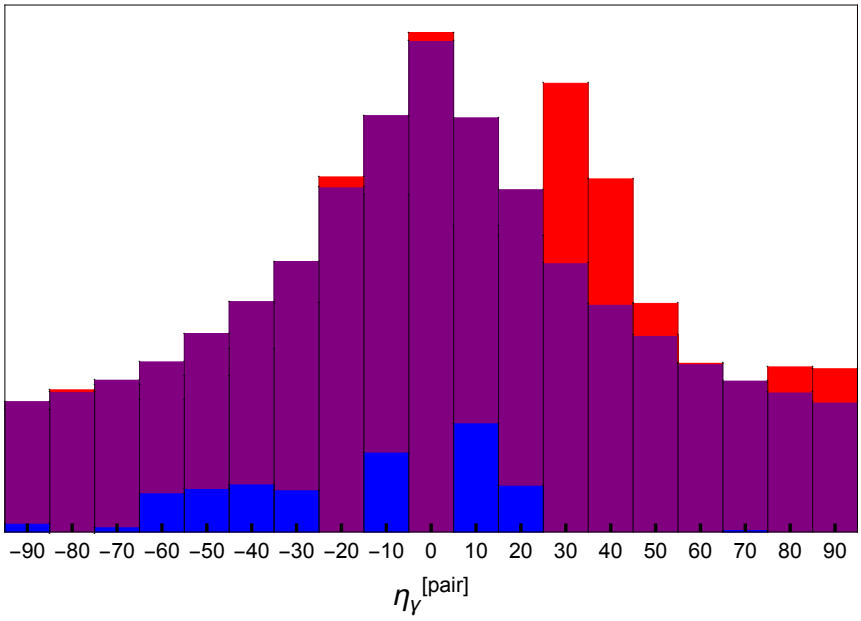

Figure 7.3. Results of a study of the type already described in the previous Fig.2, but now taking into account only pairs of photons that do not involve a "high" photon. Color coding of the bars is the same as for Fig.2.

(15 GeV $\leq E_0 \leq$ 40 GeV) and a "low" (5 GeV $\leq E_0 \leq$ 15 GeV) photon. For this case we estimate, using our simulated data obtained by time reshuffling, that the excess of occupancy of the bin $25 \leq \eta_\gamma^{[pair]} \leq 35$ visible in Fig. 7.6 should occur accidentally only in 0.2 % of cases.

7.4 Summary

In the previous sections we discussed a total of 4 analyses which are to a large extent independent, though not totally independent. Each analysis uses different pairs but for example the results reported in Fig. 7.6 and Fig. 7.5 could be used to anticipate to some extent the results of Fig. 7.2. Considering the (rather high) level of independence of the different analyses it is striking that in all cases we found an excess of results with η_γ between 25 and 35. We found that 3 of our analyses have significance between 0.2 % and 1.2 %, while the fifth analysis has significance of about 14 %. The present data situation is surely intriguing, but dwelling on percentages is in our opinion premature. We therefore prudently quote in the main text an overall significance of about 0.5 %, but surely more refined techniques of analysis of the overall statistical significance would produce an even more striking estimate.

In summary we found rather striking indications in favor of values of η_γ of about 30 in GRB data for all photons with energy at emission greater than 5 GeV. We used data that were already available at the time of the studies that led to Fig. 6.2 (which in particular focused on photons with energy at emission greater than 40 GeV) but nobody had looked before at those data for photons with energy at emission

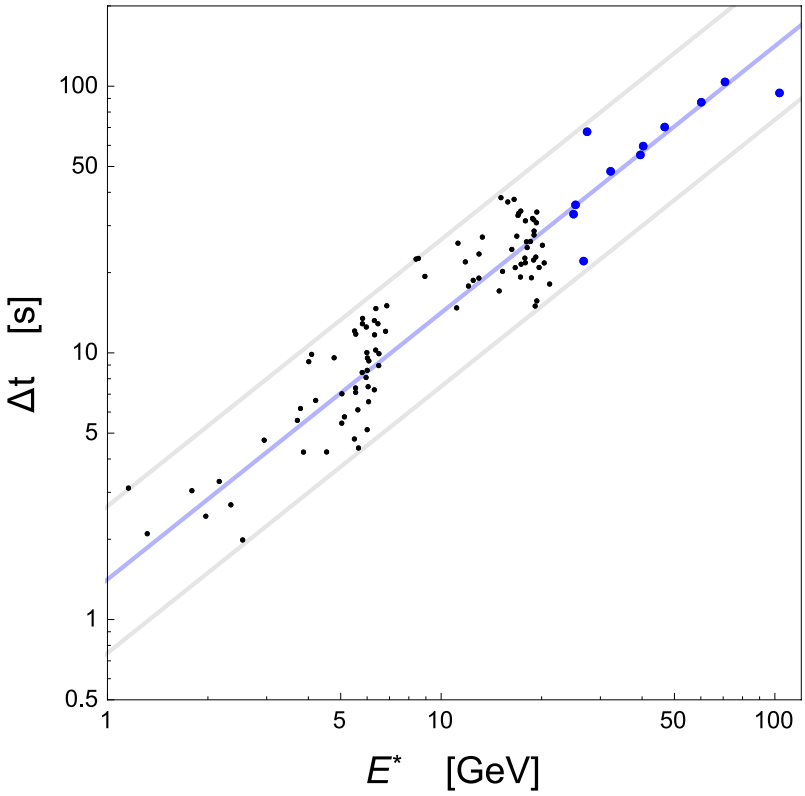

Figure 7.4. Blue points here are for the GRB photons discussed in Refs.[135] and in Chap. 6 (with energy at emission greater than 40 GeV). Black points give the E^*_{pair} and the Δt_{pair} for our pairs of GRB photons, including only cases in which both photons have energy at emission lower than 40 GeV and the associated value of $\eta_\gamma^{[pair]}$ falls within the range of values of η_γ favored by the blue points (region delimited by the gray lines). Only cases with a rather sharp determination of $\eta_\gamma^{[pair]}$ are shown (relative error of less than 30%). The violet line is for $\eta_\gamma = 34$ and intends to help the reader notice the similarity of statistical properties between the distribution of black and blue points, that goes perhaps even beyond the quantitative aspects exposed in our histograms.

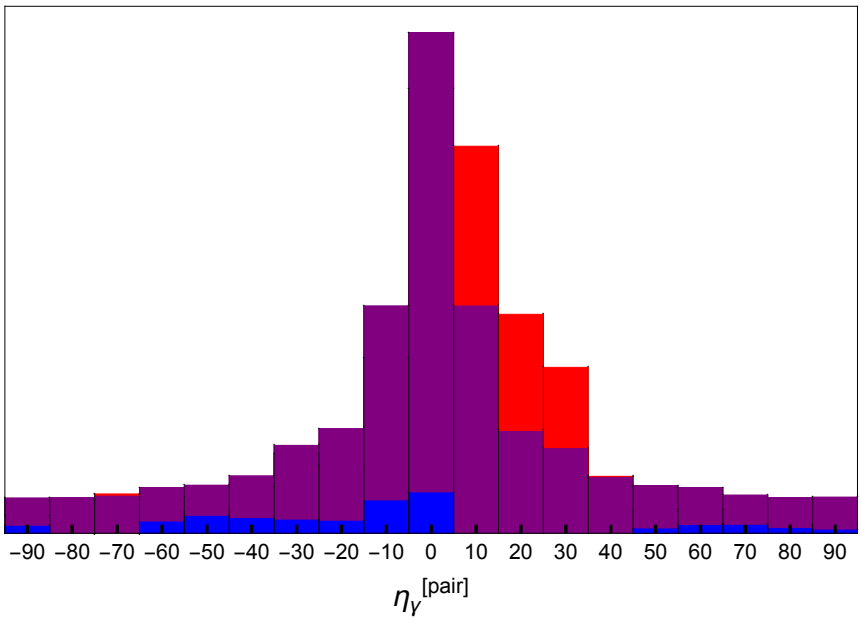

Figure 7.5. Results of a study of the type already described in the previous Figs. 7.2 and 7.3, but now we require the pair to be made of a "high" and a "low" photon.

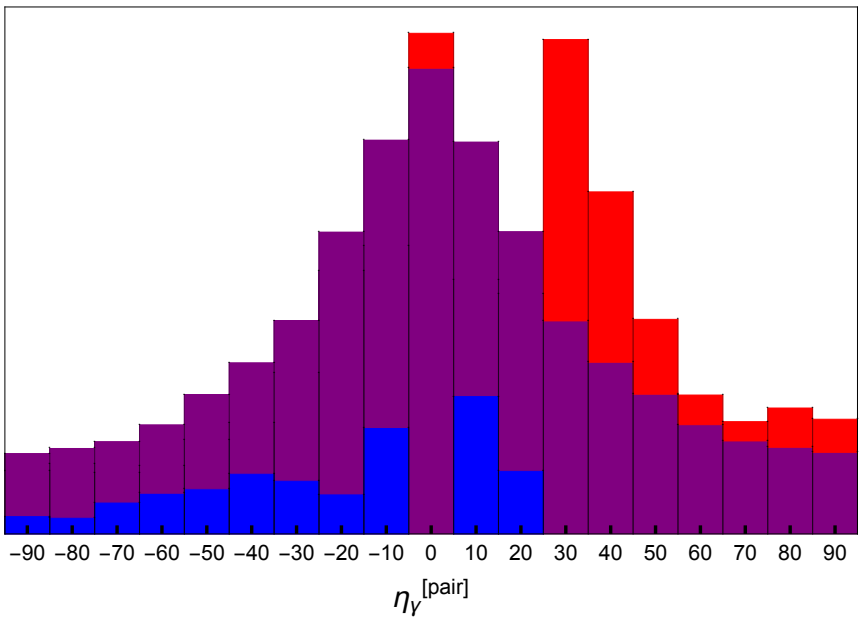

Figure 7.6. Here we show the same type of results already shown in the previous Figs. 7.2, 7.3 and 7.5 , but now taking into account only pairs composed of a "medium" and a "low" photon.

between 5 and 40 GeV, from the perspective of Fig. 6.2. We therefore feel that it might be legitimate to characterize what we here reported as a successful prediction originating from the analyses on which Fig. 6.2 was based. Combining the statistical significance here exposed with the already noteworthy statistical significance of the analyses exposed in the previous chapters, whose findings were summarized in Fig. 6.4, we are starting to lean toward expecting that not all of this is accidental, in the sense that on future similar-size GRB data samples one should find again at least some partial manifestation of the same feature. We are of course much further from establishing whether this feature truly is connected with quantum-gravity-induced in-vacuo dispersion, rather than being some intrinsic property of GRB signals. Within our analysis the imprint of in-vacuo dispersion is coded in the $D(z)$ for the distance dependence and, while that does give a good match to the data, one should keep in mind that only a few redshifts (a few GRBs) were relevant for our analysis. If we are actually seeing some form of in-vacuo dispersion it would most likely be of statistical ("fuzzy") nature since other studies have provided evidence strongly disfavoring the possibility that this type of in-vacuo-dispersion effects would affect systematically all photons [15].

GRB080916C			Redshift: 4.35		GBM trigger: 243216766.000 s				
			RA: 119.88°				Dec: -56.59°		
6.7 s	1.7 GeV	7.2 s	1.3 GeV	7.5 s	2.1 GeV	8.1 s	1.5 GeV	10.8 s	1.1 GeV
13.6 s	1.0 GeV	17.2 s	12.4 GeV	17.4 s	1.2 GeV	20.3 s	1.4 GeV	22.8 s	2.6 GeV
23.0 s	1.0 GeV	24.5 s	1.6 GeV	26.9 s	2.5 GeV	27.7 s	1.7 GeV	28.8 s	6.7 GeV
41.1 s	27.4 GeV	43.5 s	1.0 GeV	44.6 s	5.7 GeV	66.1 s	1.0 GeV	134.5 s	1.2 GeV
154.5 s	1.3 GeV	165.4 s	1.0 GeV	197.7 s	0.9 GeV	658.5 s	2.7 GeV	1206.6 s	1.8 GeV
1447.6 s	1.2 GeV	1472.7 s	6.5 GeV	1919.8 s	1.9 GeV				
GRB090510			Redshift: 0.903		GBM trigger: 263607781.970 s				
			RA: 333.400°				Dec: -26.767°		
0.7 s	3.5 GeV	0.8 s	29.9 GeV	0.8 s	6.6 GeV	1.6 s	4.4 GeV	3.4 s	2.6 GeV
3.7 s	3.7 GeV	483.4 s	5.4 GeV	531.7 s	6.4 GeV	580.2 s	10.8 GeV		
GRB090902B			Redshift: 1.822		GBM trigger: 273582310.310 s				
			RA: 265.00°				Dec: 27.33°		
8.9 s	1.8 GeV	9.3 s	3.1 GeV	9.9 s	3.1 GeV	10.0 s	7.7 GeV	10.7 s	2.1 GeV
11.0 s	2.0 GeV	11.7 s	11.9 GeV	11.8 s	1.8 GeV	13.9 s	2.0 GeV	14.2 s	14.2 GeV
14.9 s	2.0 GeV	15.4 s	5.2 GeV	16.4 s	2.2 GeV	16.5 s	2.5 GeV	17.7 s	2.5 GeV
19.1 s	5.4 GeV	19.7 s	1.9 GeV	19.9 s	2.6 GeV	21.6 s	3.3 GeV	23.3 s	2.9 GeV
23.4 s	2.2 GeV	23.4 s	5.4 GeV	23.8 s	5.6 GeV	26.2 s	18.1 GeV	26.8 s	1.8 GeV
27.5 s	1.9 GeV	41.6 s	3.3 GeV	42.4 s	12.7 GeV	43.3 s	1.9 GeV	45.6 s	15.4 GeV
49.3 s	2.1 GeV	65.2 s	2.8 GeV	81.7 s	39.9 GeV	85.9 s	3.6 GeV	104.4 s	5.5 GeV
108.5 s	2.9 GeV	170.9 s	4.7 GeV	258.8 s	2.2 GeV	277.7 s	2.4 GeV	296.5 s	4.2 GeV
331.9 s	21.7 GeV	438.7 s	3.6 GeV	527.0 s	6.0 GeV	829.1 s	2.3 GeV		
GRB090926A			Redshift: 2.1071		GBM trigger: 275631628.990 s				
			RA: 353.56°				Dec: -66.34°		
9.5 s	3.3 GeV	11.8 s	2.0 GeV	14.7 s	2.2 GeV	15.5 s	2.7 GeV	16.5 s	2.0 GeV
16.7 s	2.1 GeV	16.9 s	2.5 GeV	19.8 s	1.8 GeV	24.8 s	19.5 GeV	34.7 s	2.2 GeV
39.0 s	6.2 GeV	45.6 s	2.2 GeV	59.5 s	3.1 GeV	60.3 s	7.7 GeV	64.3 s	2.6 GeV
77.8 s	3.9 GeV	91.6 s	2.8 GeV	92.0 s	6.3 GeV	111.6 s	2.4 GeV	199.0 s	2.1 GeV
218.9 s	5.0 GeV	255.8 s	1.9 GeV	271.9 s	4.7 GeV	313.9 s	1.7 GeV		
GRB100414A			Redshift: 1.368		GBM trigger: 292904423.990 s				
			RA: 191.59°				Dec: 8.57°		
33.4 s	29.8 GeV	39.3 s	4.4 GeV	49.7 s	2.2 GeV	288.3 s	5.4 GeV	358.5 s	25.1 GeV
GRB130427A			Redshift: 0.34		GBM trigger: 388741629.420 s				
			RA: 173.148°				Dec: 27.709°		
11.0 s	8.7 GeV	15.0 s	9.9 GeV	18.6 s	77.1 GeV	20.2 s	5.3 GeV	20.8 s	4.8 GeV
21.8 s	4.3 GeV	23.2 s	10.9 GeV	23.5 s	12.0 GeV	23.9 s	8.3 GeV	37.6 s	9.9 GeV
47.6 s	28.4 GeV	64.5 s	12.2 GeV	78.4 s	38.7 GeV	80.5 s	12.9 GeV	84.7 s	26.9 GeV
119.3 s	14.9 GeV	123.1 s	6.6 GeV	129.4 s	8.2 GeV	141.1 s	25.4 GeV	149.4 s	4.0 GeV
184.7 s	5.8 GeV	213.3 s	5.1 GeV	213.9 s	11.7 GeV	217.5 s	17.1 GeV	243.1 s	94.1 GeV
256.3 s	57.4 GeV	469.1 s	5.8 GeV	486.7 s	4.8 GeV	536.8 s	7.5 GeV	610.6 s	43.7 GeV
GRB160509A			Redshift: 1.17		GBM trigger: 484477148.360 s				
			RA: 311.3°				Dec: 76.1°		
6.1 s	2.3 GeV	58.4 s	51.9 GeV	115.7 s	3.9 GeV	194.1 s	8.8 GeV	224.1 s	41.5 GeV
582.9 s	3.7 GeV	1757.4 s	6.5 GeV	2180.6 s	20.5 GeV	NA s	NA GeV		

Table 7.1. Here reported the difference in times in seconds of observation from the GBM trigger and the observed energy in GeV for each of the 148 photons considered in this analysis. For each of the 7 GRBs it is also reported the value of its redshift, its trigger time expressed in MJD (Modified Julian Date) and its location expressed in right ascension (RA) and declination (Dec).

Chapter 8

Conclusions

This thesis work has been devoted to address the challenge to find the first macroscopic and indirect evidence of Planck-scale effects in astrophysical observations. We focused in particular on those effects, like the in-vacuo dispersion or the dual gravity lensing, whose prediction relies on the possibility of breaking or modifying the relativistic symmetries at the Planck the scale . As shown in Chap. 1, these kind of speculations finds support in those quantum-gravity models in which one has to abandon the special-relativistic framework by introducing either a a preferred reference frame (this is what happens in Lorentz-symmetry-breaking theories) or by deforming the transformation laws between inertial at the Planck scale (like in DSR theories). The main result of this thesis work is probably summarized at best in Fig. 6.4 of Chap. 6 and in Fig. 7.4 of Chap. 7, in which the feature that has been discovered for both neutrinos and photons is shown, along with the consistency between them. Our statistical analysis suggest that these features are unlikely due to chance, as shown vividly by the small values of the false alarm probabilities found in our Monte Carlo simulations.

Our work for the neutrino feature of Chaps. 4 and 5 took off from the analogous study reported in Ref. [36], with additional motivation found in what had been reported in Ref. [124]. We looked within IceCube data from June 2010 to May 2014 for the same feature which had been already noticed in Ref. [36], in an analysis based on much poorer IceCube data for the period from April 2008 to May 2010. The study of Ref. [36] was intriguing but ultimately appeared to be little more than an exercise in data-analysis strategy, since it could only consider 3 neutrinos, none of which could be viewed as a promising GRB-neutrino candidate. The 109-TeV event considered in Ref. [36] could be easily dismissed as likely the result of a cosmic-ray air shower, and the other two neutrinos were of much lower energy, energies at which atmospheric neutrinos are very frequent. Yet what we found here is remarkably consistent with what had been found in Ref. [36]. We chose to rely exclusively on data unavailable to Ref. [36], IceCube data from June 2010 to May 2014, and on these new data alone the feature is present very strongly, characterized by a false alarm probability which we estimated fairly at 0.03 % and ultraconservatively at 1 %. We feel this should suffice to motivate a vigorous program of further investigation of the scenarios analyzed in Chap. 4. Particularly over these last few decades of fundamental physics, results even more encouraging than ours have then gradually

faded away, as more data was accrued, and we are therefore well prepared to see our neutrinos have that fate. We are more confident that our strategy of analysis will withstand the test of time. The main ingredient of novelty is the central role played by the correlation between the energy of a neutrino and the difference between the time of observation of that neutrino and the trigger time of a GRB. The advantage of focusing on this correlation is that it is expected in a rather broad class of phenomenological models of particle propagation in a quantum spacetime.

The analyses reported in Chaps. 6 and 7 took off instead from studies reported in Refs. [138, 136, 135]. Our quantification of statistical significance gave impressive results also for the photon features (which we estimate of about 0.5%), as well as for the consistency between them. We still feel that the overall situation should be assessed in depth, since the class of effects we explored here would imply, if truly discovered, that fundamental physics goes beyond its current horizons. Steps like these, rare as they are in fundamental physics, must require extremely high statistical evidence, and so more data is required. Nonetheless it is inevitable to assess and find possible interpretations for the present situation.

More data will soon be available both for our photons and for our neutrinos. Particularly for neutrinos a much improved analysis should become soon possible, since so far we only analyzed the IceCube data publicly available up to May of 2014, while the inclusion in the analysis of the events from 2014 to 2016, at the time of writing this thesis, is an on-going project. Moreover we know that some additional 2 years of data have been collected by IceCube but have not yet been publicly released. For photons our main reference is the Fermi telescope, which has been operating since 2008. In about 8 year of operation Fermi provided 7 GRBs contributing to the photon side of our analysis of Chaps. 6 and 7, so we can expect to have roughly one GRB per year adding data to our photon feature.

If the neutrino feature was confirmed it would be very hard to even imagine an astrophysical origin for that feature. The relevant effects are of the order of a couple of days, and neutrinos observed two days before or after a GRB could not possibly be GRB neutrinos (unless in-vacuo dispersion takes place). If the neutrino feature is confirmed when more abundant data become available we would know that something not of astrophysical origin has been discovered. In this respect the photon feature is very different. The size of the effects is between a few and ~ 100 seconds, which may well be the time scale of some mechanisms intrinsic of GRBs. For photons instead our intuition, while being open to ultimately finding conclusive evidence of in-vacuo dispersion, presently favors the possibility of a scenario in which the feature is confirmed by additional data but in the end the correct description be given in terms of some properties of the astrophysical sources. We would welcome feedback from the astrophysics community on the type of "mechanisms at the source" that could produce such a feature for photons.

Appendix A

IceCube-neutrinos catalog

ID	Dep. Energy (TeV)	Time (MJD)	Decl. (deg.)	R.A. (deg.)	Ang. Err. (deg.)	Topology
1	$47.6^{+6.5}_{-5.4}$	55351.32	−1.8	35.2	16.3	Shower
2	117^{+15}_{-15}	55351.47	−28.0	282.6	25.4	Shower
3	$78.7^{+10.8}_{-8.7}$	55451.07	−31.2	127.9	$\lesssim 1.4$	Track
4	165^{+20}_{-15}	55477.39	−51.2	169.5	7.1	Shower
5	$71.4^{+9.0}_{-9.0}$	55512.55	−0.4	110.6	$\lesssim 1.2$	Track
6	$28.4^{+2.7}_{-2.5}$	55567.64	−27.2	133.9	9.8	Shower
7	$34.3^{+3.5}_{-4.3}$	55571.26	−45.1	15.6	24.1	Shower
8	$32.6^{+10.3}_{-11.1}$	55608.82	−21.2	182.4	$\lesssim 1.3$	Track
9	$63.2^{+7.1}_{-8.0}$	55685.66	33.6	151.3	16.5	Shower
10	$97.2^{+10.4}_{-12.4}$	55695.27	−29.4	5.0	8.1	Shower
11	$88.4^{+12.5}_{-10.7}$	55714.59	−8.9	155.3	16.7	Shower
12	104^{+13}_{-13}	55739.44	−52.8	296.1	9.8	Shower
13	253^{+26}_{-22}	55756.11	40.3	67.9	$\lesssim 1.2$	Track
14	1041^{+132}_{-144}	55782.52	−27.9	265.6	13.2	Shower
15	$57.5^{+8.3}_{-7.8}$	55783.19	−49.7	287.3	19.7	Shower
16	$30.6^{+3.6}_{-3.5}$	55798.63	−22.6	192.1	19.4	Shower
17	200^{+27}_{-27}	55800.38	14.5	247.4	11.6	Shower
18	$31.5^{+4.6}_{-3.3}$	55923.53	−24.8	345.6	$\lesssim 1.3$	Track
19	$71.5^{+7.0}_{-7.2}$	55925.80	−59.7	76.9	9.7	Shower
20	1141^{+143}_{-133}	55929.40	−67.2	38.3	10.7	Shower
21	$30.2^{+3.5}_{-3.3}$	55936.54	−24.0	9.0	20.9	Shower
22	220^{+21}_{-24}	55941.98	−22.1	293.7	12.1	Shower
23	$82.2^{+8.6}_{-8.4}$	55949.57	−13.2	208.7	$\lesssim 1.9$	Track
24	$30.5^{+3.2}_{-2.6}$	55950.85	−15.1	282.2	15.5	Shower
25	$33.5^{+4.9}_{-5.0}$	55966.74	−14.5	286.0	46.3	Shower
26	210^{+29}_{-26}	55979.26	22.7	143.4	11.8	Shower
27	$60.2^{+5.6}_{-5.6}$	56008.68	−12.6	121.7	6.6	Shower
28	$46.1^{+5.7}_{-4.4}$	56048.57	−71.5	164.8	$\lesssim 1.3$	Track
29	$32.7^{+3.2}_{-2.9}$	56108.26	41.0	298.1	7.4	Shower
30	129^{+14}_{-12}	56115.73	−82.7	103.2	8.0	Shower
31	$42.5^{+5.4}_{-5.7}$	56176.39	78.3	146.1	26.0	Shower

32	—	56211.74	—	—	—	Coincident
33	$385\,^{+46}_{-49}$	56221.34	7.8	292.5	13.5	Shower
34	$42.1\,^{+6.5}_{-6.3}$	56228.61	31.3	323.4	42.7	Shower
35	$2004\,^{+236}_{-262}$	56265.13	−55.8	208.4	15.9	Shower
36	$28.9\,^{+3.0}_{-2.6}$	56308.16	−3.0	257.7	11.7	Shower
37	$30.8\,^{+3.3}_{-3.5}$	56390.19	20.7	167.3	$\lesssim 1.2$	Track
38	$200.5\,^{+16.4}_{-16.4}$	56470.11	14.0	93.3	<1.2	Track
39	$101.3\,^{+13.3}_{-11.6}$	56480.66	-17.9	106.2	14.2	Shower
40	$157.3\,^{+15.9}_{-16.7}$	56501.16	-48.5	143.9	11.7	Shower
41	$87.6\,^{+8.4}_{-10.0}$	56603.11	3.3	66.1	11.1	Shower
42	$76.3\,^{+10.3}_{-11.6}$	56613.26	-25.3	42.5	20.7	Shower
43	$46.5\,^{+5.9}_{-4.5}$	56628.57	-22.0	206.6	<1.3	Track
44	$84.6\,^{+7.4}_{-7.9}$	56671.88	0.0	336.7	<1.2	Track
45	$429.9\,^{+57.4}_{-49.1}$	56679.20	-86.3	219.0	<1.2	Track
46	$158.0\,^{+15.3}_{-16.6}$	56688.07	-22.3	150.5	7.6	Shower
47	$74.3\,^{+8.3}_{-7.2}$	56704.60	67.4	209.4	<1.2	Track
48	$104.7\,^{+13.5}_{-10.2}$	56705.94	-33.2	213.0	8.1	Shower
49	$59.9\,^{+8.3}_{-7.9}$	56722.41	-26.3	203.2	21.8	Shower
50	$22.2\,^{+2.3}_{-2.0}$	56737.20	59.3	168.6	8.2	Shower
51	$66.2\,^{+6.7}_{-6.1}$	56759.22	54.0	88.6	6.5	Shower
52	$158.1\,^{+16.3}_{-18.4}$	56763.54	-54.0	252.8	7.8	Shower
53	$27.6\,^{+2.6}_{-2.2}$	56767.07	-37.7	239.0	<1.2	Track
54	$54.5\,^{+5.1}_{-6.3}$	56769.03	6.0	170.5	11.6	Shower
55	0.0	56798.73	—	—	—	Coincident
56	$104.2\,^{+9.7}_{-10.0}$	56817.39	-50.1	280.5	06.5	Shower
57	$132.1\,^{+18.1}_{-16.8}$	56830.53	-42.2	123.0	14.4	Shower
58	$52.6\,^{+5.2}_{-5.7}$	56859.76	-32.4	102.1	<1.3	Track
59	$124.6\,^{+11.6}_{-11.7}$	56922.59	-03.9	63.3	08.8	Shower
60	$93.0\,^{+12.9}_{-11.7}$	56931.93	-37.9	32.7	13.3	Shower
61	$53.8\,^{+7.2}_{-6.3}$	56970.21	-16.5	55.6	<1.2	Track
62	$75.8\,^{+6.7}_{-7.1}$	56987.77	13.3	187.9	<1.3	Track
63	$97.4\,^{+9.6}_{-9.6}$	57000.14	06.5	160.0	<1.2	Track
64	$70.8\,^{+8.1}_{-7.7}$	57036.74	-27.3	144.5	10.6	Shower
65	$43.3\,^{+5.9}_{-5.2}$	57051.66	-33.5	72.8	17.5	Shower
66	$84.2\,^{+10.7}_{-9.9}$	57053.13	38.3	128.7	18.3	Shower
67	$165.7\,^{+16.5}_{-15.5}$	57079.97	3	335.7	7.0	Shower
68	$59.1\,^{+8.0}_{-6.0}$	57081.54	-15.7	294.3	11.7	Shower
69	$18.0\,^{+2.2}_{-2.0}$	57133.79	0.3	236.2	15.7	Shower
70	$98.8\,^{+12.0}_{-11.1}$	57134.40	-33.5	93.9	12.3	Shower
71	$73.5\,^{+10.0}_{-10.5}$	57140.47	-20.8	80.7	<1.2	Track
72	$35.3\,^{+4.6}_{-4.1}$	57144.30	28.3	203.2	19.5	Shower
73	$26.2\,^{+2.6}_{-2.3}$	57154.84	11.1	278.4	6.9	Shower
74	$71.3\,^{+9.1}_{-8.1}$	57157.00	-0.9	341.0	12.7	Shower
75	$164.0\,^{+20.7}_{-21.4}$	57168.40	70.5	259.0	13.1	Shower
76	$126.3\,^{+12.0}_{-12.7}$	57276.57	-0.4	240.2	<1.2	Track

77	$39.5^{+3.8}_{-3.7}$	57285.02	2.1	278.4	7.2	Shower
78	$56.7^{+7.0}_{-6.9}$	57363.44	7.5	0.4	<1.2	Track
79	$158.2^{+20.3}_{-19.8}$	57365.75	-11.1	24.6	14.6	Shower
80	$85.6^{+11.1}_{-10.6}$	57386.36	-3.6	146.6	16.1	Shower
81	$151.8^{+13.9}_{-21.6}$	57480.65	-79.4	45.0	13.5	Shower
82	$159.3^{+15.5}_{-15.3}$	57505.24	9.4	240.9	<1.2	Track

Table A.1. Properties of the events observed in six years of data taking from early 2010 to early 2016 for a total livetime of 2078 days [95]. The "Dep. Energy" column shows the electromagnetic-equivalent deposited energy of each event. Events 28, 32 and 55 have coincident hits in the IceTop surface array, implying that they are almost certainly produced in cosmic ray air showers. "Ang. Err" shows the median angular error including systematic uncertainties.

Appendix B

Gamma-ray-bursts catalog

In the next pages we show, laid out in two columns, the relevant properties, taken from the GRB-web catalog [83], of all GRBs used in this research thesis. For the sake of brevity we only show the name of the GRB (first column), its right ascension (second column) and declination (third column), the angular error (fourth column), its T90 (fifth column), the time of the day at which the GRB was observed (sixth column) and its redshift (last column). If the redshift is not measured a redshift of 2.15 (0.5) is assigned for Long (Short) GRBs.

Name	RA	Decl	ERR	T90	Time	z
100604A	248.3	-73.19	3.64	13.44	06:53:34	2.15
100605A	273.43	-67.6	7.67	8.19	18:35:10	2.15
100606A	350.627	-66.241	3e-04	480	19:12:41	2.15
100608A	30.54	20.45	5.33	30.21	09:10:06	2.15
100609A	90.48	42.78	2.53	230.41	18:48:11	2.15
100612A	63.53	13.74	2.69	0.58	13:04:21	0.5
100612B	352	-1.83	1.58	8.58	17:26:06	2.15
100614A	263.499	49.234	3e-04	225	21:38:26	2.15
100614B	224.76	40.87	2.99	172.29	11:57:23	2.15
100615A	177.205	-19.481	3e-04	39	01:59:03	1.398
100616A	342.91	3.09	45.74	0.19	18:32:32	0.5
100619A	84.622	-27.005	3e-04	97.5	00:21:07	2.15
100620A	80.1	-51.68	1.46	51.84	02:51:29	2.15
100621A	315.305	-51.106	3e-04	63.6	03:03:32	0.542
100621B	103.83	37.35	2.81	123.91	10:51:18	2.15
100621C	160.86	14.72	11.41	1.03	12:42:16	0.5
100625A	15.796	-39.088	3e-04	0.192	18:32:27	0.5
100625B	338.26	20.29	4.45	29.18	21:22:45	2.15
100628A	225.943	-31.653	0.0213	0.036	08:16:40	0.5
100629A	231.21	27.81	3.32	0.83	19:14:03	0.5
100701B	43.109	-2.224	0.0923	15	11:45:19	2.15
100702A	245.693	-56.549	0.0142	0.16	01:03:47	0.5
100703A	9.522	-25.71	0.0284	0.07	17:43:37	0.5
100704A	133.641	-24.203	3e-04	197.5	03:35:08	2.15
100706A	255.16	46.89	12.23	0.13	16:38:18	0.5
100707A	358.019	-8.658	1.1217	12	00:46:38	2.15
100709A	142.53	17.38	4.47	100.1	14:27:32	2.15
100713A	255.209	28.39	0.0253	20	14:36:06	2.15
100713B	82.06	13	3.74	7.61	23:31:34	2.15
100714A	106.37	51.14	3.69	35.58	16:07:23	2.15
100714B	307.94	61.3	9.69	5.63	16:27:20	2.15
100715A	299.27	-54.71	9.32	14.84	11:27:17	2.15
100717A	287.06	-0.66	8.84	5.96	08:55:06	2.15
100717B	304.31	19.53	9.19	2.43	10:41:47	2.15
100718A	298.47	41.43	10.24	38.66	19:06:22	2.15
100718B	121.83	-46.18	5.93	32.64	03:50:09	2.15
100719A	112.319	-5.857	0.0243	36.0	03:30:57	2.15
100719B	304.87	-67.14	15.41	1.6	07:28:17	0.5
100719C	231.41	18.56	10.32	3.07	19:48:08	2.15
100719D	113.3	5.4	1	21.82	23:44:04	2.15
100722A	238.77	-15.61	1.07	7.17	02:18:37	2.15
100722B	31.81	56.23	8.06	1.28	06:58:24	0.5
100724A	194.543	-11.103	3e-04	1.4	00:42:19	1.288
100724B	120.04	76.74	1.1	103	00:42:04	2.15
100725A	166.482	-26.67	3e-04	141	07:12:52	2.15
100725B	290.033	76.956	3e-04	200	11:24:34	2.15
100727A	154.177	-21.39	3e-04	84	05:42:17	2.15
100728A	88.758	-15.255	2e-04	198.5	02:18:24	1.567
100728B	163.488	-45.473	1e-04	10.24	10:31:54	2.106
100730A	339.79	-22.23	5.4	63.88	11:06:14	2.15
100802A	2.468	47.755	3e-04	487	05:45:36	2.15
100804A	248.97	27.45	1	6.59	02:29:26	2.15
100805A	299.877	52.628	1e-04	15.0	04:12:42	2.15
100805B	22.8	34.19	7.65	0.07	07:12:12	0.5
100805C	112.72	-35.93	3.75	58.43	20:16:29	2.15
100807A	55.3	67.672	3e-04	7.9	09:13:13	2.15
100810A	124.77	-1.61	5.65	2.56	01:10:34	2.15
100811A	345.87	15.86	6.04	0.38	02:35:49	0.5
100811B	108.14	62.19	3.57	78.08	18:44:09	2.15
100814A	22.473	-17.995	3e-04	110	03:50:08	2.15
100814B	122.82	18.49	2.6	7.43	08:25:25	2.15
100816A	351.74	26.579	3e-04	2.05	00:37:50	0.8034
100816B	102.12	-26.66	1.06	62.4	00:12:41	2.15
100819A	279.6	-50.04	3.86	12.54	11:56:35	2.15
100820A	258.79	-18.51	2.14	8.96	08:56:58	2.15
100823A	20.704	5.835	4e-04	NA	17:25:33	2.15
100825A	253.44	-56.57	6.34	3.33	06:53:48	2.15
100826A	279.593	-22.128	1.6037	150	22:58:29	2.15
100827A	193.9	71.89	5.68	0.58	10:55:49	0.5
100829A	90.409	30.314	0.2693	10	21:02:07	2.15
100829B	115.45	-3.99	4.66	94.97	08:59:07	2.15
100831A	161.26	33.65	10.16	40.2	15:37:25	2.15
100901A	27.265	22.759	4e-04	439	13:34:10	1.408
100902A	48.629	30.979	3e-04	428.8	19:31:54	2.15
100902B	306.04	42.31	7.2	22.28	23:45:19	2.15
100904A	172.907	-16.185	0.0182	37.5	01:33:43	2.15
100905A	31.55	14.929	3e-04	3.4	15:08:14	2.15
100905B	262.65	13.08	4	11.52	21:46:22	2.15
100906A	28.684	55.631	2e-04	114.4	13:49:27	1.727
100907A	177.29	-40.63	6.9	5.38	18:01:11	2.15
100909A	73.951	54.654	0.0203	60	09:04:00	2.15
100910A	238.1	-34.62	1.02	13.83	19:37:43	2.15
100911A	151.32	58.99	11.77	5.63	19:35:39	2.15
100915A	315.694	65.673	3e-04	200	01:31:05	2.15
100915B	85.394	25.095	0.0203	7.8	05:49:39	2.15
100916A	151.96	-59.38	3.48	12.8	18:41:12	2.15
100917A	289.25	-17.12	0.0213	66	05:03:25	2.15
100918A	308.41	-45.96	1	86.02	20:42:18	2.15
100919A	163.24	6.02	1.81	49.6	21:12:16	2.15
100922A	356.98	-25.19	15.03	4.35	14:59:43	2.15
100923A	106.12	39.6	5.35	51.71	20:15:10	2.15
100924A	0.672	7.004	0.0101	96.0	03:58:08	2.15
100925A	254.736	-15.236	0.0304	NA	08:05:05	2.15
100926A	222.75	-72.35	3.81	32.25	14:17:03	2.15
100926B	43.58	-11.1	12	37.89	16:39:54	2.15
100928A	223.037	-28.542	0.0233	3.3	02:19:52	2.15
100929A	166.33	62.29	13.39	8.19	05:38:52	2.15
100929B	243.62	33.33	23.83	4.61	07:33:04	2.15
100929C	183.03	-24.94	7.79	0.32	21:59:45	0.5
101002A	323.35	-27.47	16.36	7.17	06:41:26	2.15
101003A	175.85	2.49	7.39	9.98	05:51:08	2.15
101004A	232.22	-43.99	7.29	161.03	10:13:49	2.15
101008A	328.875	37.067	3e-04	104	16:43:15	2.15
101010A	47.19	43.56	18.63	65.03	04:33:46	2.15
101011A	48.294	-65.982	2e-04	71.5	16:58:35	2.15
101013A	292.08	-49.64	1.6	15.36	09:52:42	2.15
101014A	26.94	-51.07	1	449.41	04:11:52	2.15
101015A	73.16	15.46	5.94	500.55	13:24:02	2.15
101016A	133.04	-4.62	2.81	3.84	05:50:16	2.15
101017A	291.386	-35.145	4e-04	45	10:32:41	2.15
101017B	27.47	-26.55	4.92	47.87	14:51:29	2.15
101020A	189.607	23.129	0.0345	175.0	23:40:41	2.15
101021A	0.87	-23.71	1.33	120.77	00:13:25	2.15
101021B	0.46	47.34	12.81	1.53	01:30:31	0.5
101023A	317.964	-65.389	3e-04	80.8	22:50:12	2.15
101024A	66.506	-77.265	3e-04	24.45	11:39:33	2.15
101025A	240.19	-8.49	24.35	14.33	03:30:18	2.15
101026A	263.7	-0.37	7.57	0.26	00:49:16	0.5
101027A	79.02	43.97	11.39	1.34	05:30:30	0.5
101030A	166.382	-16.378	3e-04	95.74	15:56:30	2.15
101031A	184.12	-7.47	15.87	0.38	14:59:32	0.5
101101A	13.55	45.75	3.06	3.32	17:51:34	2.15
101101B	266.04	-29	5.45	31.23	21:34:08	2.15
101102A	284.68	-37.03	7.85	43.52	20:10:07	2.15
101104A	161.02	-7.08	8.53	1.28	19:26:14	0.5
101107A	168.33	22.43	4.09	375.82	00:16:25	2.15
101112A	292.218	39.359	0.0217	10	22:10:24	2.15
101112B	100.1	9.62	5.13	82.94	23:36:55	2.15
101113A	29.08	0.21	2.67	12.29	11:35:36	2.15
101114A	303.193	14.029	0.0182	NA	00:32:50	2.15
101116A	32	-81.2	7.26	0.58	11:32:26	0.5
101117A	57.19	-26.87	1.75	50.18	11:54:45	2.15
101117B	173.002	-72.663	1e-04	5.2	19:13:23	2.15
101119A	226.49	59.61	16.19	0.64	16:27:02	0.5
101123A	131.381	5.563	0.3407	103.94	22:51:34	2.15
101126A	84.77	-22.55	1	43.84	04:44:27	2.15
101127A	290.31	7.89	23.17	29.44	02:13:59	2.15
101127B	70.95	-11.32	6.55	60.67	02:27:30	2.15
101128A	145.47	-35.2	5.7	8.2	07:44:04	2.15
101129A	155.921	-17.645	0.0304	0.4	15:39:30	2.15
101129B	271.54	1.01	8.22	0.57	17:25:25	0.5
101130A	61.803	-16.75	0.196	65.792	09:39:26	2.15
101130B	274.61	26.62	23.61	4.86	01:45:54	2.15
101201A	1.955	-16.196	0.0203	112.64	10:01:49	2.15
101202A	254.02	58.48	6.13	18.43	03:41:53	2.15
101204A	167.537	-20.42	3e-04	10	23:53:29	2.15
101204B	191.91	55.67	10.37	0.12	08:14:18	0.5
101205A	322.1	-39.1	11.1	7.94	07:24:24	2.15
101206A	164.08	-38.11	3.5	34.82	00:52:17	2.15
101207A	175.75	8.72	3.73	61.44	12:51:41	2.15
101208A	212.4	4.04	11.7	0.19	04:52:56	0.5

101208B	280.94	-59.02	1.41	2.05	11:57:01	2.15
101211A	31.84	10.06	11.25	13.57	11:37:54	2.15
101213A	241.314	21.897	3e-04	32	10:49:19	0.414
101213B	260.99	-64.51	7.06	6.65	20:22:26	2.15
101214A	0.69	-28.27	5.56	2.24	17:57:03	2.15
101214B	181.13	-31.06	5.73	11.52	23:50:00	2.15
101216A	284.27	-20.97	2.12	1.92	17:17:52	0.5
101219A	74.586	-2.527	0.0101	0.6	02:31:29	0.718
101219B	12.231	-34.567	3e-04	34	16:27:53	0.5519
101220A	241.57	46.14	1.25	72.45	13:49:58	2.15
101220B	2.7	27.2	1.48	31.74	20:43:54	2.15
101223A	250.55	48.22	4.34	56.07	20:00:18	2.15
101224A	285.939	45.706	0.0213	1.72	05:27:13	0.5
101224B	289.14	-55.25	4.82	44.74	13:52:58	2.15
101224C	290.16	34.46	8.86	25.6	14:43:32	2.15
101224D	325.17	-38.66	8.29	18.69	23:57:34	2.15
101225A	0.198	44.6	2e-04	1088.0	18:37:45	0.4
101225B	60.68	32.77	1.81	81.22	09:02:53	2.15
101227A	186.79	-83.55	7.16	95.49	04:40:28	2.15
101227B	240.5	-24.5	1.62	153.34	09:45:06	2.15
101227C	150.87	-49.44	2.59	28.87	12:51:46	2.15
101231A	191.71	17.64	1.41	23.62	01:36:50	2.15
110101A	264.26	36.54	11.17	3.58	04:50:20	2.15
110101B	105.5	34.58	16.49	235.53	12:08:21	2.15
110102A	245.881	7.614	1e-04	264	18:52:25	2.15
110105A	85.11	-17.12	2.03	123.39	21:02:39	2.15
110106A	79.306	64.173	3e-04	4.3	15:25:16	0.093
110106B	134.154	47.003	3e-04	35.52	21:26:16	0.618
110107A	299.89	41.889	0.0304	NA	21:15:51	2.15
110108A	11.62	-9.64	2.67	51.45	23:26:18	2.15
110112A	329.932	26.456	5e-04	0.5	04:12:18	0.5
110112B	10.599	64.406	0.0263	0.5	22:24:54	2.15
110117A	130.87	47.59	9.63	72.45	08:44:50	2.15
110117B	129.51	-12.88	3.57	43.27	15:01:27	2.15
110118A	226.57	-39.55	4.07	34.56	20:34:18	2.15
110119A	348.586	5.986	3e-04	208	22:20:58	2.15
110120A	61.6	-12	0.4	6.4	15:59:39	2.15
110123A	246.97	28.03	1.16	17.86	19:17:45	2.15
110124A	53.83	36.35	9.14	5.38	18:49:09	2.15
110125A	331.35	-46.21	5.76	4.8	21:27:28	2.15
110128A	193.896	28.065	2e-04	12.16	01:44:36	2.339
110130A	111.51	38.25	6.75	47.36	05:31:52	2.15
110131A	183.79	72.91	14.52	0.38	18:42:38	0.5
110201A	137.489	88.61	0.0132	13.0	09:35:08	2.15
110204A	1.82	-17.4	4.03	28.67	04:17:11	2.15
110205A	164.63	67.525	3e-04	330	02:02:41	2.22
110205B	359.73	-80.44	9.24	6.4	00:39:04	2.15
110205C	312.69	-55.85	10.12	158.72	14:07:20	2.15
110206A	92.355	-58.808	0.0203	20	18:08:05	2.15
110206B	333.7	1.61	15.47	12.29	04:50:36	2.15
110207A	12.54	-10.79	0.0132	37.88	11:17:20	2.15
110207B	179	-58.43	9.03	7.68	23:00:26	2.15
110208A	22.462	-20.593	3e-04	37.4	21:10:46	2.15
110209A	329.7	-21.93	10.63	5.64	03:58:08	2.15
110210A	13.057	7.78	3e-04	233	09:52:41	2.15
110212A	69.025	43.716	0.0142	3.3	01:09:08	2.15
110212B	311.33	-74.5	4.33	0.07	13:12:33	0.5
110213A	42.964	49.273	3e-04	48.0	05:17:29	1.46
110213B	41.768	0.952	0.304	50	14:31:33	1.083
110213C	6.28	27.54	10.82	0.32	21:00:51	0.5
110217A	274.74	32.35	8.49	60.67	14:10:46	2.15
110220A	185.49	16.58	6.06	33.02	18:16:21	2.15
110221A	15.18	66.05	1.24	13.06	05:51:19	2.15
110223A	345.854	87.558	3e-04	7.0	20:56:59	2.15
110223B	150.233	-68.302	3e-04	54.0	21:25:48	2.15
110226A	199.29	35.77	7.07	14.08	23:44:31	2.15
110227A	148.72	-54.04	11.93	1.73	00:12:28	0.5
110227B	25.24	15.89	7.45	18.43	05:30:10	2.15
110227C	232.73	-9.94	4.99	25.6	10:04:12	2.15
110228A	10.27	-45.67	2.56	44.48	00:15:58	2.15
110228B	245.09	16.41	4.74	17.15	18:59:50	2.15
110301A	229.35	29.4	1	5.7	05:08:43	2.15
110302A	122.35	2.91	6.84	38.34	01:01:51	2.15
110304A	322.93	33.27	4.23	19.52	01:42:33	2.15
110305A	260.881	-15.802	3e-04	12.0	06:38:01	2.15
110307A	193.12	15.64	7.58	2.3	23:19:08	2.15
110311A	117.59	34.29	9.68	6.4	19:29:21	2.15
110312A	157.481	-5.263	3e-04	28.7	17:55:37	2.15
110315A	279.195	17.539	2e-04	77	23:57:04	2.15
110316A	46.7	-67.58	17.8	2.95	03:19:41	2.15
110318A	338.292	-15.278	0.0101	16.0	13:14:19	2.15
110318B	211.678	-51.579	3e-04	4.8	15:27:09	2.15
110319A	356.502	-66.011	3e-04	19.3	02:16:41	2.15
110319B	326.088	-56.774	0.0101	NA	19:34:02	2.15
110319C	207.96	-51.58	4.94	15.34	15:04:45	2.15
110321A	13.31	-21.81	11.83	30.72	08:17:42	2.15
110322A	99.04	-48.9	4.72	36.1	13:23:42	2.15
110328A	251.208	57.583	3e-04	NA	12:57:45	2.15
110328B	117.65	43.1	1.7	141.32	12:29:19	2.15
110331A	6.66	25.99	4.66	3.2	14:29:06	2.15
110401A	268.56	26.87	3.76	2.37	22:04:19	2.15
110402A	197.402	61.253	3e-04	70	00:12:58	2.15
110406A	17.34	35.809	0.1707	8	03:44:06	2.15
110407A	186.031	15.712	4e-04	145	14:06:41	2.15
110407B	97.41	-11.95	1	9.03	23:56:57	2.15
110409A	238.7	-34.32	10.89	0.13	04:17:20	0.5
110410A	30.94	-15.95	3.67	61.95	03:10:52	2.15
110410B	337.17	-21.96	17.39	8.07	18:31:19	2.15
110411A	291.442	67.712	3e-04	80.3	19:34:11	2.15
110411B	210.3	-64.99	6.28	23.55	15:05:15	2.15
110412A	133.491	13.488	0.0193	23.4	07:33:21	2.15
110413A	352.67	32.33	11.64	54.28	22:31:09	2.15
110414A	97.873	24.362	3e-04	152.0	07:42:14	2.15
110415A	213.82	9.05	9.23	166.14	12:59:22	2.15
110420A	2.164	-37.887	1e-04	11.8	11:02:24	2.15
110420B	320.045	-41.277	0.0223	0.12	22:42:11	0.5
110421A	277.23	50.8	1.71	40.45	18:10:39	2.15
110422A	112.047	75.107	3e-04	40	15:41:42	1.77
110422B	226.69	43.02	21.52	0.32	00:41:48	0.5
110424A	293.31	-11.12	12.35	0.67	18:11:36	0.5
110426A	219.93	-8.72	1.2828	356.36	15:06:26	2.15
110428A	5.3	64.8	0.15	5	09:18:30	2.15
110428B	128.44	19.94	2.94	101.63	08:07:05	2.15
110430A	147.06	67.95	2.53	32.52	09:00:13	2.15
110503A	132.776	52.208	1e-04	10.0	17:35:45	1.613
110503B	70.51	-10.9	4.29	7.94	03:28:26	2.15
110505A	16.81	-32.3	3.09	4.09	04:52:56	2.15
110509A	180.81	-34	4.6	68.87	03:24:38	2.15
110509B	74.65	-26.98	8.3	0.64	11:24:15	0.5
110511A	214.1	-45.42	10.62	5.89	14:47:12	2.15
110517A	296.09	-73.76	8.97	0.57	10:52:35	0.5
110517B	190.15	6.29	2.11	23.04	13:44:47	2.15
110517C	85.6	47.28	8.3	NA	21:38:48	0.5
110518A	67.18	-34.195	0.2003	35	20:38:10	2.15
110519A	261.638	-23.426	0.0101	27.2	02:12:16	2.15
110520A	134.341	56.427	3e-04	15.7	20:28:48	2.15
110520B	71.01	-85.93	12.41	12.29	07:14:26	2.15
110521A	120.133	45.827	3e-04	13.8	15:51:31	2.15
110521B	57.54	-62.34	1.31	6.14	11:28:58	2.15
110522A	228.91	55.53	5.56	28.16	06:08:17	2.15
110522B	184.46	49.33	6.4	27.14	07:06:01	2.15
110522C	180.57	-26.81	12.5	58.12	15:11:56	2.15
110523A	219.03	-15.42	4.5	44.54	08:15:54	2.15
110526A	102.48	-16.42	5.84	0.45	17:09:01	0.5
110528A	44.79	-6.87	2.48	69.63	14:58:44	2.15
110529A	118.33	67.91	1.5	0.57	00:48:40	2.15
110529B	172.6	8.79	2.1	45.82	06:17:41	2.15
110529C	340.62	1.86	4.82	34.82	19:27:12	2.15
110530A	282.068	61.929	2e-04	19.6	15:31:02	2.15
110531A	190.51	11.85	11.06	38.65	10:45:10	2.15
110601A	310.71	11.48	3	52.21	16:20:16	2.15
110604A	271.003	18.472	0.0507	45	14:49:45	2.15
110605A	14.95	52.46	1	82.69	04:23:32	2.15
110605B	242.09	-3.14	10.13	1.54	18:42:49	0.5
110609A	327.83	44.59	12.72	9.99	04:26:11	2.15
110609B	317.63	-38.16	4.71	33.03	10:12:06	2.15
110610A	308.179	74.825	3e-04	47	15:22:06	2.15
110613A	336.86	-3.47	2.79	40.2	15:08:46	2.15
110616A	274.45	-34.02	11.96	12.55	15:33:25	2.15
110618A	176.808	-71.688	0.502	163.84	08:47:36	2.15
110618B	147.05	-7.48	2.1	89.6	18:14:16	2.15
110622A	133.96	19.46	1.79	70.4	03:47:19	2.15
110624A	65.02	-15.95	17.34	3.52	21:44:25	2.15
110625A	286.751	6.755	0.0132	24	21:08:22	2.15

110625B	315.33	-39.44	4.6	35.58	13:53:24	2.15
110626A	131.91	5.56	7.66	6.4	10:44:54	2.15
110629A	69.37	25.01	4.82	61.7	04:09:58	2.15
110702A	5.62	-37.66	4.75	34.37	04:29:28	2.15
110703A	155.39	-29.3	3.76	6.72	13:22:15	2.15
110705A	156.024	40.099	0.161	0.25	03:37:09	2.15
110705B	122.96	28.8	3.08	19.2	08:43:43	2.15
110706A	100.08	6.14	8.03	12.04	04:51:04	2.15
110706B	94.15	-50.77	2.04	73.22	11:26:15	2.15
110706C	9.06	31.73	4.11	16.89	17:27:56	2.15
110706D	347.47	7.11	2.58	33.22	23:26:51	2.15
110708A	340.121	53.96	0.0162	50	04:43:22	2.15
110708B	170.382	-50.569	0.1633	60	13:59:46	2.15
110709A	238.891	40.924	3e-04	44.7	15:24:29	2.15
110709B	164.654	-23.455	2e-04	48	21:32:44	2.15
110709C	155.38	23.12	1.53	24.06	11:06:53	2.15
110709D	156.21	-41.79	10.84	5.37	20:40:50	2.15
110710A	229.09	48.4	3.87	22.72	22:53:50	2.15
110715A	237.684	-46.236	4e-04	8	13:13:49	0.82
110716A	329.68	-76.98	3.86	7.17	00:25:19	2.15
110717A	308.47	-7.85	7.45	0.12	04:19:50	0.5
110717B	312.84	-14.84	1.2	90.37	07:39:55	2.15
110719A	24.581	34.586	4e-04	41.0	06:09:11	2.15
110720A	198.65	-44.29	2.6	11.2	04:14:32	2.15
110721A	333.4	-39	0.75	21.82	04:47:43	2.15
110722A	215.06	5	1.99	73.47	16:39:16	2.15
110722B	8.28	62.74	4.66	14.34	17:01:45	2.15
110725A	270.14	-25.2	9.06	20.22	05:39:42	2.15
110726A	286.717	56.071	1e-04	5.2	01:30:40	1.036
110726B	317.71	2.47	3.82	29.95	05:03:59	2.15
110728A	166.6	20.11	2.56	0.71	01:20:22	0.5
110729A	353.39	4.97	1.36	408.58	03:25:05	2.15
110730A	263.08	-22.78	4.28	28.42	00:11:54	2.15
110730B	335.1	-2.89	3.8	33.85	15:50:43	2.15
110731A	280.504	-28.537	1e-04	6.56	11:09:30	2.83
110801A	89.437	80.956	1e-04	385	19:49:42	1.858
110801B	248.27	-57.06	7.3	0.39	08:01:43	0.5
110802A	44.455	32.593	0.1163	0.6	15:19:16	0.5
110803A	300.42	-11.44	7.49	186.89	18:47:25	2.15
110806A	112.04	2.38	2.42	28.41	22:25:31	2.15
110807A	278.696	-8.76	0.0304	NA	19:57:46	2.15
110808A	57.267	-44.195	5e-04	48	06:18:54	2.15
110808B	266.181	-37.74	0.0693	0.5	15:44:55	0.5
110809A	172.17	-13.93	1.84	12.54	11:03:34	2.15
110812A	358.409	72.206	0.0304	30	00:20:08	2.15
110812B	77.76	1.71	2.49	11.26	21:35:08	2.15
110813A	61.24	34.56	1	22.78	05:40:50	2.15
110815A	85.297	32.442	0.1137	20	09:40:55	2.15
110817A	336.04	-45.84	1.54	5.95	04:35:12	2.15
110818A	317.337	-63.981	2e-04	103	20:37:49	2.15
110819A	139.49	-76.64	3.19	16.38	15:57:54	2.15
110820A	343.192	70.298	4e-04	256	17:38:27	2.15
110820B	157.583	-54.605	0.5	200	21:27:48	2.15
110820C	90.51	21.63	3.96	11.27	11:25:44	2.15
110824A	152.05	1.32	1.68	76.61	00:13:09	2.15
110825A	44.896	15.4	0.3437	6.9	02:27:03	2.15
110825B	251.31	-80.28	5.18	51.07	06:22:11	2.15
110827A	164.059	53.817	0.0223	8.5	00:01:52	2.15
110828A	110.58	-23.81	1.04	44.67	13:48:14	2.15
110831A	352.35	33.66	5.86	98.88	06:45:26	2.15
110901A	141.28	-15.79	3.37	22.53	05:31:44	2.15
110903A	197.061	58.985	0.0203	370	02:39:33	2.15
110903B	164.21	42.08	1.18	28.67	00:13:06	2.15
110904A	359.69	35.9	2.63	83.91	02:58:15	2.15
110904B	190.4	-28.85	6.11	51.46	03:54:36	2.15
110904C	323.74	23.94	1.68	20.48	12:44:19	2.15
110905A	278.958	-19.269	0.0314	NA	05:48:40	2.15
110906A	296.891	-26.209	0.0385	94	12:25:13	2.15
110906B	26.32	17.65	4.03	23.94	07:15:13	2.15
110909A	347.34	-24.22	1.98	20.74	02:46:58	2.15
110911A	258.58	-66.98	50	8.96	01:41:41	2.15
110915A	310.824	-0.723	6e-04	78.76	13:20:44	2.15
110915B	77.548	1.925	0.0405	18	18:24:19	2.15
110916A	4.11	40.36	21.86	1.79	00:23:01	0.5
110918A	32.575	-27.281	0.0557	69.376	21:27:02	0.982
110919A	279.97	66.43	1	35.07	15:12:15	2.15
110920A	87.57	38.76	5	9.73	08:07:16	2.15
110920B	209.82	-27.56	1	160.77	13:05:43	2.15
110921A	294.098	36.329	3e-04	48.00	13:51:20	2.15
110921B	6.09	-5.83	7.31	149.51	10:38:48	2.15
110921C	17.97	-27.75	1	17.66	21:52:45	2.15
110923A	323.4	-10.89	3.69	46.4	20:01:58	2.15
110924A	234.748	-66.308	0.0304	NA	09:03:20	2.15
110926A	69.44	10.43	3.27	75.27	02:33:36	2.15
110928A	257.733	36.536	4e-04	26.7	01:51:31	2.15
110928B	153.4	34.29	1.42	148.23	04:19:51	2.15
110929A	288.19	-62.21	4.03	5.12	04:28:53	2.15
110930A	187.31	-53.66	5.05	37.89	13:32:31	2.15
111001A	340.01	-15.33	15.11	0.39	19:17:58	0.5
111003A	276.76	-62.32	1.11	16.64	11:10:00	2.15
111005A	223.315	-19.722	0.0213	26	08:05:14	2.15
111005B	340.3	75.8	5.28	30.72	09:33:03	2.15
111008A	60.451	-32.709	3e-04	63.46	22:12:58	5
111008B	220.75	-5.67	4.34	42.5	23:49:01	2.15
111009A	183.04	-56.82	1.08	20.74	06:45:40	2.15
111010A	87.09	43.98	3.18	82.43	05:40:34	2.15
111010B	183.54	-31.7	7.08	8.7	15:50:21	2.15
111010C	69.8	41.88	1.67	52.99	17:00:35	2.15
111010D	77.02	-14.96	7.68	18.56	21:34:13	2.15
111011A	37.96	-12.53	6.77	1.47	02:15:09	0.5
111012A	154.01	68.09	2.08	20.74	10:56:37	2.15
111012B	97.22	67.05	1.71	7.93	19:27:39	2.15
111015A	220.65	-58.41	1.96	92.74	10:15:12	2.15
111016A	153.834	27.462	3e-04	550	18:37:04	2.15
111016B	290.499	-4.578	0.1803	150	22:41:40	2.15
111017A	8.1	-7.01	1	11.07	15:45:23	2.15
111018A	271.489	-3.907	3e-04	36	17:26:24	2.15
111018B	106.08	66.14	7.15	8.19	14:16:48	2.15
111018C	124.18	81.29	7.46	29.7	18:50:14	2.15
111020A	287.052	-38.012	3e-04	0.40	06:33:49	0.5
111022A	275.871	-23.666	0.0101	24.7	16:07:04	2.15
111022B	108.965	49.684	3e-04	101.64	17:13:04	2.15
111022C	104.5	-33.11	9.32	0.19	20:29:23	0.5
111024A	222.18	25.84	0.1489	NA	07:21:27	0.5
111024B	162.74	-44.94	2.57	68.6	17:19:02	2.15
111024C	91.23	-1.75	13.15	1.8	21:30:02	0.5
111025A	325.62	-35.52	2.73	51.71	01:52:45	2.15
111026A	244.256	-47.435	0.0182	3.62	06:47:29	2.15
111029A	44.784	57.111	4e-04	7.6	09:44:40	2.15
111103A	327.111	-10.532	0.0111	11.6	10:35:13	2.15
111103B	265.693	1.61	3e-04	167	10:59:03	2.15
111103C	201.58	-43.16	10.99	0.32	22:45:05	0.5
111105A	153.48	7.28	14.24	43.52	10:57:36	2.15
111107A	129.477	-66.52	3e-04	12.04	00:50:25	2.893
111107B	315.46	-38.53	3.53	77.19	01:49:46	2.15
111109A	118.203	-41.584	4e-04	13.0	02:57:46	2.15
111109B	133.73	-33.35	7.38	4.86	10:52:32	2.15
111109C	129.98	44.65	1.5	9.67	20:57:16	2.15
111112A	223.72	28.81	3.83	0.19	21:47:48	0.5
111113A	225.39	2.185	0.0957	0.16	05:10:13	0.5
111113B	4.32	-7.52	3.96	15.36	09:50:11	2.15
111114A	268.08	-20.01	5.72	22.02	05:35:45	2.15
111117A	12.702	23.021	0.0172	0.47	12:13:41	0.5
111117B	27.16	-16.11	6.22	23.81	12:38:00	2.15
111120A	344.6	-37.34	5.17	98.63	13:20:24	2.15
111121A	154.761	-46.671	3e-04	119	16:26:24	2.15
111123A	154.846	-20.645	3e-04	290.0	18:13:21	3.1516
111124A	94.06	4.63	9.42	8.96	07:24:10	2.15
111126A	276.057	51.461	0.0304	0.8	18:57:42	0.5
111127A	103.7	3.5	2.09	19.01	19:27:01	2.15
111129A	307.434	-52.713	3e-04	7.6	16:18:14	2.15
111201A	190.485	32.994	0.0213	16.89	14:22:45	2.15
111203A	53.22	33.47	3.23	55.55	01:17:04	2.15
111203B	242.83	-22.15	13.3	22.02	14:36:45	2.15
111204A	336.628	-31.375	4e-04	48	13:37:28	2.15
111205A	134.486	-31.972	0.1017	85	13:10:50	2.15
111207A	92.924	-39	0.0304	3	14:16:59	2.15
111207B	164.88	-17.94	9.98	0.77	12:17:16	0.5
111208A	290.215	40.669	0.0223	40.96	08:28:10	2.15
111209A	14.344	-46.801	2e-04	NA	07:12:08	0.677
111210A	191.477	-7.166	4e-04	2.52	14:37:03	2.15
111211A	153.091	11.182	0.0304	25	22:17:33	0.478

111212A	310.431	-68.613	3e-04	68.51	09:23:07	2.15
111215A	349.555	32.494	2e-04	796	14:04:08	2.15
111215B	222.403	16.439	0.0767	75	20:28:02	2.15
111216A	185.99	5.83	1.37	83.78	09:20:31	2.15
111220A	267.6	-56.05	1.39	39.04	11:40:26	2.15
111221A	10.16	-29.77	1.92	27.13	17:43:30	2.15
111222A	179.22	69.071	1e-04	0.32	14:51:55	0.5
111225A	13.155	51.572	1e-04	106.8	03:50:37	0.297
111226A	21.5	3.87	1	74.75	19:04:58	2.15
111228A	150.067	18.298	2e-04	101.20	15:44:43	0.714
111228B	330.65	14.47	3.57	2.94	10:52:50	2.15
111229A	76.29	-84.711	3e-04	25.4	22:37:52	1.3805
111230A	150.19	33.43	2.78	28.16	16:23:08	2.15
111230B	242.61	-22.12	2.02	12.74	19:39:32	2.15
120101A	185.87	52.91	8.77	0.13	08:30:06	0.5
120102A	276.225	24.714	3e-04	38.7	02:15:55	2.15
120102B	341.15	-23.16	3.58	20.22	09:59:01	2.15
120105A	203.69	40.07	2.8	22.53	14:00:35	2.15
120106A	66.108	64.038	2e-04	61.6	14:16:24	2.15
120107A	246.4	-69.93	0.5	25	09:12:12	2.15
120109A	251.33	30.8	11.33	38.66	19:46:01	2.15
120111A	95.34	5	5.38	76.8	01:13:27	2.15
120114A	317.904	57.036	0.0233	43.27	16:20:05	2.15
120114B	263.23	-75.64	11.05	2.75	10:23:39	2.15
120116A	16.241	33.931	3e-04	41.0	18:06:28	2.15
120118A	195.403	-61.644	0.0274	60	06:04:44	2.15
120118B	124.871	-7.185	3e-04	37.83	17:00:22	2.943
120118C	166.57	47.87	7.17	17.15	21:32:45	2.15
120119A	120.029	-9.082	1e-04	61	04:01:34	1.212
120119B	139.65	-61.33	2	41.73	05:29:49	2.15
120119C	65.96	-33.92	4.42	16.39	08:29:29	2.15
120120A	134.72	35.47	5.71	32.26	10:21:25	2.15
120121A	249.354	-23.962	3e-04	26.1	09:42:19	2.15
120121B	235.67	-39.34	7.86	18.43	02:25:53	2.15
120121C	208.9	-1.34	1.61	37.12	06:00:45	2.15
120122A	96.58	16.53	2.69	16.7	07:12:06	2.15
120129A	30.44	59.282	3.826	3.07	13:55:46	2.15
120129B	26.52	-8.51	15.04	1.28	07:29:14	0.5
120130A	150.04	-17.45	3.69	27.78	16:47:10	2.15
120130B	64.96	9.48	5.55	3.58	21:44:54	2.15
120130C	323.3	58.56	1	38.91	22:30:34	2.15
120202A	203.507	22.775	0.0253	100	21:40:17	2.15
120203A	339.3	-46.59	6.77	10.24	19:29:23	2.15
120204A	292.58	-3.57	1	49.08	01:17:07	2.15
120205A	243.417	25.9	23.8333	0.58	06:51:05	0.5
120206A	73.45	58.41	2.25	9.48	22:46:16	2.15
120210A	54.65	-58.52	5.51	1.34	15:35:43	0.5
120211A	87.754	-24.775	3e-04	61.7	11:58:28	2.15
120212A	43.1	-18.021	3e-04	9.22	09:11:23	2.15
120212B	303.4	-48.1	7.47	0.86	08:27:47	0.5
120213A	301.012	65.411	4e-04	48.9	00:27:19	2.15
120213B	183.49	5.76	4.2	13.82	14:32:44	2.15
120215A	30.048	8.802	3e-04	26.5	00:41:15	2.15
120217A	122.44	36.77	3.23	5.89	19:23:50	2.15
120217B	298.73	32.7	1.5	2.62	21:41:57	2.15
120218A	319.764	-25.463	0.0193	27.5	00:49:22	2.15
120218B	101.85	-1.37	3.64	256.26	06:37:02	2.15
120219A	129.79	51.032	3e-04	90.5	14:30:08	2.15
120219B	274.85	-31.11	10.94	8.13	13:31:23	2.15
120220A	206.13	-57.36	7.39	21.25	05:02:21	2.15
120222A	299.55	26.49	2.76	1.08	00:29:36	0.5
120222B	340	-36.41	5.7	29.44	02:51:54	2.15
120223A	219.61	-7.46	2.74	14.33	22:23:48	2.15
120224A	40.942	-17.761	3e-04	8.13	04:39:56	2.15
120224B	118.42	41.34	4.6	60.93	06:46:28	2.15
120224C	331.06	10.18	3.59	29.18	21:33:07	2.15
120226A	300.05	48.81	0.5	80	20:54:19	2.15
120226B	87.59	52.35	1.15	14.59	10:44:16	2.15
120227A	84.76	8.5	6.33	19.71	09:22:45	2.15
120227B	256.73	-88.86	1.21	17.4	17:24:41	2.15
120229A	20.033	-35.796	0.0193	0.22	14:35:11	0.5
120302A	122.426	29.642	0.0233	NA	01:55:30	2.15
120302B	24.09	9.71	13.87	1.6	17:19:59	0.5
120304A	127.15	-61.12	1	9.99	01:27:48	2.15
120304B	277.28	-46.22	1	5.38	05:57:47	2.15
120305A	47.536	28.492	3e-04	0.10	19:37:30	0.5
120308A	219.085	79.687	3e-04	60.6	06:13:38	2.15
120308B	30.75	55.22	1.19	25.6	14:06:05	2.15
120311A	273.092	14.296	4e-04	3.5	05:33:38	2.15
120311B	258.562	-13.051	3e-04	28.2	15:08:10	2.15
120312A	251.812	23.881	0.0213	14.2	16:06:28	2.15
120314A	17.89	-48.73	17.82	1.28	09:52:34	0.5
120316A	57.016	-56.288	0.467	24	00:11:02	2.15
120319A	69.85	-45.44	3.67	72.45	23:35:04	2.15
120320A	212.518	8.696	4e-04	25.74	11:56:15	2.15
120323A	340.407	29.717	0.118	0.5	12:10:15	2.15
120323B	211.1	-45.23	3.79	4.35	03:52:49	2.15
120324A	291.079	24.13	3e-04	118	05:59:11	2.15
120326A	273.905	69.26	3e-04	69.6	01:20:29	1.798
120327A	246.864	-29.415	3e-04	62.9	02:55:16	2.81
120327B	170.41	23.76	13	0.25	10:01:49	0.5
120328A	241.614	-39.336	3e-04	24.2	03:06:19	2.15
120328B	229.038	25.299	1.077	29.7	06:26:20	2.15
120331A	26.37	-54.84	6.51	16.39	01:19:06	2.15
120401A	58.083	-17.636	4e-04	145.69	05:24:15	2.15
120402B	223.73	-10.4	2.61	20.22	16:04:00	2.15
120403A	42.458	40.489	0.0233	1.25	01:05:23	0.5
120403B	55.276	-89.009	4e-04	7.3	20:33:56	2.15
120404A	235.01	12.885	3e-04	38.7	12:51:02	1.633
120410A	159.63	-17	8.6	1.08	14:02:00	0.5
120411A	38.07	-7.24	8.45	38.91	22:12:25	2.15
120412A	29.44	-24.67	13.47	9.73	01:18:42	2.15
120412B	38.91	7.06	2.8	101.19	22:04:40	2.15
120415A	213.54	16.73	4.36	12.54	01:49:57	2.15
120415B	190.69	4.91	6.88	0.96	21:23:41	0.5
120415C	150.46	61.27	4.96	12.54	22:59:19	2.15
120419A	187.402	-63.017	0.0253	20	12:56:25	2.15
120420A	47.89	-52.19	5.44	25.6	05:58:07	2.15
120420B	109.26	10.76	1.11	254.92	20:35:13	2.15
120422A	136.91	14.018	3e-04	5.35	07:12:03	0.28
120426A	111.537	-65.631	0.3013	2.88	02:09:14	2.15
120426B	285.49	-13.68	3.83	30.98	14:02:22	2.15
120427A	224.935	29.311	0.2193	5.63	01:17:27	2.15
120427B	114.7	50.21	26.65	22.78	03:40:37	2.15
120429A	165.98	-8.76	15.4	1.66	00:04:07	0.5
120429B	133.04	-32.23	5.34	15.36	11:37:03	2.15
120430A	47.25	18.52	5.75	14.59	23:30:43	2.15
120504A	329.94	46.83	4.06	41.98	11:13:39	2.15
120504B	200.28	-24.2	6.74	5.76	22:40:08	2.15
120506A	172.22	-33.72	9.33	2.31	03:05:02	2.15
120509A	195.39	38.31	16.8	0.7	14:52:02	0.5
120510A	44.047	72.887	8e-04	130	08:47:44	2.15
120510B	186.93	-55.24	3.75	62.47	21:36:26	2.15
120511A	226.93	-60.49	2.07	45.25	15:18:47	2.15
120512A	325.558	13.636	0.0101	40	02:41:40	2.15
120513A	140.79	74.99	10.8	23.81	12:44:00	2.15
120514A	283.001	-4.264	3e-04	164.4	01:12:49	2.15
120519A	178.366	22.407	0.634	0.72	17:18:14	2.15
120520A	45.86	35.28	8.3	5.76	22:46:24	2.15
120521A	148.725	-49.417	3e-04	0.45	05:59:42	0.5
120521B	197.01	-52.755	3e-04	31.4	09:07:48	2.15
120521C	214.286	42.145	3e-04	26.7	23:22:07	6
120522A	165.996	-62.094	0.0773	13	03:11:07	2.15
120522B	56.07	54.85	2.02	28.16	08:39:16	2.15
120524A	358.15	-15.61	10.45	0.71	03:12:54	0.5
120526A	66.28	-32.23	1.04	43.65	07:16:40	2.15
120528A	295.13	6.5	5.98	16.39	10:36:00	2.15
120528B	77.59	-37.8	0.0608	30	18:11:48	2.15
120528C	12.93	-0.95	0.0608	NA	21:21:58	2.15
120530A	175.96	78.83	3.27	77.06	02:53:41	2.15
120531A	290.4	1.22	11.03	25.35	09:26:38	2.15
120602A	87.922	-39.354	0.039	70	05:00:00	2.15
120603A	198.794	4.326	0.6427	0.38	10:32:09	2.15
120604A	163.87	-7.4	9.34	10.5	05:16:31	2.15
120604B	113.58	-2.79	11.91	12.03	08:13:40	2.15
120605A	243.61	41.51	2.62	18.11	10:52:15	2.15
120608A	229.98	-26.12	2.52	0.96	11:43:51	0.5
120608B	313.26	12.64	5.08	24.84	18:38:33	2.15
120609A	67.32	13	7.54	1.79	13:54:35	0.5
120611A	324.68	-44.79	5.28	49.92	02:36:00	2.15
120612A	126.722	-17.575	3e-04	90	02:05:19	2.15
120612B	211.88	34.56	7.08	63.24	16:19:45	2.15

120612C	39.67	-37.91	10.65	0.25	16:29:44	0.5
120614A	312.73	65.16	0.1216	NA	05:49:10	2.15
120616A	79.69	56.44	8.54	0.05	15:06:50	0.5
120617A	22.309	33.804	0.251	0.5	15:02:47	0.5
120618A	77.31	75.85	2.59	17.6	03:03:49	2.15
120618B	213.57	-2.11	4.8	47.62	22:03:34	2.15
120619A	190.74	-25.02	2.79	0.96	21:13:16	0.5
120622A	205.43	-1.71	0.2116	NA	03:21:46	2.15
120624A	4.773	7.167	0.4427	0.3	07:24:22	2.15
120624B	170.886	8.933	0.0101	274	22:19:30	2.15
120625A	51.26	51.07	1.17	7.43	02:50:46	2.15
120629A	176.16	-0.6	8.88	0.7	13:34:11	0.5
120630A	352.3	42.495	0.0274	0.6	23:17:33	0.5
120701A	80.338	-58.531	0.0132	13.8	07:50:41	2.15
120701B	182.73	-45.7	14.79	1.02	15:41:48	0.5
120702A	227.8	36.76	8.48	35.07	21:23:19	2.15
120703A	339.357	-29.724	2e-04	25.2	17:25:22	2.15
120703B	69.49	34.74	2.6	64.51	10:01:11	2.15
120703C	210.51	46.26	5.15	77.57	11:56:56	2.15
120707A	291.874	-32.77	2.1067	40.96	19:12:17	2.15
120709A	320.23	-51.13	0.5	27.33	21:11:40	2.15
120710A	120.39	-31.14	4.76	131.84	02:23:17	2.15
120711A	94.7	-70.9	0.16	46.336	02:45:55	3
120711B	331.71	59.996	0.0324	60	03:11:02	2.15
120711C	127.88	-31.83	11.03	87.55	10:42:54	2.15
120712A	169.589	-20.034	3e-04	14.7	13:42:27	4.15
120713A	161.68	40.66	16.71	13.82	05:25:29	2.15
120714A	167.983	-30.627	3e-04	16.2	07:46:46	2.15
120714B	355.412	-46.196	0.0263	159	21:18:46	0.3984
120715A	272.15	58.79	3.73	29.69	01:35:15	2.15
120716A	313.089	9.558	0.1747	234.49	17:05:03	2.48
120716B	304.53	59.41	5.09	24.96	13:51:02	2.15
120719A	204.29	-43.45	1.37	75.01	03:30:00	2.15
120722A	230.497	13.251	4e-04	42.4	12:53:26	0.9586
120724A	245.18	3.508	3e-04	72.8	06:39:02	1.48
120727A	163.26	25.09	15.27	0.9	08:29:39	0.5
120727B	37.76	16.36	1	10.49	16:20:19	2.15
120727C	250.86	-45.97	0.3	NA	00:00:00	0.5
120728A	137.095	-54.438	3e-04	32.77	22:25:12	2.15
120728B	103.772	-45.893	0.4723	250	10:25:34	2.15
120729A	13.074	49.94	3e-04	71.5	10:56:14	0.8
120801A	245.73	-47.37	2.39	479.24	22:05:21	2.15
120802A	44.842	13.768	5e-04	50	08:00:51	3.796
120803A	269.531	-6.733	0.0253	10.0	07:22:16	2.15
120803B	314.236	53.304	3e-04	37.5	11:06:06	2.15
120804A	233.948	-28.782	3e-04	0.81	00:54:14	0.5
120805A	216.538	5.825	5e-04	48.00	21:28:09	2.15
120805B	30.13	-21.51	10.11	1.86	16:56:21	0.5
120806A	308.99	6.33	4.25	26.63	00:10:08	2.15
120807A	241.26	-47.48	3e-04	20.0	07:09:37	2.15
120811A	257.184	-22.735	0.0263	166	02:35:18	2.15
120811B	43.658	-31.675	0.233	0.45	00:20:30	0.5
120811C	199.683	62.301	3e-04	26.8	15:34:52	2.671
120814A	26.19	22.45	3.71	0.89	04:49:12	0.5
120814B	90.57	33.13	10.68	0.19	19:16:06	0.5
120815A	273.958	-52.131	3e-04	9.7	02:13:58	2.358
120816A	282.143	-6.938	3e-04	7.6	19:18:34	2.15
120816B	341.155	2.156	2.51	0.768	23:58:18	0.5
120817A	250.689	-38.355	3e-04	28.2	06:49:42	2.15
120817B	8.31	-26.428	0.0507	0.11	04:02:29	2.15
120817C	259.97	-9.07	7.14	36.86	01:22:09	2.15
120819A	235.908	-7.309	3e-04	71	13:10:14	2.15
120819B	171.54	49.42	7.94	66.3	01:08:26	2.15
120820A	186.64	-12.31	4.81	107.52	14:02:21	2.15
120821A	255.269	-40.521	0.0203	12	13:23:45	2.15
120822A	181.72	80.56	7.7	1.54	15:03:56	0.5
120824A	70.92	17.63	3	111.62	14:16:00	2.15
120827A	222.74	-71.89	1.67	5.05	05:10:25	2.15
120830A	88.42	-28.81	0.86	1.28	07:07:03	0.5
120830B	337.87	-80.04	3.46	16.06	05:04:52	2.15
120830C	110.03	17.53	3.39	49.67	16:51:36	2.15
120831A	144.02	-16.21	8.54	0.39	21:37:31	0.5
120905A	355.96	16.99	1.8	195.59	15:46:21	2.15
120907A	74.75	-9.315	3e-04	5.76	00:24:24	2.15
120908A	230.64	-25.79	0.2857	66.95	22:31:00	2.15
120908B	268.67	-35.79	1.5	46.84	20:57:30	2.15
120909A	275.737	-59.449	2e-04	115	01:41:09	3.93
120911A	357.979	63.099	3e-04	22.02	07:08:33	2.15
120911B	172.03	-37.51	0.3	69	06:25:14	2.15
120913A	146.4	26.959	0.0122	40.96	20:18:22	2.15
120913B	213.66	-14.508	0.0101	126	23:55:58	2.15
120914A	267.94	1.82	5.35	10.24	03:26:42	2.15
120915A	283.56	-1.11	6.54	5.88	11:22:04	2.15
120916A	205.631	36.7	0.4953	26	04:07:46	2.15
120916B	82.04	-19.22	11.13	1.34	02:02:15	0.5
120918A	181.042	-32.762	0.0111	25.1	11:16:10	2.15
120919A	214.768	-45.564	0.0863	8	07:24:38	2.15
120919B	302.633	-37.49	0.2653	118.02	01:14:23	2.15
120919C	303.53	-66.16	11.89	22.02	19:35:41	2.15
120920A	27.12	-26.12	7.84	29.18	00:04:32	2.15
120921A	96.42	-64.77	3.2	5.64	21:03:03	2.15
120922A	234.749	-20.182	3e-04	173	22:30:28	3.1
120923A	303.795	6.221	3e-04	27.2	05:16:06	2.15
120926A	318.39	58.38	1.51	4.29	08:02:56	2.15
120926B	59.72	-37.2	3.76	60.16	10:13:16	2.15
120926C	24.61	-45.58	21.32	3.08	18:04:35	2.15
120927A	136.614	0.416	2e-04	43	22:40:46	2.15
121001A	276.032	-5.666	3e-04	147	18:23:02	2.15
121004A	137.46	-11.02	9.44	1.53	05:03:18	0.5
121005A	195.17	-2.09	9.48	96.77	00:42:51	2.15
121005B	149.73	25.4	5.39	141.57	08:09:12	2.15
121008A	340.97	-3.1	9	3.46	10:10:50	2.15
121011A	260.215	41.11	4e-04	31	11:15:30	0.58
121011B	182.809	44.113	1.4943	0.35	22:32:20	2.15
121012A	33.42	14.58	6.78	0.45	17:22:16	0.5
121014A	166.645	-29.105	0.0203	80.0	20:11:56	2.15
121014B	320.01	-53.43	17.2	0.39	15:19:00	0.5
121017A	288.83	-1.604	3e-04	4.2	19:23:28	2.15
121019A	43.47	62.14	7.52	14.34	05:35:09	2.15
121023A	313.86	-4.38	4.76	0.51	07:44:16	0.5
121024A	70.472	-12.291	2e-04	69	02:56:12	2.298
121025A	248.382	27.672	6e-04	NA	07:46:30	2.15
121027A	63.597	-58.83	3e-04	62.6	07:32:29	1.773
121027B	4.31	-47.54	2.61	166.92	00:54:19	2.15
121028A	271.899	-2.294	3e-04	3.8	05:04:31	2.15
121028B	52.56	-25.07	7.68	11.01	06:43:13	2.15
121029A	226.77	-28.2	1.65	15	08:24:18	2.15
121031A	170.77	-3.517	3e-04	242.43	22:47:15	2.15
121102A	270.901	-16.958	2e-04	20	02:27:00	2.15
121102B	258.47	14.09	12.15	2.05	01:32:47	2.15
121104A	72.14	14.08	4.05	59.13	15:02:15	2.15
121108A	83.194	54.474	3e-04	89	17:47:39	2.15
121109A	6.84	-42.57	10.37	22.14	08:06:56	2.15
121112A	78.98	-55.44	15.56	1.28	19:20:44	0.5
121113A	313.17	59.82	2.06	95.49	13:02:43	2.15
121116A	180.88	-74.79	6.98	1.34	11:00:24	0.5
121117A	31.611	7.42	1e-04	30	08:50:56	2.15
121117B	279.14	44.93	4.32	331.78	00:25:37	2.15
121118A	299.379	65.654	1.1443	33.8	13:48:54	2.15
121118B	171.704	-3.059	0.7363	50	22:27:06	2.15
121119A	311.65	-16.92	8.13	2.31	13:53:14	2.15
121122A	35.262	45.139	3.7097	8.19	21:14:52	2.15
121122B	52.67	46.47	12.89	8.7	13:31:27	2.15
121122C	355.45	6.34	2.66	125.44	20:52:49	2.15
121123A	307.318	-11.86	1e-04	317	10:02:41	2.15
121123B	30.52	-18.79	1.61	42.5	10:35:55	2.15
121124A	87.93	49.55	14.64	0.26	14:32:07	0.5
121125A	228.528	55.313	3e-04	52.2	08:32:27	2.15
121125B	177.53	38.54	5.24	12.86	11:14:47	2.15
121127A	176.438	-52.414	0.0803	0.25	21:55:57	2.15
121128A	300.6	54.3	3e-04	23.3	05:05:37	2.2
121201A	13.468	-42.943	3e-04	85	12:25:42	3.6
121202A	256.797	23.948	2e-04	20.1	04:20:05	2.15
121205A	238.59	-49.71	11.72	2.81	12:10:04	2.15
121209A	326.787	-8.235	3e-04	42.7	21:59:11	2.15
121210A	202.54	17.77	8.25	12.8	01:56:01	2.15
121211A	195.533	30.149	3e-04	5.63	13:47:03	1.023
121211B	72.37	8.63	5.23	8.96	16:41:02	2.15
121212A	177.792	78.037	3e-04	10	06:56:12	2.15
121216A	13.88	-85.44	14.15	9.22	10:03:16	2.15
121217A	153.71	-62.35	3e-04	778	07:17:47	0.8
121217B	153.71	-62.351	5e-04	828.67	07:30:01	2.15

121220A	31.07	48.28	8.3	5.12	07:28:13	2.15
121221A	214.26	33.55	4.22	38.91	21:59:29	2.15
121223A	50.11	21.37	2.74	11.01	07:11:19	2.15
121225A	264.86	-66.07	0.1702	NA	09:50:24	2.15
121225B	308.913	-34.355	1.25	53	10:01:03	2.15
121226A	168.62	-30.413	0.0203	1.00	19:09:43	0.5
121229A	190.101	-50.594	3e-04	64	05:00:21	2.707
121229B	315.59	-11.94	4.58	23.04	12:47:33	2.15
121231A	335.47	-17.78	6.46	32.77	10:41:23	2.15
130102A	311.423	49.818	3e-04	77.5	18:10:53	2.15
130102B	309.58	-72.38	0.1721	30	04:41:42	2.15
130104A	174.09	25.92	2.44	26.37	17:18:07	2.15
130106A	66.67	29.74	4.99	11.26	19:53:22	2.15
130106B	28.76	63.38	1.87	70.4	23:52:25	2.15
130109A	17.45	19.24	3.72	8.96	04:56:26	2.15
130112A	236.03	52.19	4.93	35.33	06:52:07	2.15
130112B	196.29	-31.94	5.76	2.05	08:27:47	2.15
130114A	310.19	-15.32	10.86	8.71	00:27:04	2.15
130115A	171.09	22.62	2.78	13.57	17:10:39	2.15
130116A	38.24	15.75	29.85	66.82	09:58:14	2.15
130117A	341.24	2.81	6.17	78.85	02:05:11	2.15
130118A	278.3	40.98	6.7	21.57	11:33:29	2.15
130121A	211.31	-49.49	1.14	178.69	20:01:59	2.15
130122A	194.285	59.015	3e-04	64	23:44:09	2.15
130127A	251.05	-17.07	8.46	0.45	17:50:23	0.5
130127B	301.21	-57.21	10.01	19.46	07:09:53	2.15
130131A	171.126	48.076	3e-04	51.6	13:56:22	2.15
130131B	173.956	15.038	3e-04	4.30	19:10:08	2.539
130131C	189.63	-14.48	1	147.46	12:15:13	2.15
130204A	105.64	41.92	7.07	0.19	11:36:51	0.5
130206A	140.387	-58.193	0.0193	91.59	19:36:30	2.15
130206B	269.1	49.43	2.4	11.27	11:33:34	2.15
130208A	181.6	50.93	4.67	41.47	16:24:23	2.15
130209A	33.59	-27.58	1	9.92	23:03:41	2.15
130211A	147.524	-42.33	0.0213	25.1	03:36:32	2.15
130213A	99.09	-8.1	10.62	15.36	21:43:55	2.15
130214A	325.02	-1.83	12.77	96.77	03:17:05	2.15
130214B	56.93	-0.29	1.6	13.76	19:12:21	2.15
130215A	43.486	13.387	0.0152	46.0	01:31:25	0.597
130215B	3.11	59.38	2.1	58.11	15:34:16	2.15
130216A	67.901	14.67	0.0101	6.5	22:15:24	2.15
130216B	58.866	2.036	0.0152	15.29	18:58:11	2.15
130217A	96.72	6.8	8.19	14.84	16:31:19	2.15
130218A	69.31	-69.13	2.28	37.12	06:16:25	2.15
130219A	303.73	40.83	1.21	96	18:35:51	2.15
130219B	169.29	-22.25	2.2	168.0	04:44:07	2.15
130219C	211.6	12.22	16.68	1.54	15:01:13	0.5
130220A	306.2	31.74	1.14	6.4	23:08:48	2.15
130224A	205.9	59.72	2.62	70.91	08:53:02	2.15
130228A	265.83	55.93	0.5	111.75	02:40:02	2.15
130228B	240.75	-55.21	1.28	15.42	05:05:57	2.15
130304A	98.93	53.57	1.2	67.84	09:49:53	2.15
130304B	178.87	-60.29	6.51	23.3	15:46:49	2.15
130305A	116.774	52.037	0.0182	25.6	11:39:11	2.15
130305B	73.32	-1.56	1.76	118.53	12:37:47	2.15
130306A	279.475	-11.682	0.0162	120.57	23:47:25	2.15
130307A	155.996	22.998	0.3643	0.38	03:01:44	0.5
130307B	319.52	10.77	4.42	63.49	05:42:19	2.15
130310A	141.905	-17.431	0.2177	16.0	20:09:41	2.15
130313A	236.438	-0.355	0.0263	0.26	16:08:11	0.5
130314A	206.21	46.77	1.41	142.85	03:31:16	2.15
130315A	157.541	-51.794	0.0132	233.4	12:45:32	2.15
130318A	200.74	8.12	9.94	137.99	10:56:31	2.15
130320A	192.684	-14.471	1.511	20	07:08:44	2.15
130320B	195.539	-71.259	0.486	380	13:24:11	2.15
130324A	255.43	0.05	6.03	37.76	01:00:24	2.15
130325A	122.78	-18.9	0.25	9.72	04:51:54	2.15
130325B	30.44	62.06	16.14	0.64	00:07:46	0.5
130327A	92.039	55.715	3e-04	9.0	01:47:34	2.15
130327B	218.09	-69.51	0.17	30	08:24:04	2.15
130331A	164.47	29.64	2.43	13.82	13:35:44	2.15
130403A	199.9	-46.68	8.26	22.79	20:46:47	2.15
130404A	30.75	1.54	7.24	3.33	10:15:40	2.15
130404B	146.58	-42.16	1.08	34.56	20:10:04	2.15
130404C	28.29	56.49	18.23	0.96	21:02:11	0.5
130406A	157.78	-62.05	2.09	7.93	06:55:03	2.15
130406B	109.66	-27.86	7.66	88.83	08:00:36	2.15
130406C	138.21	42.83	14.84	2.56	08:29:36	2.15
130407A	248.1	10.51	0.0608	NA	23:37:01	2.15
130407B	53.53	44.17	9.29	32.0	19:12:43	2.15
130408A	134.405	-32.361	3e-04	7	21:51:38	3.758
130408B	118.77	66.34	3.93	9.21	15:40:22	2.15
130409A	30.52	44.1	2.22	26.11	23:01:59	2.15
130416A	99.28	24.7	14.34	3.08	16:34:07	2.15
130416B	51.21	-18.25	4.86	0.19	18:28:53	0.5
130418A	149.037	13.667	3e-04	300	19:00:53	1.218
130418B	216.53	-17.54	8.46	169.48	20:14:45	2.15
130419A	355.278	9.9	0.0263	75.7	13:30:29	2.15
130420A	196.106	59.424	3e-04	123.5	07:28:29	1.297
130420B	183.128	54.391	3e-04	13.83	12:56:32	2.15
130420C	122.68	-11.43	1.19	38.91	08:14:02	2.15
130420D	117.06	-69.03	4.01	27.33	10:08:09	2.15
130425A	6.211	-70.183	2.5037	66.44	07:51:16	2.15
130427A	173.136	27.698	6e-04	162.83	07:47:57	0.34
130427B	314.898	-22.547	3e-04	27.0	13:20:41	2.78
130502A	138.569	-0.123	3e-04	3.33	17:50:30	2.15
130502B	66.648	71.084	0.093	27.392	07:51:12	2.15
130503A	214.72	-11.55	21.48	0.88	05:08:28	0.5
130504A	272.459	-16.32	0.0172	50	02:05:34	2.15
130504B	347.952	-5.739	0.228	0.430	07:31:59	2.15
130504C	91.715	3.846	0.155	67	23:29:00	2.15
130505A	137.061	17.485	3e-04	14	08:22:24	2.27
130505B	344.47	-70.47	1.5	50.24	22:55:15	2.15
130507A	319.74	-20.53	3.29	60.16	13:04:37	2.15
130508A	305.351	34.966	0.0223	42	17:08:53	2.15
130509A	240.85	-40.22	2.08	24.32	01:52:14	2.15
130509B	133.86	-11.51	8.78	28.67	20:08:43	2.15
130510A	105.71	-9.87	4.98	29.44	21:03:22	2.15
130511A	196.645	18.71	3e-04	5.43	11:30:47	1.3033
130513A	144.775	-5.244	0.0203	50	07:38:00	2.15
130514A	296.283	-7.976	3e-04	204	07:13:41	2.15
130514B	147.604	-18.969	0.0304	17.41	13:26:32	2.15
130515A	283.44	-54.279	4e-04	0.25	01:21:17	2.15
130515B	312.84	-14.95	5.37	20.48	10:18:30	2.15
130515C	146.77	11.26	10.5	2.56	18:06:51	2.15
130517A	41.86	42.66	1.5	32.52	18:44:12	2.15
130518A	355.671	47.478	0.0294	22	13:54:50	2.49
130518B	321.555	-20.148	0.0182	10	10:50:38	2.15
130518C	289.72	-4.15	2.7	3.45	13:13:08	2.15
130521A	87.568	14.47	0.0162	11.0	22:49:16	2.15
130521B	281.641	22.723	0.1207	23	21:24:31	2.15
130522A	134.15	17.62	4.9	27.9	12:14:31	2.15
130523A	22.29	29.73	2.82	17.92	02:16:09	2.15
130523B	39.49	-63.07	2.13	5.38	04:45:42	2.15
130527A	309.276	-24.725	3e-04	7.4	14:21:27	2.15
130527B	175.79	-2.52	3.08	27.78	15:02:14	2.15
130528A	139.501	87.301	3e-04	59.4	16:41:23	2.15
130528B	352.7	27.81	5.5	66.3	12:04:31	2.15
130529A	24.282	-64.147	3e-04	128	11:15:25	2.15
130530A	160.95	25.23	1.04	58.62	17:15:23	2.15
130603A	86.897	82.909	3e-04	76	05:59:32	2.15
130603B	172.201	17.071	3e-04	0.18	15:49:14	0.356
130604A	250.188	68.227	4e-04	37.7	06:54:26	2.15
130604B	292.18	-24.86	1.21	26.88	00:48:11	2.15
130605A	134.536	-33.477	0.0172	12.6	23:41:42	2.15
130606A	249.396	29.796	3e-04	276.58	21:04:39	5.91
130606B	218.574	-22.131	0.1	43.7	11:55:35	2.15
130606C	339.37	12.49	1.67	24.13	07:35:30	2.15
130608A	24.611	41.503	3e-04	44.4	23:14:21	2.15
130609A	152.669	24.132	4e-04	7.0	03:05:08	2.15
130609B	53.771	-40.174	1e-04	191.98	21:38:40	1.3
130610A	224.42	28.207	1e-04	46.4	03:12:13	2.15
130610B	176.359	-32.187	0.277	16.640	21:21:19	2.15
130611A	238.84	-25.23	2.97	66.81	12:54:20	2.15
130612A	259.794	16.72	3e-04	7.42	03:22:23	2.006
130612B	247.94	31.02	1.79	10.24	10:57:14	2.15
130614A	324.18	-33.89	1.22	4.9	23:56:09	2.15
130615A	274.829	-68.161	4e-04	304	09:44:45	2.15
130615B	184.86	69.62	6.2	21.76	09:33:07	2.15
130617A	74.73	-60.06	9.99	0.77	13:32:49	0.5
130620A	74.42	61.19	12.27	14.59	11:57:06	2.15
130622A	312.74	24.46	10.91	0.96	14:45:53	0.5

130623A	20.723	-77.784	0.0405	22.27	11:42:47	2.15
130623B	194.61	35.51	7.2	29.44	03:06:37	2.15
130623C	203.59	49.03	7.12	44.55	09:30:24	2.15
130623D	284.68	10.67	26.27	7.68	16:46:23	2.15
130623E	107.43	36.04	4.63	42.24	18:57:50	2.15
130624A	337.32	11.45	6.9	95.23	02:13:56	2.15
130625A	343.278	82.174	4e-04	38.1	07:00:39	2.15
130626A	273.128	-9.525	0.0182	1.85	10:51:03	0.5
130626B	24.89	4.93	4.03	28.16	14:17:32	2.15
130627A	184.415	-37.087	3e-04	35.84	08:55:05	2.15
130627B	181.914	-55.706	0.0182	28.6	12:00:50	2.15
130628A	6.29	-5.07	1.71	2.4	12:44:04	2.15
130628B	312.83	6.1	4.97	0.51	20:38:01	0.5
130630A	170.01	60.06	1	17.15	06:31:19	2.15
130701A	357.229	36.101	3e-04	4.38	04:17:43	1.155
130701B	97.79	-60.13	1	20.22	01:27:06	2.15
130701C	325.94	-30.89	1.68	1.6	18:15:30	0.5
130702A	216.4	15.8	0.5	26	00:05:23	0.145
130702B	292.16	10.39	12.95	16.39	22:48:59	2.15
130704A	65.56	-14.46	1	6.4	13:26:07	2.15
130705A	156.3	47.41	19.37	0.12	09:33:03	0.5
130706A	299.36	56.48	10.43	0.12	21:36:07	0.5
130707A	54.45	-21.04	5.37	76.55	12:07:48	2.15
130708A	17.474	0.003	0.0162	NA	11:43:03	2.15
130715A	287.37	-31.05	1	46	21:44:38	2.15
130716A	179.581	63.057	0.042	0.77	10:36:53	0.5
130716B	348.87	45.34	6.27	91.14	08:26:19	2.15
130717A	256.59	-13.57	12.1	55.3	17:36:20	2.15
130719A	89.038	-11.591	0.0193	177.7	05:47:49	2.15
130720A	243.5	14.97	6.58	48.64	02:46:40	2.15
130720B	338.03	-9.4	1	199.17	13:57:40	2.15
130722A	260.652	-2.973	2e-04	55.191	08:20:01	2.15
130722B	119.86	-47.45	10.12	81.41	00:29:51	2.15
130722C	352.41	-22.31	2.7	2.31	23:46:11	2.15
130723A	217.77	-16.86	8.16	8.19	02:12:34	2.15
130725A	230.06	0.624	0.0253	101.8	11:37:11	2.15
130725B	214.241	-11.128	1e-04	10.0	17:39:38	2.15
130725C	42.45	64.82	2.27	6.65	12:38:40	2.15
130727A	330.798	-65.539	2e-04	13.57	16:45:19	2.15
130730A	133.75	-60.36	3.44	27.9	05:50:19	2.15
130802A	80.28	-7.62	12.88	0.06	17:31:52	0.5
130803A	220.253	-2.492	3e-04	7.62	10:02:53	2.15
130804A	280.03	-76.15	0.76	0.96	00:33:15	2.15
130806A	35.929	67.532	4e-04	6.1	02:51:33	2.15
130807A	269.801	-27.616	0.0172	176	10:25:43	2.15
130808A	162.72	33.38	10.03	0.26	06:04:33	0.5
130811A	192.89	-17.04	3.36	44.8	04:28:01	2.15
130812A	92.396	-13.288	3e-04	7.6	22:22:52	2.15
130812B	7.405	-79.178	0.3367	33.024	10:55:16	2.15
130813A	204.03	56.34	10.47	11.26	18:59:22	2.15
130815A	164.71	49.57	1.6	236.29	10:05:07	2.15
130815B	112.37	-2.15	1	37.89	15:50:52	2.15
130816A	197.141	-58.945	3e-04	29.97	01:46:55	2.15
130816B	170.016	-57.557	3e-04	10.00	04:53:38	2.15
130818A	192.29	57.58	2.23	25.35	22:34:33	2.15
130819A	124.72	-33.76	4.93	82.69	09:27:34	2.15
130821A	314.1	-12	0.1	87.05	16:10:28	2.15
130822A	27.922	-3.209	4e-04	0.04	15:54:17	0.154
130828A	259.83	28	0.3	136.45	07:20:00	2.15
130828B	188.25	27.89	2.43	3.91	19:23:54	2.15
130829A	182.426	46.52	0.0132	42.56	05:43:33	2.15
130829B	258.51	6	1.69	6.66	16:08:01	2.15
130830A	142.97	-0.55	7.71	83.97	20:44:49	2.15
130830B	350.97	-51.57	10.49	36.35	22:06:33	2.15
130831A	358.625	29.43	3e-04	32.5	13:04:16	0.4791
130831B	192.42	-29.183	3e-04	37.8	13:48:19	2.15
130831C	267.45	61.03	8.06	24.83	01:24:13	2.15
130903A	82.133	-0.125	0.0152	70	00:47:20	2.15
130905A	275.89	-2.31	2.18	21.25	09:02:11	2.15
130906A	194.11	4.2	12.39	11.26	05:19:30	2.15
130906B	279.39	-53.38	7.6	8.19	10:26:25	2.15
130907A	215.892	45.607	2e-04	206.080	21:39:15	1.238
130907B	236.63	-25.1	7.37	3.14	18:14:46	2.15
130908A	219.16	-7.2	8.84	66.05	16:14:23	2.15
130909A	198.18	-20.79	17.24	33.79	19:36:08	2.15
130912A	47.593	13.997	3e-04	0.51	08:34:57	2.15
130913A	341.96	1.294	0.0507	10	00:28:21	2.15
130919A	207.281	-10.353	0.0162	97.3	11:07:24	2.15
130919B	297.35	-11.73	5.32	0.96	04:09:40	0.5
130919C	59.8	48.52	5.72	80.9	08:27:04	2.15
130919D	242.22	-48.29	6.78	17.41	23:38:13	2.15
130924A	28.77	-7.14	6.04	37.12	06:06:49	2.15
130924B	78.59	39.26	5.86	1.8	21:51:01	0.5
130925A	41.179	-26.153	3e-04	6.4	03:56:23	0.35
130925B	83.43	55.3	4.12	265.47	13:05:43	2.15
130928A	306.91	-44.19	3.26	133.0	12:52:35	2.15
130929A	135.024	-47.561	3e-04	11.10	09:36:33	2.15
130929B	200.93	2.8	19.67	2.3	09:00:13	2.15
130930A	190.661	-35.502	0.0304	NA	19:09:32	2.15
131001A	8.304	25.557	0.0162	NA	05:37:24	2.15
131002A	253.221	82.054	3e-04	55.04	06:55:06	2.15
131002B	75.122	-75.703	4e-04	39.10	10:54:28	2.15
131004A	296.113	-2.959	3e-04	1.54	21:41:03	0.717
131006A	325.38	-26.63	18.48	0.13	08:48:21	0.5
131006B	139.36	-0.87	5.86	41.99	20:09:52	2.15
131008A	328	-25.98	2.5	36.35	20:36:02	2.15
131011A	32.526	-4.412	0.0011	77.05	17:47:34	2.15
131014A	100.5	-19.1	0.45	3.2	05:09:00	2.15
131014B	15.05	21.43	6.94	30.21	12:18:36	2.15
131018A	98.471	-19.896	3e-04	73.22	12:47:48	2.15
131018B	304.41	23.11	0.13	39.93	16:08:39	2.15
131020A	209	51.1	19.77	2.24	02:42:25	2.15
131021A	329.12	-25.35	6.39	17.67	08:26:45	2.15
131024A	290.482	-64.603	3e-04	112.00	12:26:20	2.15
131024B	144.503	44.272	5e-04	64.00	21:35:31	2.15
131028A	61.225	71.595	2.7067	17.15	01:49:02	2.15
131028B	333.4	-56.94	6.64	14.34	02:17:51	2.15
131029A	200.785	48.298	0.26	84	23:20:48	2.15
131029B	110.28	-1.37	5.79	50.95	23:45:53	2.15
131030A	345.067	-5.368	2e-04	41.1	20:56:18	1.293
131030B	61.45	-62.8	7.77	53.25	15:40:25	2.15
131030C	186.29	-5.34	4.28	27.39	18:59:45	2.15
131031A	29.618	-1.603	0.0405	7.43	11:33:32	2.15
131102A	74.1	-28.01	14.82	62.98	14:55:44	2.15
131103A	348.919	-44.641	2e-04	17.3	22:07:25	0.5955
131105A	70.968	-62.995	3e-04	112.3	02:04:44	1.686
131108A	156.4	9.9	0.5	23.04	20:41:52	2.4
131108B	353.6	33.88	4.7	14.59	00:34:42	2.15
131110A	69.268	-17.259	0.0081	NA	11:53:11	2.15
131110B	9.81	8.16	3.96	27.32	08:57:01	2.15
131113A	157.99	-41.52	1.21	60.55	11:35:37	2.15
131117A	332.331	-31.762	3e-04	11.00	00:34:04	4.042
131117B	213.27	-2.47	2.13	93.95	18:23:30	2.15
131118A	349.863	-66.833	0.1723	139.520	22:58:58	2.15
131119A	47.96	-24.01	7.35	34.82	18:44:47	2.15
131120A	278.937	-12.026	0.0304	131	14:37:56	2.15
131122A	152.555	57.74	0.0162	70	21:25:01	2.15
131122B	261.67	33.38	1.69	23.04	11:45:05	2.15
131123A	53.24	-20.88	8.34	3.14	13:01:58	2.15
131125A	114.675	48.414	0.9113	2.81	16:32:51	2.15
131126A	215.43	53.53	0.76	0.128	03:54:08	2.15
131127A	332.73	36.609	3e-04	92.1	10:11:35	2.15
131127B	304.839	-2.83	0.9323	21.760	14:12:19	2.15
131127C	49.4	-5.67	4.07	59.65	11:31:00	2.15
131127D	246.3	33.92	8.66	15.1	16:41:46	2.15
131128A	355.308	31.306	3e-04	3.00	15:06:24	2.15
131202A	344.054	-21.662	3e-04	19.97	15:12:10	8.2
131202B	169.66	21.25	2.24	86.02	21:45:20	2.15
131204A	309.67	-69.67	4.42	29.95	22:28:57	2.15
131205A	131.628	-60.156	3e-04	37.5	09:18:38	2.15
131209A	136.5	-33.2	0.9	13.56	13:07:56	2.15
131209B	253.88	72.6	6.14	4.09	23:06:16	2.15
131211A	271.34	-40.61	3.56	44.8	12:14:49	2.15
131212A	273.63	18.11	15.27	7.42	19:32:29	2.15
131214A	183.94	-6.34	1	80.06	16:55:55	2.15
131215A	258.654	7.862	0.0608	300	09:08:20	2.15
131215B	104.07	68.26	1.38	23.04	07:08:45	2.15
131216A	94.674	-41.627	1.4397	5.69	01:56:32	2.15
131217A	86.59	30.6	6.41	0.76	02:36:11	0.5
131217B	227.73	25.16	3.12	9.21	04:23:28	2.15
131217C	57.46	43.21	10.78	NA	00:00:00	0.5
131218A	113.781	-64.737	0.0182	6	21:05:32	2.15

131224A	296.834	31.668	0.0203	0.8	16:54:37	0.5
131224B	163.722	-14.177	0.0304	NA	03:25:08	2.15
131225A	95.15	5.413	0.1824	NA	09:54:50	2.15
131226A	301.309	-64.943	0.0101	7	05:47:38	2.15
131227A	67.378	28.883	3e-04	18.0	04:44:51	2.15
131229A	85.232	-4.396	2e-04	12	06:39:29	2.15
131230A	91.11	64.29	11.07	3.07	12:41:27	2.15
131230B	73.05	4.84	3.91	49.15	19:24:09	2.15
131231A	10.59	-1.653	1e-04	31.23	04:45:16	0.642
140102A	211.919	1.333	3e-04	10.496	21:17:36	2.15
140103A	232.114	37.752	0.0172	17.3	00:30:43	2.15
140104B	218.81	-8.9	0.22	185	17:32:13	2.15
140105A	208.22	50.17	6.07	1.08	01:33:01	0.5
140105B	252.88	19.03	3.95	0.57	17:56:32	0.5
140106A	2.34	-8.75	15.81	33.02	08:16:43	2.15
140108A	325.112	58.745	4e-04	97.8	17:18:42	0.6
140109A	102.74	29.76	10.03	0.7	18:30:06	0.5
140109B	24.09	-25.05	37.45	3.32	21:03:26	2.15
140110A	28.9	-36.26	0.5	9.48	06:18:37	2.15
140110B	50.64	-69.29	11.71	0.77	09:52:04	0.5
140110C	31.86	65.16	3.19	81.15	19:31:34	2.15
140112A	8.44	11.99	7.14	12.03	01:26:46	2.15
140113A	75.63	3.18	9.99	68.87	04:23:55	2.15
140113B	329.37	18.13	12.28	4.61	14:58:25	2.15
140114A	188.522	27.951	3e-04	139.7	11:57:40	2.15
140115A	210.03	-61.41	2.2	14.91	20:43:18	2.15
140115B	94.86	-48.86	5.18	10.49	21:35:11	2.15
140118A	330.999	-17.937	0.0152	84.15	01:32:02	2.15
140122A	56.08	15.09	5.26	3.59	14:19:47	2.15
140124A	64.18	38.48	2.02	121.54	12:38:31	2.15
140126A	208.7	31.28	5.84	75.78	19:33:41	2.15
140129A	37.891	-1.595	1e-04	2.99	03:23:59	2.15
140129B	326.757	26.206	3e-04	1.36	12:51:09	0.5
140129C	183.4	-10.32	9.06	0.12	11:59:01	0.5
140204A	166.11	62.53	5.64	71.17	13:07:02	2.15
140206A	145.335	66.761	2e-04	93.6	07:17:20	2.73
140206B	315.26	-8.51	0.23	154.368	06:36:09	2.15
140209A	81.328	32.488	0.0101	21.3	07:30:57	2.15
140211A	124.233	20.237	0.0142	89.4	12:23:03	2.15
140211B	115.84	-13.59	3.99	3.46	02:10:41	2.15
140213A	105.155	-73.137	1e-04	18.62	19:21:32	1.2076
140215A	104.149	41.786	3e-04	84.2	04:07:10	2.15
140216A	194.04	31.46	13.73	2.43	07:56:04	2.15
140217A	359.39	76.75	3.08	41.48	01:01:41	2.15
140218A	347.48	44.54	3.62	53.5	10:14:29	2.15
140219A	156.44	7.46	0.9207	NA	19:45:58	2.15
140219B	221.93	50	8.23	6.08	07:38:54	2.15
140221A	107.447	-17.336	0.0608	NA	07:12:50	2.15
140223A	141.12	-30.4	5.55	17.41	11:53:06	2.15
140224A	2.78	20.37	5.93	2.3	09:10:17	2.15
140224B	23.74	39.48	3.69	17.15	18:55:19	2.15
140226A	221.492	14.994	6e-04	15	10:02:57	2.15
140227A	235.31	31.55	8.19	17.15	17:43:06	2.15
140301A	69.557	-34.257	3e-04	31.0	15:24:49	2.15
140302A	253.859	-12.878	4e-04	87.5	08:12:58	2.15
140304A	30.643	33.474	3e-04	31.75	13:22:31	5.39
140304B	354.18	-27.03	3.31	232.71	20:22:30	2.15
140305A	344.497	15.448	0.0172	13.7	15:00:20	2.15
140306A	27.943	48.975	0.1647	54	03:29:44	2.15
140308A	357.561	-33.348	0.1537	64	03:49:26	2.15
140308B	350.16	73.03	2.67	12.03	17:02:38	2.15
140311A	209.305	0.642	3e-04	71.4	21:05:16	4.95
140311B	252.325	52.724	3e-04	72.19	21:14:35	2.15
140311C	183.65	62.81	3.32	14.33	14:49:13	2.15
140311D	39.04	-25.23	5.29	14.91	10:52:04	2.15
140318A	184.089	20.209	3e-04	8.43	00:09:07	2.15
140319A	136.01	81.53	3.64	50.37	23:08:30	2.15
140320A	281.855	-11.194	8e-04	2.31	02:12:46	2.15
140320B	145.541	60.279	0.0203	100	09:26:00	2.15
140320C	134.418	71.2	0.0304	30	13:17:20	2.15
140320D	87.893	85.429	3.7177	22	20:21:38	2.15
140322A	250.3	-69.45	6.6	10.5	10:11:03	2.15
140323A	356.96	-79.905	3e-04	111.42	10:22:53	2.15
140327A	283.12	-6.15	5.31	11.52	01:33:05	2.15
140328A	320.04	17.97	14.7	4.16	13:26:26	2.15
140329A	145.698	-32.229	0.2	33.024	07:04:41	2.15
140329B	92.35	-41.08	9.18	0.06	06:31:21	0.5
140330A	325.59	-64.3	0.2	16.640	04:19:54	2.15
140331A	134.864	2.717	3e-04	209	05:49:48	2.15
140402A	207.592	5.971	0.1216	0.3	00:10:07	0.5
140402B	207.592	5.971	0.05	0.32	00:10:06	0.5
140404A	14.89	78.89	4.88	84.99	00:43:26	2.15
140404B	172.73	33.18	2.19	26.63	04:06:47	2.15
140404C	101.81	-6.95	2.59	22.78	21:36:17	2.15
140405A	119.1	-26.89	3.92	39.93	00:47:02	2.15
140406A	70.1	13.54	5.86	37.12	03:26:48	2.15
140406B	357.55	5.63	2.6	109.31	02:52:13	2.15
140408A	290.716	-12.595	4e-04	4.00	13:15:54	2.15
140412A	144.973	-65.822	4e-04	39.6	22:20:49	2.15
140413A	65.455	-51.183	3e-04	139.6	00:09:40	2.15
140414A	195.31	56.902	0.0405	NA	06:06:29	0.5
140414B	45.68	13.82	2.3	25.6	16:38:37	2.15
140416A	40.186	39.527	4.1323	32.768	01:26:36	2.15
140419A	126.99	46.24	3e-04	94.7	04:06:51	3.956
140422A	164.54	-62.62	6.85	361.47	04:38:45	2.15
140423A	197.285	49.842	2e-04	134	08:31:53	3.26
140426A	174.49	-13.95	12.52	37.57	12:21:32	2.15
140427A	131.91	27.49	23.26	13.31	16:50:21	2.15
140428A	194.365	28.331	0.0223	17.42	22:40:50	4.7
140428B	2.006	68.172	1.288	0.15	21:44:35	2.15
140429A	338.6	34.85	6.09	9.22	23:24:41	2.15
140430A	102.936	23.024	3e-04	173.6	20:33:36	1.6
140430B	146.38	-36.88	1.82	26.37	17:11:23	2.15
140501A	171.88	24.64	10.74	0.26	03:19:41	0.5
140501B	62.78	43.25	2.73	22.15	11:55:10	2.15
140502A	319.188	48.97	3e-04	16.9	08:30:20	2.15
140506A	276.775	-55.636	2e-04	64.13	21:07:36	2.15
140508A	255.631	46.747	0.2717	44.28	03:03:54	2.15
140508B	350.53	-63.78	4.98	19.45	04:17:41	2.15
140508C	272.1	72.53	3.56	50.44	15:05:26	2.15
140509A	46.595	-62.639	3e-04	23.20	02:22:13	2.15
140509B	312.966	21.016	0.0608	-	16:18:38	2.15
140511A	329.76	-30.06	8.84	1.4	02:17:11	0.5
140511B	26.25	-24.91	3.58	59.13	23:53:09	2.15
140512A	289.37	-15.094	3e-04	154.8	19:31:49	0.725
140513A	248.36	-19.5	3.93	17.15	17:22:12	2.15
140515A	186.065	15.105	3e-04	23.4	09:12:36	6.32
140515B	289.354	-11.701	0.0608	-	13:00:53	2.15
140516A	252.989	39.963	4e-04	0.19	20:30:54	0.5
140516B	115.16	4.29	7.77	33.79	16:47:38	2.15
140516C	74.28	32.85	3.81	22.01	18:21:00	2.15
140517A	127.75	13.57	2.17	20.48	19:31:17	2.15
140518A	227.231	42.396	0.0182	60.5	09:17:46	4.707
140518B	244.04	-77.86	13.43	0.7	17:00:43	0.5
140519A	278.47	34.41	5.43	47.61	01:01:44	2.15
140521A	320.177	67.587	0.0111	11.55	17:34:18	2.15
140521B	308.73	38.86	10.1	46.59	04:25:12	2.15
140523A	133.3	24.95	0.4	22	03:05:57	2.15
140526A	131.23	-4.15	3.71	79.11	10:47:04	2.15
140526B	142.99	-10.95	6.18	0.06	13:42:54	0.5
140528A	280.731	-59.08	0.226	13.57	20:05:22	2.15
140529A	228.81	-41.042	0.0122	3	09:28:06	2.15
140603A	217.45	25.91	2.13	138.24	11:24:59	2.15
140604A	263.17	-40.406	0.212	1	04:50:15	2.15
140605A	121.79	-53.86	6.08	0.51	09:02:50	0.5
140606A	201.799	37.599	0.0243	0.34	10:58:13	0.5
140606B	327.109	33.047	2.1927	8	03:11:50	0.384
140607A	86.373	18.904	0.0193	109.9	17:13:31	2.15
140608A	151.22	-50.26	1.26	66.69	03:41:00	2.15
140608B	211.96	53.82	2.91	6.4	17:07:10	2.15
140610A	286.261	3.899	0.0101	112.37	16:31:29	2.15
140610B	199.05	35.91	8.18	0.96	11:41:21	0.5
140610C	121.72	6.32	1	36.86	13:09:06	2.15
140611A	349.939	-40.111	0.0405	-	03:51:04	2.15
140612A	267.38	-64.11	4.69	38.92	07:03:33	2.15
140614A	231.17	-79.129	3e-04	720	01:04:59	4.233
140614B	322.631	14.93	3e-04	49.8	06:38:11	2.15
140614C	147.423	71.945	0.0304	-	20:06:56	2.15
140616A	104.94	-70.51	7	0.51	03:57:05	0.5
140619A	27.109	-39.259	2e-04	233.9	11:38:35	2.15
140619B	132.68	-9.66	0.06	2.82	11:24:40	2.15
140619C	233.018	-25.599	0.407	105	22:46:06	2.15

140620A	281.87	49.73	2	45.82	05:15:28	2.15
140621A	25.083	22.424	0.72	6.3	19:50:07	2.15
140622A	317.173	-14.419	4e-04	0.13	09:36:04	0.959
140623A	207.69	77.68	4.93	114.69	05:22:06	2.15
140624A	23.16	-0.56	4.57	0.1	10:08:40	0.5
140626A	77.38	-82.631	4e-04	16.4	00:33:01	2.15
140626B	120.81	38.78	6.61	1.8	20:14:14	0.5
140627A	66.49	-16.76	13.59	7.42	09:37:59	2.15
140628A	40.672	-0.378	0.0101	10.5	13:35:37	2.15
140628B	226.03	-25.83	13.04	12.55	15:01:36	2.15
140628C	359.15	31.56	9.04	75.52	16:53:18	2.15
140629A	248.977	41.877	3e-04	42.0	14:17:30	2.275
140630A	27.58	47.73	2.24	63.74	12:07:52	2.15
140701A	351.45	-28.66	3.82	25.09	13:36:11	2.15
140701B	285.44	-32.59	4.33	6.91	19:59:35	2.15
140703A	12.996	45.102	3e-04	84.22	00:37:07	3.14
140705A	293.732	21.897	4e-04	0.08	09:32:48	0.5
140705B	163.86	56.97	5.83	26.88	12:55:28	2.15
140706A	49.294	-38.052	3e-04	48.3	19:33:33	2.15
140709A	304.666	51.222	0.0101	98.6	01:13:41	2.15
140709B	146.054	63.529	4e-04	155.0	15:15:45	2.15
140710A	41.068	35.499	3e-04	3.52	10:16:40	0.558
140710B	204.646	-58.591	0.0172	11.52	21:37:37	2.15
140710C	2.8	-38.88	6.45	0.38	12:53:05	0.5
140711A	166.01	-24.6	8.46	80.89	16:35:24	2.15
140712A	319.28	-10.72	9.23	26.63	16:57:01	2.15
140712B	83.48	-73.62	1.68	28.16	23:20:51	2.15
140713A	281.105	59.634	3e-04	5.38	18:43:45	2.15
140714A	220.99	40.31	1.14	132.1	06:25:55	2.15
140715A	65.05	24.07	1.56	77.31	05:33:18	2.15
140716A	108.133	-60.15	0.0152	170	10:27:56	2.15
140716B	215.23	57.01	5.67	3.33	07:20:12	2.15
140717A	168.48	-18.94	6	80.64	19:50:58	2.15
140719A	171.601	-50.135	3e-04	48	05:53:55	2.15
140719B	39.731	-2.384	0.0172	53.0	20:49:35	2.15
140720A	175.03	-32.31	28.19	0.32	03:47:25	0.5
140720B	141.35	10.76	11.62	9.98	06:43:43	2.15
140721A	177.645	-37.735	3.6243	127.74	08:03:22	2.15
140723A	210.63	-3.73	0.35	45	01:36:30	2.15
140723B	24.63	11.19	2.23	45.06	11:58:04	2.15
140724A	314.73	-1.85	28.68	0.9	12:47:48	0.5
140725A	13.34	66.45	5.28	19.97	14:00:06	2.15
140727A	68.53	57.66	11.37	13.82	17:56:44	2.15
140729A	193.95	15.35	0.34	16	00:36:53	2.15
140730A	56.399	-66.545	4e-04	41.3	19:43:51	2.15
140801A	44.069	30.938	4e-04	7.17	18:59:53	1.32
140807A	200.16	26.49	2.53	0.51	11:59:33	0.5
140808A	221.222	49.215	6e-04	338	00:53:59	3.29
140809A	170.11	72.36	4.11	69.12	03:11:10	2.15
140810A	119.04	27.55	0.12	100	18:46:11	2.15
140814A	182.515	49.348	0.2006	-	07:12:31	2.15
140815A	86.896	-8.673	0.0253	8	21:55:05	2.15
140817A	127.264	58.19	3e-04	244	07:02:01	2.15
140817B	29.05	-44.48	5.17	26.11	05:30:02	2.15
140818A	199.554	6.888	0.0608	109.25	05:30:09	2.15
140818B	271.136	-1.386	3e-04	20.99	18:44:15	2.15
140819A	287.49	24.1	12.02	6.65	03:50:26	2.15
140821A	174.72	13.53	1	32.51	23:56:02	2.15
140824A	206.617	33.294	3e-04	3.09	08:40:28	2.15
140824B	18.33	58.64	1.49	108.8	14:33:12	2.15
140824C	55.63	4.35	2.06	4.09	13:08:46	2.15
140825A	88.715	-11.83	0.067	14	06:55:25	2.15
140825B	342.84	31.09	2.66	78.59	07:52:45	2.15
140825C	264.49	-6.92	16.32	16.39	23:30:52	2.15
140827A	130.65	35.8	1.82	20.99	18:18:03	2.15
140828A	142.029	14.569	0.0132	23.56	06:54:12	2.15
140829A	255.59	55.93	3.53	77.56	21:07:27	2.15
140831A	280.37	25.64	8.91	0.7	05:09:01	0.5
140831B	4.29	44.01	9.9	3.59	08:59:07	2.15
140901A	15.816	-32.755	0.2123	0.18	19:41:37	0.5
140901B	112.184	-29.209	0.0203	65	06:17:22	2.15
140901C	112.184	-29.209	0.1	65.02	06:17:22	2.15
140903A	238.021	27.608	0.0101	0.30	15:00:30	0.351
140905A	340.5	-25.94	2.82	110.08	10:53:45	2.15
140906A	248.36	49.51	7.66	37.63	04:11:38	2.15
140906B	185.84	0.98	1.6	20.74	10:18:02	2.15
140906C	314.961	1.939	0.1703	0.16	23:51:12	0.5
140907A	48.146	46.605	2e-04	79.2	16:07:08	1.21
140907B	163.82	-27	9.53	27.39	10:18:16	2.15
140909A	193.612	63.517	0.0012	-	06:56:51	2.15
140911A	128.39	-36.56	3.08	116.74	00:17:07	2.15
140912A	303.5	59.56	8.21	2.31	15:56:35	2.15
140916A	40.399	-39.686	3e-04	80.1	10:43:47	2.15
140916B	60.02	-10.26	5.62	31.24	05:36:49	2.15
140917A	171.37	20.41	6.18	16.52	12:17:06	2.15
140918A	356.18	-0.54	17.25	165.63	09:06:01	2.15
140919A	221.537	-32.176	3e-04	151.3	15:15:15	2.15
140927A	291.792	-65.394	3e-04	6.26	05:15:11	2.15
140928A	43.81	-56.08	0.16	17.92	10:29:53	2.15
140928B	163.77	48.47	7.07	7.68	02:23:23	2.15
140929A	177.45	-58.64	8.79	37.12	16:14:45	2.15
140930A	41.61	57.58	10.53	3.26	03:12:32	2.15
140930B	6.348	24.294	3e-04	0.84	19:41:42	2.15
141003A	321.77	-36.89	7	8.7	13:32:13	2.15
141003B	137.64	-2.21	7.02	7.42	18:55:23	2.15
141004A	76.734	12.819	3e-04	3.92	23:20:54	0.573
141004B	30.44	-77.3	2.07	9.47	03:36:28	2.15
141005A	291.093	36.095	3e-04	3.39	05:13:06	2.15
141005B	267.29	-1.09	19.56	11.26	12:49:57	2.15
141011A	257.939	-9.681	0.1153	0.1	06:46:17	2.15
141011B	259.38	-43	4.13	12.03	11:12:49	2.15
141012A	286.82	-49.88	3.06	37.64	18:33:17	2.15
141013A	315.06	-61.89	3.78	82.43	19:16:59	2.15
141015A	87.519	18.329	4e-04	11.0	09:12:59	2.15
141016A	221.45	-62.49	1.51	17.41	21:31:21	2.15
141017A	93.63	-58.582	3e-04	55.7	18:25:28	2.15
141020A	224.996	55.313	3e-04	15.55	07:48:39	2.15
141020B	214.296	7.984	0.0608	1.6	10:31:31	0.5
141022A	241.93	-72.152	0.0223	8.72	01:27:42	2.15
141022B	119.39	-75.17	1	9.22	02:04:40	2.15
141026A	44.084	26.928	3e-04	146	02:36:51	2.15
141026B	132.82	62.48	13.3	2.56	17:48:07	2.15
141028A	322.7	-0.28	0.4	31.48	10:54:46	1.82
141029A	69.413	-16.481	0.1702	-	04:32:09	2.15
141029B	102.5	25.07	1	202.44	03:13:18	2.15
141030A	161.37	33.4	6.65	21.09	17:54:13	2.15
141031A	128.608	-59.168	3e-04	920	07:18:26	2.15
141031B	356.905	41.353	3e-04	16.0	14:56:45	2.15
141031C	26.72	45.98	9.01	38.66	06:10:40	2.15
141031D	133.08	-33.68	15.62	0.16	23:57:20	0.5
141102A	208.614	-47.1	0.0405	2.62	12:51:39	2.15
141102B	223.23	-17.42	15.61	0.01	02:41:16	0.5
141102C	114.22	22.73	12.79	25.08	18:41:18	2.15
141104A	279.488	-12.702	0.1367	25	00:03:19	2.15
141105A	202.6	-32	5.67	19.2	08:35:48	2.15
141105B	16.91	29.17	4.1	1.28	09:44:47	0.5
141109A	144.531	-0.608	3e-04	94	05:49:55	1.67
141109B	222.303	73.131	3e-04	54.2	07:47:39	2.15
141109C	204.29	79.03	2.77	32.0	10:43:57	2.15
141110A	253.13	-34.09	3.8	36.61	05:33:23	2.15
141111A	51.22	43.02	14.48	1.73	10:26:59	0.5
141112A	17.4	-45.81	3.78	335.88	12:56:16	2.15
141112B	78.31	-4	7.42	63.75	19:52:03	2.15
141113A	171.02	80.26	12.15	0.44	08:17:43	0.5
141114A	6.75	-13.42	3.89	44.8	16:29:16	2.15
141118A	156.874	19.07	11.758	8.448	16:15:48	2.15
141121A	122.669	22.217	3e-04	-	03:36:43	1.47
141121B	235.89	-35.6	6.96	3.84	09:56:08	2.15
141122A	9.71	-20.02	10.9	1.28	02:05:26	0.5
141122B	280.61	-52.52	5.78	30.72	20:59:46	2.15
141122C	75.71	17.94	16.14	4.1	22:56:28	2.15
141124A	135.07	78.18	4.98	0.51	06:38:20	0.5
141125A	127.91	-29.874	0.429	-	03:33:01	2.15
141126A	243.87	59.99	17.12	0.89	05:35:56	0.5
141128A	321.8	-35.76	8.75	0.28	23:05:53	0.5
141130A	222.822	47.319	3e-04	62.9	23:10:56	2.15
141202A	143.073	54.161	0.543	1.34	11:17:05	2.15
141205A	92.859	37.876	0.0203	1.5	08:05:17	0.5
141205B	294.61	-87.58	3.9	13.05	00:25:29	2.15
141205C	92.859	37.876	0.033	1.28	08:05:17	0.5
141205D	298.77	-7.82	1.73	5.44	18:18:27	2.15
141206A	320.56	2.42	9.29	4.61	06:05:51	2.15

141207A	159.99	3.91	0.215	20	19:11:22	2.15
141208A	239.16	10.97	9.49	14.33	00:55:02	2.15
141208B	359.26	26.44	16.98	0.96	15:09:58	0.5
141209A	90.2	-30.57	3.5	78.09	03:07:59	2.15
141212A	39.124	18.147	5e-04	0.30	12:14:01	0.5
141212B	250.876	31.75	4e-04	10.5	13:23:48	2.15
141213A	248.19	18.06	8.72	0.76	07:12:15	0.5
141215A	179.056	-52.745	0.2003	15	13:26:13	2.15
141220A	195.058	32.146	0.0122	8.448	06:02:51	1.3195
141221A	198.287	8.205	3e-04	36.9	08:07:10	2.15
141221B	126.02	-74.21	3.69	32.51	21:31:48	2.15
141222A	178.04	-57.35	0.1	8.448	07:08:55	2.15
141222B	97.43	40.13	1	34.05	16:34:30	2.15
141223A	147.38	-20.71	7.48	94.2	05:45:37	2.15
141225A	138.778	33.792	3e-04	56.32	23:01:13	0.915
141226A	163.85	28.39	6.26	38.65	21:07:24	2.15
141229A	71.479	-18.956	0.0608	13.82	11:48:59	2.15
141229B	170.1	23.06	4.3	22.02	21:52:10	2.15
141230A	56.98	1.59	3.86	9.86	03:24:22	2.15
141230B	181.47	11.65	4.23	28.93	20:00:25	2.15
141230C	246.93	-40.18	10.48	0.22	20:54:05	0.5
150101A	312.603	36.733	5e-04	0.24	06:28:53	0.5
150101B	188	-10.956	0.04	0.08	15:23:34	0.093
150103A	131.666	-48.886	3e-04	49.1	20:02:18	2.15
150105A	124.32	-14.78	1	73.73	06:10:00	2.15
150106A	40.83	0.31	13.14	79.88	22:05:56	2.15
150110A	217	18.9	1	74.3	10:23:38	2.15
150110B	289.375	32.523	3e-04	10.6	22:08:30	2.15
150110C	68.576	-16.869	0.1155	-	23:41:01	2.15
150118B	240.24	-35.75	0.5	58.368	09:48:22	2.15
150118C	160.077	-27.555	0.096	0.29	22:14:32	2.15
150120A	10.319	33.995	4e-04	1.20	02:57:46	0.46
150120B	39.291	8.078	2e-04	24.30	07:21:55	2.15
150120C	48.11	26.94	9.94	56.83	16:26:17	2.15
150122A	151.23	-32.6	3.3	53.25	23:02:28	2.15
150123A	111.56	-9.691	0.0851	-	15:01:50	2.15
150126A	350.503	-12.368	0.51	96.51	20:50:35	2.15
150127A	296.953	-9.416	1.4493	52.73	09:32:44	2.15
150127B	140.184	-3.205	0.242	60.93	14:08:26	2.15
150127C	300.68	32.66	9.66	84.22	22:26:38	2.15
150128A	127.65	63.15	9.09	0.09	14:58:54	0.5
150128B	272.27	27.78	3.32	85.25	18:59:14	2.15
150131A	16.12	11.36	5.81	8.19	08:03:02	2.15
150131B	62.27	19.27	5.31	8.2	22:49:26	2.15
150201A	11.833	-37.619	3e-04	22.272	13:46:51	2.15
150201B	5.63	19.75	13.92	0.51	00:56:54	0.5
150201C	11.833	-37.619	0.0014	25.6	14:09:55	2.15
150202A	39.227	-33.148	3e-04	25.7	23:10:02	2.15
150202B	86.77	58.55	1	167.42	23:59:08	2.15
150203A	98.399	6.954	4e-04	25.8	04:09:07	2.15
150203B	156.88	-21.81	2.67	23.81	13:04:30	2.15
150204A	160.241	-64.043	0.0152	10	06:31:07	2.15
150204B	160.241	-64.043	0.02	11.01	06:31:07	2.15
150206A	10.074	-63.182	2e-04	83.2	14:30:02	2.087
150206B	220.59	57.5	6.76	5.12	09:46:27	2.15
150206C	357.94	-61.61	3.7	94.0	06:50:10	2.15
150208A	176.94	9.34	19.96	6.91	13:44:31	2.15
150208B	350.67	34.89	4.17	0.13	22:17:18	0.5
150210A	112.15	13.27	0.33	31.3	22:26:24	2.15
150211A	254.846	55.39	0.0101	13.6	11:52:11	2.15
150211B	336.56	38.98	9.08	18.43	05:44:16	2.15
150212A	285.497	47.389	0.0122	11.4	10:57:19	2.15
150213A	95.29	-4.85	1	4.1	00:01:48	2.15
150213B	253.452	34.189	3e-04	181	22:31:30	2.15
150214A	342.58	-34.17	10.47	0.19	07:01:22	0.5
150215A	305.62	3.38	14.68	0.52	00:37:26	0.5
150216A	120.68	-9.52	10.08	33.79	09:57:57	2.15
150219A	271.251	-41.594	6e-04	36.09	12:31:12	2.15
150220A	135.496	-1.597	0.1577	144.65	14:21:35	2.15
150222A	198.786	-12.152	3e-04	15.90	16:56:40	2.15
150222B	155.897	-41.17	0.0608	65.28	10:48:07	2.15
150222C	294.54	-40.94	11.32	74.75	19:58:03	2.15
150226A	63.5	22.51	1.28	1.4	05:20:26	0.5
150226B	51.1	28.48	2.58	174.6	13:05:23	2.15
150226C	157.76	18.37	11.3	32.76	22:45:49	2.15
150227A	190.3	-29.93	8.15	17.41	16:51:29	2.15
150228A	231.32	-41.87	2.03	4.13	20:16:18	2.15
150228B	7.55	-61.73	2.53	36.61	23:32:40	2.15
150301A	244.281	-48.732	0.0193	0.41	01:04:28	0.5
150301B	89.166	-57.97	1e-04	12.44	19:38:04	2.15
150301C	11.311	41.843	0.001	-	06:20:54	2.15
150302A	175.531	36.811	6e-04	23.74	05:42:36	2.15
150303A	114.81	-5.54	5.12	4.87	12:22:51	2.15
150305A	269.769	-42.648	0.0253	100	09:49:19	2.15
150305B	225.12	-44.74	11.36	16.13	17:23:13	2.15
150306A	0.63	-58.55	1	18.94	23:49:39	2.15
150309A	277.102	86.429	3e-04	242	23:03:06	2.15
150312A	285.49	-86	10.75	0.32	09:40:45	0.5
150313A	251.439	-11.707	0.0608	5.12	15:46:42	2.15
150314A	126.67	63.834	3e-04	10.69	04:54:50	1.758
150316A	15.89	53.14	11.44	1.98	09:36:09	0.5
150317A	138.985	55.466	4e-04	23.29	04:22:42	2.15
150318A	325.006	-61.457	3e-04	83.88	07:04:53	2.15
150318B	269.05	-30.22	2.19	94.72	12:29:53	2.15
150319A	7.13	28.06	2.36	10.5	06:29:49	2.15
150320A	139.98	68.93	10.55	0.06	11:05:31	0.5
150322A	125.84	-48.05	2.8	15.62	01:35:03	2.15
150323A	128.178	45.465	3e-04	149.6	02:49:14	0.593
150323B	260.447	38.316	0.025	56.32	09:28:39	2.15
150323C	192.617	50.191	3e-04	43.27	17:05:09	2.15
150324A	180.81	-42.72	4.19	4.61	03:56:10	2.15
150324B	295.21	-20.04	1.7	13.06	07:39:08	2.15
150325A	133.14	37.75	10.17	0.08	16:42:02	0.5
150326A	345.39	8.19	12.11	5.89	12:30:42	2.15
150326B	331.13	-19.65	5.94	4.1	13:00:35	2.15
150329A	163	-12.32	11.73	28.93	06:55:19	2.15
150330A	331.028	52.297	1.0617	194.560	19:52:18	2.15
150402A	173.658	40.992	0.0253	14	00:37:46	2.15
150403A	311.505	-62.711	2e-04	40.90	21:54:16	2.06
150404A	165.91	-67.37	8.87	4.87	17:35:03	2.15
150407A	216.603	38.541	0.0304	-	00:31:10	0.5
150411A	342.75	28.39	12.01	15.36	00:37:49	2.15
150412A	186.79	2.91	17.59	0.58	12:10:36	0.5
150412B	220.26	20.13	8.11	0.64	22:20:36	0.5
150413A	190.396	71.839	0.0193	263.6	13:54:58	3.139
150415A	220.63	-19.34	3.59	34.56	00:41:07	2.15
150416A	58.75	52.96	1.93	33.28	18:33:25	2.15
150418A	159.791	-4.326	0.0608	29	00:52:08	2.15
150418B	312.43	-43.53	9.17	3.84	19:39:29	2.15
150422A	215.1	-20.86	1.07	36.86	16:52:33	2.15
150422B	156.02	-53.56	10.29	30.2	07:03:30	2.15
150423A	221.579	12.283	3e-04	0.22	06:28:04	0.456
150423B	220.39	-38.84	14.73	14.34	06:50:42	2.15
150424A	152.306	-26.631	1e-04	91	07:42:57	2.15
150424B	182.759	-16.212	0.0608	36.1	09:39:59	2.15
150425A	214.23	-55.5	8.18	4.35	14:48:19	2.15
150426A	17.64	-30.23	1.46	22.53	14:15:31	2.15
150426B	283.52	0.65	3.25	61.7	22:59:10	2.15
150428A	188.539	6.954	3e-04	53.2	01:30:40	2.15
150428B	292.639	4.125	3e-04	130.9	03:12:03	2.15
150428C	60.247	67.818	0.1763	-	08:24:15	2.15
150428D	242.33	69.51	6.06	32.51	07:19:02	2.15
150430A	326.481	-27.919	0.0162	111.62	00:21:05	2.15
150501A	50	-15.57	3.25	9.73	00:24:08	2.15
150502A	241.46	42.06	1	109.31	10:25:55	2.15
150506A	176.25	7.56	1.46	6.78	09:33:47	2.15
150506B	76.32	67.81	3.21	0.51	15:07:05	0.5
150506C	29.25	-3.37	15.95	0.38	23:19:15	0.5
150507A	19.13	-3.8	1.35	63.49	00:37:29	2.15
150508A	45.93	-52.45	10.08	113.92	22:40:42	2.15
150510A	15.138	4.985	0.36	62	03:19:48	2.15
150511A	91.18	-30.35	5.05	31.24	08:41:57	2.15
150512A	200.5	59.11	3.64	123.14	10:22:25	2.15
150513A	49.044	-22.868	0.0101	162	20:31:19	2.15
150514A	74.85	-60.91	0.12	10	18:35:05	0.807
150518A	234.342	16.307	0.0608	-	00:00:00	0.256
150520A	128.53	-1.63	9.87	15.61	21:25:34	2.15
150522A	289.32	-39.67	3.81	43.77	10:23:50	2.15
150522B	130.86	58.58	10.47	1.03	22:38:44	0.5
150523A	115.36	-45.4	0.1	32	09:29:50	2.15
150523B	202.27	-39.2	5.74	114.69	16:33:56	2.15
150527A	288.96	4.202	3e-04	20.73	06:47:08	2.15

150527B	10.8	-35.6	3.03	63.23	15:53:43	2.15
150528A	350.95	-20.09	2.5	13.05	15:44:04	2.15
150530A	327.513	57.517	4e-04	6.62	11:42:18	2.15
150530B	7.496	44.29	0.0304	-	00:00:00	0.5
150601A	79.67	-53.82	6.84	0.77	21:41:10	0.5
150602A	289.87	-74.21	2.45	10.5	20:09:18	2.15
150603A	73.96	-38.39	1.06	59.64	02:31:47	2.15
150603B	274.45	-18.71	5.91	160.0	19:45:40	2.15
150604A	306.27	-46.72	7.77	52.74	06:48:27	2.15
150604B	72.44	-21.59	4.45	0.89	10:24:43	0.5
150605A	217.86	14.71	12.72	0.18	18:46:19	0.5
150607A	139.989	68.436	3e-04	26.3	07:55:09	2.15
150608A	13.389	-0.213	0.0608	-	11:45:25	2.15
150609A	52.26	31.63	14.15	0.26	07:35:19	0.5
150612A	2.28	25.09	1.78	68.35	16:51:35	2.15
150613A	106.13	-0.46	5.96	27.4	10:04:25	2.15
150613B	228.54	-7.07	6.53	46.6	23:52:36	2.15
150614A	283.26	23.95	3.49	5.12	01:44:33	2.15
150615A	107.565	-22.449	3e-04	27.6	04:42:27	2.15
150616A	314.717	-53.394	2e-04	599.5	22:49:19	2.15
150618A	238.17	28.54	6.53	45.31	16:10:47	2.15
150619A	219.69	8.64	1.44	57.09	06:53:06	2.15
150622A	252.028	-52.768	0.0608	297.25	00:02:46	2.15
150622B	267.05	33.25	1	60.68	09:26:32	2.15
150626A	111.337	-37.781	3e-04	144	02:12:49	2.15
150626B	187.633	66.772	3e-04	48.0	20:22:52	2.15
150627A	117.49	-51.56	0.05	-	04:23:26	2.15
150628A	347.02	-66.18	14.68	0.64	18:23:57	0.5
150629A	307.65	-26.45	11.18	1.92	13:32:40	0.5
150630A	116.81	-21.31	1.46	22.78	05:20:45	2.15
150630B	358.16	-47.39	2.52	39.17	22:58:58	2.15
150702A	52.78	-57	0.36	-	23:56:38	2.15
150703A	135.8	-11.19	5.13	50.18	03:34:06	2.15
150703B	341.33	46.61	2.02	46.6	06:13:33	2.15
150705A	102.49	20.86	2.97	20.99	00:13:36	2.15
150705B	66.54	-6.62	12.6	0.64	14:07:11	0.5
150707A	84.42	48.96	2.53	112.39	02:59:13	2.15
150708A	308.56	-39.36	3.13	95.24	08:08:46	2.15
150710A	194.484	14.309	0.0152	0.15	00:00:00	0.5
150710B	83.195	-46.963	0.0203	8.5	08:05:33	2.15
150710C	133.88	48.9	11.67	33.28	15:30:21	2.15
150711A	221.627	-35.456	3e-04	64.2	18:23:03	2.15
150712A	20.25	-38.46	4.3	59.65	20:18:18	2.15
150715A	157.26	23.57	19.91	0.38	03:15:28	0.5
150716A	278.481	-12.978	0.0111	44	07:06:43	2.15
150716B	286.64	14.46	8.97	32.77	13:14:38	2.15
150717A	236.55	16.14	7.31	9.98	19:04:26	2.15
150718A	124.75	-51.04	6.19	19.46	15:44:46	2.15
150720A	119.581	-28.263	3e-04	151	00:00:00	2.15
150721A	334.14	7.76	1.5	48.75	05:49:08	2.15
150721B	251.6	20.06	29.32	0.32	10:21:06	0.5
150721C	282.88	-49.41	6.97	11.52	17:34:29	2.15
150722A	218.278	-35.196	3e-04	67	09:57:53	2.15
150723A	149.86	-12.93	6.01	33.02	14:35:14	2.15
150724A	97.56	-19.165	3e-04	280	05:46:35	2.15
150724B	351.92	3.67	0.3	37.89	18:45:37	2.15
150724C	160.61	27.05	8.83	37.38	09:32:37	2.15
150726A	264.38	-36.2	3.17	46.85	21:02:30	2.15
150727A	203.968	-18.326	3e-04	88	19:02:02	0.313
150728A	292.229	33.916	7e-04	0.83	12:51:11	0.5
150728B	100.44	17.06	7.53	1.73	03:37:26	0.5
150729A	219.22	5.75	1	35.58	12:24:08	2.15
150801B	82.966	-5.389	3e-04	426	22:41:48	2.15
150802A	151.53	-62.08	4.18	313.1	03:03:02	2.15
150802B	201.54	17.18	4.54	9.98	04:57:42	2.15
150804A	334.53	27.09	2.19	51.2	19:21:11	2.15
150805A	95.76	-64.33	2.59	45.83	10:40:35	2.15
150805B	326.08	-33.4	13.14	1.41	17:54:12	0.5
150806A	106.85	1.01	2.8	85.25	08:21:41	2.15
150809A	351.03	-16.59	2.15	47.36	12:22:55	2.15
150810A	283.2	21.18	3	1.28	11:38:08	0.5
150811A	291.339	-15.425	4e-04	34.00	04:06:09	2.15
150811B	186.348	-14.105	0.99	0.7	20:22:09	2.15
150815A	289.92	-25.54	7.01	24.58	14:29:59	2.15
150817A	249.631	-12.053	3e-04	38.8	02:05:13	2.15
150817B	31.05	-41	2.41	13.31	06:00:47	2.15
150818A	230.356	68.342	3e-04	123.3	11:36:32	2.15
150819A	42.333	9.807	3e-04	52.1	00:50:08	2.15
150819B	59.386	39.701	0.5	0.96	10:33:19	2.15
150820A	258.65	-48.33	15.35	5.89	21:07:15	2.15
150821A	341.913	-57.894	3e-04	103.42	09:44:20	0.755
150822A	144.46	0.85	5.4	13.31	04:16:07	2.15
150824A	167.55	-56.767	0.15	-	01:53:30	2.15
150824B	265.72	80.99	4.84	32.77	02:59:22	2.15
150826A	317.97	-64.94	5.66	33.02	13:22:15	2.15
150827A	68.3	-60	5.14	10.5	18:50:12	2.15
150828A	193.81	65.78	2.26	12.8	07:58:55	2.15
150828B	94.24	78.64	13.34	2.05	21:37:02	2.15
150830A	207.25	-47.78	2.99	44.8	03:04:32	2.15
150831A	221.024	-25.635	3e-04	1	10:34:09	2.15
150831B	271.03	-27.243	0.0203	13.76	22:19:27	2.15
150901A	183.609	25.076	0.0274	64.0	15:26:35	2.15
150901B	1.96	12.16	22.12	0.71	22:10:44	0.5
150902A	214.926	-69.361	0.127	20	17:35:40	2.15
150904A	67.08	-20.38	10.89	23.3	11:30:20	2.15
150906A	212.04	1.09	5.19	0.32	22:38:47	0.5
150907B	255.304	-63.785	3e-04	62.0	23:26:27	2.15
150908A	157.13	-46.43	6.11	60.93	09:46:58	2.15
150910A	5.667	33.473	2e-04	112.2	09:04:48	1.36
150911A	67.434	5.735	3e-04	7.2	18:40:21	2.15
150911B	355.28	-2.9	7.32	41.73	07:32:54	2.15
150911C	33.11	-16.94	3.8	46.08	14:06:03	2.15
150912A	248.443	-21.034	0.033	30.97	10:37:38	2.15
150912B	321.36	73.26	6.38	0.32	14:24:31	0.5
150913A	241.05	-53.79	1.95	20.99	03:51:57	2.15
150915A	319.731	-34.854	0.0304	-	21:18:24	1.968
150917A	37.89	40.89	12.72	7.42	03:33:30	2.15
150919A	65.1	71.7	2.57	6.65	14:33:18	2.15
150922A	292.96	-2.25	6.76	0.15	05:37:29	0.5
150922B	90.56	21.01	10.42	15.88	17:13:42	2.15
150922C	274.14	-50.47	12.39	2.82	21:11:32	2.15
150923A	316.8	31.82	10.76	0.19	07:07:36	0.5
150923B	267.81	-40.66	6.37	0.19	10:18:17	0.5
150925A	227.52	-19.628	0.0304	-	04:09:28	0.5
150928A	83.78	34.24	4.57	53.51	08:37:19	2.15
151001A	233.729	10.967	3e-04	8.94	00:00:00	2.15
151001B	336.839	64.694	3e-04	109	00:00:00	2.15
151001C	246.74	-10.14	1.69	377.86	08:20:35	2.15
151003A	60.34	-66.37	12.56	44.03	17:29:59	2.15
151004A	213.613	-64.956	0.0233	128.40	19:09:14	2.15
151006A	147.426	70.503	3e-04	203.9	09:55:01	2.15
151009A	222	63.71	13.28	18.95	22:47:03	2.15
151011A	258.35	-9.64	2.73	25.34	03:15:27	2.15
151014A	0.39	55.07	14.17	34.3	14:13:03	2.15
151021A	337.643	-33.197	3e-04	110.2	01:29:12	2.15
151021B	104.34	-10.96	1.2	7.23	18:59:28	2.15
151022A	349.197	55.812	3e-04	134.3	14:06:32	2.15
151022B	92.14	79.08	16.56	0.38	13:51:02	0.5
151022C	34.76	-68.86	4.31	0.76	21:25:12	0.5
151023A	270.985	-8.316	4e-04	10.66	13:43:04	2.15
151023B	359.74	-17.15	16.4	10.24	02:29:25	2.15
151024A	232.86	22.95	11.11	4.61	04:17:53	2.15
151026A	228.04	-6.13	5.42	53.24	04:03:06	2.15
151026B	107.39	-73.32	3.57	63.23	12:32:38	2.15
151027A	272.487	61.353	3e-04	129.69	03:58:24	0.81
151027B	76.219	-6.45	3e-04	80.00	22:40:40	4.063
151029A	38.528	-35.386	3e-04	8.95	07:49:54	1.423
151030A	297.63	30.85	1	116.23	23:58:22	2.15
151031A	83.196	-39.121	4e-04	5.00	05:50:30	2.15
151107A	217.139	-59.68	0.0274	-	17:19:36	2.15
151107B	31.3	45.59	1.67	139.01	20:24:52	2.15
151111A	56.845	-44.162	3e-04	76.93	08:33:23	3.5
151112A	2.053	-61.663	2e-04	19.32	13:44:48	4.1
151114A	120.943	-61.028	3e-04	4.86	09:59:34	2.15
151114B	62.14	-47.9	5.81	34.81	15:28:24	2.15
151117A	19.64	-64.1	2.11	58.56	10:36:59	2.15
151118A	57.172	65.902	3e-04	23.4	03:06:30	2.15
151118B	292.98	43.4	3.59	40.9	13:18:05	2.15
151120A	157.25	-32.524	0.025	20	08:22:51	2.15
151122B	299.704	-19.899	0.05	51.2	17:00:45	2.15
151126A	338.61	30.88	10.08	8.45	07:01:17	2.15
151127A	19.478	-82.771	4e-04	0.19	09:08:49	0.5

151129A	60.82	-11.49	5.67	52.23	08:00:06	2.15
151130A	136.27	-18.82	5.8	20.22	03:50:50	2.15
151202A	326.49	-24.67	7.94	0.7	13:33:49	0.5
151205A	229.289	35.744	3e-04	62.8	15:46:00	2.15
151205B	41.19	-43.461	0.0233	1.4	21:43:14	0.5
151210A	65.116	-71.251	3e-04	94.9	03:12:56	2.15
151210B	293.97	-42.7	3.37	37.63	00:59:16	2.15
151211A	262.49	39.26	5.96	40.9	16:07:34	2.15
151212B	303.81	66.06	3.6	22.27	00:42:58	2.15
151212C	313.68	58.25	1.69	13.31	01:32:04	2.15
151215A	93.584	35.516	4e-04	17.8	03:01:28	2.59
151218A	9.45	-30.73	10.77	3.33	20:33:31	2.15
151219A	351.19	11.37	5.05	62.72	13:36:22	2.15
151222A	355.18	36.7	2.89	0.77	08:10:13	2.15
151227A	205.5	65.87	1.53	3.39	01:44:07	2.15
151227B	287.89	31.94	1	48	05:13:47	2.15
151228A	214.017	-17.665	0.0182	0.25	03:05:12	0.5
151228B	344.425	8.081	3e-04	48.0	22:47:14	2.15
151229A	329.37	-20.732	3e-04	3.46	06:50:27	2.15
151229C	346.49	6.91	16.11	0.16	11:40:06	0.5
151231A	65.63	-61.54	1	91	10:37:47	2.15
151231B	150.08	28.81	3.05	0.83	13:38:08	0.5
160101A	219.651	-13.815	8e-04	4.6	00:43:51	2.15
160101B	1.36	55.23	1.37	22.02	05:10:12	2.15
160102B	223.77	6.38	5.81	25.34	11:59:22	2.15
160102C	143.44	38.75	3.46	10.49	22:28:16	2.15
160104A	76.796	11.324	3e-04	16.2	11:24:10	2.15
160104C	280.43	-8.34	6	44.29	22:01:26	2.15
160106A	181.61	17.45	1.11	39.43	22:45:30	2.15
160107A	299.67	6.413	0.17	113.92	22:20:41	2.15
160111B	310.24	-32.78	5.68	26.88	02:45:03	2.15
160113A	187.26	11.53	1.2	24.57	09:32:30	2.15
160117A	20.367	-0.677	0.0182	118.58	10:13:39	2.15
160117B	132.195	-16.367	3e-04	-	13:59:27	0.86
160118A	17.72	59.78	1.49	46.85	01:25:42	2.15
160119A	211.922	20.461	3e-04	215	00:00:00	2.15
160119B	231.99	47.17	6.31	23.3	01:44:12	2.15
160121A	109.088	-23.592	3e-04	12.0	13:50:37	1.645
160123A	150.313	-33.775	3e-04	3.95	08:58:20	2.15
160123B	314.22	-22.18	10.75	37.63	02:17:25	2.15
160125A	76.78	13.01	10.85	16.9	08:49:30	2.15
160127A	225.982	0.073	3e-04	6.16	08:43:07	2.15
160131A	78.168	-7.05	4e-04	325	08:20:31	0.97
160131B	333.69	-41.44	9.16	34.82	02:46:24	2.15
160131C	113.03	15.49	4.71	205.32	04:09:56	2.15
160201A	312.67	69.32	2.9	40.51	21:11:42	2.15
160203A	161.951	-24.789	3e-04	20.2	02:13:10	3.52
160206B	184.26	52.41	4.17	21.5	10:19:12	2.15
160211A	123.2	53.43	4.97	0.96	02:50:48	0.5
160215A	356.79	1.73	3.44	141.32	18:33:30	2.15
160216A	311.684	-71.548	3e-04	-	19:10:30	2.15
160218A	33.33	-26.45	9.69	20.22	17:03:39	2.15
160219A	1.352	-21.957	20	3.52	06:56:18	2.15
160219B	238.03	33.67	2.56	145.93	16:09:47	2.15
160220A	236.953	-18.566	3e-04	8.3	01:25:25	2.15
160220B	259.865	-18.124	3e-04	31.4	11:10:53	2.15
160220C	326.89	6.05	15.78	22.52	20:50:12	2.15
160221B	232.082	-28.434	0.04	11.52	23:49:45	2.15
160222A	309.58	-23.77	9.57	18.17	01:41:23	2.15
160223A	147.603	9.369	0.0101	127	01:44:25	2.15
160223B	94.994	33.408	0.0367	17.92	09:59:01	2.15
160223C	18.11	-48.54	4.87	288.01	16:04:41	2.15
160224A	319.87	0.75	9.41	0.38	21:51:22	0.5
160225A	164.23	53.67	3e-04	157	14:20:56	2.15
160225B	150.19	-34.71	1	64.26	19:24:25	2.15
160225C	80.59	-9.19	1.25	70.15	17:16:40	2.15
160226A	92.3	-2.87	6.07	105.47	21:54:21	2.15
160227A	194.807	78.679	3e-04	316.5	19:32:08	2.38
160227B	123.43	-48.27	1.29	7.68	19:57:06	2.15
160228A	107.316	26.932	4e-04	98.36	17:34:32	1.64
160228B	32.21	39.38	12.43	16.12	00:48:52	2.15
160301A	114.4	2.29	3.48	29.69	05:10:18	2.15
160303A	168.701	22.742	3e-04	5.0	10:54:42	2.15
160303B	163.49	56.94	9.05	48.13	04:49:32	2.15
160303C	302.2	-65.68	8	27.13	23:18:32	2.15
160308A	128.27	20.19	10.75	88.06	17:00:39	2.15

Bibliography

[1] Aartsen, M., et al. First observation of pev-energy neutrinos with icecube. *Physical review letters*, **111** (2013), 021103.

[2] Aartsen, M., et al. Energy reconstruction methods in the icecube neutrino telescope. *Journal of Instrumentation*, **9** (2014), P03009.

[3] Aartsen, M., et al. Evidence for astrophysical muon neutrinos from the northern sky with icecube. *Physical review letters*, **115** (2015), 081102.

[4] Aartsen, M., et al. Extending the search for muon neutrinos coincident with gamma-ray bursts in icecube data. *The Astrophysical Journal*, **843** (2017), 112.

[5] Aartsen, M. G. et al. Energy Reconstruction Methods in the IceCube Neutrino Telescope. *JINST*, **9** (2014), P03009. arXiv:1311.4767, doi:10.1088/1748-0221/9/03/P03009.

[6] Aartsen, M. G. et al. Atmospheric and astrophysical neutrinos above 1 TeV interacting in IceCube. *Phys. Rev.*, **D91** (2015), 022001. arXiv:1410.1749, doi:10.1103/PhysRevD.91.022001.

[7] Aartsen, M. G. et al. Flavor Ratio of Astrophysical Neutrinos above 35 TeV in IceCube. *Phys. Rev. Lett.*, **114** (2015), 171102. arXiv:1502.03376, doi:10.1103/PhysRevLett.114.171102.

[8] Aartsen, M. G. et al. The IceCube Neutrino Observatory - Contributions to ICRC 2015 Part II: Atmospheric and Astrophysical Diffuse Neutrino Searches of All Flavors. In *Proceedings, 34th International Cosmic Ray Conference (ICRC 2015): The Hague, The Netherlands, July 30-August 6, 2015* (2015). Available from: https://inspirehep.net/record/1398539/files/arXiv:1510.05223.pdf, arXiv:1510.05223.

[9] Aartsen, M. G. et al. Observation and Characterization of a Cosmic Muon Neutrino Flux from the Northern Hemisphere using six years of IceCube data. *Astrophys. J.*, **833** (2016), 3. arXiv:1607.08006, doi:10.3847/0004-637X/833/1/3.

[10] Aartsen, M. G. et al. Search for Astrophysical Tau Neutrinos in Three Years of IceCube Data. *Phys. Rev.*, **D93** (2016), 022001. arXiv:1509.06212, doi:10.1103/PhysRevD.93.022001.

[11] Aartsen, M. G. et al. Measurement of the multi-TeV neutrino cross section with IceCube using Earth absorption. *Nature*, (2017). arXiv:1711.08119, doi:10.1038/nature24459.

[12] Aartsen, M. G. et al. Search for astrophysical sources of neutrinos using cascade events in IceCube. *Astrophys. J.*, **846** (2017), 136. arXiv:1705.02383, doi:10.3847/1538-4357/aa8508.

[13] Aartsen, M. G. et al. The IceCube Neutrino Observatory - Contributions to ICRC 2017 Part II: Properties of the Atmospheric and Astrophysical Neutrino Flux. (2017). arXiv:1710.01191.

[14] Abbott, B. P., et al. Gw170817: observation of gravitational waves from a binary neutron star inspiral. *Physical Review Letters*, **119** (2017), 161101.

[15] Abdo, A., et al. A limit on the variation of the speed of light arising from quantum gravity effects. *Nature*, **462** (2009), 331.

[16] Achterberg, A., et al. First year performance of the icecube neutrino telescope. *Astroparticle Physics*, **26** (2006), 155 . Available from: http://www.sciencedirect.com/science/article/pii/S0927650506000855, doi:https://doi.org/10.1016/j.astropartphys.2006.06.007.

[17] Ade, P. A., et al. Planck 2015 results-xiii. cosmological parameters. *Astronomy & Astrophysics*, **594** (2016), A13.

[18] Ahlers, M., Gonzalez-Garcia, M. C., and Halzen, F. GRBs on probation: testing the UHE CR paradigm with IceCube. *Astropart. Phys.*, **35** (2011), 87. arXiv:1103.3421, doi:10.1016/j.astropartphys.2011.05.008.

[19] Alfaro, J., Morales-Tecotl, H. A., and Urrutia, L. F. Quantum gravity corrections to neutrino propagation. *Physical Review Letters*, **84** (2000), 2318.

[20] Amelino-Camelia, G. Testable scenario for relativity with minimum length. *Physics Letters B*, **510** (2001), 255.

[21] Amelino-Camelia, G. Quantum-gravity phenomenology: Status and prospects. *Modern Physics Letters A*, **17** (2002), 899.

[22] Amelino-Camelia, G. Relativity in spacetimes with short-distance structure governed by an observer-independent (planckian) length scale. *International Journal of Modern Physics D*, **11** (2002), 35.

[23] Amelino-Camelia, G. Fate of lorentz symmetry in relative-locality momentum spaces. *Physical Review D*, **85** (2012), 084034.

[24] Amelino-Camelia, G. Quantum-spacetime phenomenology. *Living Reviews in Relativity*, **16** (2013), 5.

[25] Amelino-Camelia, G., Arzano, M., Bianco, S., and Buonocore, R. J. The dsr-deformed relativistic symmetries and the relative locality of 3d quantum gravity. *Classical and Quantum Gravity*, **30** (2013), 065012.

[26] Amelino-Camelia, G., Barcaroli, L., D'Amico, G., Loret, N., and Rosati, G. IceCube and GRB neutrinos propagating in quantum spacetime. *Phys. Lett.*, **B761** (2016), 318. arXiv:1605.00496, doi:10.1016/j.physletb.2016.07.075.

[27] Amelino-Camelia, G., Barcaroli, L., D'Amico, G., Loret, N., and Rosati, G. Quantum-gravity-induced dual lensing and icecube neutrinos. *International Journal of Modern Physics D*, **26** (2017), 1750076.

[28] Amelino-Camelia, G., Barcaroli, L., Gubitosi, G., and Loret, N. Dual redshift on planck-scale-curved momentum spaces. *Classical and Quantum Gravity*, **30** (2013), 235002.

[29] Amelino-Camelia, G., Barcaroli, L., and Loret, N. Modeling transverse relative locality. *International Journal of Theoretical Physics*, **51** (2012), 3359.

[30] Amelino-Camelia, G., D'Amico, G., Fiore, F., Puccetti, S., and Ronco, M. In-vacuo-dispersion-like spectral lags in gamma-ray bursts. *arXiv preprint arXiv:1707.02413*, (2017).

[31] Amelino-Camelia, G., D'Amico, G., Rosati, G., and Loret, N. In-vacuo-dispersion features for GRB neutrinos and photons. *Nat. Astron.*, **1** (2017), 0139. arXiv:1612.02765, doi:10.1038/s41550-017-0139.

[32] Amelino-Camelia, G., Ellis, J., Mavromatos, N., Nanopoulos, D. V., and Sarkar, S. Tests of quantum gravity from observations of γ-ray bursts. *Nature*, **393** (1998), 763.

[33] Amelino-Camelia, G., Fiore, F., Guetta, D., and Puccetti, S. Quantum-spacetime scenarios and soft spectral lags of the remarkable grb130427a. *Advances in High Energy Physics*, **2014** (2014).

[34] Amelino-Camelia, G., Freidel, L., Kowalski-Glikman, J., and Smolin, L. Principle of relative locality. *Physical Review D*, **84** (2011), 084010.

[35] Amelino-Camelia, G., Freidel, L., Kowalski-Glikman, J., and Smolin, L. Relative locality: A deepening of the relativity principle. *International Journal of Modern Physics D*, **20** (2011), 2867.

[36] Amelino-Camelia, G., Guetta, D., and Piran, T. Icecube neutrinos and lorentz invariance violation. *The Astrophysical Journal*, **806** (2015), 269.

[37] Amelino-Camelia, G., Loret, N., and Rosati, G. Speed of particles and a relativity of locality in κ-minkowski quantum spacetime. *Physics Letters B*, **700** (2011), 150.

[38] Amelino-Camelia, G. and Majid, S. Waves on noncommutative space–time and gamma-ray bursts. *International Journal of Modern Physics A*, **15** (2000), 4301.

[39] Amelino-Camelia, G., Mandanici, G., Procaccini, A., and Kowalski-Glikman, J. Phenomenology of doubly special relativity. *International Journal of Modern Physics A*, **20** (2005), 6007.

[40] Amelino-Camelia, G., Matassa, M., Mercati, F., and Rosati, G. Taming nonlocality in theories with planck-scale deformed lorentz symmetry. *Physical review letters*, **106** (2011), 071301.

[41] Amelino-Camelia, G., Ng, Y. J., and Van Dam, H. Anomalous particle-production thresholds through systematic and non-systematic quantum-gravity effects. *Astroparticle Physics*, **19** (2003), 729.

[42] Amelino-Camelia, G. and Smolin, L. Prospects for constraining quantum gravity dispersion with near term observations. *Physical Review D*, **80** (2009), 084017.

[43] Ardenghi, J. S., Castagnino, M., and Campoamor-Stursberg, R. The nonrelativistic limit of (central-extended) poincaré group and some consequences for quantum actualization. *Journal of Mathematical Physics*, **50** (2009), 103526.

[44] Atwood, W., et al. The large area telescope on the fermi gamma-ray space telescope mission. *The Astrophysical Journal*, **697** (2009), 1071.

[45] Baerwald, P., Hümmer, S., and Winter, W. Magnetic field and flavor effects on the gamma-ray burst neutrino flux. *Physical Review D*, **83** (2011), 067303.

[46] Bell, A. R. Particle acceleration by shocks in supernova remnants. *Braz. J. Phys.*, **44** (2014), 415. [,1286(2013)]. arXiv:1311.5779, doi:10.1007/s13538-014-0219-5.

[47] Berger, E. Short-duration gamma-ray bursts. *Annual Review of Astronomy and Astrophysics*, **52** (2014), 43.

[48] Bourbaki, N. Lie groups and lie algebras. In *Elements of the History of Mathematics*, pp. 247–267. Springer (1994).

[49] Bourrely, C., Soffer, J., and Teryaev, O. V. Positivity constraints for lepton polarization in neutrino deep inelastic scattering. *Phys. Rev.*, **D69** (2004), 114019. arXiv:hep-ph/0403176, doi:10.1103/PhysRevD.69.114019.

[50] Bustamante, M. and Connolly, A. Measurement of the Energy-Dependent Neutrino-Nucleon Cross Section Above 10 TeV Using IceCube Showers. (2017). arXiv:1711.11043.

[51] Butterfield, J. On symmetry and conserved quantities in classical mechanics. In *Physical theory and its interpretation*, pp. 43–100. Springer (2006).

[52] Calmet, X., Hsu, S. D., and Reeb, D. Grand unification and enhanced quantum gravitational effects. *Physical review letters*, **101** (2008), 171802.

[53] Calmet, X., Hsu, S. D., and Reeb, D. Grand unification through gravitational effects. *Physical Review D*, **81** (2010), 035007.

[54] Chianese, M., Mele, R., Miele, G., Migliozzi, P., and Morisi, S. Use of ANTARES and IceCube data to constrain single power-law neutrino flux. (2017). arXiv:1707.05168.

[55] Chianese, M., Miele, G., and Morisi, S. Interpreting IceCube 6-year HESE data as an evidence for hundred TeV decaying Dark Matter. *Phys. Lett.*, **B773** (2017), 591. arXiv:1707.05241, doi:10.1016/j.physletb.2017.09.016.

[56] Cianfrani, F., Kowalski-Glikman, J., and Rosati, G. Generally covariant formulation of relative locality in curved spacetime. *Physical Review D*, **89** (2014), 044039.

[57] Cohen, A. G. and Glashow, S. L. Pair creation constrains superluminal neutrino propagation. *Physical Review Letters*, **107** (2011), 181803.

[58] Collaboration, I. et al. Multimessenger observations of a flaring blazar coincident with high-energy neutrino icecube-170922a. *Science*, **361** (2018), eaat1378.

[59] Connolly, A., Thorne, R. S., and Waters, D. Calculation of High Energy Neutrino-Nucleon Cross Sections and Uncertainties Using the MSTW Parton Distribution Functions and Implications for Future Experiments. *Phys. Rev.*, **D83** (2011), 113009. arXiv:1102.0691, doi:10.1103/PhysRevD.83.113009.

[60] Cooper-Sarkar, A., Mertsch, P., and Sarkar, S. The high energy neutrino cross-section in the Standard Model and its uncertainty. *JHEP*, **08** (2011), 042. arXiv:1106.3723, doi:10.1007/JHEP08(2011)042.

[61] Costa, E., et al. Discovery of an x-ray afterglow associated with the γ-ray burst of 28 february 1997. *Nature*, **387** (1997), 783.

[62] Cucchiara, A., et al. A photometric redshift of z 9.4 for grb 090429b. *The Astrophysical Journal*, **736** (2011), 7.

[63] D'Amico, G. Flavor and energy inference for the high-energy icecube neutrinos. *Astroparticle Physics*, **101** (2018), 8.

[64] découvre le Ξb, C. Icecube observations challenge ideas on cosmic-ray origins. *CERN Courier*, (2012).

[65] Denton, P. B., Marfatia, D., and Weiler, T. J. The Galactic Contribution to IceCube's Astrophysical Neutrino Flux. *JCAP*, **1708** (2017), 033. arXiv:1703.09721, doi:10.1088/1475-7516/2017/08/033.

[66] Dutta, S. I., Reno, M. H., and Sarcevic, I. Tau neutrinos underground: Signals of muon-neutrino —> tau neutrino oscillations with extragalactic neutrinos. *Phys. Rev.*, **D62** (2000), 123001. arXiv:hep-ph/0005310, doi:10.1103/PhysRevD.62.123001.

[67] Einstein, A. et al. On the electrodynamics of moving bodies. *Annalen der Physik*, **17** (1905), 50.

[68] Ellis, J., Mavromatos, N. E., Sakharov, A. S., and Sarkisyan-Grinbaum, E. K. Limits on neutrino lorentz violation from multimessenger observations of txs 0506+ 056. *arXiv preprint arXiv:1807.05155*, (2018).

[69] Fishman, G. Batse–the burst and transient source experiment on the gamma ray observatory. *Gamma-Ray Bursts-Observations, Analyses and Theories*, (1992), 265.

[70] Freidel, L. and Smolin, L. Gamma ray burst delay times probe the geometry of momentum space. *arXiv preprint arXiv:1103.5626*, (2011).

[71] Gambini, R. and Pullin, J. Nonstandard optics from quantum space-time. *Physical Review D*, **59** (1999), 124021.

[72] Gandhi, R., Quigg, C., Reno, M. H., and Sarcevic, I. Ultrahigh-energy neutrino interactions. *Astropart. Phys.*, **5** (1996), 81. arXiv:hep-ph/9512364, doi:10.1016/0927-6505(96)00008-4.

[73] Gandhi, R., Quigg, C., Reno, M. H., and Sarcevic, I. Neutrino interactions at ultrahigh-energies. *Phys. Rev.*, **D58** (1998), 093009. arXiv:hep-ph/9807264, doi:10.1103/PhysRevD.58.093009.

[74] Garay, L. J. Quantum gravity and minimum length. *International Journal of Modern Physics A*, **10** (1995), 145.

[75] Gehrels, N., et al. The swift gamma-ray burst mission. *The Astrophysical Journal*, **611** (2004), 1005.

[76] Gelfand, A. E. Gibbs sampling. *Journal of the American Statistical Association*, **95** (2000), 1300. Available from: http://www.tandfonline.com/doi/abs/10.1080/01621459.2000.10474335, arXiv:http://www.tandfonline.com/doi/pdf/10.1080/01621459.2000.10474335, doi:10.1080/01621459.2000.10474335.

[77] Ghirlanda, G., Ghisellini, G., and Nava, L. The onset of the gev afterglow of grb 090510. *Astronomy & Astrophysics*, **510** (2010), L7.

[78] Girelli, F. and Livine, E. R. Special relativity as a noncommutative geometry: lessons for deformed special relativity. *Physical Review D*, **81** (2010), 085041.

[79] Glashow, S. L. Resonant scattering of antineutrinos. *Phys. Rev.*, **118** (1960), 316. Available from: https://link.aps.org/doi/10.1103/PhysRev.118.316, doi:10.1103/PhysRev.118.316.

[80] Goldstein, H., Poole, C., and Safko, J. Classical mechanics addison-wesley. *Reading, MA*, (1980), 426.

[81] Gomboc, A. Unveiling the secrets of gamma ray bursts. *Contemporary Physics*, **53** (2012), 339.

[82] Gomboc, A., et al. Optical flashes, reverse shocks and magnetization. In *AIP Conference Proceedings*, vol. 1133, pp. 145–150. AIP (2009).

[83] GRBweb, I. Available from: `http://grbweb.icecube.wisc.edu`.

[84] Guetta, D., Hooper, D., Alvarez-MuÃ±iz, J., Halzen, F., and Reuveni, E. Neutrinos from individual gamma-ray bursts in the batse catalog. *Astroparticle Physics*, **20** (2004), 429 . Available from: `http://www.sciencedirect.com/science/article/pii/S0927650503002111`, `doi:https://doi.org/10.1016/S0927-6505(03)00211-1`.

[85] Guetta, D., Hooper, D., Alvarez-Muniz, J., Halzen, F., and Reuveni, E. Neutrinos from individual gamma-ray bursts in the batse catalog. *Astroparticle Physics*, **20** (2004), 429.

[86] Hagiwara, K., Mawatari, K., and Yokoya, H. Tau polarization in tau neutrino nucleon scattering. *Nucl. Phys.*, **B668** (2003), 364. [Erratum: Nucl. Phys.B701,405(2004)]. `arXiv:hep-ph/0305324`, `doi:10.1016/S0550-3213(03)00575-3`.

[87] Harding, A. K. The physics of gamma-ray bursts. *Physics Reports*, **206** (1991), 327.

[88] Hümmer, S., Baerwald, P., and Winter, W. Neutrino emission from gamma-ray burst fireballs, revised. *Physical Review Letters*, **108** (2012), 231101.

[89] Inönü, E. and Wigner, E. P. Representations of the galilei group. *Il Nuovo Cimento (1943-1954)*, **9** (1952), 705.

[90] Isham, C. Structural issues in quantum gravity. *arXiv preprint gr-qc/9510063*, (1995).

[91] Jacob, U. and Piran, T. Neutrinos from gamma-ray bursts as a tool to explore quantum-gravity-induced lorentz violation. *Nature Physics*, **3** (2007), 87.

[92] Jacob, U. and Piran, T. Lorentz-violation-induced arrival delays of cosmological particles. *Journal of Cosmology and Astroparticle Physics*, **2008** (2008), 031.

[93] Kapner, D., Cook, T., Adelberger, E., Gundlach, J., Heckel, B. R., Hoyle, C., and Swanson, H. Tests of the gravitational inverse-square law below the dark-energy length scale. *Physical Review Letters*, **98** (2007), 021101.

[94] Klebesadel, R. W., Strong, I. B., and Olson, R. A. Observations of gamma-ray bursts of cosmic origin. *The Astrophysical Journal*, **182** (1973), L85.

[95] Kopper, C., Collaboration, I., et al. Observation of astrophysical neutrinos in six years of icecube data. In *35th International Cosmic Ray Conference*, vol. 301, p. 981. SISSA Medialab (2017).

[96] Kouveliotou, C., Meegan, C. A., Fishman, G. J., Bhat, N. P., Briggs, M. S., Koshut, T. M., Paciesas, W. S., and Pendleton, G. N. Identification of two classes of gamma-ray bursts. *The Astrophysical Journal*, **413** (1993), L101.

[97] Kowalski-Glikman, J. and Nowak, S. Non-commutative space–time of doubly special relativity theories. *International Journal of Modern Physics D*, **12** (2003), 299.

[98] Liberati, S. and Mattingly, D. Lorentz breaking effective field theory models for matter and gravity: theory and observational constraints. In *Gravity: Where Do We Stand?*, pp. 367–417. Springer (2016).

[99] Lipari, P. Lepton spectra in the earth's atmosphere. *Astroparticle Physics*, **1** (1993), 195 . Available from: `http://www.sciencedirect.com/science/article/pii/0927650593900226`, `doi:https://doi.org/10.1016/0927-6505(93)90022-6`.

[100] Loret, N., Barcaroli, L., and Rosati, G. Longitudinal and transverse relativity of spacetime locality in planck-scale-deformed phase spaces. In *Journal of Physics: Conference Series*, vol. 360, p. 012060. IOP Publishing (2012).

[101] Lukierski, J., Ruegg, H., and Zakrzewski, W. J. Classical and quantum mechanics of free k relativistic systems. Tech. rep. (1993).

[102] Magueijo, J. and Smolin, L. Generalized lorentz invariance with an invariant energy scale. *Physical Review D*, **67** (2003), 044017.

[103] Majid, S. and Ruegg, H. Bicrossproduct structure of κ-poincaré group and non-commutative geometry. *Physics Letters B*, **334** (1994), 348.

[104] Majumdar, D. and Ghosal, A. Probing deviations from tri-bimaximal mixing through ultra high energy neutrino signals. *Phys. Rev.*, **D75** (2007), 113004. `arXiv:hep-ph/0608334`, `doi:10.1103/PhysRevD.75.113004`.

[105] Mattingly, D. Modern tests of lorentz invariance. *Living Reviews in relativity*, **8** (2005), 5.

[106] Meegan, C., Fishman, G., Wilson, R., Paciesas, W., Pendleton, G., Horack, J., Brock, M., and Kouveliotou, C. Spatial distribution of γ-ray bursts observed by batse. *Nature*, **355** (1992), 143.

[107] Meegan, C., et al. The fermi gamma-ray burst monitor. *The Astrophysical Journal*, **702** (2009), 791.

[108] Mészáros, P. and Rees, M. J. Multi-gev neutrinos from internal dissipation in gamma-ray burst fireballs. *The Astrophysical Journal Letters*, **541** (2000), L5.

[109] Metzger, M., Djorgovski, S., Kulkarni, S., Steidel, C., Adelberger, K., Frail, D., Costa, E., and Frontera, F. Spectral constraints on the redshift of the optical counterpart to the γ-ray burst of 8 may 1997. *Nature*, **387** (1997), 878.

[110] Myers, R. C. and Pospelov, M. Ultraviolet modifications of dispersion relations in effective field theory. *Physical Review Letters*, **90** (2003), 211601.

[111] Nunokawa, H., Panes, B., and Zukanovich Funchal, R. How Unequal Fluxes of High Energy Astrophysical Neutrinos and Antineutrinos can Fake New Physics. *JCAP*, **1610** (2016), 036. arXiv:1604.08595, doi:10.1088/1475-7516/2016/10/036.

[112] O'Connell, A. D., et al. Quantum ground state and single-phonon control of a mechanical resonator. *Nature*, **464** (2010), 697.

[113] Paciesas, W. S., et al. The fourth batse gamma-ray burst catalog (revised). *The Astrophysical Journal Supplement Series*, **122** (1999), 465.

[114] Palladino, A., Pagliaroli, G., Villante, F. L., and Vissani, F. What is the Flavor of the Cosmic Neutrinos Seen by IceCube? *Phys. Rev. Lett.*, **114** (2015), 171101. arXiv:1502.02923, doi:10.1103/PhysRevLett.114.171101.

[115] Palomares-Ruiz, S., Mena, O., and Vincent, A. C. On the flavor composition of the high-energy neutrinos in icecube. *Nuclear and Particle Physics Proceedings*, **273-275** (2016), 433 . 37th International Conference on High Energy Physics (ICHEP). Available from: http://www.sciencedirect.com/science/article/pii/S2405601415005520, doi:https://doi.org/10.1016/j.nuclphysbps.2015.09.063.

[116] Palomares-Ruiz, S., Vincent, A. C., and Mena, O. Spectral analysis of the high-energy IceCube neutrinos. *Phys. Rev.*, **D91** (2015), 103008. arXiv:1502.02649, doi:10.1103/PhysRevD.91.103008.

[117] Piran, T. Gamma-ray bursts and the fireball model. *Physics Reports*, **314** (1999), 575.

[118] Piran, T. The physics of gamma-ray bursts. *Reviews of Modern Physics*, **76** (2005), 1143.

[119] Rachen, J. P. and Meszaros, P. Cosmic rays and neutrinos from gamma-ray bursts. *AIP Conf. Proc.*, **428** (1998), 776. arXiv:astro-ph/9811266, doi:10.1063/1.55402.

[120] Radel, L. and Wiebusch, C. Calculation of the Cherenkov light yield from electromagnetic cascades in ice with Geant4. *Astropart. Phys.*, **44** (2013), 102. arXiv:1210.5140, doi:10.1016/j.astropartphys.2013.01.015.

[121] Ramirez-Ruiz, E. and Fenimore, E. Pulse width evolution in gamma-ray bursts: evidence for internal shocks. *The Astrophysical Journal*, **539** (2000), 712.

[122] Robinson, S. P. and Wilczek, F. Gravitational correction to running of gauge couplings. *Physical review letters*, **96** (2006), 231601.

[123] Rosati, G., Amelino-Camelia, G., Marcianò, A., and Matassa, M. Planck-scale-modified dispersion relations in frw spacetime. *Physical Review D*, **92** (2015), 124042.

[124] Stecker, F. W., Scully, S. T., Liberati, S., and Mattingly, D. Searching for traces of planck-scale physics with high energy neutrinos. *Physical Review D*, **91** (2015), 045009.

[125] Szabo, R. J. Quantum field theory on noncommutative spaces. *Physics Reports*, **378** (2003), 207.

[126] Tavani, M., et al. The agile mission. *Astronomy & Astrophysics*, **502** (2009), 995.

[127] Vasileiou, V., Granot, J., Piran, T., and Amelino-Camelia, G. A planck-scale limit on spacetime fuzziness and stochastic lorentz invariance violation. *Nature Physics*, **11** (2015), 344.

[128] Vasileiou, V., Jacholkowska, A., Piron, F., Bolmont, J., Couturier, C., Granot, J., Stecker, F. W., Cohen-Tanugi, J., and Longo, F. Constraints on lorentz invariance violation from fermi-large area telescope observations of gamma-ray bursts. *Physical Review D*, **87** (2013), 122001.

[129] Waxman, E. Cosmological gamma-ray bursts and the highest energy cosmic rays. *Physical Review Letters*, **75** (1995), 386.

[130] Waxman, E. and Bahcall, J. N. High-energy neutrinos from cosmological gamma-ray burst fireballs. *Phys. Rev. Lett.*, **78** (1997), 2292. arXiv:astro-ph/9701231, doi:10.1103/PhysRevLett.78.2292.

[131] Waxman, E. and Bahcall, J. N. High-energy neutrinos from astrophysical sources: An Upper bound. *Phys. Rev.*, **D59** (1999), 023002. arXiv:hep-ph/9807282, doi:10.1103/PhysRevD.59.023002.

[132] Waxman, E. and Bahcall, J. N. Neutrino afterglow from gamma-ray bursts:˜ 1018 ev. *The Astrophysical Journal*, **541** (2000), 707.

[133] Whitehorn, N. A search for high-energy neutrino emission from gamma-ray bursts. (2012).

[134] Winkler, C., et al. The integral mission. *Astronomy & Astrophysics*, **411** (2003), L1.

[135] Xu, H. and Ma, B.-Q. Light speed variation from gamma ray burst grb 160509a. *Physics Letters B*, **760** (2016), 602.

[136] Xu, H. and Ma, B.-Q. Light speed variation from gamma-ray bursts. *Astroparticle Physics*, **82** (2016), 72.

[137] Zhang, B. and Kumar, P. Model-dependent high-energy neutrino flux from gamma-ray bursts. *Physical Review Letters*, **110** (2013), 121101.

[138] Zhang, S. and Ma, B.-Q. Lorentz violation from gamma-ray bursts. *Astroparticle Physics*, **61** (2015), 108.